UNIVERSITY OF CALIFORNIA SAN DIEGO

Structure Activity Relationships of Microtubule (MT)-Targeting 1,2,4-Triazolo[1,5-a]pyrimidines as Candidates for Neurodegenerative Tauopathies

A Thesis submitted in partial satisfaction of the requirements
for the degree Master of Science

in

Chemistry

by

Bobby Ray Lucero

Committee in charge:

Professor Carlo Ballatore, Chair
Professor Jerry Yang, Co-Chair
Professor Thomas Hermann

The Thesis of Bobby Ray Lucero is approved, and it is acceptable in quality and form for publication on microfilm and electronically:

_____

_____
Co-Chair

_____
Chair

University of California San Diego

2019

TABLE OF CONTENTS

LIST OF ABBREVIATIONS

Meaning	**Abbreviation**
Neurofibrillary tangle	NFT
Alzheimer's disease	AD
Amyloid beta	Aβ
Central nervous system	CNS
Microtubule associated protein	MAP
Microtubule	MT
Blood-brain barrier	BBB
Epothilone D	EpoD
Transgenic	Tg
P-glycoprotein	Pgp
Acetylated alpha tubulin	AcTub
Detyrosynated (glu)-tubulin	gluTub
Pharmacokinetic	PK
Triazolopyrimidine	TPD
Phenylpyrimidine	PPD
Blood to plasma	B/P
Tubulin	Tub
Structure-activity relationship	SAR
Sodium hydride	NaH
Copper (I) bromide	CuBr
Potassium carbonate	K_2CO_3
N,*N*-Dimethylformamide	DMF
Phosphoryl (V) trichloride	$POCl_3$
Dimethyl sulfoxide	DMSO
meta-Chloroperoxybenzoic acid	m-CPBA
Dichloromethane	CH_2Cl_2
Ammonium chloride	NH_4Cl

LIST OF ABBREVIATIONS

Meaning	**Abbreviation**
Tetrahydrofuran	THF
Lithium hexamethyldisilazane	LiHMDS
Trifluoroacetic acid	TFA
Di*iso*propylethylamine	DIPEA
Thin layer chromatography	TLC
Nuclear magnetic resonance	NMR
Melting point	mp
Infrared	IR
High performance liquid chromatography	HPLC

LIST OF SYMBOLS

Meaning	**Symbol**
Micro	μ
Degree	°
Alpha	α
Beta	β

LIST OF FIGURES

LIST OF FIGURES

LIST OF SCHEMES

LIST OF TABLES

ACKNOWLEDGMENTS

I would like to acknowledge Professor Carlo Ballatore for his support as the chair of my committee. His guidance was truly invaluable.

This work, in part, is coauthored with Ballatore, Carlo and Brunden, Kurt R. The thesis author was the primary author of this work.

ABSTRACT OF THE THESIS

Structure Activity Relationships of Microtubule (MT)-Targeting 1,2,4-Triazolo[1,5-a]pyrimidines as Candidates for Neurodegenerative Tauopathies

by

Bobby Ray Lucero

Master of Science in Chemistry

University of California San Diego, 2019

Professor Carlo Ballatore, Chair
Professor Jerry Yang, Co-Chair

A subset of neurodegenerative diseases known as tauopathies, of which Alzheimer's disease (AD) is the most prominent example, are defined by the presence of proteinaceous inclusions comprised of hyperphosphorylated tau protein within neurons. Tau has been shown to provide stability to microtubules (MTs), key constituents of the cytoskeleton that are involved in a variety of cellular functions, including cell communication and transport. Tau hyperphosphorylation and mutation causes it to detach from MTs and causes them to destabilize leading to axonal transport deficits and, ultimately, neuronal loss. A possible strategy of therapeutic intervention calls for the development of brain penetrant MT-stabilizing agents that

could compensate for the loss of tau function in neurons. Through a screen of non-naturally occurring small molecules, a few selected classes of molecules were found to have advantages over MT stabilizing natural products, in terms of synthetic accessibility and drug like physicochemical properties. Preliminary evaluation and SAR of those selected classes led to the identification of a preferred subset of triazolopyrimidines which were shown to be brain penetrant, orally bioavailable, and possess other favorable pharmacokinetic properties. The initial cellular assessment of triazolopyrimidines (TPDs) found that depending on the substitution pattern TPDs can either preserve or disrupt MT integrity in cells. Presented here are the design, synthesis and *in vitro* evaluation of a set of triazolopyrimidine congeners bearing a range of structural modifications at position 6 and/or 7. These studies complement and expand prior SAR studies and characterize the role that substituents of the triazolopyrimidine scaffold can have in determining MT-stabilizing activity.

Introduction

Though characterized by decline in cognitive function, neuron loss, and synaptic dysfunction, the presence of senile plaques and neurofibrillary tangles (NFTs) in an autopsied brain is the conclusive diagnosis of Alzheimer's Disease (AD). [1, 2] Senile plaques are formed primarily of deposits of the amyloid β (Aβ) peptide, while NFT are composed of protein tau aggregates. Much of the research in AD have focused on identifying therapeutics that decrease levels of Aβ peptides and consequently, senile plaques. Despite strong preclinical data, no Aβ targeting therapeutics have demonstrated clinical efficacy.[3] In the last several years, an increase in tau-focused research can be observed. This is, in part, caused by the discovery that inherited forms of Parkinsonism and frontotemporal dementia resulted in mutations in the tau gene[4-6] – illustrating that tau aggregates are involved in the neurodegenerative process rather than just indicators of dying neurons.

In addition to AD, the presence of tau aggregates are characteristic of many neurodegenerative diseases including corticobasal degeneration, progressive supranuclear palsy, and Pick's disease.[7] Tau is a microtubule associated protein (MAP); in cells, microtubules (MTs) are responsible for cell movement, intracellular transport machinery, and structure. In neurons, MTs that lie in the axons form polarized linear arrays between the synapses and the cell body, providing both structural support and serve as a track for motor proteins in intracellular transport.[8] As a MAP, tau provides stability to the MTs in axons,[9] regulation of motor proteins kinesin and dynein,[10, 11] and modulate the accessibility of MT-severing enzymes.[12, 13] The formation of tau aggregates are caused by hyperphosphorylation by various kinases,[14] which cause tau to lose affinity for MTs, misfold, and aggregate to form NFTs (Figure 1). The loss of

the MT-stabilizing function of tau leads to alterations in MT dynamics and organization, and consequently to axonal transport defects (Figure 1).[15-17]

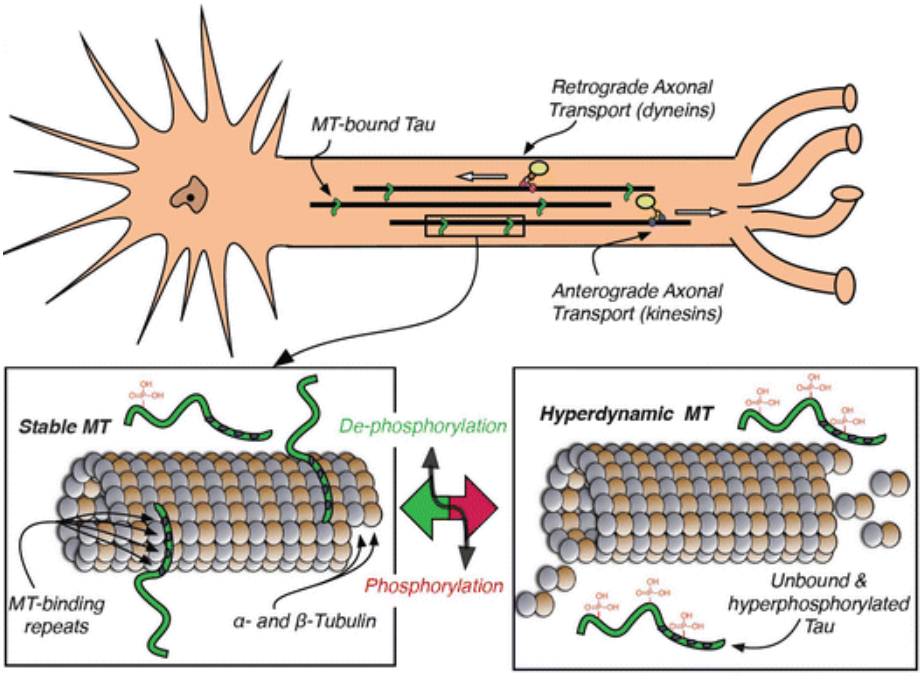

Figure 1. The role of Tau on MT dynamics and organization. Tau stabilizes MTs in axons. Under pathological conditions tau becomes hyperphosphorylated and disengaged from MTs with a consequent disruption of MT integrity and axonal transport. Disengaged tau then becomes misfolded and aggregates to form NFTs.

One of the possible strategies to treat tau-mediated neurodegeneration is to compensate for the loss of MT-stabilizing tau function by administering exogenous, brain-penetrant MT-stabilizing compounds.[18] A number of MT-stabilizing agents have been studied in preclinical animal models of human tauopathies.[3] Paclitaxel (**1**, Figure 2), was the first MT-stabilizing compound to be investigated in tau transgenic (Tg) mice (T44).[17] These studies, which established that treatment with **1** resulted in a recovery of axonal transport deficits that are observed in vehicle treated T44 mice, provided a first *in vivo* proof-of-concept validating the therapeutic strategy. However, since T44 mice exhibit tau pathology in motor neurons that reside outside of the central nervous system (CNS), **1** was not required to gain access into the brain in order to be effective. Since paclitaxel is known to have very limited ability to traverse

the blood-brain barrier (BBB), this compound could not be considered for further studies in animal models that recapitulate tau pathology in the CNS.[19] Originally of interest for their antifungal properties, epothilones, were found to have MT-stabilizing properties like that of taxol.[20] One analogue, Epothilone D (EpoD, **2**, Figure 2) was confirmed to penetrate the BBB and exhibited a long brain half-life.[16] *In vivo* studies in tau Tg mice showed that EpoD was efficacious at the onset of tau pathology[16] and also in models with developed neurodegeneration,[21] and confirmed by further independent studies by Bristol-Myers Squibb.[22] Dictyostatin (**3**, Figure 2) was isolated for interest in its antineoplastic properties in 1994[23] shared similar MT-stabilizing activity as EpoD, and was both brain penetrant and retentive.[24] Further studies showed that at the low dose of 0.1 mg/kg dictyostatin showed the desired effects, but at higher doses led to gastrointestinal complications and death of some PS19 mice.[25]

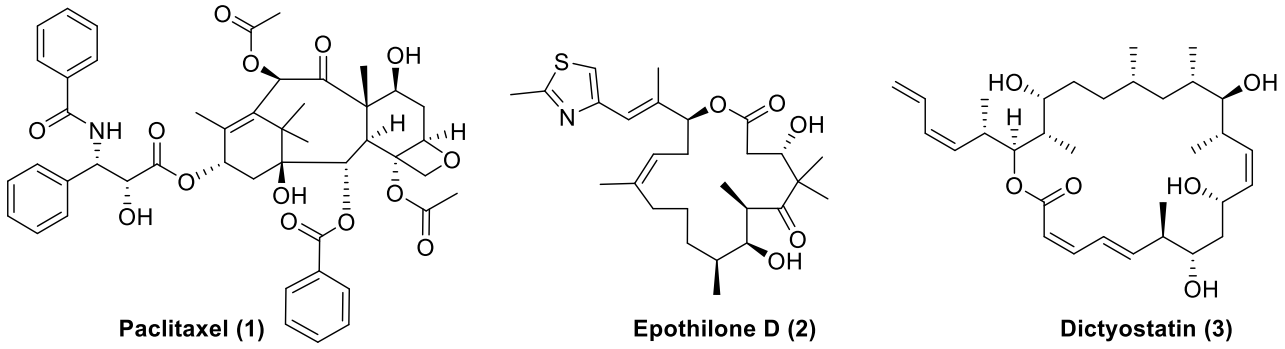

Figure 2. Selected, representative examples of MT-stabilizing natural products

While different naturally occurring compounds have been identified that show promising combination of MT-stabilizing properties and brain penetration, these molecules generally lack the oral bioavailability found in promising drug candidates and had to be administered intravenously.[19] Additionally, several of these (*e.g.*, EpoD **2** and dictyostatin **3**) are found to be potent inhibitors of the P-glycoprotein (Pgp) which could lead to CNS toxicities.[26] For these reasons, the development of alternative MT-stabilizing compounds that are suitable for CNS

indications is clearly desirable. In the recent years, a number of non-naturally occurring MT-stabilizing agents have been reported (Figure 3). Several of these compounds exhibit potential advantages over the existing classes of MT-stabilizing natural products, in terms of drug-like physicochemical properties and synthetic accessibility. Studies in the laboratory evaluated various non-naturally occurring agents – including triazolopyrimidines (TPD; **4**, **5**, and similar compounds), phenylpyrimidines (PPD; **6** and similar compounds) – based on MT-stabilizing ability, Pgp interactions, pharmacokinetic (PK) properties, and brain pharmacodynamic (PD) effects. QBI293 cells were used to monitor increase in acetylation of α-tubulin (AcTub) – a post-translational modification that occurs in polymerized tubulin.[27] The study showed that the compounds increased AcTub, exhibited desirable pharmacokinetic (PK) properties, such as good brain penetration and oral bioavailability, and did not disrupt Pgp function.[28] Among PPDs, compound 51549 (**6**, Figure 3) was found to be both brain penetrant and orally bioavailable.

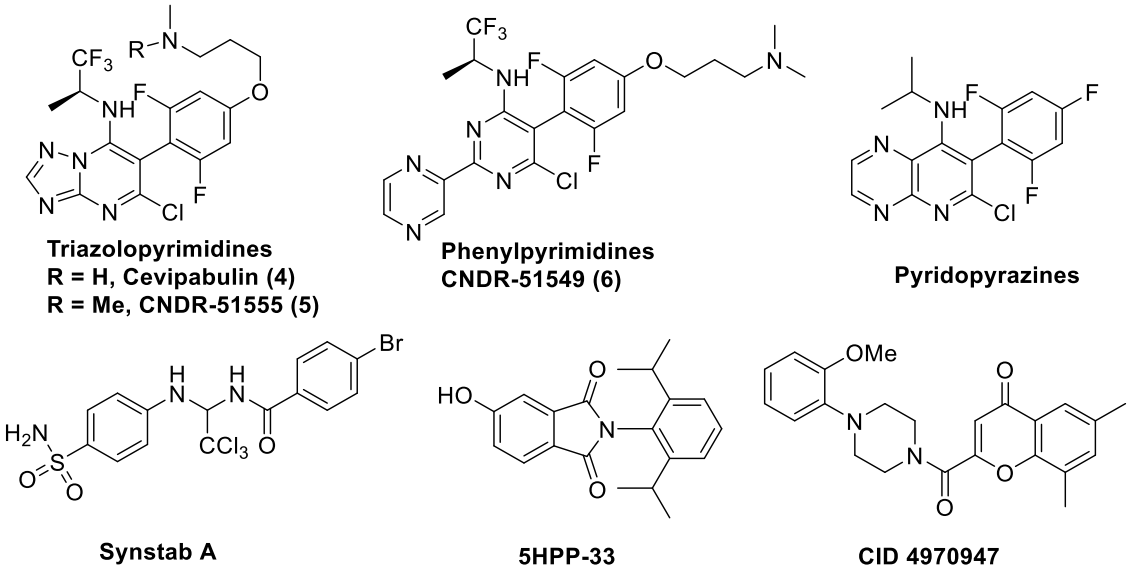

Figure 3. Representative examples of Non-naturally occurring MT-stabilizing agents.

Among TPDs, one particular example, cevipabulin (**4**, Figure 3), was known to possess promising drug-like properties including oral bioavailability, water solubility (0.89 mg/mL), and MT-stabilizing activity higher than that of EpoD.[29] Although cevipabulin was unable to cross the BBB and therefore would not be of any therapeutic use for neurodegenerative disease,[28] small changes to the terminal amine present in the side chain result in brain penetrant derivatives, such as 51555 (**5**, Figure 3). Thus, based on these promising findings, TPDs and PPDs were selected for further studies. Interestingly, investigations into the MT-stabilizing properties of TPDs and related PPDs in cell-based assays of MT-stabilization revealed that varying the scaffold (*i.e.*, TPD or PPD) or substitution pattern results in molecules that can either promote MT stabilization or, conversely, disrupt MT integrity.[30] For example, an evaluation of a representative set of TPDs and PPDs for their ability to produce elevations in known markers of stable MTs,[31] such as acetylated and de-tyrosinated α-tubulin (AcTub and GluTub, respectively), in cells revealed that typically the PPDs (*e.g.*, 51549, **6**, Figure 3) produce an unusual bell-shaped concentration-response curve in these assays. In addition, these compounds cause a concentration-dependent decrease in total cellular α- and β-tubulin resulting from proteasome-mediated degradation with a visible reduction of MT networks.[30] Interestingly, although similar observations were made for some TPDs, such as 51555 (**5**, Figure 3), replacement of the alkoxide chain of these molecules with a fluorine atom (*e.g.* 51597, **7**, Figure 4) had a dramatic positive impact on the MT-stabilizing properties of the compounds as demonstrated by the fact that the latter molecule caused the desired linear concentration-dependent increase in MT stabilization and MT mass in cells, without decreased cellular tubulin levels or changing MT morphology.[30] The observation that specific structural features within the TPDs are critical to elicit an increase in MT stability and mass led to a more systematic exploration of the SAR of the TPD scaffold.

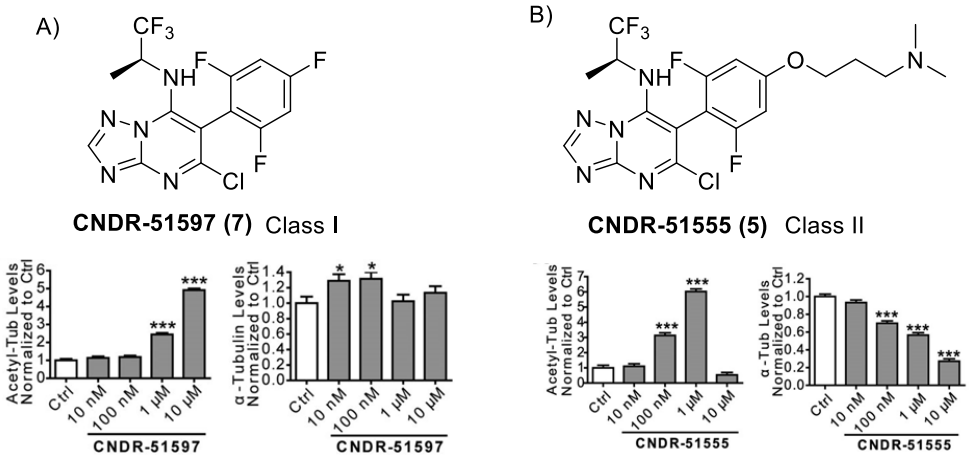

Figure 4. Results from prototypical TPD compounds in MT-stabilizing assay quantifying markers of stable MT and total tubulin. A) results from CNDR-51597, exhibiting class I characteristics. B) Results from CNDR-51555 that exhibits the characteristics of class II.

Design and Preliminary SAR

Since the ultimate goal would be to develop CNS-active, MT-stabilizing molecules that would be able of compensating for the loss of tau function in tauopathy neurons and maintain appropriate MT-structures in their axons, ideally, MT-stabilizing compounds should increase levels of AcTub and gluTub (markers of MT-stabilization), without affecting total α-Tub and β-Tub levels. Results from CNDR-51957 showed that, *in vitro*, there was a linear dose response in the AcTub assay with the concentrations tested (10 nM, 100 nM, 1 µM, and 10 µM). CNDR-51957 also maintained levels of α-Tub and β-Tub in active doses and did not show altered MT structure. Compounds eliciting this kind of cellular response are potentially appropriate for treatment of tauopathies and are classified as "Class I" compounds (Figure 4A). CNDR-51555, on the other hand, produced a bell-shaped dose response in the AcTub assay and were found to disrupt the integrity of MT-network causing a decrease total levels of α-Tub and β-Tub, similar to the undesirable response described above for PPD compounds. Compounds eliciting this kind of cellular response are classified as "Class II" (Figure 4B) and are likely unsuitable for tauopathy treatment.

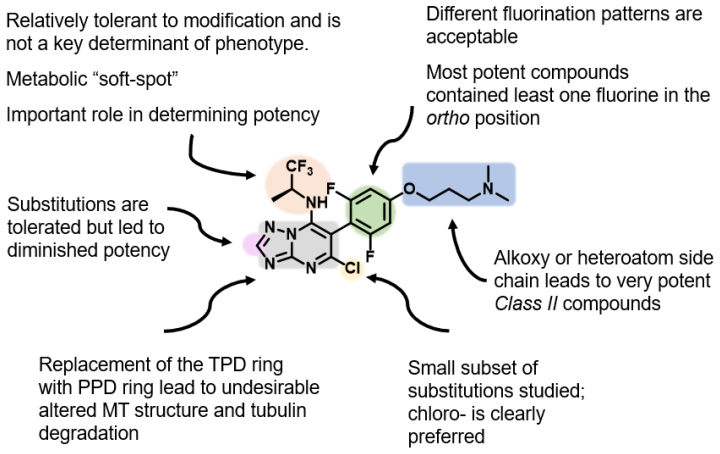

Figure 5 Summary of preliminary SAR with example compounds of differing fluorination patterns, alkoxide chain replacements, amine fragments, chloro replacements and scaffold replacements.

Preliminary SAR studies were performed, and results are summarized in Figure 5. The SAR explored included an investigation of the amine fragment at C7 (*a*); the fluorination pattern of the phenyl ring linked at C6 (*b*); the nature of the alkoxide chains (*c*); the effect of replacing the halogen at C5 (*d*); and the effect of substitutions at C2 (*e*).The amine fragment at C7 was found to be relatively tolerant to modification and is not a key determinant of phenotype (Class I vs II). However, this fragment has shown to be the metabolic "soft-spot" and therefore plays an important role in determining both potency and ADME-PK properties. Generally, lipophilic aliphatic amines at C7 appeared to be preferred for optimal MT-stabilizing activity. Examination of the nature of the alkoxide chain, found that compounds made with varying chain lengths and different substituents on the terminal amine led to compounds that varied only in levels of activity but still elicited the undesirable Class II phenotype. Compounds lacking the side chain and bearing different fluorination patterns on the phenyl ring were evaluated: active compounds were Class I. This result indicated that the fluorination pattern may be important in determining the phenotype elicited by these TPDs; moreover, the presence of one or more fluoro substituents in the ring can have impacts in terms of potency. In particular, it was found that in order to retain appreciable MT-stabilizing activity at least one fluoride had to remain in the *ortho*-position on the phenyl ring. Of all the compounds tested, the 2,4,6-trifluorophenyl pattern remained the most active. A few substitutions on C2 and C5 were also explored. The C2 position was substituted with a methyl and a phenyl group, both of which resulted in reduction of potency. The chloro substitution at C5 was replaced with a methyl group or different amines, resulting generally in dramatic reduction of potency without qualitative changes of cellular response. While these preliminary findings tell us that phenotype is dictated primarily by the substitution in C6 and potency is dictated by the substituents at C2, C5, and C7, additional SAR is necessary to better

define the structural determinants for Class and potency, and ultimately identify candidates for future clinical development.

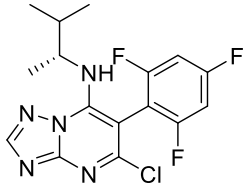

CNDR-51657 (**8**)

Figure 6. Structure of CNDR-51657.

Among the previously evaluated compounds, CNDR-51657 (**8**, Figure 6) was chosen for full characterization and *in vivo* testing.[30] The compound exhibited the desired MT-stabilizing activity including increased AcTub levels, increased gluTub levels, and maintained levels of α-Tub and β-Tub. Additionally, the compound displayed a desirable brain-to-plasma (B/P) ratio of 2.7 indicative of BBB permeability. *In vivo* testing began with pharmacodynamic studies by first confirming that compound treatment resulted in elevated AcTub levels in the CNS of wild type (WT) mice after peripheral administration. The results of these studies revealed that the compound elicits the desired MT-stabilizing activity in the brain. Moreover, although CNDR-51657 exhibit relatively short half-life in both brain and plasma (~1–2h), the pharmacodynamic studies showed that the MT-stabilizing effect was retained for an extended period after drug clearance. Evaluation of compound efficacy and safety was conducted by administering for 3 months either 10 or 3 mg/kg of CNDR-51657 to 9-month-old female PS19 tau Tg mice, which exhibit low but discernable tau pathology. The results from these *in vivo* efficacy/tolerability studies demonstrated that low, infrequent dosing of TPD, CNDR-51657, was effective in normalizing the MT-deficits of the tau Tg mice and in reducing tau pathology in the CNS. Moreover, compound treatment was not associated with overt signs of toxicity. However, despite *in vivo* support of a TPD as MT-stabilizing agent, prototype CNDR-51657 may feature

suboptimal properties as clinical candidate, including limited aqueous solubility (~50 μM) and rather short plasma half-life in mice (~1–2 h). These findings further support a need for a better TPD compound that has suitable pharmacokinetic profile, all while having comparable or better activity.

In order to identify a clinical candidate, more compounds need to be designed, synthesized, and evaluated to expand the SAR. Based on what is known from the existing SAR, a number of details still need to be investigated. For example, we know that the replacement of the fluorine with an alkoxy-group can have a dramatic effect in determining the MT-stabilizing activity of the compounds (*i.e.*, Class I vs Class II phenotype), but further studies are needed to more accurately define the stereo-electronic properties of the substituent in the *para* position that may be important to elicit Class I phenotype. Likewise, although it was found that a variety of different amines can be tolerated at C7, several details concerning the nature and characteristics of the fragment linked at C7 remain unclear and need to be elucidated.

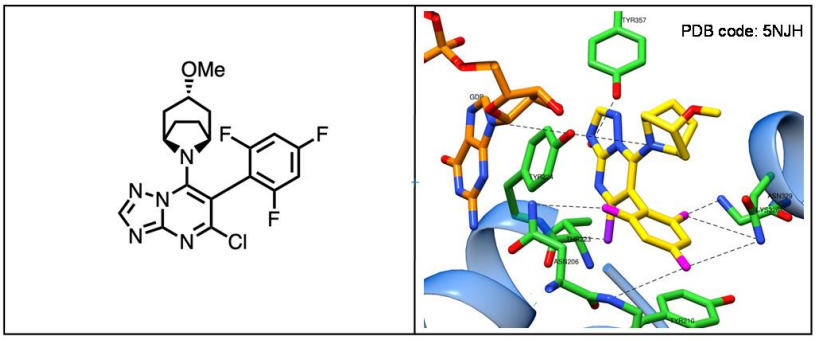

Figure 7. The Co-crystal structure of a TPD bound to tubulin (right) and the TPD compound from which it was resolved (left).

During the preliminary SAR, the crystal structure of a class I TPD MT-stabilizing compound bound to tubulin was solved (Figure 7).[32] This crystal structure has enabled us to use computation methods in designed new TPD compounds. *In silico* methods for the amine substitution at C7 have been developed and has allowed for us to screen many commercially

available amines to prioritize for synthesis and evaluation; and in an iterative process, results are fed back to improve the existing *in silico* calculations to result in further compounds that are predicted to be potent.

The goal is to develop a more comprehensive SAR to elucidate the structural determinants of Class I and Class II compounds, and with better understanding of the SAR, we could develop compounds with better drug-like properties, and of desired cellular phenotype for treatments in neurodegenerative tauopathies. Lead compound CNDR-51657, had good results *in vitro* and *in vivo* and is orally bioavailable but with what was known of the SAR at the time of the development left some questions unanswered. Further understanding of the SAR could optimize the MT-stabilizing activity and metabolic stability of the compound. Ultimately the information obtained from the SAR will allow us to design novel compounds that exhibit the desired Class I phenotype, while having a suitable ADME-PK and physicochemical profile that would identify a potential clinical candidate.

Synthesis

During the course of this thesis project, a total of 30 TPD derivatives have been synthesized, bearing modification at the fragment linked at C7 and/or the phenyl ring at C6. The general synthetic approach to access most of the TPD analogues is depicted in Scheme 1 and is largely based on published reports.[29, 33, 34] In general all test compounds were synthesized at 30 mg scale, which was considered sufficient to complete both *in vitro* characterization of biological activity, as well as a preliminary assessment of *in vivo* PK. The structural integrity and purity of each test compound was determined by NMR, HRMS, and IR (see Appendix).

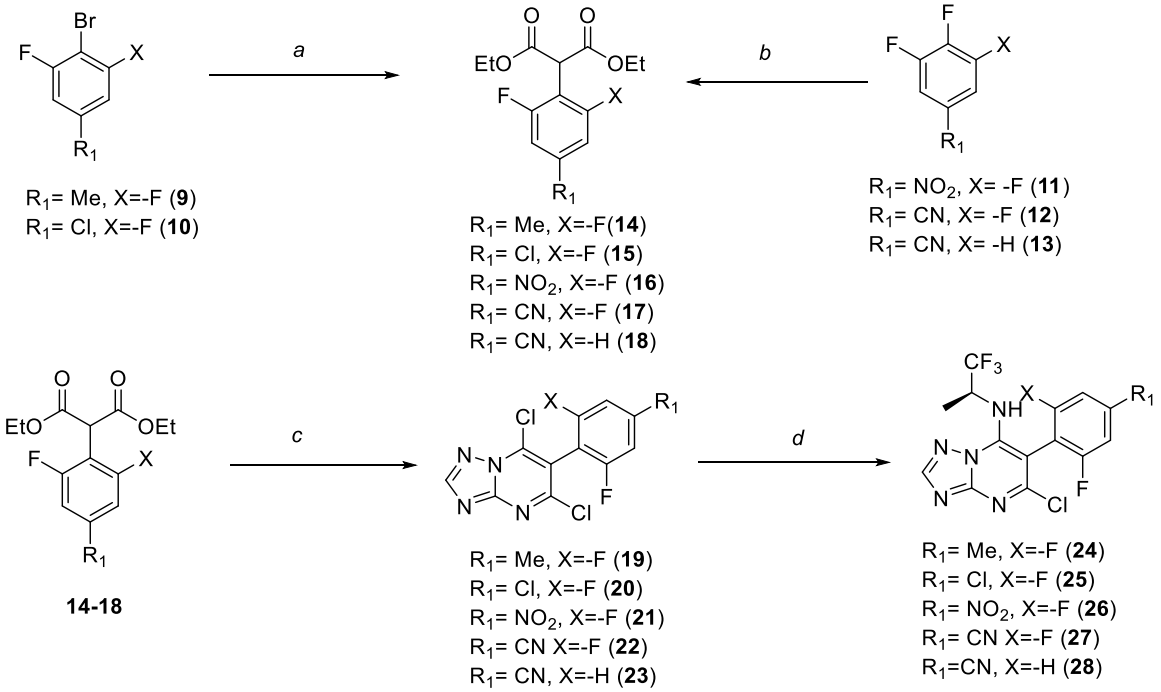

Scheme 1. Synthesis of TPD derivatives **24-28**. *Reagents and reaction conditions:* (*a*) Diethyl malonate, NaH, CuBr, dioxane 60-100 °C (60–80%), 16 hr; (*b*) Diethyl malonate, K_2CO_3, DMF, 60 °C (73–85%), 5 hr; (*c*) 3-amino-1,2,4-triazole, tributylamine, 170 °C, 2 hr; (*ii*) $POCl_3$, 130 °C (59–90%), 6 hr; (*d*) (*S*)-1,1,1-trifluoropropan-2-amine, DMF, 50 °C (45–90%), 1–16 hr.

The synthesis of compounds with varying R_1 followed similar methods, beginning with commercially available diethyl malonate and fluorinated benzenes (Scheme 1). Compounds **14** and **15** were synthesized in good yields (60–80%) by coupling diethyl malonate and the

appropriate difluorobromobenzenes (**9** and **10**) in the presence of NaH, and stoichiometric CuBr at elevated temperatures (60 to 100 °C), via a modified Hurtley arylation[35-38] adapted from procedure.[33] Nucleophilic aromatic substitution of **11**–**13** with diethyl malonate afforded compounds **16**–**18** in good yields (73%–85%). Cyclocondensation of **14–18** with 3-amino-1,2,4-triazole at 170 °C afforded crude bisodic salts that were used without further purification, followed by subsequent bis-chlorination using $POCl_3$ at 130 °C, with yields up to 90%. Compounds **19–23** were usually adequately pure as determined via NMR and used in the next step without further purification. From **19–23**, TPD analogues **24–28** were synthesized by chemoselective nucleophilic substitution of (*S*)-1,1,1-trifluoropropan-2-amine in DMF to replace the 7-chloro exclusively,[29, 34] also confirmed by X-ray crystallography. Substitution of 9-chloro was not observed. All final compounds were purified using reversed phased HPLC and were 95+% in purity.

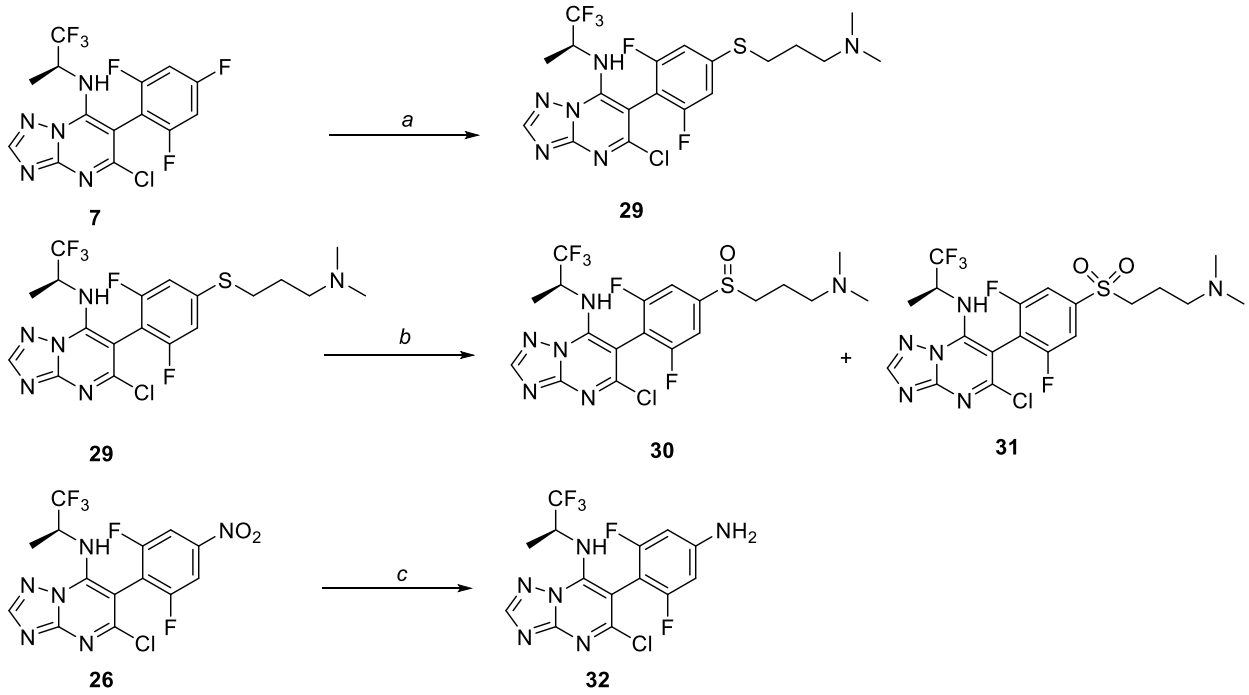

Scheme 2. Synthesis of compounds **29**–**32** *Reagents and reaction conditions:* (*a*) 3-mercapto-*N*,*N*-dimethylpropan-1-aminium chloride, NaH, DMSO, 60 °C; (*b*) m-CPBA, CH_2Cl_2, r.t.; (*c*) NH_4Cl, Fe, ethanol/water, 80 °C.

Compound **29** was synthesized from nucleophilic aromatic substitution of the fluoride in compound **7** and with 3-mercapto-*N*,*N*-dimethylpropan-1-aminium chloride in DMSO, in the presence of NaH in good yield (81%). Compound **29** was oxidized using *m*-CPBA, resulting in both compounds **30** and **31** (32% and 52%, respectively), which were separable via reversed phased HPLC. Compound **32** was synthesized from the Bechamp reduction[39, 40] of compound **26**, resulting in good yield as well (69%).

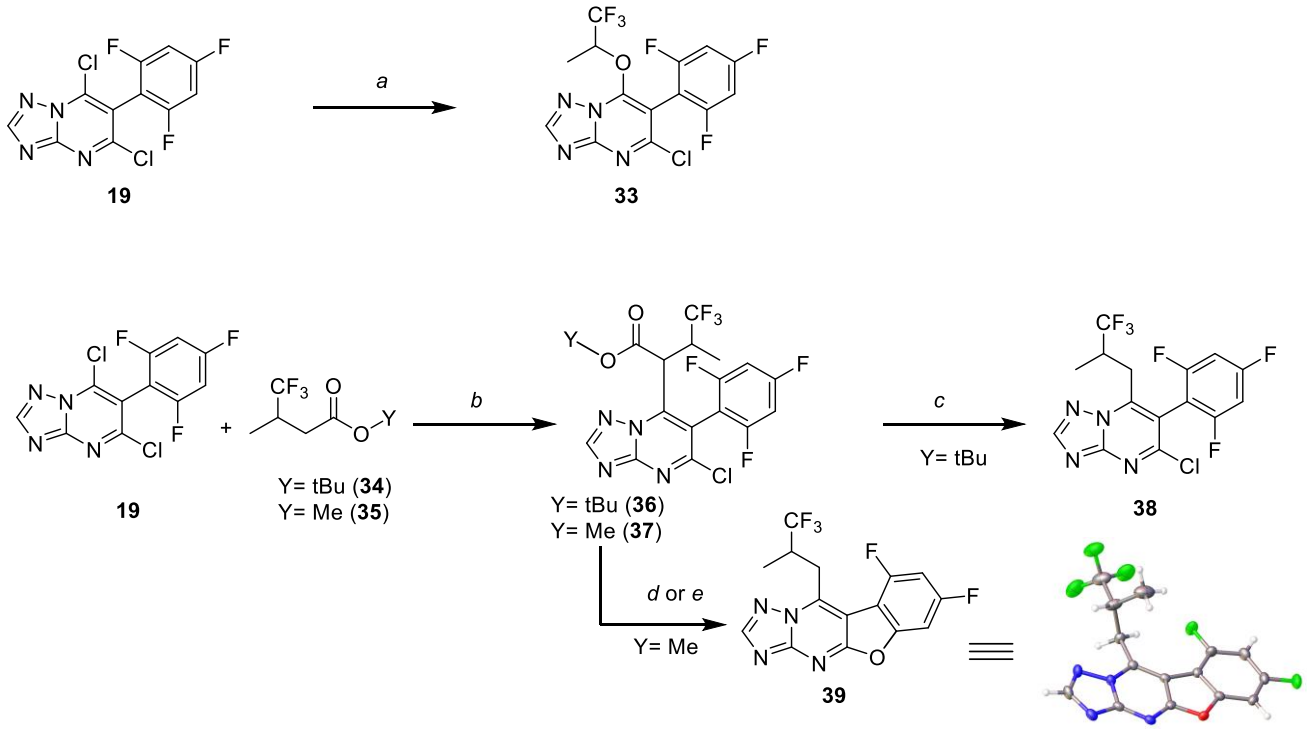

Scheme 3. Synthesis of **33**–**39**. *Reagents and reaction conditions:* (*a*) 1,1,1-trifluoropropan-2-ol, NaH, THF, 60 °C (37%); (*b*) LiHMDS, THF, -78 °C; (*c*) TFA, CH_2Cl_2 (68%) r.t.; (*d*) LiCl, DMSO, 140 °C, 3h (46%); (*e*) LiOH, Water/Methanol r.t. 16h.

Starting from dichloride **19**, which was previously described,[29] compound **33** was synthesized from substitution of the 7-chloro with 1,1,1-trifluoropropan-2-ol in the presence of NaH at 60 °C, resulting in 37% yield. LCMS analysis suggested that substitution of the *para*-fluoro of the phenyl ring formed as well, though the byproduct was not fully characterized. Initial attempts at the synthesis of final compound **38** was to synthesize and add ester **35** to **19**

using LiHMDS in THF at -78 ℃ and follow this by an *in situ* decarboxylation of intermediate **36** using lithium hydroxide in a water/methanol mixture to yield **38**. This method was adapted from a procedure[41] that was used to generate the same type of alkyl linkage to a TPD scaffold; however, it did not yield the desired compound. This led to the isolation of intermediate **35** to attempt decarboxylation at different conditions varying pH and temperature to find that there were no reactions occurring. Subjecting **36** to Krapcho decaboxylation[42] conditions found that compound **39** was formed exclusively as confirmed by X-ray crystallography. It was later confirmed that **39** was also made from the previously mentioned conditions (*i.e.*, Scheme 3). One possibility that was speculated is that the presence of trace amounts of water could lead to the undesired byproduct and another synthesis had to be designed that used anhydrous conditions and an intermediate that could be cleaved under milder conditions. Desired compound **38** was ultimately made using a similar approach instead attaching *tert*-butyl ester **34** to **19** in THF, in the presence of LiHMDS at -78 ℃ to afford intermediate **37** followed by decarboxylation by using TFA in CH_2Cl_2 at room temperature.

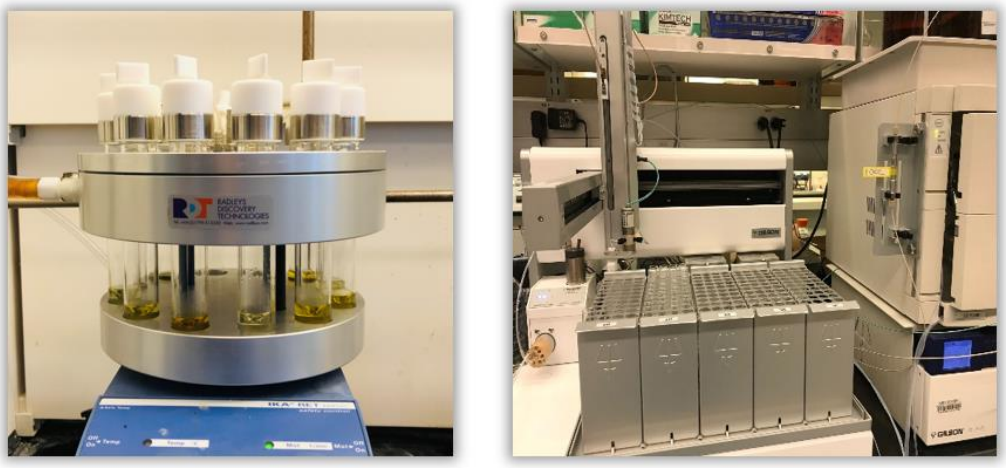

Figure 8. Pictures of the Parallel synthesis set-up (left) and the preparative reverse phase preparative HPLC.

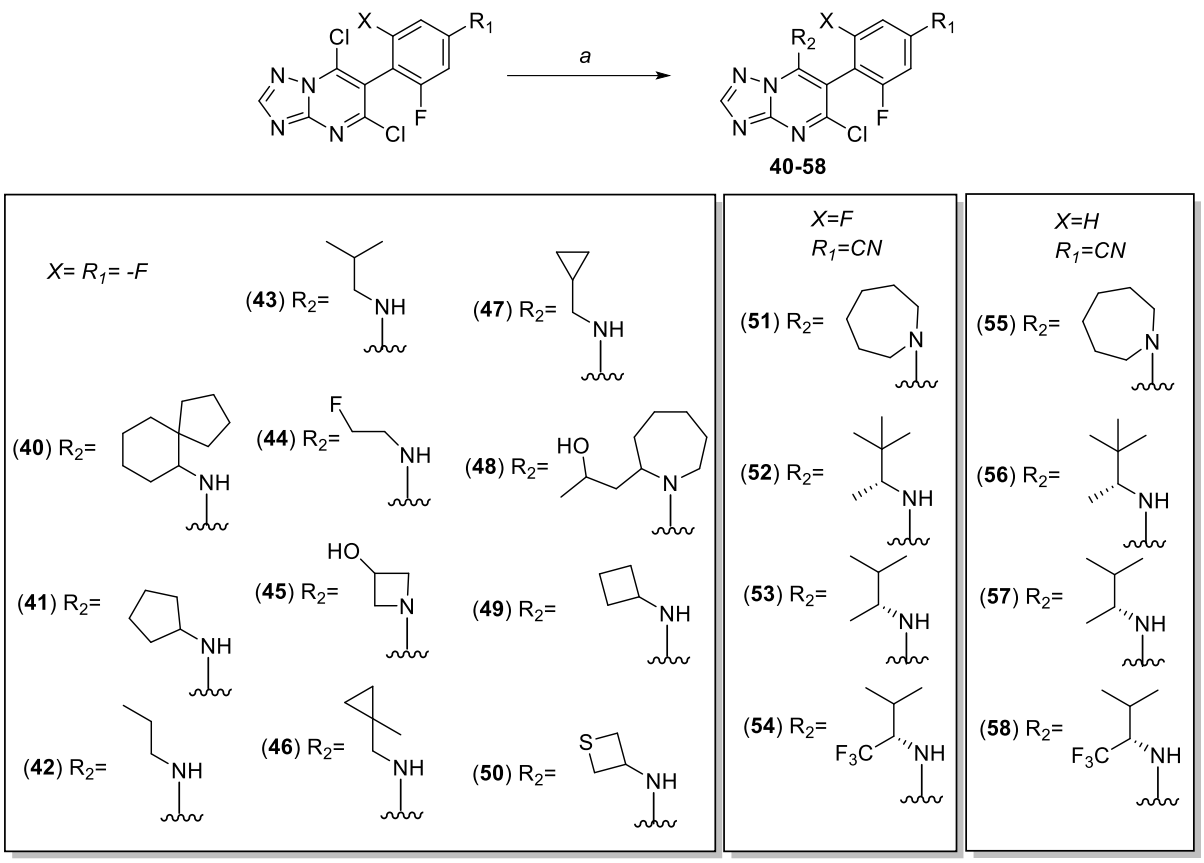

Scheme 4. Synthesis of compounds **40**–**58.** *Reagents and reaction conditions:* (*a*) Amine, DIPEA, r.t. (5-95%), 1-16h

Compounds **40**–**58** with varying amine substituents at R_2 were synthesized in one step by reacting the appropriate TPD dichloride and amines. Nucleophilicities of the amines that afforded compounds **40**–**48** allowed the reactions to be conducted in parallel followed by an automated reverse phase preparative HPLC purification (Figure 8). Compound series **51**–**58** were synthesized in a similar manner to produce compounds in generally good to excellent yields (5–95%) with the sole exception of compounds **54**, and **58** which were only obtained in amounts that provide a partial characterization.

Results and Discussion

All test compounds were evaluated by collaborators at the University of Pennsylvania in a previously described cell-based assay of MT-stabilization,[30] in which compound-dependent changes in tubulin polymerization and total tubulin levels were determined after 4 h of incubation of QBI293 cells with 1 and 10 μM compound via quantification of acetylated α-tubulin and total tubulin in cell lysates by ELISA. Previous evaluations of the MT-stabilizing activity of selected examples of TPDs in this assay revealed that the nature of the substituent in the *para* position of the fluorinated phenyl can elicit one of two distinct cellular responses. The first is characterized by a linear concentration-dependent increase of markers of stable MTs (*i.e.*, acetylated- and detyrosinated-α-tubulin) with no effect on total tubulin levels, which is typically observed in compounds fluorinated in the *para* position (*e.g.*, **7**); and the other by a proteasome-dependent degradation of tubulin that is often accompanied by a bell-shaped concentration-response relationship that may not always manifest at typical assay concentrations, with such compounds typified by those bearing the dimethylaminopropanoxy side-chain (*e.g.*, **6**). To facilitate the presentation and discussion of the SAR results, we will refer here to these two distinct cellular responses as “Class I” and “Class II”, respectively, and TPDs **5** and **6** are used as comparators and defining examples of these classes. The results are shown in the tables below where the SAR examines the affects changes in the substituents in (A) the *para*-position of the phenyl ring at C6 and (B) the fragment linked at the C7 position of the TPD scaffold, which are designated R_1 and R_2 respectively.

Table 1. Activities (AcTub, α-Tub) at 1 μM and 10 μM, and Class of TPD compounds with varying R_1. All compounds were tested against a vehicle-treated control. [a]AcTub is measured as fold-increase in acetylated alpha-tubulin versus the control. [b]α-Tub is the total level of α-tubulin. [c]Two distinct TPD phenotypes are observed: Class I and Class II. Class I compounds are characterized by a linear dose response in the AcTub assay with the concentrations tested and by maintained levels of α-Tub in active doses. Class II compounds are characterized by a decrease in total levels of α-Tub. Class II compounds are classified as compounds that lead to α-Tub reduction by at least 20% at any concentration tested. NS=Not significant. [*]Compounds were previously synthesized by other members of the lab.

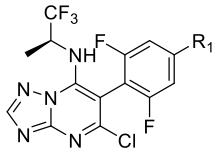

Compound	R_1	AcTub[a] at 1 μm	AcTub[a] at 10 μm	α-Tub[b] at 1 μm	α-Tub[b] at 10 μm	Class[c]
7	-F	2.78 ± 0.17	5.04 ± 0.45	1.18 ± 0.09	1.22 ± 0.18	I
6	$-O(CH_2)_3N(CH_3)_2$	13.2 ± 1.8	1.92 ± 0.14	0.74 ± 0.05	0.40 ± 0.01	II
24	-Me	1.62 ± 0.18	2.73 ± 0.18	0.99 ± 0.09	0.78 ± 0.07	II
25	-Cl	1.88 ± 0.03	4.20 ±0.17	0.93 ± 0.02	0.81 ± 0.06	I
26	$-NO_2$	3.24 ± 0.36	6.65 ± 0.45	0.96 ± 0.01	0.94 ± 0.05	I
22	-CN	1.90 ± 0.06	3.56 ± 0.31	0.94 ± 0.02	0.95 ± 0.05	I
32	$-NH_2$	NS	NS	NS	NS	NA
59*	-H	2.20 ± 0.13	5.28 ± 0.54	1.06 ± 0.14	1.02 ± 0.04	I
60*	-OH	1.22 ± 0.73	4.11 ± 0.76	0.84 ± 0.07	0.57 ± 0.02	II
61*	-OMe	3.16 ± 0.29	2.07 ± 0.07	0.72 ± 0.09	0.51 ± 0.05	II
62*	$-CF_3$	1.09 ± 0.04	1.39 ± 0.11	1.06 ± 0.02	1.02 ± 0.03	I
29	$-S(CH_2)_3N(CH_3)_2$	3.90 ± 0.66	1.49 ± 0.48	0.83 ± 0.05	0.73 ± 0.59	II
30	$-S(O)(CH_2)_3N(CH_3)_2$	NS	NS	NS	NS	NA
31	$-S(O)_2(CH_2)_3N(CH_3)_2$	NS	NS	NS	NS	NA

Table 2. Activities (AcTub, α-Tub) at 1 μm and 10 μm, and Class of TPD compounds with varying R_2. All compounds were tested against a control vehicle. [a]AcTub is measured as fold-increase in acetylated alpha-tubulin versus the control. [b]α-Tub is the total level of α-tubulin. [c]Two distinct TPD phenotypes are observed: Class I and Class II. Class I compounds are characterized by a linear dose response in the AcTub assay with the concentrations tested and by maintained levels of α-Tub in active doses. Class II compounds are characterized by a decrease in total levels of α-Tub. Class II compounds are classified as compounds that lead to α-Tub reduction by at least 20% at any concentration tested. NS=Not significant.*Compounds were previously synthesized by other members of the lab.

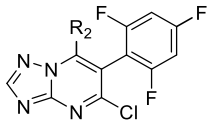

Compound	R_2	AcTub[a] at 1 μm	AcTub[a] at 10 μm	α-Tub[b] at 1 μm	α-Tub[b] at 10 μm	Class
49		0.97 ± 0.15	1.75 ± 0.03	0.94 ± 0.01	0.95 ± 0.02	I
41	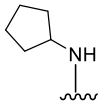	2.03 ± 0.04	4.83 ± 0.04	1.07 ± 0.05	0.99 ± 0.05	I
63*	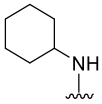	1.13 ± 0.11	3.51 ± 0.19	1.07 ± 0.05	0.99 ± 0.05	I
64*		1.14 ± 0.37	2.74 ± 0.23	1.12 ± 0.31	1.18 ± 0.10	I
65*		2.21 ± 0.36	5.84 ± 1.38	1.23 ± 0.05	1.20 ± 0.22	I
66*	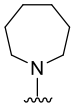	4.16 ± 0.97	6.87 ± 0.04	0.99 ± 0.03	0.99 ± 0.04	I
67*	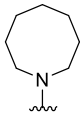	3.70 ± 0.32	7.16 ± 0.11	0.99 ± 0.03	0.99 ± 0.04	I
42	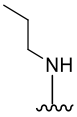	NS	NS	NS	NS	NA
43	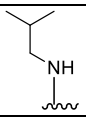	NS	NS	NS	NS	NA
68*	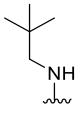	2.04 ± 0.11	4.79 ± 0.74	1.03 ± 0.07	1.06 ± 0.08	I

Table 2. Activities (AcTub, α-Tub) at 1 μm and 10 μm, and Class of TPD compounds with varying R_2. All compounds were tested against a control vehicle. [a]AcTub is measured as fold-increase in acetylated alpha-tubulin versus the control. [b]α-Tub is the total level of α-tubulin. [c]Two distinct TPD phenotypes are observed: Class I and Class II. Class I compounds are characterized by a linear dose response in the AcTub assay with the concentrations tested and by maintained levels of α-Tub in active doses. Class II compounds are characterized by a decrease in total levels of α-Tub. Class II compounds are classified as compounds that lead to α-Tub reduction by at least 20% at any concentration tested. NS=Not significant.*Compounds were previously synthesized by other members of the lab. Continued.

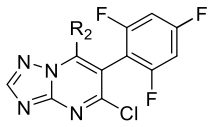

Compound	R_2	AcTub[a] at 1 μm	AcTub[a] at 10 μm	α-Tub[b] at 1 μm	α-Tub[b] at 10 μm	Class
46	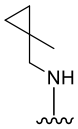	2.68	5.06	1.04	0.97	II
47	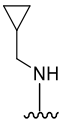	1.37	3.21	1.12	1.02	I
69*	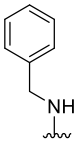	NS	NS	NS	NS	NA
70*	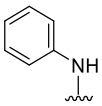	NS	NS	NS	NS	NA
71*	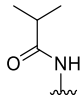	NS	NS	NS	NS	NA
72*		NS	NS	NS	NS	NA
45	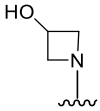	NS	NS	NS	NS	NA
50	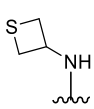	1.29	4.60	1.12	1.02	I
44	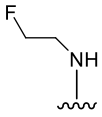	NS	NS	NS	NS	NA

Table 2. Activities (AcTub, α-Tub) at 1 μm and 10 μm, and Class of TPD compounds with varying R_2. All compounds were tested against a control vehicle. [a]AcTub is measured as fold-increase in acetylated alpha-tubulin versus the control. [b]α-Tub is the total level of α-tubulin. [c]Two distinct TPD phenotypes are observed: Class I and Class II. Class I compounds are characterized by a linear dose response in the AcTub assay with the concentrations tested and by maintained levels of α-Tub in active doses. Class II compounds are characterized by a decrease in total levels of α-Tub. Class II compounds are classified as compounds that lead to α-Tub reduction by at least 20% at any concentration tested. NS=Not significant. *Compounds were previously synthesized by other members of the lab. Continued.

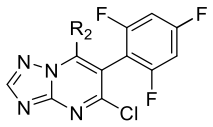

Compound	R_2	AcTub[a] at 1 μm	AcTub[a] at 10 μm	α-Tub[b] at 1 μm	α-Tub[b] at 10 μm	Class
40	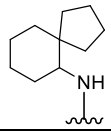	NS	NS	NS	NS	NA
48	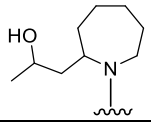	NS	NS	NS	NS	NA
33		NS	NS	NS	NS	NA
38		2.30 ± 0.59	2.29 ± 0.38	1.03 ± 0.07	0.78 ± 0.05	II

Exploration into the structural determinants of Class II compounds started with the design of compounds **60** and **61** that would represent complete truncation of the alkoxide chain in R_2. The compounds—although at different potencies—were found to elicit the Class II phenotype. Compound **25** was then synthesized to assess if a different halo-substituent would be tolerated. It was discovered that a chloro-substituent resulted in decrease in potency compared to that of **7**, and reduction of total α-tubulin levels at 10 μM that is just above the threshold set for Class II classification (20% reduction in α-tubulin). An interesting observation can be made from compounds **24** and **62**. Compound **24** and its isosteric analogue **62** resulted in different biological responses. While compound **24** with the methyl group resulted in a Class II phenotype,

compound **62** with the trifluoromethyl group resulted in Class I. These results in combination with the results of the preliminary SAR—which only evaluated terminal amine substitutions of the alkoxide chain present in **6** and various homologs thereof—suggest that it is not a steric factor that influences phenotype but more the electronic factor of the substituent present at C6. With this observation in mind, additional compounds were designed to further explore the effects of C6 groups with varying electronegativities on the phenotype and potency. Compounds **22** and **21**—containing electron-withdrawing groups (EWGs) cyano- and nitro group, respectively— are both active Class I compounds and therefore best support this finding. Both compounds showed comparable activity to comparator Class I compound **7**.

To further elucidate the SAR at R_1, compound **29** was synthesized, followed by **30** and **31**. Compound **29** bearing the thioether resulted in a Class II compound that is weakly active. Compounds **30** and **31,** the sulfoxide and sulfone derivatives, were synthesized in effort to combine the effects of having an EWG in R_1 and the carbon chain length present in potent Class II compound **6** but resulted in inactive compounds. One possible explanation for this is that the sulfur, sulfoxide, and sulfone add too much steric bulk that renders the compounds unfit for binding to the active site.

Compounds **40–50** were synthesized as a result of an *in-silico* screening iteration. These compounds were found to be mostly inactive at the tested concentrations with a few exceptions. Compounds **40–43** provided information that would be important for the completion of the SAR. There is a trend that activity in R_2 is greatly influenced by both size and lipophilicity of the amine fragment. Endocyclic, tertiary amine compounds **64-67** appear to follow a pattern in which increasing ring size lead to more potent compounds. Compound **67** bearing the 8-membered endocyclic amine, however, resulted in decrease of activity compared to that of the 7-

membered endocyclic amine **66**. This break in pattern suggests that there may be a steric limitation at the C7 site, and that ring sizes greater than 7 lead to increasing steric hindrance. Amines containing larger rings and ring systems **40** and **48** are inactive, which further supports the observation of this steric limitation. Exocyclic, secondary amines **41, 49,** and **63**, however, do not follow a distinct pattern. Compound **41** with the secondary amine bearing the cyclopentane group is more potent than that of **49** bearing the cyclobutane group and **63** bearing the cyclohexane group. Compounds **69** and **70** bearing aryl and benzyl rings were also evaluated and found to be inactive. Since a number of ring-bearing amines, including cyclohexane bearing **63**, are active, these results suggest that having unsaturated fragments lead to loss of activity. This observation is further supported by inactive compounds **71** and **72**, which both contain unsaturated amine fragments at C7.

Compound **50** bearing the 3-thietane was surprisingly active considering compound **49** bearing the cyclobutane show very little activity. This may be due to the fact that the thietane group is sterically larger than the cyclobutane group; this observation follows the trend mentioned in which larger fragments are preferred at C7. A similar conclusion can be made of compound **45** which bears the smaller 3-hydroxyazetidine fragment, which in addition to the smaller ring size has a more polar hydroxy group leading to a less lipophilic, inactive compound. Compounds **42**, **43**, and **68** further show the importance of having a sterically bulky, branched amine fragment. While compounds **42** and **43** were inactive, changing the degree of branching to a more bulky, branched *tert*-butyl fragment in compound **68** yielded a potent compound. Compounds **46** and **47** bearing the cyclopropyl fragments showed good activity with the sterically larger compound **47** showing a more potent response comparable to that of **68**. It

should be noted that compounds bearing the moiety present in **47** have been previously evaluated as a *tert*-butyl isostere.[43]

Compounds **33** and **39** were synthesized to gain a better understanding of the nature of the substituent directly at the R_2, including substituents that do not have nitrogen. Replacing from an amine to an ether linkage in **33** resulted in a compound with no activity in the tested concentrations. This suggests that having an oxygen directly at the R_2 position lead to loss of activity and are therefore not of interest. Alkyl analogue **38** surprisingly resulted in a compound with moderate Class II activity. This result suggests that while various amine fragments at R_2 do not influence the phenotype, non-nitrogen atoms at R_2 can have an impact on the phenotype and can lead to undesirable Class II type cellular response. Results from these compounds further support the observation that an amine substitution at R_2 is necessary to obtain desirable, potent, Class I compounds.

As previously mentioned, compound **22** bearing the cyano- group at R_1 retained the desired phenotype and activity. It is also expected that the predicted lipophilicity of the scaffold would decrease to a more acceptable range, compared to that of comparator compound **7**. Additionally, the preliminary SAR found that compounds bearing at least one fluorine in the *ortho* position of the phenyl ring lead to the most potent compounds. These compounds are also predicted to have a lower lipophilicity than the standard 2,4,6-fluorination pattern found in compound **7**. Thus, based on the new elements of SAR defined as part of this study, second-generation compounds **51**–**58** were designed and synthesized that combine features expected to provide optimal Class I activity while keeping overall physicochemical properties within a desirable range. Results are summarized in Table 3.

Table 3. ClogP and AcTub of compounds with varying R_1, R_2 and phenyl ring substitutions. [a]CLogP values calculated from ChemDraw. [b]All compounds were found to be class I and only levels of AcTub are shown. *Compounds were previously synthesized by other members of the lab.

Compound	CLogP[a]	**AcTub[b]**	Compound	CLogP[a]	**AcTub[b]**
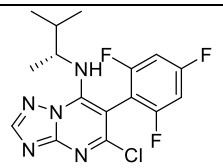 **8***	4.64	2.14 (1 μM) 2.57 (10 μM)	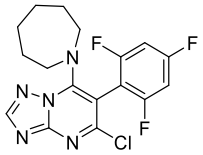 **67***	4.21	4.16 (1 μM) 6.87 (10 μM)
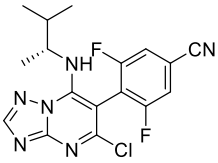 **53**	3.93	2.5 (1 μM) 3.5 (10 μM)	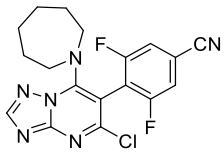 **51**	3.50	6.5 (1 μM) 11.5 (10 μM)
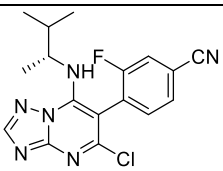 **57**	3.79	4.4 (1 μM) 7.3 (10 μM)	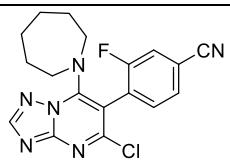 **55**	3.35	In Progress
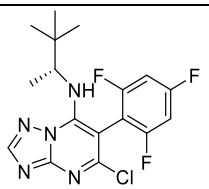 **70***	5.04	5.70 (1 μM) 8.42 (10 μM)	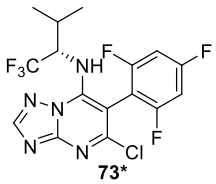 **73***	4.90	3.12 (1 μM) 6.78 (10 μM)
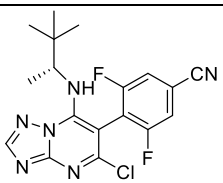 **52**	4.33	In Progress	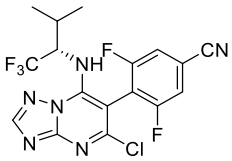 **54**	4.20	In Progress
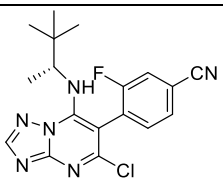 **56**	4.19	4.5 (1 μM) 7.5 (10 μM)	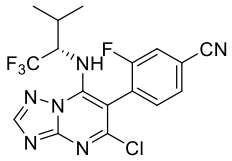 **58**	4.05	In Progress

The calculated values of partition coefficients between *n*-octanol and water (CLogP) of each compound in Table 3 confirm that when the degree of fluorination in the phenyl ring is

decreased and/or replaced with a cyano- group at R_1, the lipophilicity decreases per compound series. As shown in Table 3, compounds with less fluorine counts in the C6 phenyl ring lead to compounds with lower lipophilicity (CLogP). This trend can be seen in all parallel compounds: compounds **55**-**58** bearing the 2-fluoro, 4-cyano phenyl ring have lower CLogP values than that of compounds **51**-**54** bearing the 2,6-difluoro, 4-cyano phenyl group. Compounds **51**-**58** have lower ClogP values than that of compound **8, 70, 67,** and **73** bearing the 2,4,6-trifluoro phenyl ring. There results confirm that the C6 substitution can be altered not only to affect phenotype and improve potency, but also to improve ADME-PK and physicochemical properties.

As expected, these compounds retained Class I phenotype, as well as maintained or improved potency. Perhaps the most interesting result lies with the compounds that were designed to improve upon lead candidate CNDR-51657 (**8**). Compound **53** bearing the 2,6-fluoro-, 4-cyano- phenyl substitution demonstrated comparable potency to that of CNDR-51657; compound **57** bearing the 2-fluoro, 4-cyano phenyl substitution, on the other hand, demonstrated increased potency. These compounds are very informative in designing the next generation of MT-stabilizing TPD compounds.

Conclusion

MT-stabilizing triazolopyrimidines hold promise as candidate therapeutics for Alzheimer's disease and related neurodegenerative tauopathies. In this thesis project, 30 new triazolopyrimidine analogues were designed, synthesized and evaluated with the goal of further elucidating the SAR and ultimately provide guidance on what subset of molecules to prioritize in the search for clinical candidates with optimal activity, ADME-PK and physicochemical properties. The results of the SAR found that, in order to retain a Class I phenotype, a fluorine in R_1 is not strictly required; other groups with electron withdrawing properties are acceptable. Out of various R_2 substitutions and linkages (amine, amide, ether, and alkyl), active compounds contained amine substituents. Of the amine substituents, the most potent were generally aliphatic, branched, relatively bulky and lipophilic amines (Figure 9).

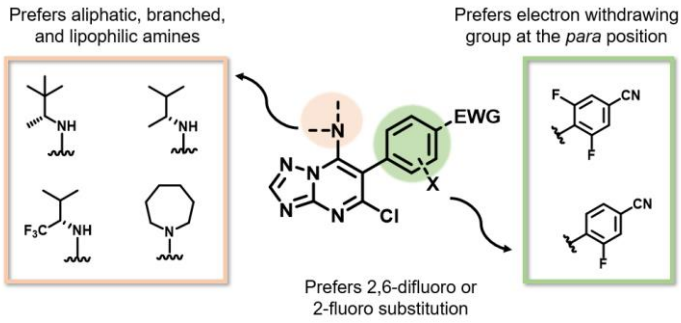

Figure 9. SAR at the C5 prefers aliphatic, branched, and lipophilic amines, with the best results from the amine shown (left). The phenyl substitution at C6 prefers the 2,6-difluoro, or 2-fluoro substitution pattern, with electron withdrawing groups preferred in the *para*-position. It was found that having the preferred fluorination patterns in the phenyl ring along with an EWG such as the cyano- group in the *para*-position could lead to compounds with desirable MT-stabilizing activity and PK profiles.

Findings from the SAR were used to design next generation compounds, taking the following into consideration: the preferred R_2 substituents, the preferred phenyl ring substitutions, and calculated LogP values. Compound designed were found to maintain comparable or higher MT-stabilizing activity than the previously evaluated compounds containing the 2,4,6-trifluorophenyl substitution pattern. The most interesting results from this

screen would be of the compounds that were analogues of the previously developed lead (CNDR-51657), compounds **53** and **57**. Compound **57** containing the 2-fluoro-, 4-cyano- phenyl substitution resulted in a significant increase in potency, *in vitro*, all while having a more desirable lipophilic profile (Figure 10).

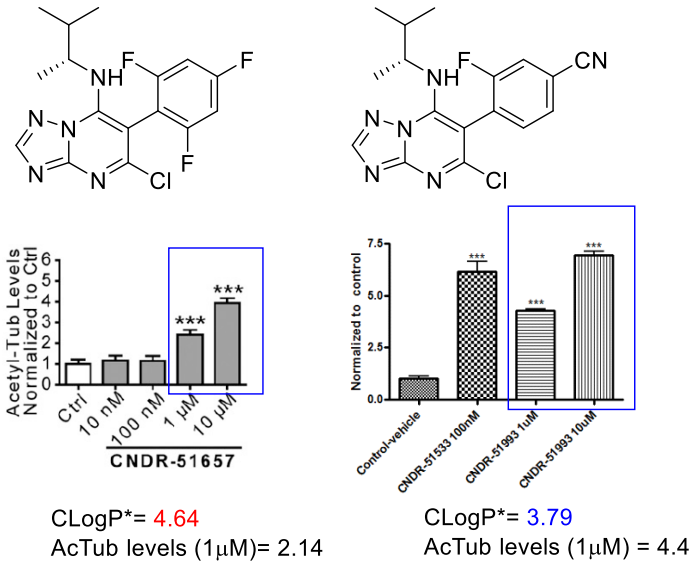

Figure 10. Comparison of lipophilicity (ClogP, obtained from ChemDraw) and AcTub levels (1 μM) of previously developed lead candidate CNDR-51657 and newly developed compound **55**.

In conclusion, the findings from this thesis has led to a greater understanding of the SAR of triazolopyrimidine MT-stabilizing compounds. The SAR elucidation has led to identification of desirable Class I compounds with increased potency and more desirable predicted ADME-PK and physicochemical properties. These novel compounds will ultimately help in the identification of a clinical candidate for treatments of neurodegenerative tauopathies.

This work, in part, is coauthored with Ballatore, Carlo and Brunden, Kurt R. The thesis author was the primary author of this work.

Experimental

Materials and Methods.

All solvents were reagent grade. All reagents were purchased from Aldrich or Acros and used as received. Thin layer chromatography (TLC) was performed with 0.25 mm E. Merck precoated silica gel plates. Silica gel column chromatography was performed with silica gel 60 (particle size 0.040−0.062 mm) supplied by Silicycle and Sorbent Technologies. TLC spots were detected by viewing under a UV light. Melting points (mp) were acquired on a Mel-Temp II (model : 1001) and are uncorrected. Infrared (IR) spectra were recorded on a Bruker, model Alpha spectrometer (part number 1003271/03). Proton (^{1}H) and carbon (^{13}C) NMR spectra were recorded on a 500 MHz Bruker AMX-500 spectrometer or 600 MHz Bruker Avance III spectrometer. Chemical shifts were reported relative to solvents. High-resolution mass spectra were measured using an Agilent 6230 time-of-flight mass spectrometer (TOFMS) with Jet stream electrospray ionisation source (ESI). Single-crystal X-ray structure determinations were performed Bruker MicroStar with an APEX II detector, double-bounce micro-focus optics and a Cu rotating anode source. Analytical reverse-phase (Sunfire C18; 4.6 mm × 50 mm, 5 mL) high-performance liquid chromatography (HPLC) was performed with a Gilson HPLC equipped with UV and mass detector. All samples were analyzed employing a linear gradient from 10% to 90% of CH_3CN in water over 8 min and flow rate of 1 mL/min, and unless otherwise stated, the purity level was >95%. Preparative reverse-phase HPLC purifications were performed on a Gilson instrument employing Waters SunFire preparative C_{18} OBD columns (5 μm 19 mm × 50 mm or 19 mm × 100 mm). Purifications were carried out employing a linear gradient from 10% to 90% of CH_3CN in water for 15 min with a flow rate of 20 mL/min. Unless otherwise stated, all final compounds were found to be >95% pure as determined by HPLC/MS and NMR.

General Procedure A (synthesis of diethylmalonate derivatives):

To a suspension of NaH (60 wt % in mineral oil) (1.00 equiv) in anhydrous 1,4-dioxane (previously degassed with N_2) (1.75 mol/L from aryl bromide derivate) at 60°C under N_2 diethyl malonate (3.00 equiv) was slowly added and the resulting mixture was stirred for 10 min. CuBr (1.20 equiv) and aryl bromide derivate were added and the reaction mixture was heated at reflux overnight. The reaction was then quenched by adding HCl 12N (1.40 equiv) at r.t.. The mixture was filtered, washed with H_2O, and extracted with EtOAc (x3). The combined organic extracts were washed with brine, dried over $MgSO_4$, filtered and concentrated in vacuo. Purification by silica gel column chromatography or by preparative reverse-phase HPLC furnished the desired diethylmalonate derivatives.

General procedure B (synthesis of dichloro-triazolopyrimidine derivatives):

A mixture of diethylmalonate derivate (1.00 equiv), 3-amino-1,2,4-triazole (1.05 equiv) and tributylamine (1.05 equiv) in sealed tube was stirred at 170 °C for 2 h. After cooling at 130 °C, toluene was added (1.00 mol/L from diethylmalonate derivative). Then, the reaction was cooled at 50°C and an aqueous solution of NaOH (50% wt) (160 µL/mmol from diethylmalonate derivate) was added. After that, the mixture was stirred at 0°C for 10 min and filtered. The solid formed was washed with cooled toluene and dried. This disodic derivate (1.00 equiv) and $POCl_3$ (17.80 equiv) were mixed in a sealed tube and heated at 130 °C for 6 h. Then, the reaction was quenched with H_2O and extracted with EtOAc (×2). The combined organic extracts were washed with water (×5), brine, dried over $MgSO_4$, filtered and concentrated in vacuo. The resulting product was directly used in the next reaction without further purification.

General procedure C (addition of the amine):

According to a reported procedure[29], to 5,7-dichloro-6-(2,4,6-trifluorophenyl)-[1,2,4]triazolo[1,5-a]pyrimidine (**19**,1.0 equiv) in DMF (0.1 M) at room temperature was added i-Pr_2NEt (3.0 equiv) or Et_3N (3.0 equiv) if necessary and the appropriate amine (3.0 equiv). The reaction mixture was stirred for 0.5-16 h and diluted with H2O. The organic layer was washed with a 1N solution of hydrochloric acid (2x), the aqueous phase was extracted with EtOAc (3x), and the combined organic layers were washed with brine (2x), dried (MgSO4), filtered, and concentrated. The products were purified by flash chromatography or reverse-phase HPLC.

General procedure D (addition of the side chain):

According to reported procedure,[29] to a suspension of NaH (4.0 equiv) in a 2:1 mixture of DMSO and THF (0.35 M) was added the aminoalcohol (4.0 equiv), and the mixture was heated to 60 °C for 1 h. The resulting solution was treated with a solution of trifluoroarene (1.0 equiv) in a 1:1 mixture DMSO and THF (0.5 M). The reaction mixture was stirred at 60 °C for 3 h and monitored by LCMS. If the starting material remained after 3 h, additional aminoalcohol (4.0 equiv) and NaH (4.0 equiv) were added, sequentially, and the reaction mixture was heated for 16 h. Following complete consumption of the starting material, the reaction mixture was cooled to room temperature and diluted with H_2O and EtOAc. The organic layer was washed with H_2O and brine, and the combined aqueous layers were extracted with EtOAc (x3). The combined organic layers were dried ($MgSO_4$), filtered, and concentrated. The crude products were purified by reverse-phase HPLC.

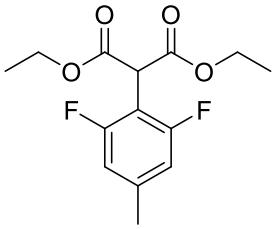

Diethyl 2-(2,6-difluoro-4-methylphenyl)malonate (14):

Following General Procedure A using diethyl malonate (4.18 g, 26.10 mmol) and 2-bromo-1,3-difluoro-5-methylbenzene (1.80 g, 8.69 mmol), silica gel column chromatography (0−8% EtOAc in Hexanes) purification provided the title compound as a colorless oil (2.00 g, 6.99 mmol, 80%).

^{1}H NMR (600 MHz, $CDCl_3$) δ 6.67 (m, 2H), 4.83 (d, *J* = 3.0 Hz, 1H), 4.20 – 4.14 (m, 4H), 2.27 (d, *J* = 3.2 Hz, 3H), 1.22 – 1.17 (m, 6H) ppm.

^{13}C NMR (150 MHz, $CDCl_3$) δ 166.89 , 160.75 (dd, *J* = 249.1, 8.1 Hz), 141.32 , 115.89 – 110.83 (m), 107.42 (t, *J* = 18.8 Hz), 61.99 , 46.98 , 21.23 (d, *J* = 1.9 Hz), 13.87 ppm.

IR: 3000, 1678, 1106, 1017 cm^{-1}

LCMS: $[M + H]^+$ 287

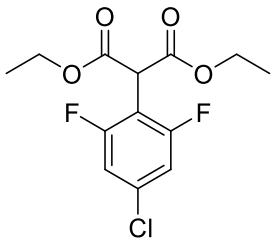

Diethyl 2-(4-chloro-2,6-difluorophenyl)malonate (15):

Following General Procedure A using diethyl malonate (6.39 g, 39.57 mmol) and 2-bromo-5-chloro-1,3-difluorobenzene (3.00 g, 13.19 mmol). Purification via silica gel column chromatography (0−8% EtOAc in Hexanes) provided the title compound as a colorless oil (1.42 g, 4.63 mmol, 35%).

^{1}H NMR (600 MHz, $CDCl_3$) δ 6.96 (m, 2H), 4.89 (s, 1H), 4.24 (q, *J* = 7.2 Hz, 4H), 1.28 – 1.24 (m, 6H) ppm.

^{13}C NMR (150 MHz, $CDCl_3$) δ 166.40 , 161.05 (dd, *J* = 252.7, 8.8 Hz), 135.40 (t, *J* = 13.4 Hz), 113.18 – 112.42 (m), 109.85 (t, *J* = 18.8 Hz), 62.41 , 47.07 , 14.01 ppm.

IR: 2838, 1678, 1642, 1249 cm^{-1}

LCMS: $[M + H]^+$ 308

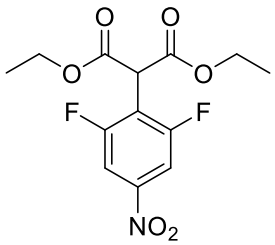

Diethyl 2-(2,6-difluoro-4-nitrophenyl)malonate (16):

A mixture of 1,2,3-trifluoro-5-nitrobenzene (1.00 g, 5.65 mmol, 1 equiv), potassium carbonate (1.56 g, 11.29 mmol, 2.00 equiv), and diethyl malonate (0.914 g, 5.71 mmol, 1.01 equiv), in anh. DMF (6.37 ml) under N_2 was stirred at 65°C until starting material was consumed as indicated by TLC. The reaction mixture was cooled to r.t. and washed with 1 N HCl (50 mL) and extracted with EtOAc (3x). The organic layers were combined, washed with satd. aq. NaCl, dried over anh. Na_2SO_4, filtered, and concentrated in vacuo. Purification by silica gel column chromatography (up to 30% EtOAc in hexanes) provided the title compound as a white solid (1.53 g, 4.85 mmol, 86%)

^{1}H NMR (600 MHz, $CDCl_3$) δ 7.84 (d, *J* = 7.2 Hz, 2H), 5.00 (s, 1H), 4.27 (q, *J* = 7.1 Hz, 4H), 1.28 (t, *J* = 7.2 Hz, 6H) ppm.

^{13}C NMR (150 MHz, $CDCl_3$) δ 165.55 , 160.93 (dd, *J* = 254.8, 7.7 Hz), 148.60 (t, *J* = 11.2 Hz), 118.05 (t, *J* = 18.7 Hz), 108.15 – 107.61 (m), 62.84 , 47.49 , 14.04 ppm.

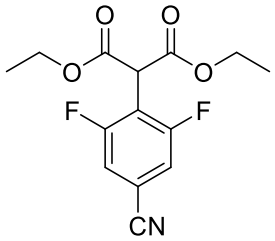

Diethyl 2-(4-cyano-2,6-difluorophenyl)malonate (17):

A mixture of 3,4,5-trifluorobenzonitrile (1.00 g, 6.37 mmol, 1 equiv), potassium carbonate (1.76 g, 12.7 mmol, 2.00 equiv), and diethyl malonate (1.03 g, 6.43 mmol, 1.01 equiv) in anh. DMF (6.37 ml) under N_2 was stirred at 65 °C until starting material was consumed as indicated by TLC. The reaction mixture was cooled to r.t., washed with 1M HCl (50 mL), and extracted with EtOAc (3x). The organic layers were combined, washed with satd. aq. NaCl, dried over anh. Na_2SO_4, filtered, and concentrated in vacuo. Purification by silica gel column chromatography (up to 30% EtOAc in hexanes) provided the title compound as a white solid (1.40 g, 4.69 mmol, 73%)

^{1}H NMR (600 MHz, $CDCl_3$) δ 7.30 (d, *J* = 7.0 Hz, 2H), 5.01 (s, 1H), 4.31 – 4.24 (m, 4H), 1.29 (t, *J* = 7.4 Hz, 6H) ppm.

^{13}C NMR (150 MHz, $CDCl_3$) δ 165.54 , 161.02 (dd, *J* = 254.0, 7.8 Hz), 116.78 (t, *J* = 18.5 Hz), 116.20 (t, *J* = 3.4 Hz), 115.94 – 115.48 (m), 113.88 (t, *J* = 12.4 Hz), 62.60 , 47.24 , 13.87 ppm.

IR: 2856, 2178, 1695 cm^{-1}

LCMS: $[M + H]^+$ 298

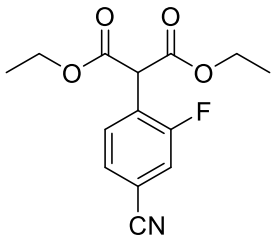

Diethyl 2-(4-cyano-2-fluorophenyl)malonate (18):

To a dry flask, under nitrogen, was added 3,4-difluorobenzonitrile (4.00 g, 28.8 mmol, 1 equiv), potassium carbonate (7.95 g, 57.5 mmol, 2.00 equiv), diethyl malonate (4.66 g, 29.1 mmol, 1.01 equiv), and anhydrous DMF (24 ml) and was heated at 65°C until starting material was consumed based on TLC. The reaction mixture was cooled to r.t. and added to a separatory funnel containing 50 ml of 1 N HCl. The mixture extracted with EtOAc (x3), and the combined organic layers were washed with water and satd. aq. NaCl. The organic layer was dried over anh. Na_2SO_4, filtered, and concentrated in vacuo. Purification by silica gel column chromatography (up to 30% EtOAc in hexanes) Provided the title compound as a colorless oil (6.73 g, 24.1 mmol, 84%)

^{1}H NMR (600 MHz, $CDCl_3$) δ 7.64 (t, *J* = 7.6 Hz, 1H), 7.47 (dd, *J* = 8.0, 1.6 Hz, 1H), 7.38 (dd, *J* = 9.2, 1.6 Hz, 1H), 4.98 (s, 1H), 4.28 – 4.18 (m, 4H), 1.26 (t, *J* = 7.2 Hz, 6H).

^{13}C NMR (150 MHz, $CDCl_3$) δ 166.55 , 160.04 (d, *J* = 252.0 Hz), 131.98 (d, *J* = 3.5 Hz), 128.26 (d, *J* = 4.0 Hz), 126.21 (d, *J* = 14.4 Hz), 119.23 (d, *J* = 26.0 Hz), 117.28 (d, *J* = 2.9 Hz), 113.71 (d, *J* = 9.8 Hz), 62.55 , 50.44 (d, *J* = 2.9 Hz), 14.00 .

LCMS: $[M + H]^+$ 280

IR: 2984, 2236, 1733, 1219 cm^{-1}

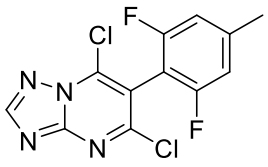

5,7-Dichloro-6-(2,6-difluoro-4-methylphenyl)-[1,2,4]triazolo[1,5-a]pyrimidine (19):

Following General Procedure B using diethyl 2-(2,6-difluoro-4-methylphenyl)malonate (800 mg, 2.79 mmol) and 3-amino-1,2,4-triazole (247 mg, 2.93 mmol). Then using the intermediate sodium 6-(2,6-difluoro-4-methylphenyl)-[1,2,4]triazolo[1,5-a]pyrimidine-5,7-bis(olate) (500 mg, 1.55 mmol) and $POCl_3$ (4.24 g, 27.6 mmol) provide the title compound as a brown solid (334 mg, 1.06 mmol, 68%).

^{1}H NMR (600 MHz, $CDCl_3$) δ 8.59 (s, 1H), 6.92 (d, *J* = 8.5 Hz, 2H), 2.46 (s, 3H) ppm.

^{13}C NMR (150 MHz, $CDCl_3$) δ 159.92 (dd, *J* = 251.1, 6.6 Hz), 157.07 , 157.01 , 153.85 , 144.81 (d, *J* = 19.7 Hz), 141.44 , 113.44 , 112.74 (dd, *J* = 20.7, 3.5 Hz), 106.01 (d, *J* = 39.9 Hz), 21.88 (d, *J* = 1.9 Hz) ppm.

IR: 3071, 1606, 1571, 1356 cm^{-1}

LCMS: $[M + H]^+$ 317

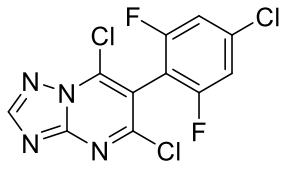

5,7-Dichloro-6-(4-chloro-2,6-difluorophenyl)-[1,2,4]triazolo[1,5-a]pyrimidine (20):

Following General Procedure B using diethyl 2-(4-chloro-2,6-difluorophenyl)malonate (1.2 g, 3.9 mmol)and 3-amino-1,2,4-triazole (350 mg, 4.10 mmol). Then using the intermediate sodium 6-(4-chloro-2,6-difluorophenyl)-[1,2,4]triazolo[1,5-a]pyrimidine-5,7-bis(olate) (1.00 g, 2.92 mmol) and $POCl_3$ (7.97 g, 52.0 mmol) provide the title compound as a brown solid (710 mg, 2.12 mmol, 73%).

^{1}H NMR (600 MHz, $CDCl_3$) δ 8.62 (s, 1H), 7.18 (d, *J* = 7.1 Hz, 2H) ppm.

^{13}C NMR (150 MHz, $CDCl_3$) δ 161.29 – 159.09 (m), 157.36 , 156.45 , 153.95 , 141.55 , 138.63 (t, *J* = 13.0 Hz), 113.78 – 113.35 (m), 112.29 , 108.08 (t, *J* = 20.0 Hz) ppm.

IR: 3106, 1642, 1427, 1391, 1071 cm^{-1}

LCMS: $[M + H]^+$ 336

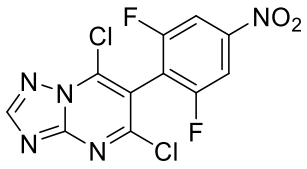

5,7-Dichloro-6-(2,6-difluoro-4-nitrophenyl)-[1,2,4]triazolo[1,5-a]pyrimidine (21):

Following General Procedure B using diethyl 2-(2,6-difluoro-4-nitrophenyl)malonate (500 mg, 1.58 mmol)and 3-amino-1,2,4-triazole (139 mg, 1.65 mmol). Then using the intermediate sodium 6-(2,6-difluoro-4-nitrophenyl)-[1,2,4]triazolo[1,5-a]pyrimidine-5,7-bis(olate) (150 mg, 0.425 mmol) and $POCl_3$ (1.16 g, 7.56 mmol) provide the title compound as a brown solid (100 mg, 0.289 mmol, 68%).

^{1}H NMR (600 MHz, $CDCl_3$) δ 8.64 (s, 1H), 8.04 (d, *J* = 6.8 Hz, 2H) ppm.

^{13}C NMR (150 MHz, $CDCl_3$) δ 160.22 (dd), 157.70 , 156.90 , 155.39 , 154.08 , 150.51 (d, *J* = 10.5 Hz), 141.48 , 116.12 – 115.19 (m), 111.63 , 108.69 – 108.36 (m) ppm.

IR: 2916, 2848, 1698, 1601, 1532 cm^{-1}

LCMS: $[M + H]^+$ 347

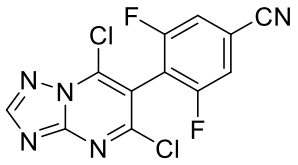

4-(5,7-Dichloro-[1,2,4]triazolo[1,5-a]pyrimidin-6-yl)-3,5-difluorobenzonitrile (22):

Following General Procedure B using diethyl 2-(4-cyano-2,6-difluorophenyl)malonate (500 mg, 1.68 mmol)and 3-amino-1,2,4-triazole (148 mg, 1.77 mmol). Intermediate sodium 6-(4-cyano-2,6-difluorophenyl)-[1,2,4]triazolo[1,5-a]pyrimidine-5,7-bis(olate) (400 mg, 1.20 mmol) and $POCl_3$ (3.28 g, 21.4 mmol) provide the title compound as a brown solid (210 mg, 1.20 mmol, 53%).

^{1}H NMR (600 MHz, $CDCl_3$) δ 8.65 (s, 1H), 7.47 (d, *J* = 6.2 Hz, 2H) ppm.

^{13}C NMR (150 MHz, $CDCl_3$) δ 161.21 (d, *J* = 6.4 Hz), 159.51 (d, *J* = 6.2 Hz), 157.66 , 155.57 , 116.85 , 116.62 – 116.30 (m), 115.86 (t, *J* = 3.5 Hz), 114.64 (t, *J* = 19.6 Hz) ppm.

IR: 3087, 2195, 1571, 1338, 1195 cm^{-1}

LCMS: $[M + H]^+$ 327

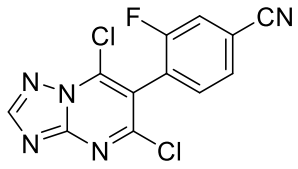

4-(5,7-Dichloro-[1,2,4]triazolo[1,5-a]pyrimidin-6-yl)-3-fluorobenzonitrile (23):

Following General Procedure B using diethyl 2-(4-cyano-2,6-difluorophenyl)malonate (500 mg, 1.68 mmol)and 3-amino-1,2,4-triazole (148 mg, 1.77 mmol). Then using the intermediate sodium 6-(4-cyano-2-fluorophenyl)-[1,2,4]triazolo[1,5-a]pyrimidine-5,7-bis(olate) (3.00g, 9.52 mmol) and $POCl_3$ (26.0 g, 169 mmol to provide the title compound as a brown solid (1.97 g, 9.52 mmol, 67%).

^{1}H NMR (600 MHz, $CDCl_3$) δ 8.61 (s, 1H), 7.68 (dd, *J* = 7.9, 1.5 Hz, 1H), 7.61 (dd, *J* = 8.6, 1.5 Hz, 1H), 7.54 (t, *J* = 7.4 Hz, 1H) ppm.

^{13}C NMR (150 MHz, $CDCl_3$) δ 160.47 , 158.79 , 157.48 , 155.52 , 153.79 , 140.73 , 133.32 , 128.86 (d, *J* = 4.6 Hz), 124.68 (d, *J* = 15.7 Hz), 120.42 (d, *J* = 24.9 Hz), 116.76 (d, *J* = 2.9 Hz), 116.69 , 116.36 (d, *J* = 9.3 Hz) ppm.

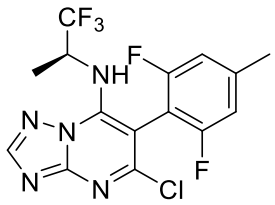

(*S*)-5-Chloro-6-(2,6-difluoro-4-methylphenyl)-N-(1,1,1-trifluoropropan-2-yl)-[1,2,4]triazolo[1,5-a]pyrimidin-7-amine (24):

Following general procedure C using 5,7-dichloro-6-(2,6-difluoro-4-methylphenyl)-[1,2,4]triazolo[1,5-a]pyrimidine (0.050 g, 0.16 mmol), *(S)*-1,1,1-trifluoropropan-2-amine (38 mg, 0.33 mmol). (28 mg, 0.071 mmol, 65%)

^{1}H NMR (600 MHz, $CDCl_3$) δ 8.36 (s, 1H), 6.91 (d, *J* = 9.0 Hz, 2H), 6.00 – 5.94 (m, 1H), 4.73 (s, 1H), 2.45 (s, 3H), 1.39 (d, *J* = 7.0 Hz, 3H) ppm.

^{13}C NMR (150 MHz, $CDCl_3$) δ 160.75 (dd, *J* = 251.4, 7.0 Hz), 160.50 (dd, *J* = 249.9, 7.3 Hz), 158.07 , 155.34 , 154.11 , 145.83 , 144.86 (t, *J* = 10.2 Hz), 124.59 (q, *J* = 282.1 Hz), 112.93 (ddd, *J* = 65.8, 21.3, 4.0 Hz), 105.67 (t, *J* = 20.9 Hz), 92.50 , 22.72 – 20.28 (m), 15.19 ppm.

HRMS (ES+) calculated for $C_{15}H_{12}N_5ClF_5$ $[M + H]^+$ 392.0696, found 392.0693

IR: 1618, 1559, 1143, 840 cm^{-1}

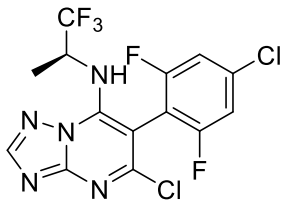

(*S*)-5-Chloro-6-(4-chloro-2,6-difluorophenyl)-*N*-(1,1,1-trifluoropropan-2-yl)-[1,2,4]triazolo[1,5-a]pyrimidin-7-amine (25):

Following general procedure C using 5,7-dichloro-6-(4-chloro-2,6-difluorophenyl)-[1,2,4]triazolo[1,5-a]pyrimidine (50 mg, 0.15 mmol) and (*S*)-1,1,1-trifluoropropan-2-amine (35 mg, 0.31 mmol). Purification by silica gel column chromatography (0−40% EtOAc in Hexanes) provided the title compound as a white powder (35 mg, 0.085 mmol, 57%).

^{1}H NMR (600 MHz, $CDCl_3$) δ 8.40 (s, 1H), 7.18 (m, 2H), 5.93 – 5.88 (m, 1H), 4.75 (s, 1H), 1.43 (d, *J* = 6.9 Hz, 3H) ppm.

^{13}C NMR (150 MHz, $CDCl_3$) δ 160.84 (ddd, *J* = 253.4, 48.9, 9.1 Hz), 157.67 , 155.57 , 154.21 , 145.82 , 138.62 (t, *J* = 14.0 Hz), 124.53 (q, *J* = 280.5 Hz), 114.47 – 113.17 (m), 51.00 (q, *J* = 32.9 Hz), 15.27 ppm.

HRMS (ES+) calculated for $C_{14}H_9Cl_2F_5N_5$ $[M + H]^+$ 412.0150, found 412.0146

IR: 3000, 1571, 1517, 1142 cm^{-1}

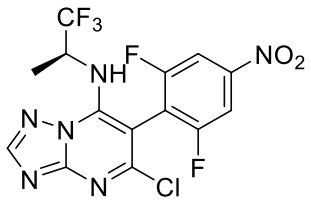

(*S*)-5-Chloro-6-(2,6-difluoro-4-nitrophenyl)-N-(1,1,1-trifluoropropan-2-yl)-[1,2,4]triazolo[1,5-a]pyrimidin-7-amine (26):

Following general procedure C 5,7-dichloro-6-(2,6-difluoro-4-nitrophenyl)-[1,2,4]triazolo[1,5-a]pyrimidine (70 mg, 0.20 mmol) and (*S*)-1,1,1-trifluoropropan-2-amine (48 mg, 0.42 mmol). Purification by silica gel column chromatography (0−40% EtOAc in Hexanes) provided the title compound as a white powder (75 mg, 0.18 mmol, 88%).

^{1}H NMR (600 MHz, $CDCl_3$) δ 8.41 (s, 1H), 8.00 (m, 2H), 5.99 (d, *J* = 10.6 Hz, 1H), 4.78 (s, 1H), 1.46 (d, *J* = 6.8 Hz, 3H) ppm.

^{13}C NMR (150 MHz, $CDCl_3$) δ 161.15 (dd, *J* = 257.2, 5.8 Hz), 160.73 (dd, *J* = 255.3, 6.1 Hz), 156.78 , 155.75 , 154.37 , 150.43 (t, *J* = 10.5 Hz), 145.80 , 124.47 (q, *J* = 282.2 Hz), 116.00 (t, *J* = 20.5 Hz), 108.53 (ddd, *J* = 61.2, 27.3, 4.0 Hz), 90.62 , 51.38 (q, *J* = 32.1 Hz), 15.20 (d, *J* = 1.5 Hz) ppm.

HRMS (ES+) calculated for $C_{14}H_9ClF_5N_6O_2$ $[M + H]^+$ 423.0390, found 423.0384

IR: 1618, 1530, 1489, 1143, 1043 cm^{-1}

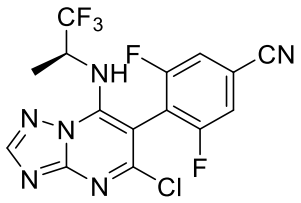

(*S*)-4-(5-Chloro-7-((1,1,1-trifluoropropan-2-yl)amino)-[1,2,4]triazolo[1,5-a]pyrimidin-6-yl)-3,5-difluorobenzonitrile (27):

Following general procedure C using 4-(5,7-dichloro-[1,2,4]triazolo[1,5-a]pyrimidin-6-yl)-3,5-difluorobenzonitrile (30 mg, 0.094 mmol) and (*S*)-1,1,1-trifluoropropan-2-amine (22 mg, 0.190 mmol). Purification by silica gel column chromatography (0−40% EtOAc in Hexanes) provided the title compound as a white powder (20 mg, 0.050 mmol, 54%).

^{1}H NMR (600 MHz, $CDCl_3$) δ 8.41 (s, 1H), 7.44 (t, *J* = 7.1 Hz, 2H), 6.00 (d, *J* = 10.7 Hz, 1H), 4.77 (s, 1H), 1.45 (d, *J* = 6.9 Hz, 3H) ppm.

^{13}C NMR (150 MHz, $CDCl_3$) δ 161.28 (dd, *J* = 256.4, 5.9 Hz), 160.87 (dd, *J* = 254.7, 6.0 Hz), 156.84 , 155.68 , 154.32 , 124.46 (q, *J* = 282.1 Hz), 116.58 (t, *J* = 11.8 Hz), 116.47 (ddd, *J* = 67.6, 25.4, 4.1 Hz), 115.79 (d, *J* = 3.5 Hz), 114.93 (t, *J* = 20.0 Hz), 90.61 , 51.27 (q, *J* = 32.2 Hz), 29.83 , 15.14 ppm.

HRMS (ES+) calculated for $C_{15}H_9N_6ClF_5$ $[M + H]^+$ 403.0492, found 403.0486.

IR: 2923, 2239, 1617, 1556, 1141 cm^{-1}

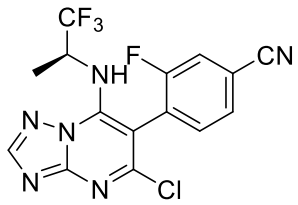

(*S*)-4-(5-Chloro-7-((1,1,1-trifluoropropan-2-yl)amino)-[1,2,4]triazolo[1,5-a]pyrimidin-6-yl)-3-fluorobenzonitrile (28):

Following general procedure C using) 4-(5,7-dichloro-[1,2,4]triazolo[1,5-a]pyrimidin-6-yl)-3-fluorobenzonitrile (40 mg, 0.13 mmol) and *(S)*-1,1,1-trifluoropropan-2-amine (31 mg, 0.27 mmol). Purification by reversed phase HPLC provided the title compound as a white powder (31 mg, 0.070 mmol, 54%).

Mixture of atropoisomers

^{1}H NMR (600 MHz, $CDCl_3$) δ 8.41 (s, 1H), 7.68 (ddd, *J* = 7.8, 3.8, 1.5 Hz, 1H), 7.61 (ddd, *J* = 8.4, 3.8, 1.5 Hz, 1H), 7.57 (t, *J* = 7.4 Hz, 1H), 7.50 (t, *J* = 7.3 Hz, 1H), 5.94 (d, *J* = 11.0 Hz, 1H), 5.57 (d, *J* = 10.8 Hz, 1H), 4.97 (s, 1H), 4.50 (s, 1H), 1.40 (d, *J* = 6.9 Hz, 3H) ppm.

^{13}C NMR (150 MHz, $CDCl_3$) δ 161.29 (d, *J* = 52.0 Hz), 159.61 (d, *J* = 50.4 Hz), 156.65 (d, *J* = 24.9 Hz), 155.72 (d, *J* = 11.0 Hz), 154.20 (d, *J* = 57.5 Hz), 145.65 (d, *J* = 62.8 Hz), 135.00 (d, *J* = 2.0 Hz), 133.84 (d, *J* = 2.2 Hz), 129.21 (d, *J* = 4.2 Hz), 124.97 (dd, *J* = 16.2, 13.1 Hz), 124.67 (qd, *J* = 282.3, 34.7 Hz), 120.62 (dd, *J* = 74.3, 25.2 Hz), 116.67 (d, *J* = 2.8 Hz), 116.33 (dd, *J* = 9.3, 5.2 Hz), 97.66 , 96.61 , 51.26 (dq, *J* = 37.9, 31.8 Hz), 15.13 , 14.99 ppm.

HRMS (ES+) calculated for $C_{15}H_{10}ClF_4N_6$ $[M + H]^+$ 385.0586, found 385.0589.

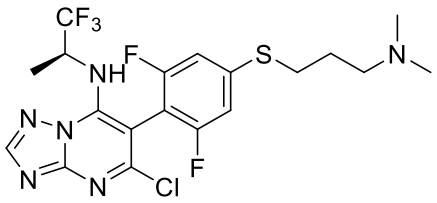

(*S*)-5-Chloro-6-(4-((3-(dimethylamino)propyl)thio)-2,6-difluorophenyl)-N-(1,1,1-trifluoropropan-2-yl)-[1,2,4]triazolo[1,5-a]pyrimidin-7-amine (29):

Following General Procedure D using 3-mercapto-*N*,*N*-dimethylpropan-1-aminium chloride (449 mg, 2.88 mmol) (*S*)-5-chloro-6-(2,4,6-trifluorophenyl)-*N*-(1,1,1-trifluoropropan-2-yl)-[1,2,4]triazolo[1,5-a]pyrimidin-7-amine (285 mg, 0.720 mmol) and NaH (60 wt % in mineral oil) (230 mg, 5.76 mmol) the reaction was stirred at 60 °C overnight. Purification by preparative reverse-phase HPLC provided the title compound as a crystalline solid (290 mg, 0.586 mmol, 81%).

^{1}H NMR (600 MHz, $CDCl_3$) δ 8.34 (s, 1H), 6.97 (d, *J* = 8.3 Hz, 2H), 4.89 (s, 1H), 3.06 (t, *J* = 7.2 Hz, 2H), 2.58 (s, 1H), 2.47 (t, *J* = 7.0 Hz, 2H), 2.26 (s, 7H), 1.89 (q, *J* = 7.1 Hz, 2H), 1.40 (d, *J* = 6.9 Hz, 3H) ppm.

^{13}C NMR (150 MHz, $CDCl_3$) δ 160.99 (dd, J = 252.9, 6.7 Hz), 160.68 (dd, J = 251.8, 6.9 Hz), 157.96 , 155.29 , 154.20 , 146.06 , 145.40 (t, J = 10.3 Hz), 124.62 (q, J = 282.2 Hz), 110.50 – 109.10 (m), 104.75 (t, J = 20.7 Hz), 92.35 , 57.96 , 50.90 (q, J = 31.9 Hz), 45.27 , 41.01 , 29.98 , 26.33 , 15.09 ppm.

HRMS (ES+) calculated for $C_{19}H_{21}ClF_5N_6S$ $[M + H]^+$ 495.1152, found 495.1148

IR: 2820, 1579, 1535, 1356 cm^{-1}

To a solution of (*S*)-5-chloro-6-(4-((3-(dimethylamino)propyl)thio)-2,6-difluorophenyl)-*N*-(1,1,1-trifluoropropan-2-yl)-[1,2,4]triazolo[1,5-a]pyrimidin-7-amine (50 mg, 0.100 mmol) in CH_2Cl_2 (1.00 ml) was added MCPBA (70%, 25 mg, 0.100 mmol). After 2 hr, the reaction mixture was concentrated in vacuo and purified by reversed phase HPLC (**30, 17 mg, 32%)** and **(31, 27 mg, 52%).**

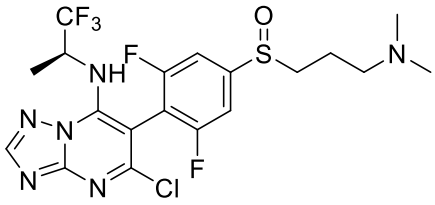

5-Chloro-6-(4-((3-(dimethylamino)propyl)sulfinyl)-2,6-difluorophenyl)-*N*-((*S*)-1,1,1-trifluoropropan-2-yl)-[1,2,4]triazolo[1,5-a]pyrimidin-7-amine (30):

^{1}H NMR (600 MHz, $CDCl_3$) δ 8.37 (s, 1H), 8.19 (s, 1H), 7.02 (d, *J* = 8.0 Hz, 2H), 6.69 (s, 1H), 5.41 (s, 1H), 3.76 – 3.67 (m, 2H), 3.40 (d, *J* = 10.2 Hz, 7H), 3.22 – 3.15 (m, 2H), 2.44 – 2.37 (m, 2H), 1.43 (d, *J* = 6.9 Hz, 3H) ppm.

^{13}C NMR (150 MHz, $CDCl_3$) δ 166.95 , 161.56 (dd, *J* = 253.3, 6.8 Hz), 160.98 (dd, *J* = 252.6, 6.6 Hz), 157.65 , 155.36 , 154.85 , 146.84 , 125.91 (q), 112.00 – 110.04 (m), 107.56 – 105.57 (m), 92.69 , 68.14 , 57.73 (d, *J* = 11.8 Hz), 51.16 (q, *J* = 31.8 Hz), 29.62 (d, *J* = 2.0 Hz), 22.63 (d, *J* = 1.7 Hz), 14.82 ppm.

HRMS (ES+) calculated for $C_{19}H_{21}ClF_5N_6OS$ $[M + H]^+$ 511.1101, found 511.1100.

IR: 3053, 1589, 1535, 1178 cm^{-1}

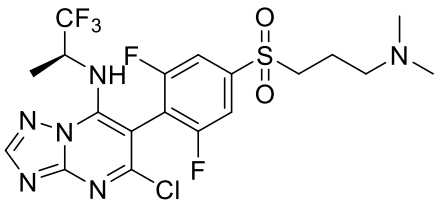

(*S*)-5-Chloro-6-(4-((3-(dimethylamino)propyl)sulfonyl)-2,6-difluorophenyl)-*N*-(1,1,1-trifluoropropan-2-yl)-[1,2,4]triazolo[1,5-a]pyrimidin-7-amine (31):

Mixture of atropoisomers

^{1}H NMR (600 MHz, $CDCl_3$) δ 8.38 (s, 1H), 8.11 (s, 1H), 7.50 (dd, *J* = 16.6, 7.4 Hz, 1H), 7.17 (d, *J* = 7.0 Hz, 0.5H), 5.88 (s, 0.5H), 5.59 (s, 0.5H), 3.86 – 3.78 (m, 1H), 3.77 – 3.70 (m, 0.5H), 3.69 – 3.62 (m, 1H), 3.36 (dd, *J* = 25.9, 3.6 Hz, 6H), 3.40 – 3.27 (m, 0.5H), 2.99 – 2.90 (m, 1H), 2.51 – 2.40 (m, 1H), 2.36 – 2.26 (m, 1H), 1.42 (dd, *J* = 6.9, 2.9 Hz, 3H) ppm.

^{13}C NMR (150 MHz, $CDCl_3$) δ 167.52 , 163.09 – 161.10 (m), 161.44 (ddd, *J* = 256.9, 21.4, 4.9 Hz), 157.00 , 156.86 , 155.45 – 155.33 (m), 155.12 , 129.28 – 119.96 (m), 112.17 (td, *J* = 20.5, 4.6 Hz), 109.28 – 107.40 (m), 92.88 , 92.30 , 67.84 , 67.54 , 58.59 , 58.51 , 57.34 , 56.93 , 52.19 , 51.77 , 51.29 (td, *J* = 31.8, 17.1 Hz), 15.61 , 15.10 , 14.68 , 14.46 (d, *J* = 1.7 Hz) ppm.

HRMS (ES+) calculated for $C_{19}H_{21}ClF_5N_6O_2S$ $[M + H]^+$ 527.1050, found 527.1045.

IR: 3285, 1589, 1535, 1142 cm^{-1}

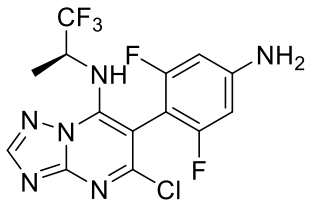

(*S*)-6-(4-amino-2,6-difluorophenyl)-5-chloro-*N*-(1,1,1-trifluoropropan-2-yl)-[1,2,4]triazolo[1,5-a]pyrimidin-7-amine (32):

To a solution of (*S*)-5-chloro-6-(2,6-difluoro-4-nitrophenyl)-*N*-(1,1,1-trifluoropropan-2-yl)-[1,2,4]triazolo[1,5-a]pyrimidin-7-amine (25 mg, 0.059 mmol) in 0.100 ml of 1:1 water : methanol was added iron powder (17 mg 0.30 mmol) and ammonium chloride (13 mg, 0.24 mmol). The mixture was stirred at 80 °C for 2h and then filtered and rinsed with hot methanol. The filtrate was evaporated in vacuo, and the resulting mixture was purified by HPLC to afford the product as a white solid (16 mg, 0.041 mmol, 69%).

^{1}H NMR (600 MHz, $CDCl_3$) δ 8.37 (s, 1H), 6.37 (t, *J* = 9.8 Hz, 2H), 5.93 (s, 1H), 4.86 (s, 1H), 4.28 (s, 2H), 2.17 (s, 1H), 1.41 (m, 3H) ppm.

^{13}C NMR (150 MHz, $CDCl_3$) δ 161.86 (ddd, *J* = 246.8, 32.1, 8.7 Hz), 158.99 , 155.32 , 154.09 , 151.02 (t, *J* = 13.9 Hz), 146.15 , 130.31 , 128.98 , 124.72 (q, *J* = 281.8 Hz), 98.19 (ddd, *J* = 63.6, 25.1, 3.2 Hz), 97.13 (t, *J* = 21.1 Hz), 92.99 , 50.71 (q, *J* = 32.4 Hz), 31.08 , 15.35 ppm.

HRMS (ES+) calculated for $C_{14}H_{11}ClF_5N_6$ $[M + H]^+$ 393.0648, found 393.0646

IR: 3341, 1651, 1614, 1587, 1346 cm^{-1}

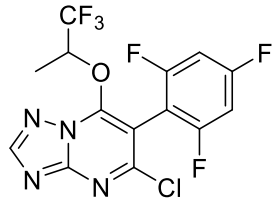

5-Chloro-6-(2,4,6-trifluorophenyl)-7-((1,1,1-trifluoropropan-2-yl)oxy)-[1,2,4]triazolo[1,5-a]pyrimidine (33):

Sodium Hydride (15 mg, 0.376 mmol) suspended in THF (3.0 ml) was added 1,1,1-trifluoropropan-2-ol (34.1 μL, 0.376 mmol) and stirred at reflux for 2 hrs. After 2 hrs at reflux 5,7-dichloro-6-(2,4,6-trifluorophenyl)-[1,2,4]triazolo[1,5-a]pyrimidine (100 mg, 0.313 mmol) was added at rt. The reaction mixture was stirred for 20 min before the reaction was quenched with water (5 ml), and extracted with EtOAc (3x). The mixture was dried in vacuo and purified by silica gel column chromatograph (46 mg, 37%).

^{1}H NMR (600 MHz, $CDCl_3$) δ 8.51 (s, 1H), 6.89 – 6.77 (m, 2H), 6.21 – 6.12 (m, 1H), 1.63 (d, *J* = 6.6 Hz, 4H) ppm.

^{13}C NMR (150 MHz, $CDCl_3$) δ 164.14 (dt, *J* = 253.1, 15.2 Hz), 161.12 (ddd, J = 252.7, 15.1, 8.7 Hz), 160.86 (ddd, J = 251.3, 15.0, 8.6 Hz), 158.43 , 156.71 , 155.59 (d, J = 43.8 Hz), 151.92 , 123.23 (q, J = 281.1 Hz), 104.10 (td, J = 20.5, 4.9 Hz), 102.40 – 98.42 (m), 76.02 (q, J = 32.7, 31.8 Hz), 14.07 , 12.80 ppm.

HRMS (ES+) calculated for $C_{14}H_8N_4ClF_6O$ $[M + H]^+$ 397.0285, found 397.0279.

IR: 2925, 2854, 1606, 1517, 1493 cm^{-1}

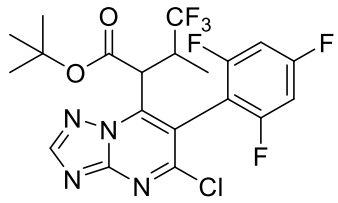

tert-butyl 2-(5-chloro-6-(2,4,6-trifluorophenyl)-[1,2,4]triazolo[1,5-a]pyrimidin-7-yl)-4,4,4-trifluoro-3-methylbutanoate (36) :

To a solution of HMDS (54 mg, 70 µL, 0.33 mmol) in THF (3 mL) at -78°C was added butyllithium (21 mg, 0.18 mL, 0.33 mmol) and the mixture was stirred at 0°C for 30 min. Then tert-butyl 4,4,4-trifluoro-3-methylbutanoate (66 mg, 0.31 mmol) was added dropwise at -78°C and was stirred for 1h.after stirring a solution of 5,7-dichloro-6-(2,4,6-trifluorophenyl)-[1,2,4]triazolo[1,5-a]pyrimidine (66 mg, 0.21 mmol, 1 equiv.) in THF (500 µL) was added at -78°C and stirred for 2.5 h and was quenched with 1M HCl. The aqueous layer was then extracted EtOAc (2x) and washed with sat. Aq. NaCl, dried and concentrated in vacuo. The crude residue was purified by silica gel chromatography using Hexanes/EtOAc (5-20%) to afford the product (26 mg, 25 %) as a white solid.

^{1}H NMR (600 MHz, $CDCl_3$) mixture of diastereomers δ 8.56 (s, 0.6H), 8.55 (s, 0.4H), 6.91 (m, 2H), 4.14 – 4.04 (m, 0.4H), 3.95 – 3.83 (m, 1.2H), 3.72 (d, 0.4H), 1.38 (d, *J* = 6.7 Hz, 1.3H), 1.27 (s, 3.5H), 1.25 (s, 6.8H), 0.80 (d, *J* = 7.0 Hz, 2H).

IR: 2922, 2852, 1598, 1736, 1493, 1460, 1441, 1371, 1271, 1252, 1201, 1182, 1173 cm^{-1}

HRMS (ES+) calculated for $C_{20}H_{18}ClF_6N_4O_2$ $[M + H]^+$ 495.1017, found 495.1010

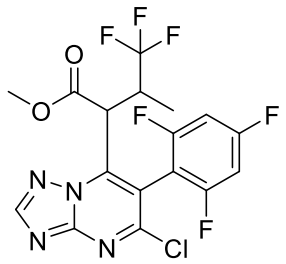

methyl 2-(5-chloro-6-(2,4,6-trifluorophenyl)-[1,2,4]triazolo[1,5-a]pyrimidin-7-yl)-4,4,4-trifluoro-3-methylbutanoate (37):

To a solution of HMDS (101 mg, 130 µL, 0.627 mmol) in THF (0.632 mL) at -78°C was added butyllithium (40 mg, 0.369 mL, 0.627 mmol) and the mixture was stirred at 0°C for 1h. Then methyl 4,4,4-trifluoro-3-methylbutanoate (117 mg, 0.690 mmol) was added dropwise at -78°C and was stirred for 1h.then a solution of 5,7-dichloro-6-(2,4,6-trifluorophenyl)-[1,2,4]triazolo[1,5-a]pyrimidine (200 mg, 0.627 mmol,) in THF (500 µL) was added at -78°C and stirred for 2.5 h and was quenched with 1M HCl. The aqueous layer was then extracted EtOAc (2x) and washed with sat. Aq. NaCl, dried and concentrated in vacuo. The crude residue was purified by silica gel chromatography using Hexanes/EtOAc (5-20%) to afford the product (200 mg, 70 %) as a white solid.

Mixture of stereoisomers

^{1}H NMR (600 MHz, $CDCl_3$) δ 8.53 (d, *J* = 6.6 Hz, 1H), 6.94 – 6.86 (m, 2H), 4.04 (d, *J* = 7.4 Hz, 1H), 3.92 – 3.85 (m, 1H), 3.62 (d, *J* = 10.4 Hz, 3H), 1.38 (d, *J* = 6.6 Hz, 1H), 0.80 (d, *J* = 7.4 Hz, 2H).

HRMS (ES+) calculated for $C_{17}H_{12}ClF_6N_4O_2[M + H]^+$ 453.0547, found 453.0542

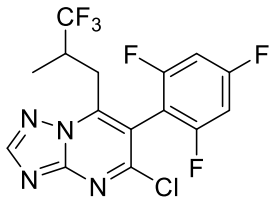

5-chloro-7-(3,3,3-trifluoro-2-methylpropyl)-6-(2,4,6-trifluorophenyl)-[1,2,4]triazolo[1,5-a]pyrimidine (38) :

To a solution of tert-butyl 2-(5-chloro-6-(2,4,6-trifluorophenyl)-[1,2,4]triazolo[1,5-a]pyrimidin-7-yl)-4,4,4-trifluoro-3-methylbutanoate (26 mg, 53 µmol, 1 equiv.) in DCM (2 mL) at rt was added TFA (0.18 g, 0.12 mL, 1.6 mmol, 30 equiv.). The mixture was then stirred 16h at rt. It was then diluted with DCM and quenched with a saturated $NaHCO_3$ solution. The aqueous layer was then extracted with DCM and the combined organic layers were dried and concentrated inv vacuo. The crude residue was purified by HPLC to afford the product as a white solid (14 mg, 68 %).

^{1}H NMR (600 MHz, $CDCl_3$) δ 8.56 (s, 1H), 6.92 (m, 2H), 3.34 (dd, *J* = 13.9, 6.2 Hz, 1H), 3.22 (m, 1H), 3.05 (dd, *J* = 13.9, 8.4 Hz, 1H), 1.03 (d, *J* = 7.0 Hz, 4H).

^{13}C NMR (150 MHz, $CDCl_3$) δ 164.45 (dt, 256.7, 18.1 Hz), 160.86 (ddd, 252.2, 15.1, 9.1 Hz), 160.61 (ddd, 250.7, 15.1, 9.06 Hz), 157.19, 157.02, 154.03, 148.77, 127.25 (q, 280.11 Hz) 112.29, 106.39 (td, 21.14, 4.9 Hz), 101.48 (dtd, *J* = 30.1, 25.9, 4.1 Hz), 35.37 (q, *J* = 27.6 Hz), 30.65, 12.88.

IR: 1639, 1609, 1599, 1516, 1495, 1442, 1278, 1265, 1207, 1186, 1172, 1146, 1122 cm^{-1}

HRMS (ES+) calculated for $C_{15}H_9ClF_6N_4$ $[M + H]^+$ 395.0493, found 395.0486

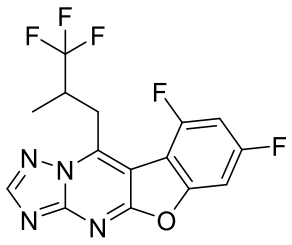

7,9-difluoro-10-(3,3,3-trifluoro-2-methylpropyl)benzofuro[2,3-d][1,2,4]triazolo[1,5-a]pyrimidine (39):

methyl 2-(5-chloro-6-(2,4,6-trifluorophenyl)-[1,2,4]triazolo[1,5-a]pyrimidin-7-yl)-4,4,4-trifluoro-3-methylbutanoate (20 mg, 0.044 mmol), LiCl (2.0 mg, 0.044 mmol), and DMSO (200 µL) were stirred at 130 ℃ for 2h. purification by reverse phase HPLC provided the title compound as a white solid (12 mg, 76%). Product confirmed by XRD.

^{1}H NMR (600 MHz, Chloroform-*d*) δ 8.55 (s, 1H), 8.01 (s, 1H), 7.01 (ddd, *J* = 11.0, 9.3, 2.2 Hz, 1H), 6.86 – 6.79 (m, 3H), 4.11 – 4.05 (m, 2H), 3.88 – 3.78 (m, 2H), 3.30 (p, *J* = 7.3 Hz, 1H), 3.20 (dd, *J* = 13.9, 5.8 Hz, 2H), 3.05 (dt, *J* = 15.1, 7.6 Hz, 2H), 2.79 (dd, *J* = 14.0, 8.7 Hz, 2H), 1.20 (d, *J* = 7.0 Hz, 3H), 1.02 (d, *J* = 7.0 Hz, 3H).

^{13}C NMR (150 MHz, Chloroform-*d*) δ 165.15 – 164.48 (m), 163.01 (d, *J* = 15.1 Hz), 162.26 – 160.00 (m), 158.41 , 156.38 , 152.47 , 150.91 , 145.88 , 143.80 , 127.47 (dd, *J* = 279.5, 28.1 Hz), 108.69 , 106.96 , 106.21 – 104.64 (m), 102.08 – 100.00 (m), 97.85 (dd, *J* = 27.4, 4.6 Hz), 36.01 (q, *J* = 28.3, 27.6 Hz), 30.84 , 29.86 .

HRMS (ES+) calculated for $C_{15}H_9F_5N_4O[M + H]^+$ 357.0769, found 357.0768

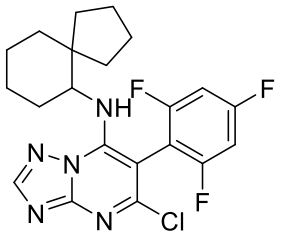

5-Chloro-*N*-(spiro[4.5]decan-6-yl)-6-(2,4,6-trifluorophenyl)-[1,2,4]triazolo[1,5-a]pyrimidin-7-amine (40):

Following general procedure C using 5,7-dichloro-6-(2,4,6-trifluorophenyl)-[1,2,4]triazolo[1,5-a]pyrimidine (40 mg, 0.13 mmol) and spiro[4.5]decan-6-amine (40 mg, 0.26 mmol). Purification by reversed phase HPLC provided the title compound as a white powder (25 mg, 0.057 mmol, 46%).

^{1}H NMR (600 MHz, $CDCl_3$) δ 8.32 (d, *J* = 1.4 Hz, 1H), 6.89 – 6.84 (m, 2H), 6.61 (s, 1H), 2.98 (s, 1H), 1.66 – 1.58 (m, 2H), 1.57 – 1.43 (m, 9H), 1.41 – 1.36 (m, 2H), 1.35 – 1.29 (m, 2H), 1.28 – 1.17 (m, 2H) ppm.

^{13}C NMR (150 MHz, $CDCl_3$) δ 164.07 (dt, *J* = 253.9, 15.1 Hz), 161.71 (ddd, *J* = 250.6, 14.8, 8.5 Hz), 161.40 (ddd, *J* = 250.6, 14.9, 8.3 Hz), 158.18 , 154.96 , 153.57 , 146.11 , 107.72 (td, *J* = 21.2, 5.2 Hz), 100.93 (qd, *J* = 25.8, 4.1 Hz), 88.46 , 58.78 , 46.55 , 37.81 , 30.84 , 25.88 , 25.32 , 22.03 ppm.

HRMS (ES+) calculated for $C_{21}H_{22}ClF_3N_5$ $[M + H]^+$ 436.1510, found 436.1507.

IR: 2936, 1636, 1571, 1494, 1426 cm^{-1}

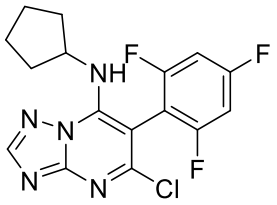

5-Chloro-*N*-cyclopentyl-6-(2,4,6-trifluorophenyl)-[1,2,4]triazolo[1,5-a]pyrimidin-7-amine (41):

Following general procedure C using 5,7-dichloro-6-(2,4,6-trifluorophenyl)-[1,2,4]triazolo[1,5-a]pyrimidine (30 mg, 0.094 mmol) and cyclopentanamine (17 mg, 0.20 mmol). Purification by silica gel column chromatography (0−40% EtOAc in Hexanes) provided the title compound as a white powder (27 mg, 0.073 mmol, 78%).

^{1}H NMR (600 MHz, $CDCl_3$) δ 8.31 (s, 1H), 6.84 (m, 2H), 6.42 (d, *J* = 8.3 Hz, 1H), 3.63 (s, 1H), 1.82 – 1.59 (m, 4H), 1.62 – 1.38 (m, 4H) ppm.

^{13}C NMR (150 MHz, $CDCl_3$) δ 163.99 (dt, *J* = 253.7, 15.2 Hz), 161.66 (ddd, *J* = 250.5, 15.0, 8.4 Hz), 158.19 , 154.93, 145.81 , 101.30 – 100.53 (m), 88.98 , 55.11 , 34.64 , 23.92 ppm.

HRMS (ES+) calculated for $C_{16}H_{14}N_5ClF_3$ $[M + H]^+$ 368.0884, found 368.0881.

IR: 3195, 2838, 1678, 1553 cm^{-1}

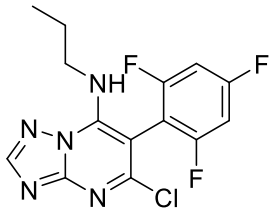

5-Chloro-*N*-propyl-6-(2,4,6-trifluorophenyl)-[1,2,4]triazolo[1,5-a]pyrimidin-7-amine (42):

Following general procedure C using 5,7-dichloro-6-(2,4,6-trifluorophenyl)-[1,2,4]triazolo[1,5-a]pyrimidine (30 mg, 0.094 mmol) and propan-1-amine (12 mg, 0.20 mmol). Purification by silica gel column chromatography (0−40% EtOAc in Hexanes) provided the title compound as a white powder (20 mg, 0.059 mmol, 62%).

^{1}H NMR (600 MHz, $CDCl_3$) δ 8.33 (s, 1H), 6.84 (m, 2H), 6.48 (t, *J* = 5.9 Hz, 1H), 2.98 (q, *J* = 6.7 Hz, 2H), 1.57 (h, *J* = 7.3 Hz, 2H), 0.85 (t, *J* = 7.4 Hz, 4H) ppm.

^{13}C NMR (150 MHz, $CDCl_3$) δ 163.93 (dt, *J* = 253.7, 15.4 Hz), 161.77 (ddd, *J* = 250.6, 14.9, 8.5 Hz), 158.16 , 155.07 , 153.65 , 146.36 , 107.18 (td, *J* = 20.8, 4.9 Hz)., 101.12 – 100.62 (m), 88.91 , 45.31 , 29.83 , 23.33 , 11.04 ppm.

HRMS (ES+) calculated for $C_{14}H_{12}N_5ClF_3$ $[M + H]^+$ 342.0728, found 342.0725.

IR: 2923, 1573, 1439, 1122 cm^{-1}

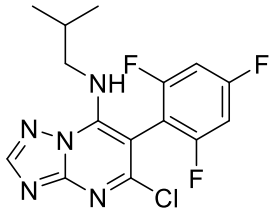

5-Chloro-*N*-*iso*butyl-6-(2,4,6-trifluorophenyl)-[1,2,4]triazolo[1,5-a]pyrimidin-7-amine (43):

Following general procedure C using 5,7-dichloro-6-(2,4,6-trifluorophenyl)-[1,2,4]triazolo[1,5-a]pyrimidine (30 mg, 0.094 mmol) and 2-methylpropan-1-amine (14 mg, 0.20 mmol). Purification by silica gel column chromatography (0−40% EtOAc in Hexanes) provided the title compound as a white powder (27 mg, 0.076 mmol, 81%).

^{1}H NMR (600 MHz, $CDCl_3$) δ 8.33 (s, 1H), 6.88 – 6.81 (m, 2H), 6.56 (t, J = 6.1 Hz, 1H), 2.84 (t, J = 6.5 Hz, 2H), 1.77 – 1.70 (m, 1H), 0.84 (d, J = 6.7 Hz, 8H) ppm.

^{13}C NMR (150 MHz, $CDCl_3$) δ 164.05 (dt, *J* = 253.8, 15.1 Hz), 161.72 (ddd, *J* = 250.4, 14.9, 8.4 Hz), 158.13 , 155.05 , 153.63 , 146.42 , 107.31 (td, *J* = 20.8, 4.8 Hz), 102.26 – 98.14 (m), 88.95 , 50.83 , 29.05 , 19.79 ppm.

HRMS (ES+) calculated for $C_{15}H_{14}N_5ClF_3$ $[M + H]^+$ 356.0884, found 356.0887.

IR: 2961, 2924, 1637, 1577, 1434 cm^{-1}

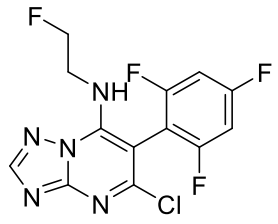

5-Chloro-*N*-(2-fluoroethyl)-6-(2,4,6-trifluorophenyl)-[1,2,4]triazolo[1,5-a]pyrimidin-7-amine (44):

Following general procedure C using 5,7-dichloro-6-(2,4,6-trifluorophenyl)-[1,2,4]triazolo[1,5-a]pyrimidine (30 mg, 0.094 mmol) and fluoroethan-1-amine (6.5 mg, 0.10 mmol), and DIPEA (36 mg, 0.28 mmol). Purification by reversed phase HPLC provided the title compound as a white powder (20 mg, 0.058 mmol, 62%).

^{1}H NMR (600 MHz, $CDCl_3$) δ 8.35 (s, 1H), 6.85 (t, 2H), 6.63 (s, 1H), 4.53 (dt, *J* = 47.0, 4.7 Hz, 2H), 3.66 – 3.48 (m, 2H) ppm.

^{13}C NMR (150 MHz, $CDCl_3$) δ 164.08 (dt, *J* = 254.5, 15.2 Hz), 161.50 (ddd, *J* = 251.2, 15.0, 8.3 Hz), 157.85 , 155.14 , 146.49 , 106.36 (d, *J* = 5.2 Hz), 101.78 – 100.54 (m), 89.77 , 81.56 (d, *J* = 171.3 Hz), 43.93 (d, *J* = 20.1 Hz) ppm.

HRMS (ES+) calculated for $C_{13}H_9ClF_4N_5$ $[M + H]^+$ 346.0477, found 346.0479.

IR: 1626, 1597, 1567, 1557, 1034 cm^{-1}

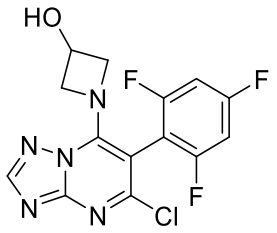

1-(5-Chloro-6-(2,4,6-trifluorophenyl)-[1,2,4]triazolo[1,5-a]pyrimidin-7-yl)azetidin-3-ol (45):

Following general procedure C using 5,7-dichloro-6-(2,4,6-trifluorophenyl)-[1,2,4]triazolo[1,5-a]pyrimidine (30 mg, 0.094 mmol), azetidin-3-ol (7.6 mg, 0.10 mmol), and DIPEA (36 mg, 0.28 mmol). Purification by reversed phase HPLC provided the title compound as a white powder (20 mg, 0.058 mmol, 62%).

^{1}H NMR (600 MHz, $CDCl_3$) δ 8.21 (s, 1H), 6.83 – 6.76 (m, 2H), 4.71 – 4.65 (m, 1H), 4.47 (d, *J* = 193.8 Hz, 4H) ppm.

^{13}C NMR (150 MHz, $CDCl_3$) δ 164.05 (dt, *J* = 253.8, 15.3 Hz), 162.11 (ddd, *J* = 249.7, 14.9, 8.1 Hz), 157.76 , 154.38 , 146.39 , 106.63 (td, *J* = 21.0, 4.8 Hz), 100.64 (td, *J* = 25.9, 4.0 Hz), 89.22 , 61.75 ppm.

HRMS (ES+) calculated for $C_{14}H_{10}ClF_3N_5O$ $[M + H]^+$ 356.0520, found 356.0520.

IR: 3241, 1638, 1595, 1557, 1035 cm^{-1}

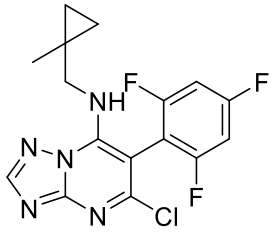

5-Chloro-*N*-((1-methylcyclopropyl)methyl)-6-(2,4,6-trifluorophenyl)-[1,2,4]triazolo[1,5-a]pyrimidin-7-amine (46):

Following general procedure C using 5,7-dichloro-6-(2,4,6-trifluorophenyl)-[1,2,4]triazolo[1,5-a]pyrimidine (30 mg, 0.094 mmol), (1-methylcyclopropyl)methanaminium chloride (11 mg, 0.094 mmol) and DIPEA (36 mg, 0.28 mmol). Purification by reversed phase HPLC provided the title compound as a white powder (25 mg, 0.068 mmol, 72%).

^{1}H NMR (600 MHz, $CDCl_3$) δ 8.36 (s, 1H), 6.92 – 6.78 (m, 2H), 6.43 (t, *J* = 5.2 Hz, 1H), 2.81 (d, *J* = 5.1 Hz, 2H), 1.09 (s, 3H), 0.49 – 0.33 (m, 3H) ppm.

^{13}C NMR (150 MHz, $CDCl_3$) δ 164.93 (t, *J* = 15.2 Hz), 163.24 (t, *J* = 15.2 Hz), 161.71 (ddd, *J* = 250.5, 14.9, 8.4 Hz), 158.14 , 155.10 , 146.48 , 107.32 (td, *J* = 20.8, 4.8 Hz), 101.54 – 100.19 (m), 88.96 , 52.69 , 29.84 , 21.00 , 11.94 ppm.

HRMS (ES+) calculated for $C_{16}H_{14}ClF_3N_5$ $[M + H]^+$ 368.0884, found 368.0881

IR: 2915, 1637, 1598, 1559, 1035 cm^{-1}

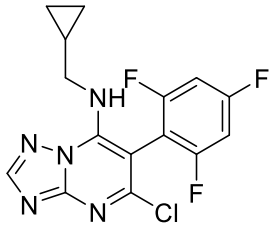

5-Chloro-*N*-(cyclopropylmethyl)-6-(2,4,6-trifluorophenyl)-[1,2,4]triazolo[1,5-a]pyrimidin-7-amine (47):

Following general procedure C using 5,7-dichloro-6-(2,4,6-trifluorophenyl)-[1,2,4]triazolo[1,5-a]pyrimidine (30 mg, 0.094 mmol) and cyclopropylmethanamine (15 mg, 0.21 mmol). Purification by reversed phase HPLC provided the title compound as a white powder (20 mg, 0.057 mmol, 60%).

^{1}H NMR (600 MHz, $CDCl_3$) δ 8.35 (s, 1H), 6.85 – 6.81 (m, 2H), 6.51 (s, 1H), 2.85 (dd, *J* = 7.3, 5.1 Hz, 2H), 1.06 – 0.98 (m, 1H), 0.63 – 0.59 (m, 2H), 0.20 (q, *J* = 5.3 Hz, 2H) ppm.

^{13}C NMR (150 MHz, $CDCl_3$) δ 164.09 (dt, *J* = 253.7, 15.1 Hz), 161.80 (ddd, *J* = 250.5, 14.9, 8.4 Hz), 158.15 , 155.06 , 153.72 , 146.13 , 107.28 (td, *J* = 20.8, 4.8 Hz), 101.34 – 100.49 (m), 89.03 , 48.80 , 11.12 , 3.93 ppm.

HRMS (ES+) calculated for $C_{15}H_{12}ClF_3N_5$ $[M + H]^+$ 354.0728, found 354.0727

IR: 2917, 2849, 1639, 1574, 1557, 1035 cm^{-1}

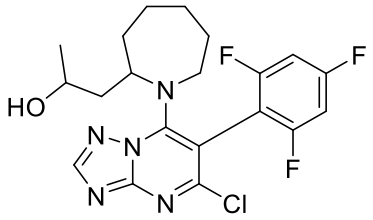

1-(1-(5-chloro-6-(2,4,6-trifluorophenyl)-[1,2,4]triazolo[1,5-a]pyrimidin-7-yl)azepan-2-yl)propan-2-ol (48):

Following general procedure C using 5,7-dichloro-6-(2,4,6-trifluorophenyl)-[1,2,4]triazolo[1,5-a]pyrimidine (30 mg, 0.094 mmol) and -(azepan-2-yl)propan-2-ol (33 mg, 0.21 mmol). Purification by reversed phase HPLC provided the title compound as a white powder (24 mg, 0.055 mmol, 58%). A mixture of stereoisomers was obtained.

^{1}H NMR (600 MHz, $CDCl_3$) δ 8.41 (1H) , 6.92 – 6.85 (m, 2H), 4.23 – 4.15 (m, 1H), 4.01 – 3.94 (m, 1H), 3.70 – 3.63 (m, 1H), 3.32 – 3.22 (m, 1H), 2.00 – 1.93 (m, 1H), 1.69 – 1.62 (m, 6H), 1.47 – 1.38 (m, 3H), 1.33 – 1.24 (m, 3H), 1.22 – 1.13 (m, 2H), 1.10 (d, *J* = 6.1 Hz, 3H) ppm.

^{13}C NMR (150 MHz, $CDCl_3$) *δ* 163.67 (dt, *J* = 253.1, 15.3 Hz), 161.47 (ddd, *J* = 249.7, 15.3, 8.9 Hz), 161.18 – 159.20 (m), 158.26 , 155.57 , 154.96 , 151.85 , 102.52 , 101.57 – 100.94 (m), 65.25 , 59.74 , 47.46 , 44.85 , 34.07 , 32.84 , 30.62 , 30.61 , 29.03 , 24.69 , 24.07 ppm.

HRMS (ES+) calculated for $C_{20}H_{22}ClF_3N_5O$ $[M + H]^+$ 440.1459, found 440.1457.

IR: 3373, 2918, 1634, 1594, 1504 cm^{-1}

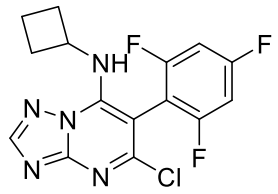

5-Chloro-*N*-cyclobutyl-6-(2,4,6-trifluorophenyl)-[1,2,4]triazolo[1,5-a]pyrimidin-7-amine (49):

Following general procedure C using 5,7-dichloro-6-(2,4,6-trifluorophenyl)-[1,2,4]triazolo[1,5-a]pyrimidine (30 mg, 0.094 mmol) and cyclobutanamine (14 mg, 0.20 mmol). Purification by silica gel column chromatography (0−40% EtOAc in Hexane) provided the title compound as a white powder (25 mg, 0.071 mmol, 75%).

^{1}H NMR (600 MHz, $CDCl_3$) δ 8.35 (s, 1H), 6.85 (m, 2H), 6.61 (d, *J* = 7.5 Hz, 1H), 3.71 (q, *J* = 7.7 Hz, 1H), 2.08 – 1.94 (m, 4H), 1.80 – 1.73 (m, 1H), 1.60 – 1.51 (m, 1H), 1.24 (s, 1H) ppm.

^{13}C NMR (150 MHz, $CDCl_3$) δ 164.03 (dt, *J* = 253.8, 15.4 Hz), 161.71 (ddd, *J* = 250.5, 15.1, 8.4 Hz), 158.22 , 155.04 , 145.33 , 120.10 , 102.32 – 99.71 (m), 89.07 , 48.80 , 31.96 , 14.62 ppm.

HRMS (ES+) calculated for $C_{15}H_{12}ClF_3N_5$ $[M + H]^+$ 354.0728, found 354.0726.

IR: 3285, 2838, 2178, 1571 cm^{-1}

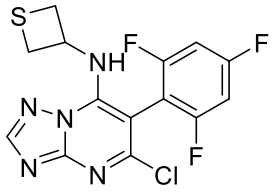

5-chloro-N-(thietan-3-yl)-6-(2,4,6-trifluorophenyl)-[1,2,4]triazolo[1,5-a]pyrimidin-7-amine (50):

Following general procedure C using 5,7-dichloro-6-(2,4,6-trifluorophenyl)-[1,2,4]triazolo[1,5-a]pyrimidine (30 mg, 0.094 mmol thietan-3-aminium chloride (12 mg, 0.094 mmol) and DIPEA (36 mg, 0.28 mmol). Purification by reversed phase HPLC provided the title compound as a white powder (23 mg, 0.062 mmol, 66%)

^{1}H NMR (600 MHz, $CDCl_3$) δ 8.36 (s, 1H), 6.92 – 6.87 (m, 2H), 6.78 (d, *J* = 8.7 Hz, 1H), 4.80 – 4.72 (m, 1H), 3.44 – 3.05 (m, 4H) ppm.

^{13}C NMR (150 MHz, $CDCl_3$) δ 164.30 (dt, *J* = 255.3, 15.2 Hz), 161.48 (ddd, *J* = 251.4, 15.0, 8.4 Hz), 158.14 , 155.28 , 153.79 , 144.69 , 134.44 , 128.78 – 128.34 (m), 106.39 (td, *J* = 20.8, 5.1 Hz), 101.81 – 101.09 (m), 89.94 , 51.10 , 36.13 ppm.

HRMS (ES+) calculated for $C_{14}H_{10}ClF_3N_5S$ $[M + H]^+$ 372.0292, found 372.0289

IR: 1610, 1555, 1437, 1034 cm^{-1}

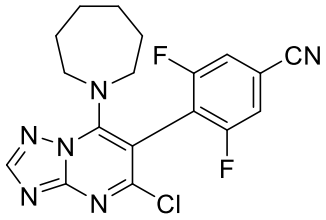

4-(7-(Azepan-1-yl)-5-chloro-[1,2,4]triazolo[1,5-a]pyrimidin-6-yl)-3,5-difluorobenzonitrile (51):

Following general procedure C using 4-(5,7-dichloro-[1,2,4]triazolo[1,5-a]pyrimidin-6-yl)-3,5-difluorobenzonitrile (20 mg, 0.060 mmol) and azepane (13 mg, 0.13 mmol). Purification by reversed phase HPLC provided the title compound as a white powder (15 mg, 0.039 mmol, 63%).

^{1}H NMR (600 MHz, $CDCl_3$) δ 8.38 (s, 1H), 7.40 (d, *J* = 6.0 Hz, 2H), 3.45 – 3.39 (m, 4H), 1.78 – 1.70 (m, 4H), 1.64 – 1.60 (m, 4H) ppm.

^{13}C NMR (150 MHz, $CDCl_3$) δ 160.74 (dd, *J* = 253.4, 6.6 Hz), 157.14 , 155.26 , 152.10 , 118.61 (t, *J* = 19.7 Hz), 116.30 – 115.97 (m), 115.12 (t, *J* = 11.9 Hz), 97.32 , 53.99 , 51.22 , 28.27 , 28.17 , 27.28 , 27.07 ppm.

HRMS (ES+) calculated for $C_{18}H_{16}ClF_2N_6$ $[M + H]^+$ 389.1088, found 389.1085.

IR: 2928, 2857, 2238, 1589, 1515, 1422 cm^{-1}

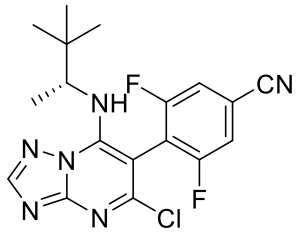

(*R*)-4-(5-Chloro-7-((3,3-dimethylbutan-2-yl)amino)-[1,2,4]triazolo[1,5-a]pyrimidin-6-yl)-3,5-difluorobenzonitrile (52):

Following general procedure C using 4-(5,7-dichloro-[1,2,4]triazolo[1,5-a]pyrimidin-6-yl)-3,5-difluorobenzonitrile (20 mg, 0.060 mmol) and (*R*)-3,3-dimethylbutan-2-amine (13 mg, 0.13 mmol). Purification by reversed phase HPLC provided the title compound as a white powder (18 mg, 0.046 mmol, 75%).

^{1}H NMR (600 MHz, $CDCl_3$) δ 8.36 (s, 1H), 7.45 – 7.41 (m, 2H), 6.52 (d, *J* = 10.8 Hz, 1H), 2.94 (s, 1H), 1.02 (d, *J* = 6.7 Hz, 3H), 0.84 (s, 9H) ppm.

^{13}C NMR (150 MHz, $CDCl_3$) δ 161.33 (dd, *J* = 253.8, 6.2 Hz), 161.05 (dd, *J* = 253.8, 6.2 Hz), 157.12 , 155.22 , 146.03 , 116.22 (d, *J* = 4.0 Hz), 116.13 – 115.95 (m), 115.95 – 115.82 (m), 58.57 , 34.93 , 25.86 , 16.56 ppm.

HRMS (ES+) calculated for $C_{18}H_{18}ClF_2N_6$ $[M + H]^+$ 391.1244, found 391.1241.

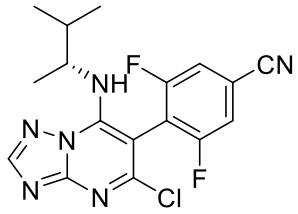

***(R)*-4-(5-chloro-7-((3-methylbutan-2-yl)amino)-[1,2,4]triazolo[1,5-a]pyrimidin-6-yl)-3,5-difluorobenzonitrile (53):**

Following general procedure C using 4-(5,7-dichloro-[1,2,4]triazolo[1,5-a]pyrimidin-6-yl)-3,5-difluorobenzonitrile (30 mg, 0.092 mmol) and *(R)*-3-methylbutan-2-amine (17 mg, 0.190 mmol). Purification by reversed phase HPLC provided the title compound as a white powder (28 mg, 0.074 mmol, 81%).

^{1}H NMR (600 MHz, DMSO-d_6) δ 8.62 (s, 1H), 8.11 (t, J = 7.8 Hz, 2H), 7.88 (s, 1H), 1.78 (dq, J = 13.9, 6.8 Hz, 1H), 1.10 (d, J = 6.6 Hz, 3H), 0.74 (dd, J = 6.8, 2.9 Hz, 6H).

^{13}C NMR (151 MHz, DMSO-d_6) δ 160.71 (dd, J = 249.2, 6.8 Hz), 160.38 (dd, J = 249.5, 6.3 Hz), 155.02 , 146.81 , 117.00 (ddd, J = 26.3, 12.6, 3.9 Hz), 116.48 (d, J = 3.5 Hz), 114.83 (t, J = 12.8 Hz).

HRMS (ES+) calculated for $C_{17}H_{16}ClF_2N_6$ $[M + H]^+$ 377.1088, found 377.1089

IR: 2966, 2220, 1690, 1562, 1422, 1204 cm^{-1}

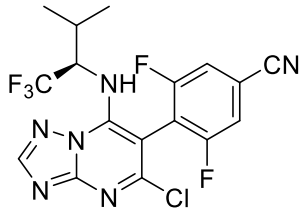

***(R)*-4-(5-chloro-7-((1,1,1-trifluoro-3-methylbutan-2-yl)amino)-[1,2,4]triazolo[1,5-a]pyrimidin-6-yl)-3,5-difluorobenzonitrile (54):**

Following general procedure C using 4-(5,7-dichloro-[1,2,4]triazolo[1,5-a]pyrimidin-6-yl)-3,5-difluorobenzonitrile (30 mg, 0.092 mmol) and *(R)*-1,1,1-trifluoro-3-methylbutan-2-amine (29 mg, 0.20 mmol). Purification by reversed phase HPLC provided the title compound as a white powder (2 mg, 0.005 mmol, 5%).

HRMS (ES+) calculated for $C_{17}H_{13}ClF_5N_6$ $[M + H]^+$ 431.0805, found 431.0800

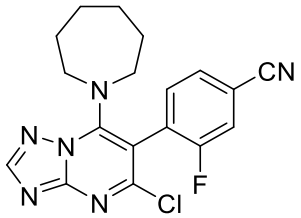

4-(7-(Azepan-1-yl)-5-chloro-[1,2,4]triazolo[1,5-a]pyrimidin-6-yl)-3-fluorobenzonitrile (55):

Following general procedure C using 4-(5,7-dichloro-[1,2,4]triazolo[1,5-a]pyrimidin-6-yl)-3-fluorobenzonitrile (40 mg, 0.13 mmol) and azepane (27 mg, 0.27 mmol). Purification by reversed phase HPLC provided the title compound as a white powder (27 mg, 0.073 mmol, 56%).

^{1}H NMR (600 MHz, $CDCl_3$) δ 8.34 (s, 1H), 7.61 (dd, *J* = 7.9, 1.6 Hz, 1H), 7.53 (dd, *J* = 8.7, 1.6 Hz, 1H), 7.48 (t, *J* = 7.5 Hz, 1H), 3.38 – 3.33 (m, 4H), 1.71 (dq, *J* = 8.0, 4.2 Hz, 4H), 1.60 (p, *J* = 3.0 Hz, 4H) ppm.

^{13}C NMR (150 MHz, $CDCl_3$) δ 160.85 , 159.18 , 156.93 , 155.27 , 155.18 , 151.61 , 134.44 (d, *J* = 2.8 Hz), 128.60 (d, *J* = 3.9 Hz), 128.48 , 120.11 , 119.94 , 117.09 (d, *J* = 2.8 Hz), 114.68 (d, *J* = 9.2 Hz), 103.59 , 54.05 , 28.27 , 28.03 ppm.

HRMS (ES+) calculated for $C_{18}H_{17}ClFN_6$ $[M + H]^+$ 371.1182, found 371.1180.

IR: 2926, 2235, 1589, 1519, 1446 cm^{-1}

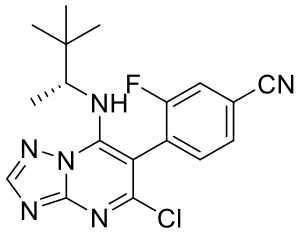

(*R*)-4-(5-Chloro-7-((3,3-dimethylbutan-2-yl)amino)-[1,2,4]triazolo[1,5-a]pyrimidin-6-yl)-3-fluorobenzonitrile (56):

Following general procedure C using 4-(5,7-dichloro-[1,2,4]triazolo[1,5-a]pyrimidin-6-yl)-3-fluorobenzonitrile (40 mg, 0.13 mmol) and *(R)*-3,3-dimethylbutan-2-amine (28 mg, 0.27 mmol). Purification by reversed phase HPLC provided the title compound as a white powder (27 mg, 0.072 mmol, 56%).

Mixture of atropoisomers

^{1}H NMR (600 MHz, $CDCl_3$) δ 8.41 – 8.34 (m, 1H), 7.67 – 7.61 (m, 1H), 7.60 – 7.55 (m, 1H), 7.55 – 7.49 (m, 1H), 6.37 (s, 1H), 2.94 (m, 1H), 1.01 (d, *J* = 6.7 Hz, 1H), 0.94 (d, *J* = 6.7 Hz, 2H), 0.82 (s, 5H), 0.81 (s, 4H) ppm.

^{13}C NMR (150 MHz, $CDCl_3$) δ 161.71 – 159.28 (m), 156.76 , 156.67 , 145.96 , 135.28 (d, *J* = 2.4 Hz), 133.96 (d, *J* = 2.3 Hz), 128.65 (d, *J* = 4.1 Hz), 128.43 (d, *J* = 4.1 Hz), 119.96 (dd, *J* = 37.6, 25.4 Hz), 116.86 (d, *J* = 2.8 Hz), 115.42 (dd, *J* = 16.7, 9.3 Hz), 94.27 , 94.14 , 58.27 , 58.07 , 35.01 , 34.82 , 25.77 (d, *J* = 1.9 Hz), 16.42 (d, *J* = 2.2 Hz) ppm.

HRMS (ES+) calculated for $C_{18}H_{19}ClFN_6$ $[M + H]^+$ 373.1338, found 373.1338.

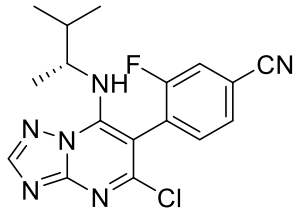

***(R)*-4-(5-chloro-7-((3-methylbutan-2-yl)amino)-[1,2,4]triazolo[1,5-a]pyrimidin-6-yl)-3-fluorobenzonitrile (57):**

Following general procedure C using 4-(5,7-dichloro-[1,2,4]triazolo[1,5-a]pyrimidin-6-yl)-3-fluorobenzonitrile (30 mg, 0.097 mmol) and *(R)*-3-methylbutan-2-amine (18 mg, 0.20 mmol). Purification by reversed phase HPLC provided the title compound as a white powder (30 mg, 0.097 mmol, 86%).

^{1}H NMR (600 MHz, Methanol-d_4) δ 8.45 (s, 1H), 7.85 (dt, *J* = 9.0, 2.1 Hz, 1H), 7.81 (ddd, *J* = 8.1, 6.6, 1.8 Hz, 1H), 7.76 (t, *J* = 7.5 Hz, 1H), 1.74 (dtd, *J* = 13.4, 6.7, 2.4 Hz, 1H), 1.10 (dd, *J* = 15.2, 6.6 Hz, 3H), 0.84 – 0.78 (m, 6H).

^{13}C NMR (150 MHz, Methanol-d_4) δ 161.91 (dd, *J* = 249.3, 4.2 Hz), 157.93 (d, *J* = 13.3 Hz), 155.38 , 155.29 – 154.81 (m), 147.88 , 136.32 (dd, *J* = 143.3, 2.6 Hz), 130.18 (dd, *J* = 10.7, 4.3 Hz), 128.29 (dd, *J* = 42.8, 16.8 Hz), 121.18 (dd, *J* = 26.0, 5.5 Hz), 118.02 (d, *J* = 3.2 Hz), 116.87 – 116.06 (m), 96.68 – 94.92 (m), 34.76 (d, *J* = 15.6 Hz), 19.26 (d, *J* = 14.4 Hz), 18.79 – 18.25 (m), 17.88 (d, *J* = 20.5 Hz).

HRMS (ES+) calculated for $C_{17}H_{17}ClFN_6$ $[M + H]^+$ 359.1182, found 359.1184

IR: 2963, 2220, 1608, 1570, 1260, 1156 cm^{-1}

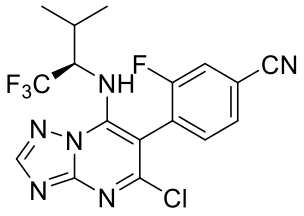

***(R)*-4-(5-chloro-7-((1,1,1-trifluoro-3-methylbutan-2-yl)amino)-[1,2,4]triazolo[1,5-a]pyrimidin-6-yl)-3-fluorobenzonitrile (58):**

Following general procedure C using 4-(5,7-dichloro-[1,2,4]triazolo[1,5-a]pyrimidin-6-yl)-3-fluorobenzonitrile (30 mg, 0.097 mmol) and *(R)*-1,1,1-trifluoro-3-methylbutan-2-amine (19 mg, 0.13 mmol)Purification by reversed phase HPLC provided the title compound as a white powder (2.6 mg, 0.006 mmol, 10%).

HRMS (ES+) calculated for $C_{17}H_{14}ClF_4N_6$ $[M + H]^+$ 413.0899, found 413.0894

Appendix

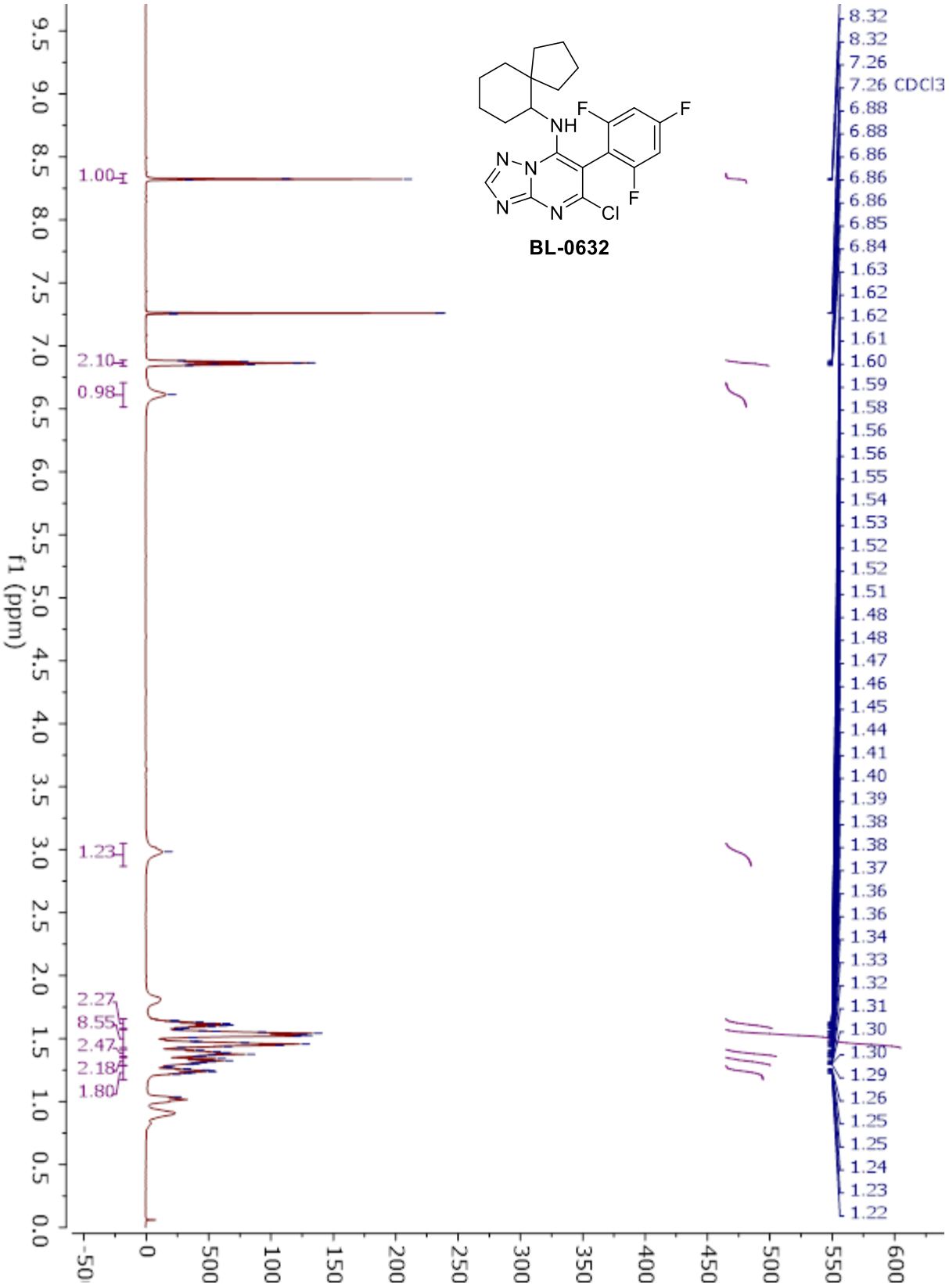
BL-0632
f1 (ppm)
1.00
2.10
0.98
1.23
2.27
8.55
2.47
2.18
1.80
8.32
8.32
7.26
7.26 CDCl3
6.88
6.88
6.86
6.86
6.86
6.85
6.84
1.63
1.62
1.62
1.61
1.60
1.59
1.58
1.56
1.56
1.55
1.54
1.53
1.52
1.52
1.51
1.48
1.48
1.47
1.46
1.45
1.44
1.41
1.40
1.39
1.38
1.38
1.37
1.36
1.36
1.34
1.33
1.32
1.31
1.30
1.30
1.29
1.26
1.25
1.25
1.24
1.23
1.22

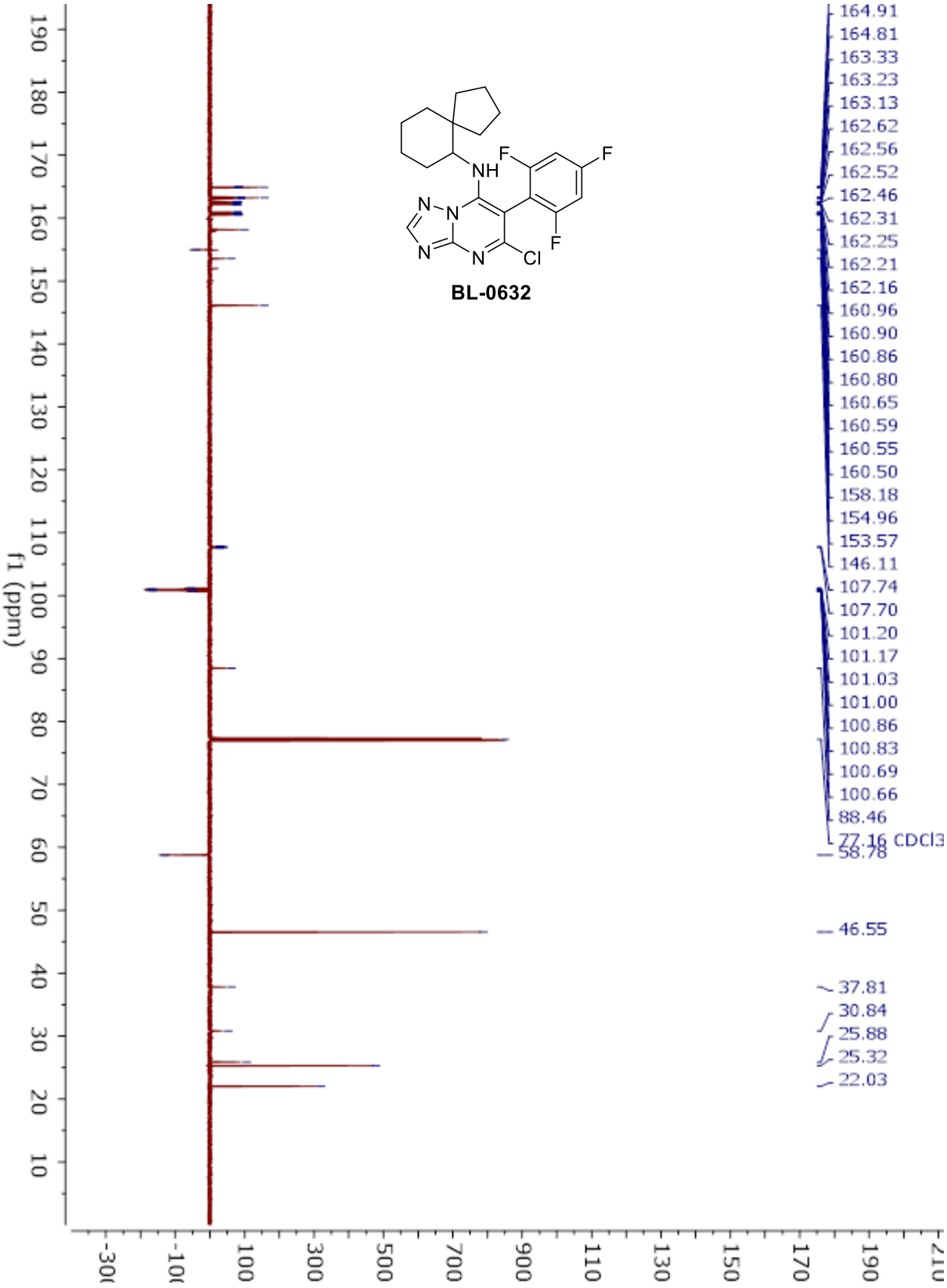
BL-0632
f1 (ppm)
164.91
164.81
163.33
163.23
163.13
162.62
162.56
162.52
162.46
162.31
162.25
162.21
162.16
160.96
160.90
160.86
160.80
160.65
160.59
160.55
160.50
158.18
154.96
153.57
146.11
107.74
107.70
101.20
101.17
101.03
101.00
100.86
100.83
100.69
100.66
88.46
77.16 CDCl3
58.78
46.55
37.81
30.84
25.88
25.32
22.03

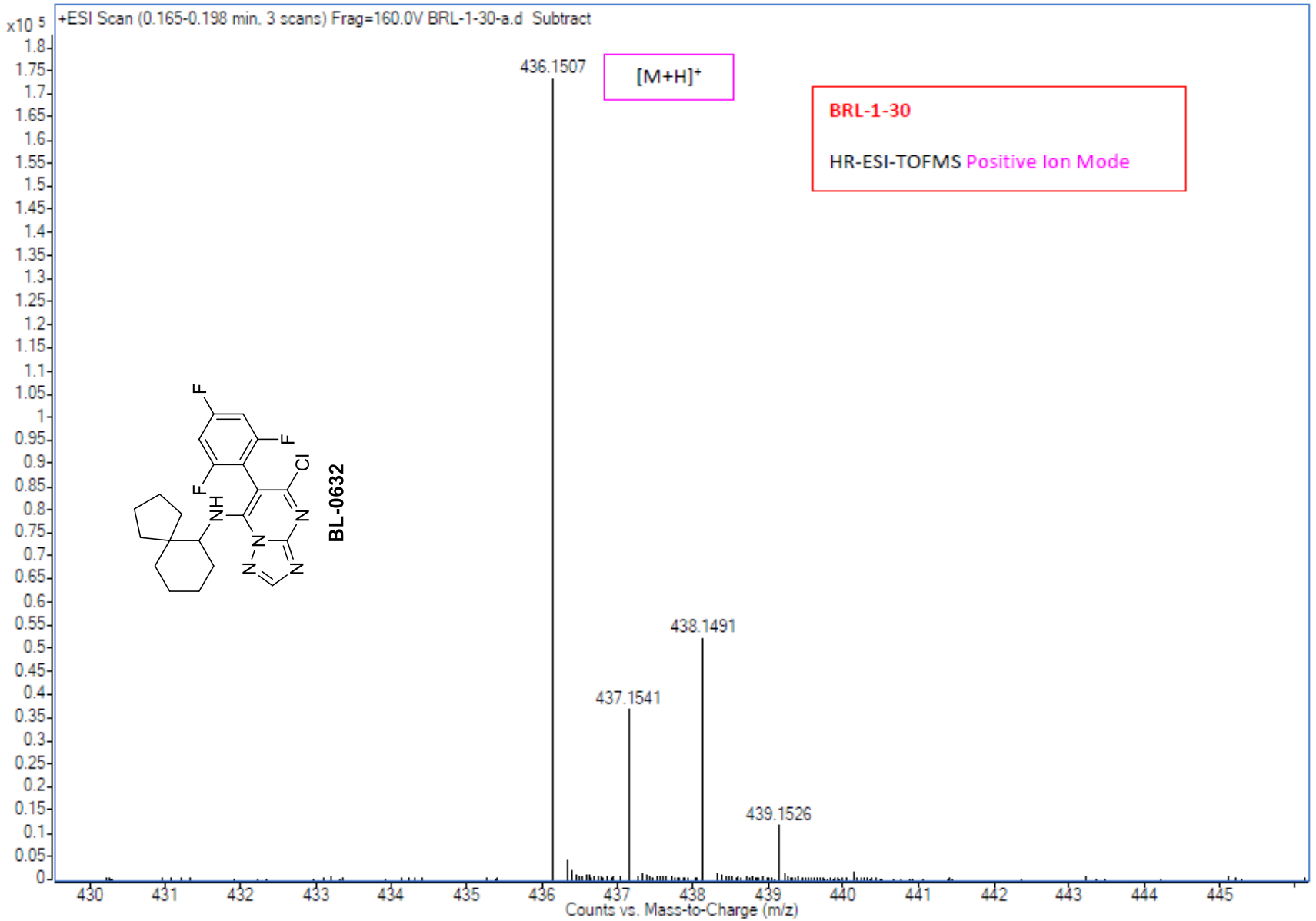
+ESI Scan (0.165-0.198 min, 3 scans) Frag=160.0V BRL-1-30-a.d Subtract
x10 5
436.1507
[M+H]+
BRL-1-30
HR-ESI-TOFMS Positive Ion Mode
BL-0632
438.1491
437.1541
439.1526
Counts vs. Mass-to-Charge (m/z)

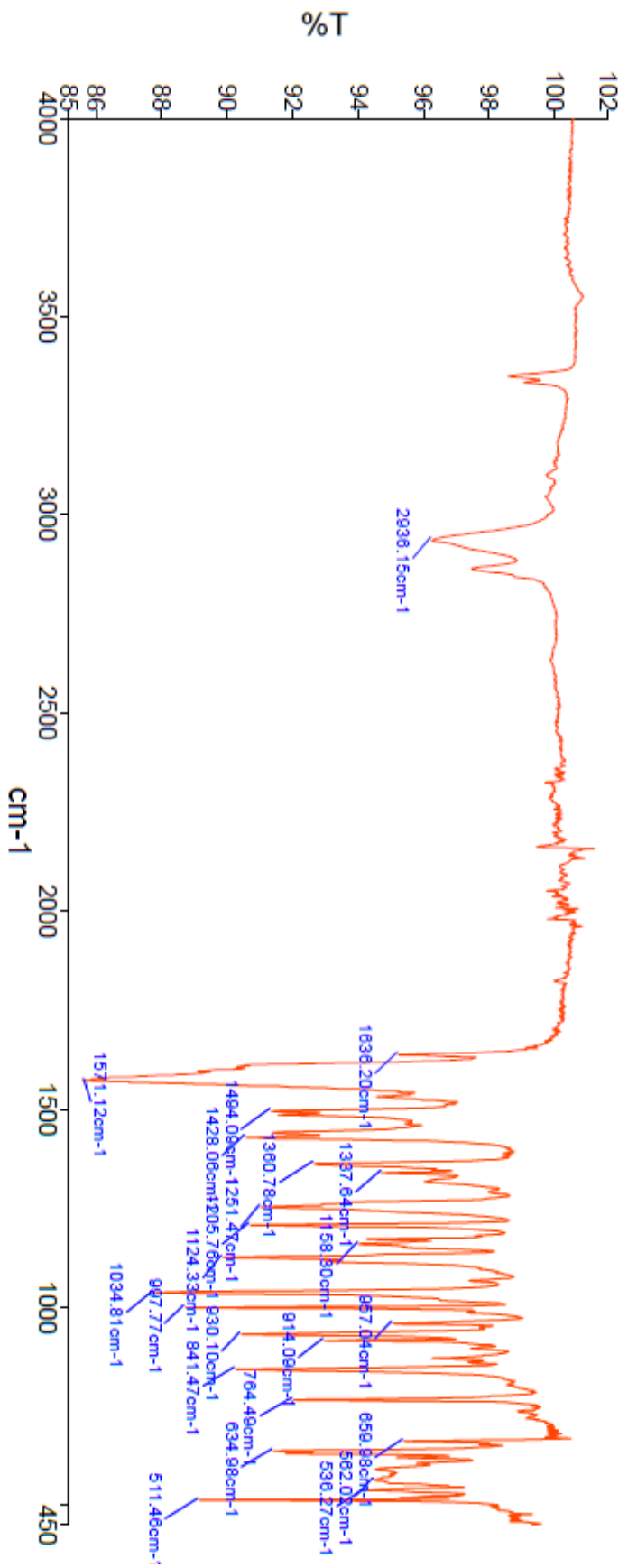
%T
cm-1
2936.15cm-1
1638.20cm-1
1571.12cm-1
1494.08cm-1
1428.06cm-1
1360.78cm-1
1387.64cm-1
1251.47cm-1
1205.76cm-1
1158.80cm-1
1124.33cm-1
1034.81cm-1
997.77cm-1
930.10cm-1
914.09cm-1
887.04cm-1
841.47cm-1
764.49cm-1
659.98cm-1
634.98cm-1
562.03cm-1
538.27cm-1
511.46cm-1

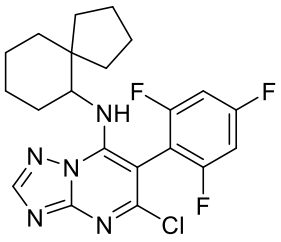

BL-0632

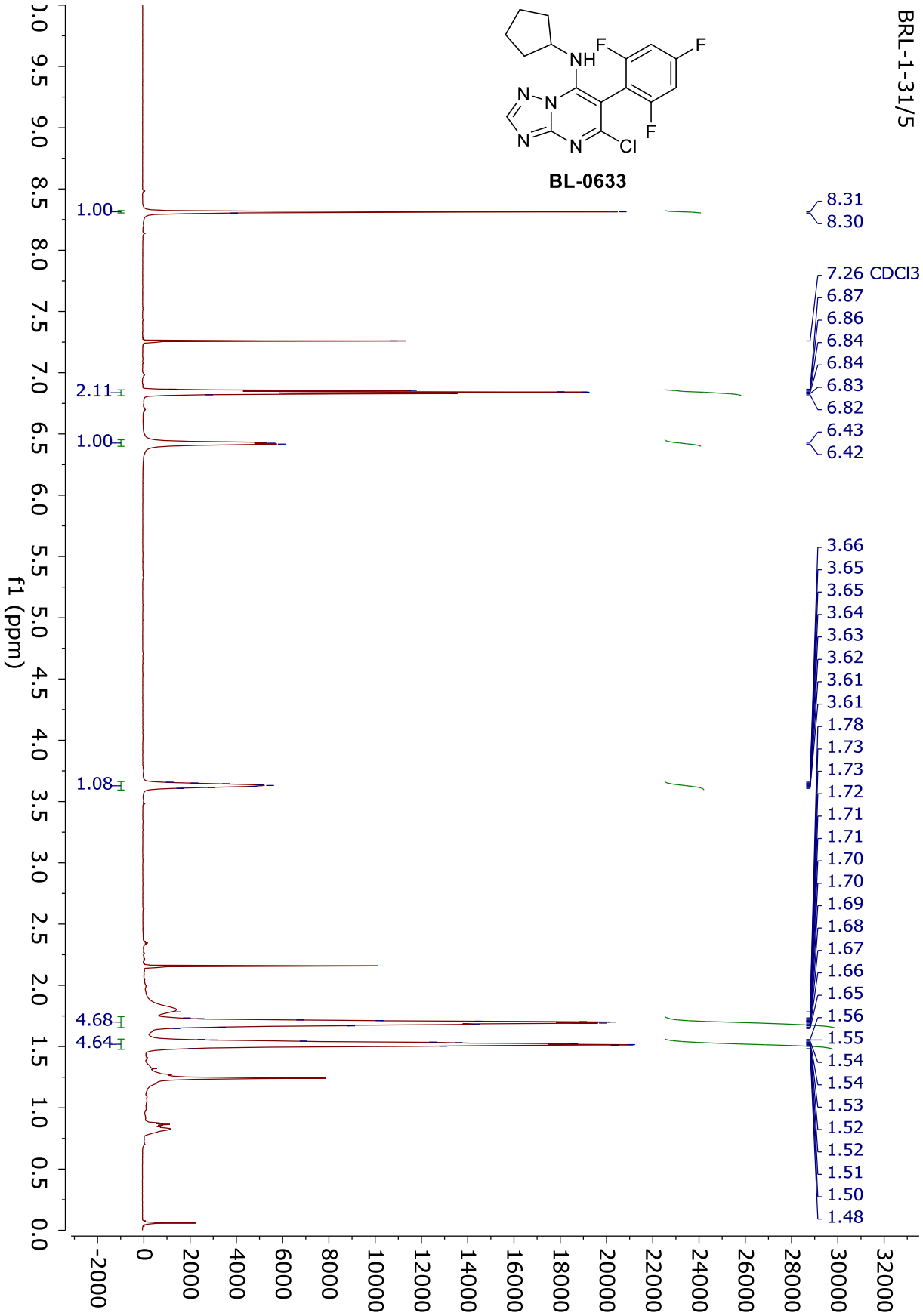
BRL-1-31/5
BL-0633
NH
F
F
F
N
N
N
N
Cl
1.00
2.11
1.00
1.08
4.68
4.64
8.31
8.30
7.26 CDCl3
6.87
6.86
6.84
6.84
6.83
6.82
6.43
6.42
3.66
3.65
3.65
3.64
3.63
3.62
3.61
3.61
1.78
1.73
1.73
1.72
1.71
1.71
1.70
1.70
1.69
1.68
1.67
1.66
1.65
1.56
1.55
1.54
1.54
1.53
1.52
1.52
1.51
1.50
1.48
f1 (ppm)

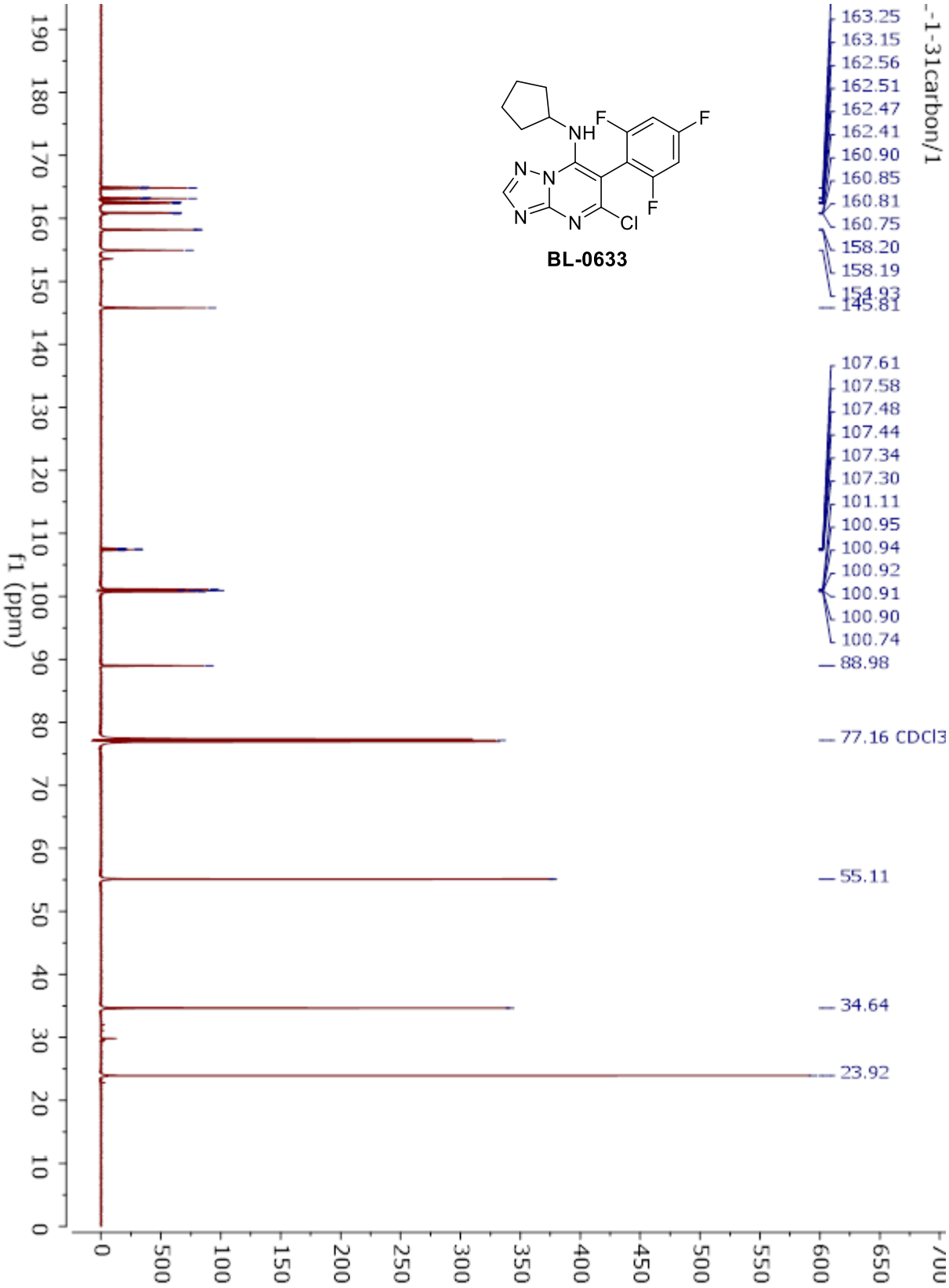
BL-0633
-1-31carbon/1
163.25
163.15
162.56
162.51
162.47
162.41
160.90
160.85
160.81
160.75
158.20
158.19
154.93
145.81
107.61
107.58
107.48
107.44
107.34
107.30
101.11
100.95
100.94
100.92
100.91
100.90
100.74
88.98
77.16 CDCl3
55.11
34.64
23.92
f1 (ppm)

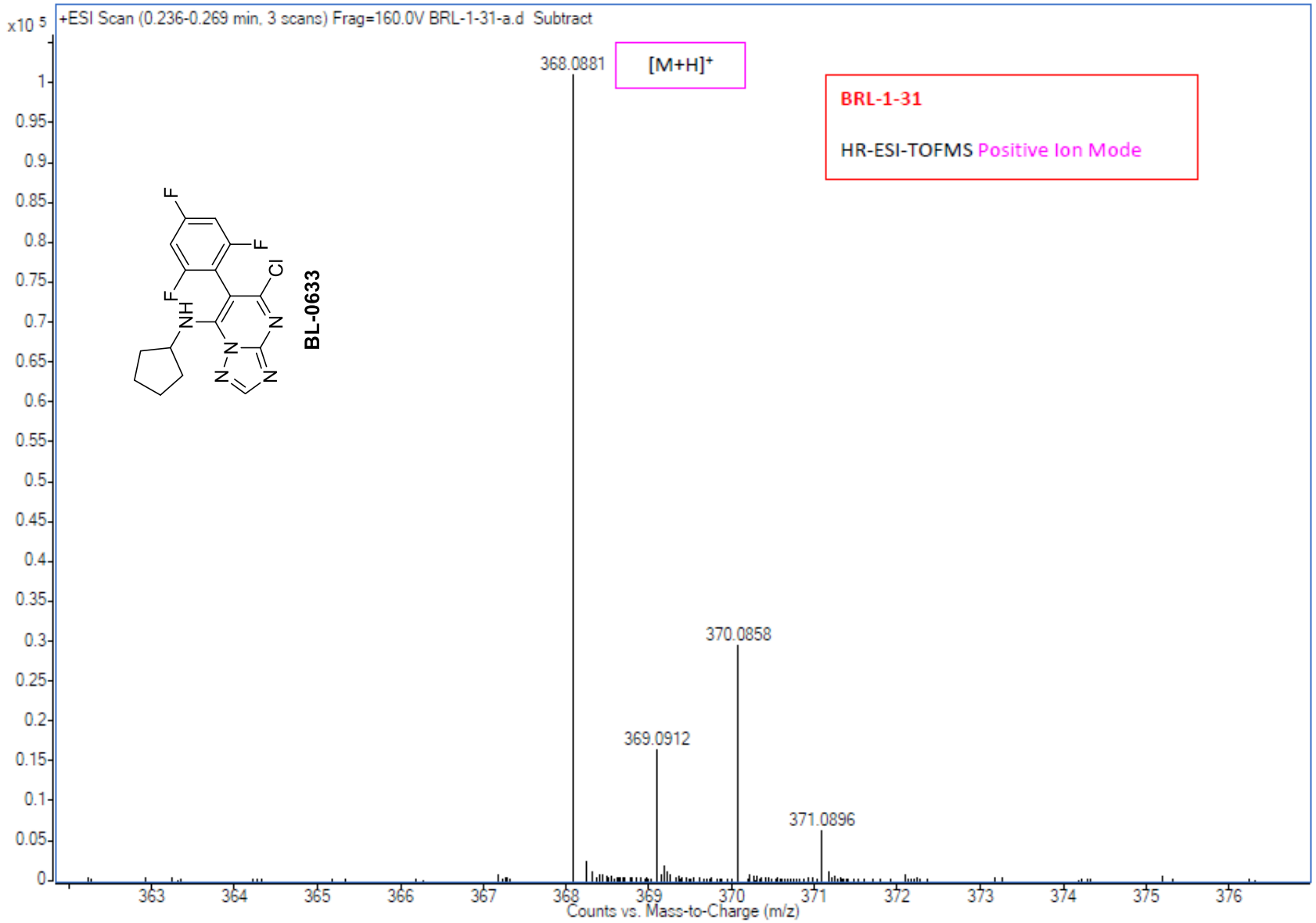
+ESI Scan (0.236-0.269 min, 3 scans) Frag=160.0V BRL-1-31-a.d Subtract
x10 5
368.0881
[M+H]+
BRL-1-31
HR-ESI-TOFMS Positive Ion Mode
BL-0633
370.0858
369.0912
371.0896
Counts vs. Mass-to-Charge (m/z)

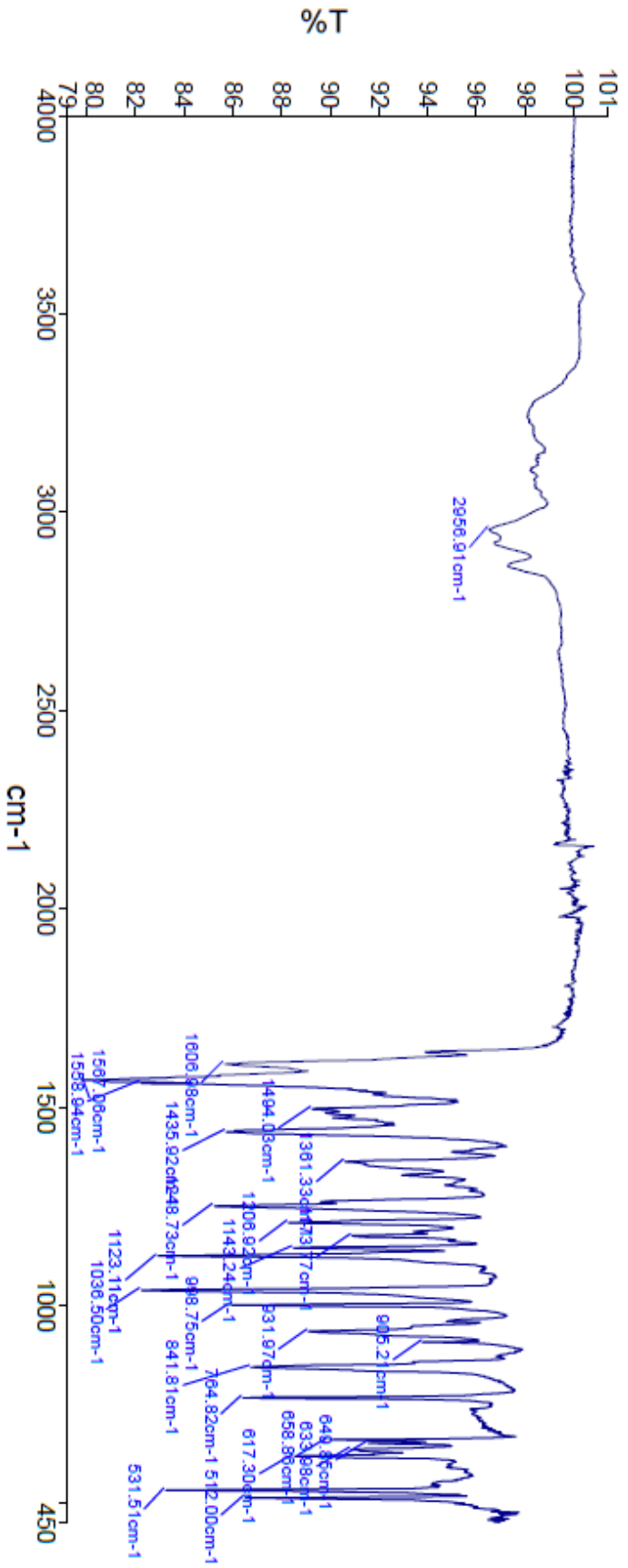
%T
cm-1
2956.91cm-1
1606.98cm-1
1435.92cm-1
1494.03cm-1
1381.33cm-1
1248.73cm-1
1106.92cm-1
1143.24cm-1
1123.11cm-1
1038.50cm-1
998.75cm-1
931.97cm-1
905.21cm-1
841.81cm-1
764.82cm-1
658.86cm-1
617.30cm-1
531.51cm-1
512.00cm-1

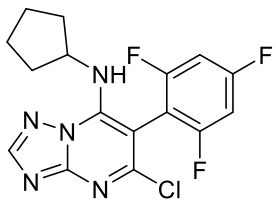
NH
F
F
F
N
N
N
N
Cl

BL-0633

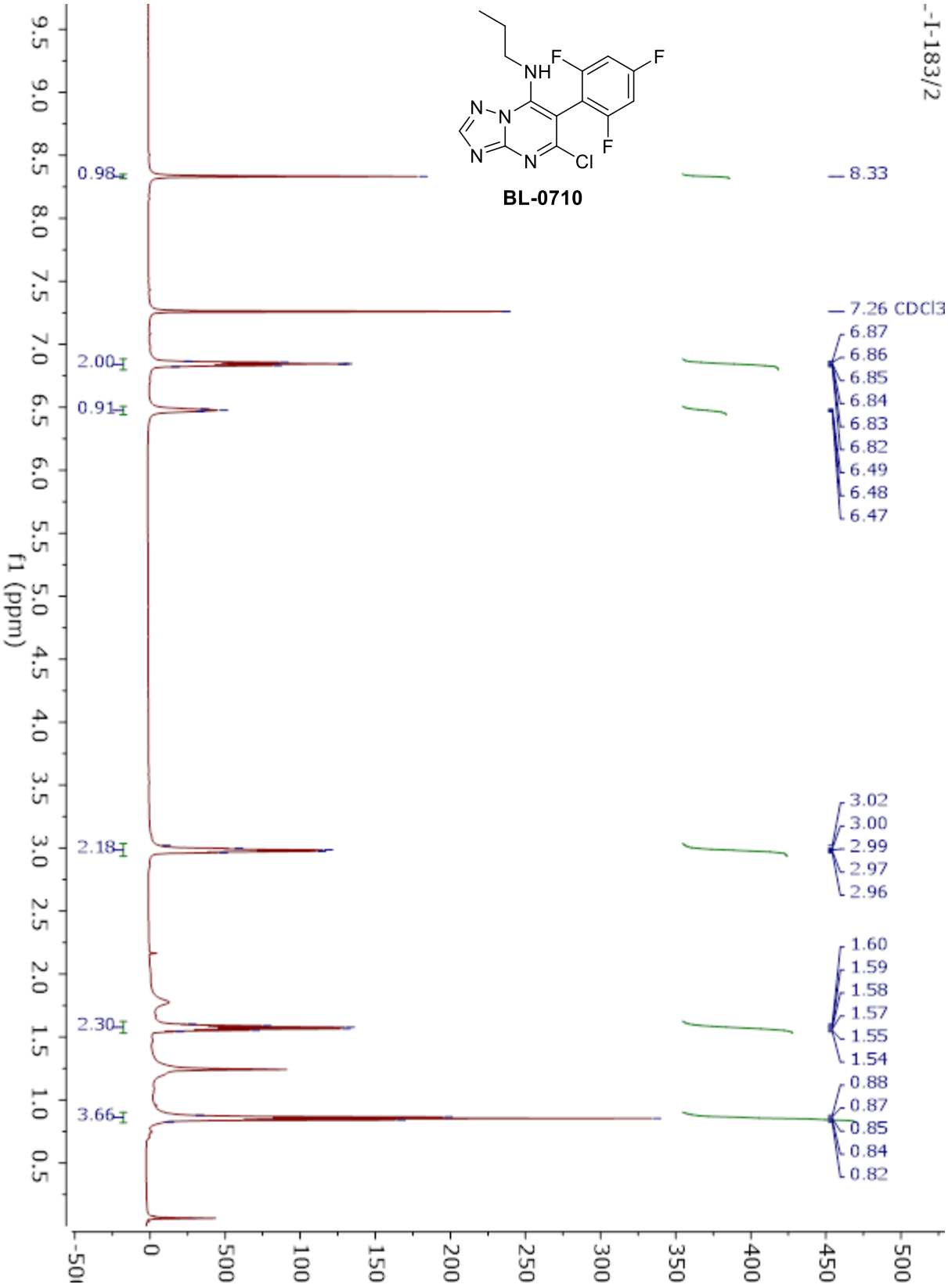
-I-183/2
BL-0710
f1 (ppm)
0.98
2.00
0.91
2.18
2.30
3.66
8.33
7.26 CDCl3
6.87
6.86
6.85
6.84
6.83
6.82
6.49
6.48
6.47
3.02
3.00
2.99
2.97
2.96
1.60
1.59
1.58
1.57
1.55
1.54
0.88
0.87
0.85
0.84
0.82

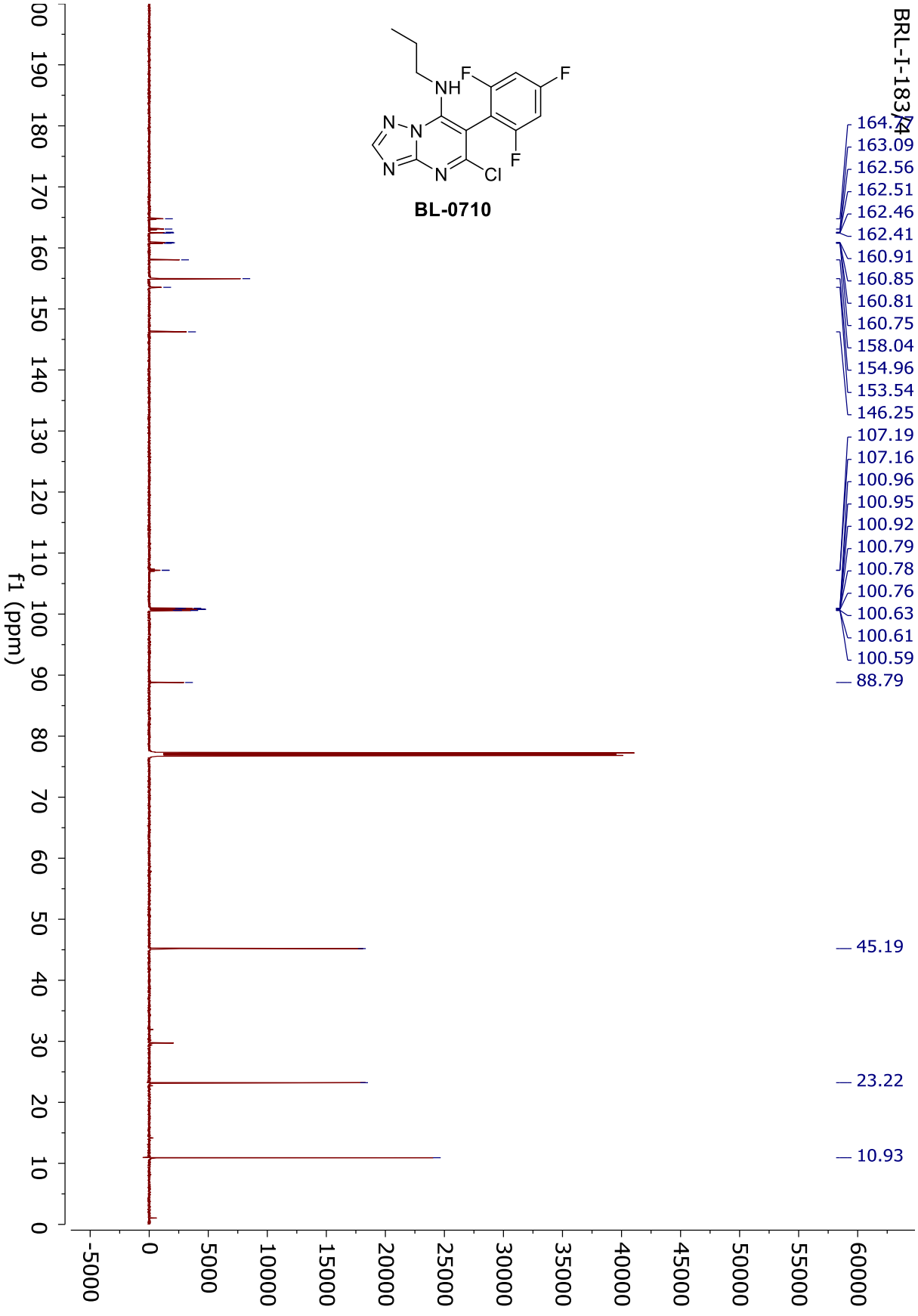
BRL-I-183-4
BL-0710
164.74
163.09
162.56
162.51
162.46
162.41
160.91
160.85
160.81
160.75
158.04
154.96
153.54
146.25
107.19
107.16
100.96
100.95
100.92
100.79
100.78
100.76
100.63
100.61
100.59
88.79
45.19
23.22
10.93
f1 (ppm)

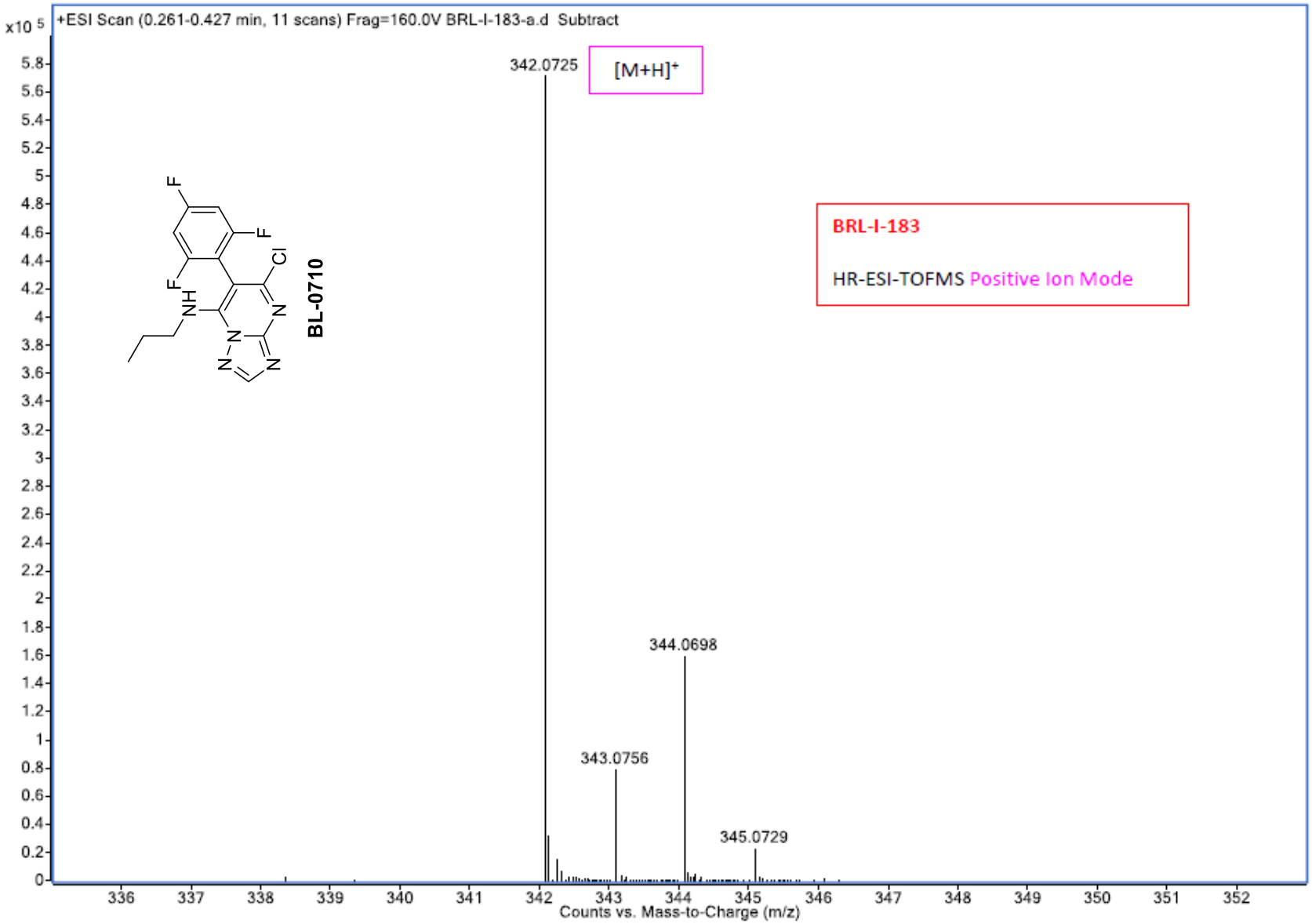
+ESI Scan (0.261-0.427 min, 11 scans) Frag=160.0V BRL-I-183-a.d Subtract
x10 5
342.0725
[M+H]+
344.0698
343.0756
345.0729
BRL-I-183
HR-ESI-TOFMS Positive Ion Mode
BL-0710
Counts vs. Mass-to-Charge (m/z)

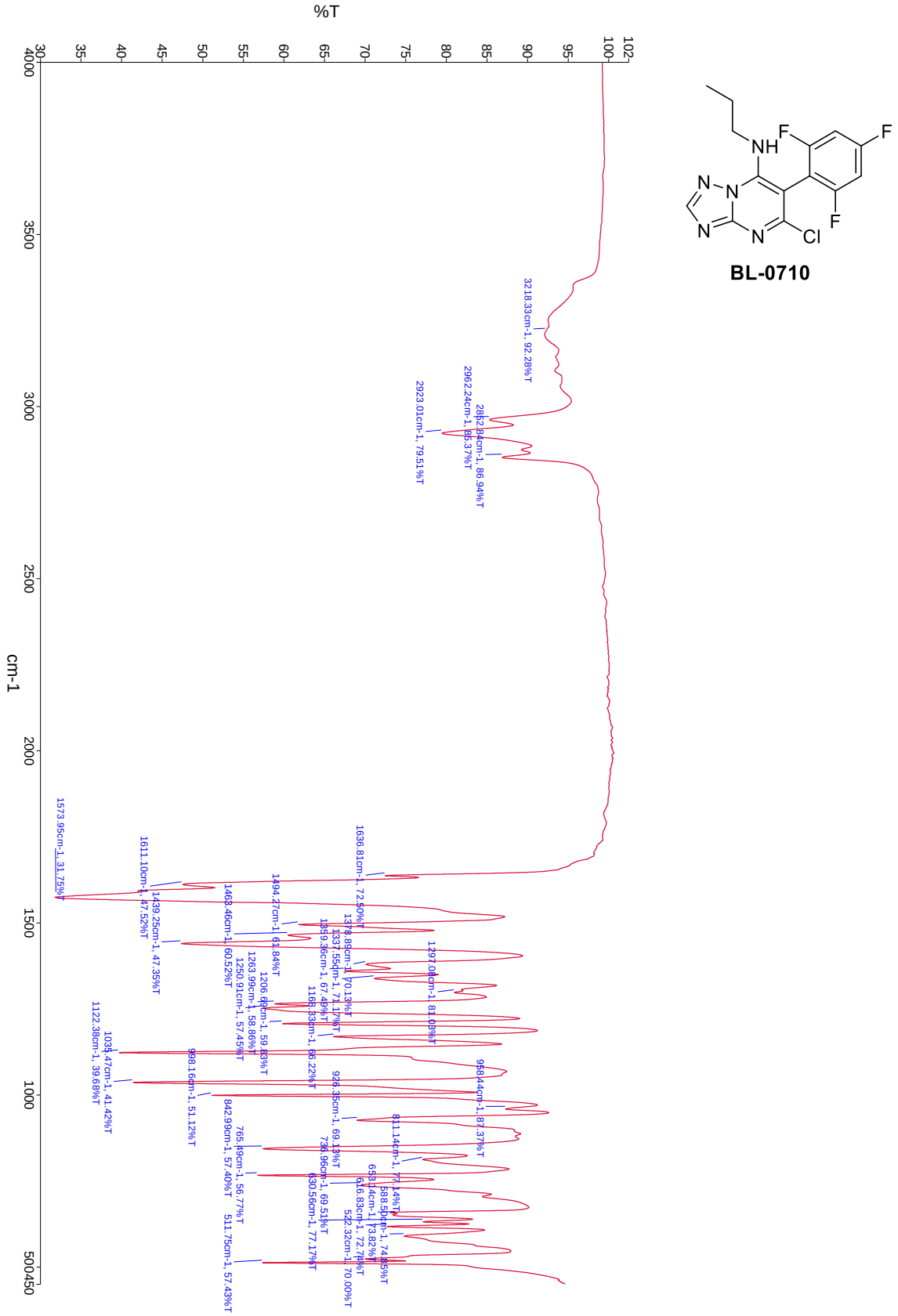
%T
cm-1
3218.33cm-1, 92.28%T
2962.24cm-1, 85.37%T
2923.01cm-1, 79.51%T
1636.81cm-1, 72.50%T
1573.95cm-1, 31.75%T
1611.10cm-1, 47.52%T
1494.27cm-1, 61.84%T
1468.46cm-1, 60.52%T
1439.25cm-1, 47.35%T
1378.88cm-1, 70.13%T
1337.55cm-1, 71.17%T
1291.08cm-1, 81.08%T
1263.99cm-1, 58.86%T
1250.91cm-1, 57.45%T
1206.69cm-1, 59.83%T
1168.33cm-1, 66.22%T
1122.38cm-1, 39.68%T
1034.47cm-1, 41.42%T
998.16cm-1, 51.12%T
960.44cm-1, 87.37%T
926.35cm-1, 69.13%T
842.99cm-1, 57.40%T
811.14cm-1, 77.14%T
765.49cm-1, 56.77%T
736.96cm-1, 69.51%T
658.14cm-1, 73.82%T
630.56cm-1, 77.17%T
616.83cm-1, 72.74%T
522.32cm-1, 70.00%T
511.75cm-1, 57.43%T
F
F
F
NH
N
N
N
N
Cl
BL-0710

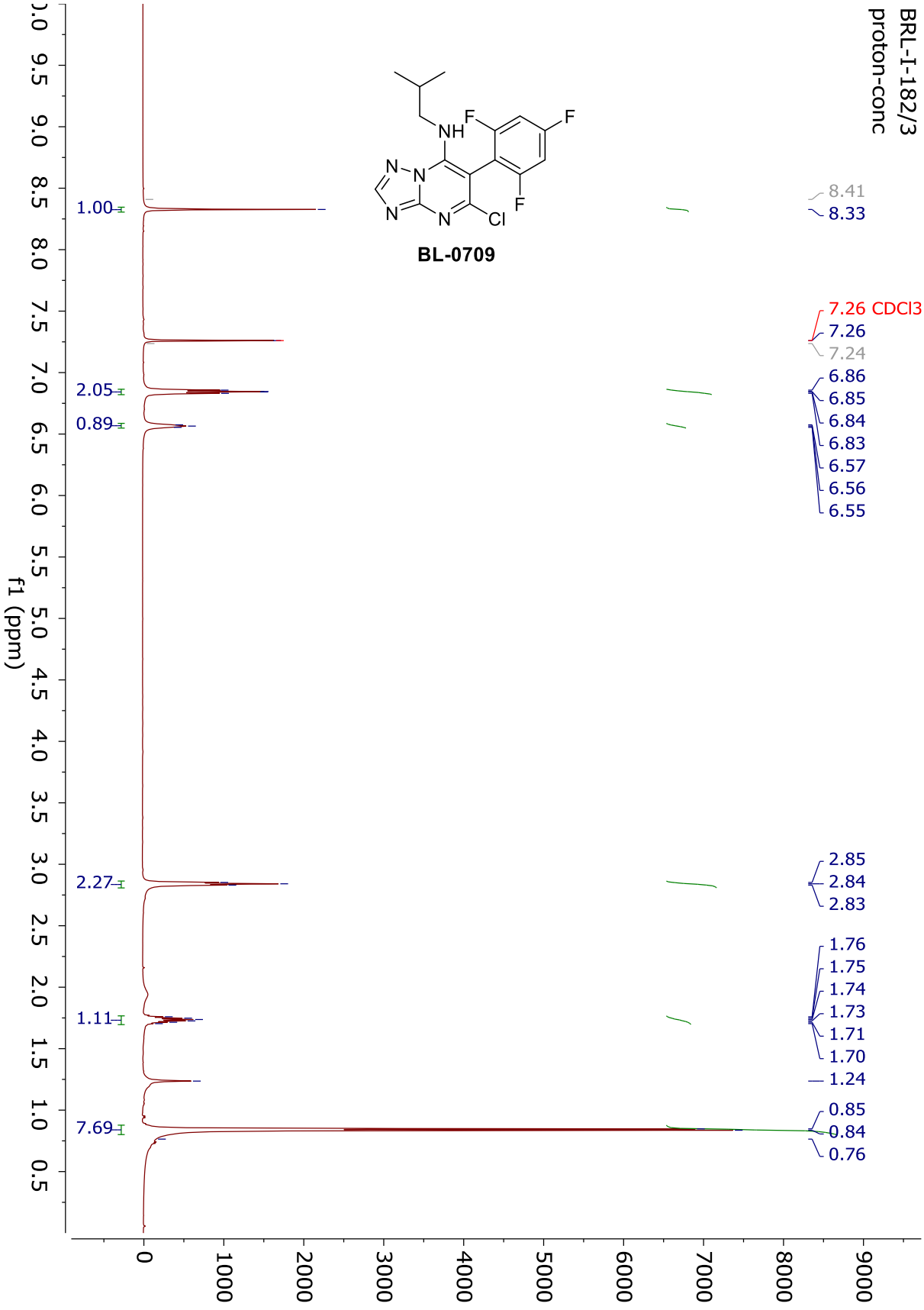
BRL-I-182/3
proton-conc
BL-0709
NH
F
F
F
N
N
N
N
Cl
1.00
2.05
0.89
2.27
1.11
7.69
8.41
8.33
7.26 CDCl3
7.26
7.24
6.86
6.85
6.84
6.83
6.57
6.56
6.55
2.85
2.84
2.83
1.76
1.75
1.74
1.73
1.71
1.70
1.24
0.85
0.84
0.76
f1 (ppm)
0
1000
2000
3000
4000
5000
6000
7000
8000
9000

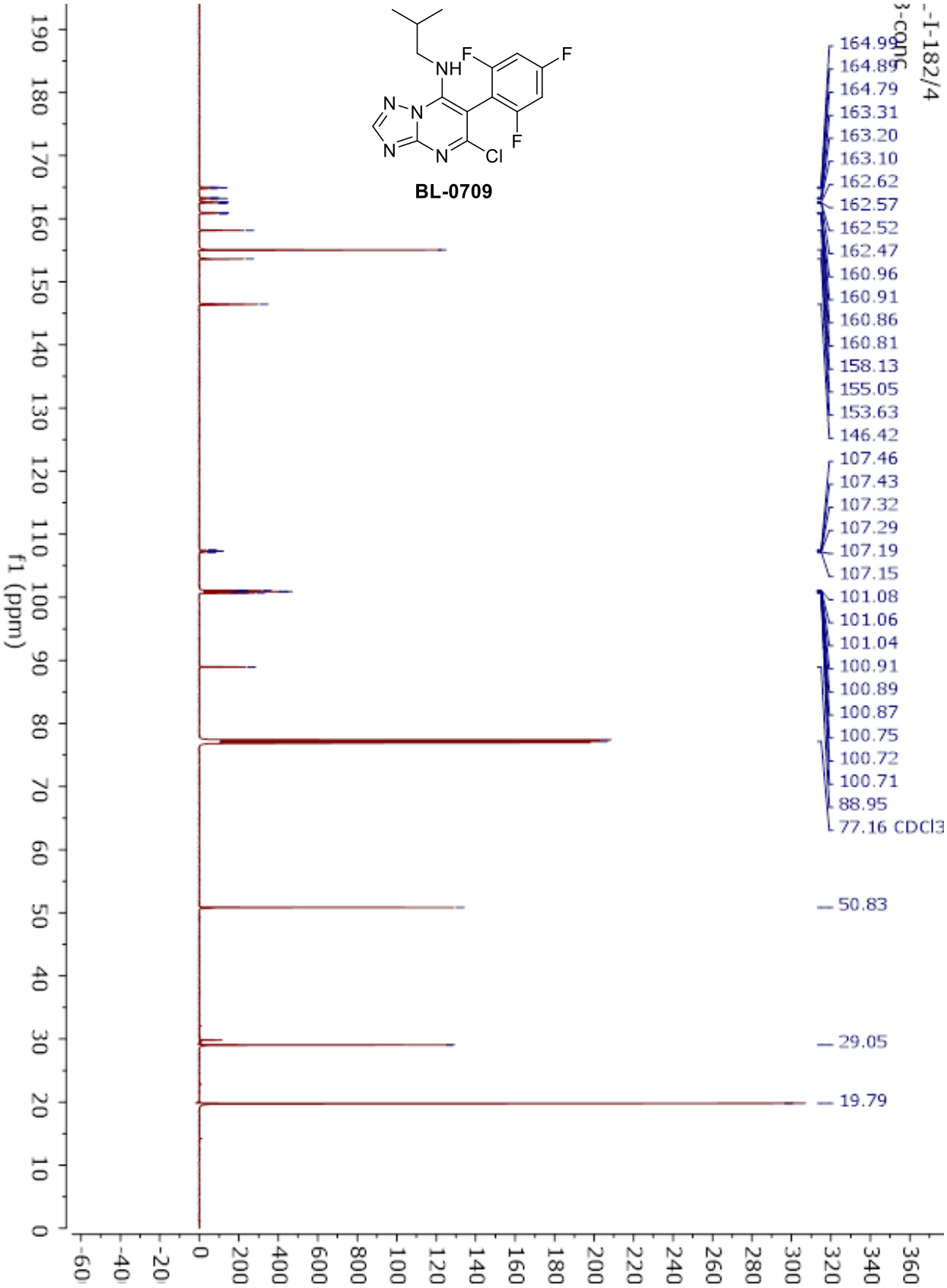
BL-0709
-I-182/4
164.99
164.89
164.79
163.31
163.20
163.10
162.62
162.57
162.52
162.47
160.96
160.91
160.86
160.81
158.13
155.05
153.63
146.42
107.46
107.43
107.32
107.29
107.19
107.15
101.08
101.06
101.04
100.91
100.89
100.87
100.75
100.72
100.71
88.95
77.16 CDCl3
50.83
29.05
19.79
f1 (ppm)

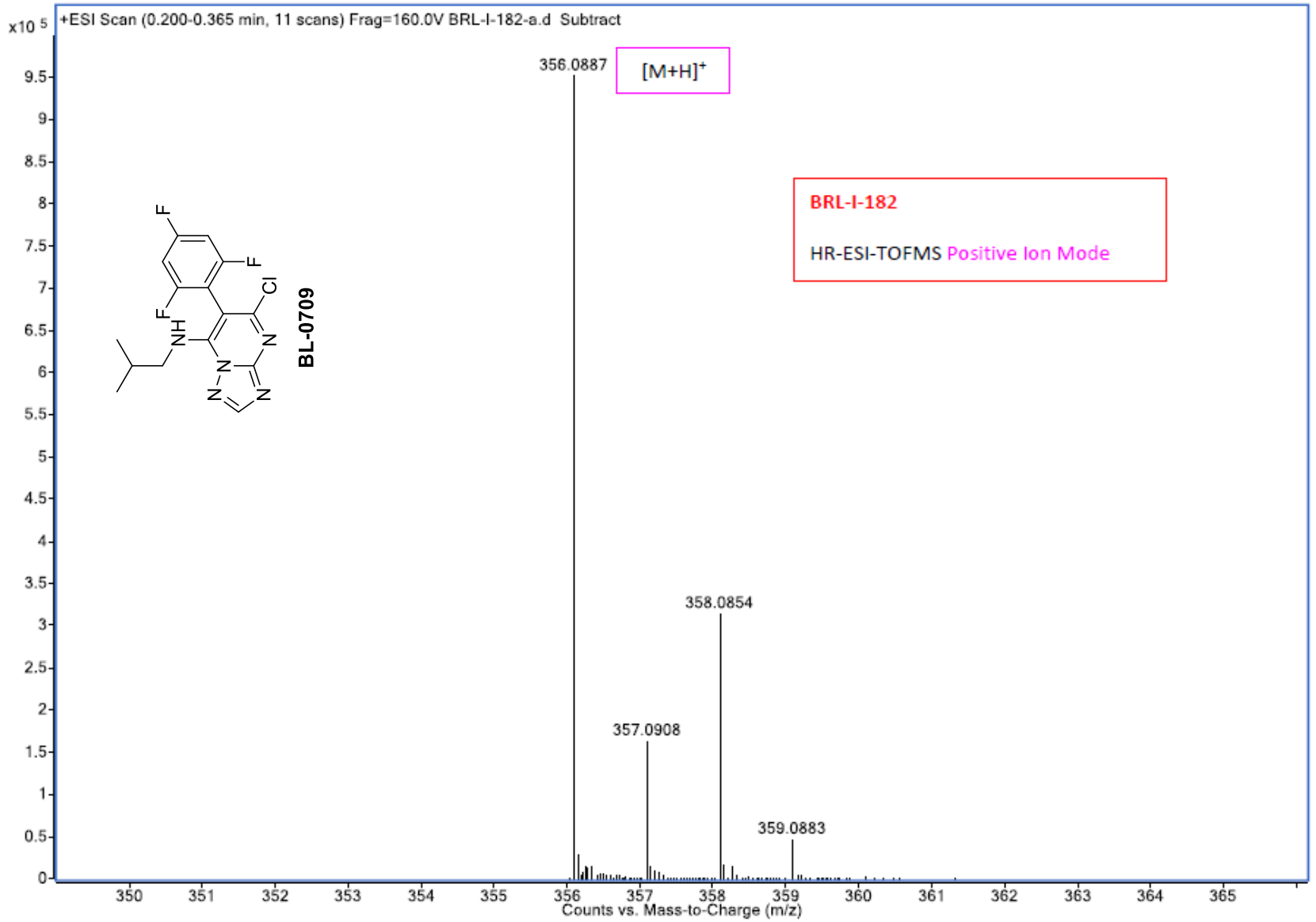
+ESI Scan (0.200-0.365 min, 11 scans) Frag=160.0V BRL-I-182-a.d Subtract
x10 5
356.0887
[M+H]+
BRL-I-182
HR-ESI-TOFMS Positive Ion Mode
BL-0709
358.0854
357.0908
359.0883
Counts vs. Mass-to-Charge (m/z)

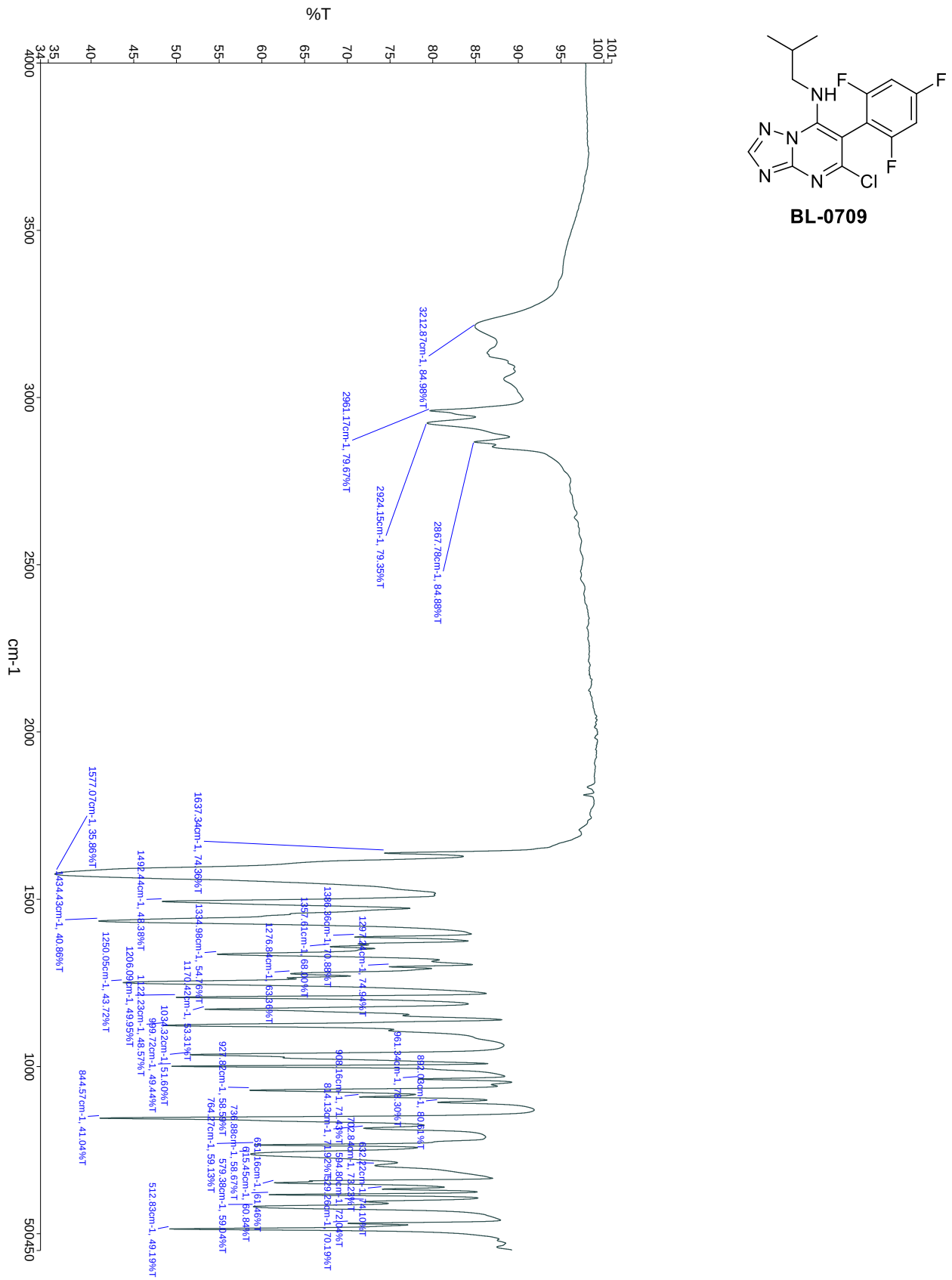
%T
cm-1
3212.87cm-1, 84.98%T
2961.17cm-1, 79.67%T
2924.15cm-1, 79.35%T
2867.78cm-1, 84.88%T
1637.34cm-1, 74.36%T
1577.07cm-1, 35.86%T
1492.44cm-1, 48.38%T
1434.43cm-1, 40.86%T
1357.61cm-1, 68.10%T
1334.98cm-1, 54.76%T
1276.84cm-1, 63.86%T
1250.05cm-1, 43.72%T
1206.09cm-1, 49.95%T
1170.42cm-1, 53.31%T
1122.23cm-1, 48.57%T
1034.32cm-1, 51.60%T
999.72cm-1, 49.44%T
961.34cm-1, 78.30%T
927.82cm-1, 58.59%T
908.16cm-1, 71.43%T
882.70cm-1, 80.61%T
844.57cm-1, 41.04%T
814.13cm-1, 71.92%T
764.77cm-1, 59.13%T
738.88cm-1, 58.67%T
702.84cm-1, 78.23%T
651.16cm-1, 61.46%T
632.22cm-1, 74.10%T
615.45cm-1, 60.84%T
584.80cm-1, 72.04%T
579.38cm-1, 59.04%T
529.26cm-1, 70.19%T
512.83cm-1, 49.19%T

NH
F
F
F
N
N
N
N
Cl

BL-0709

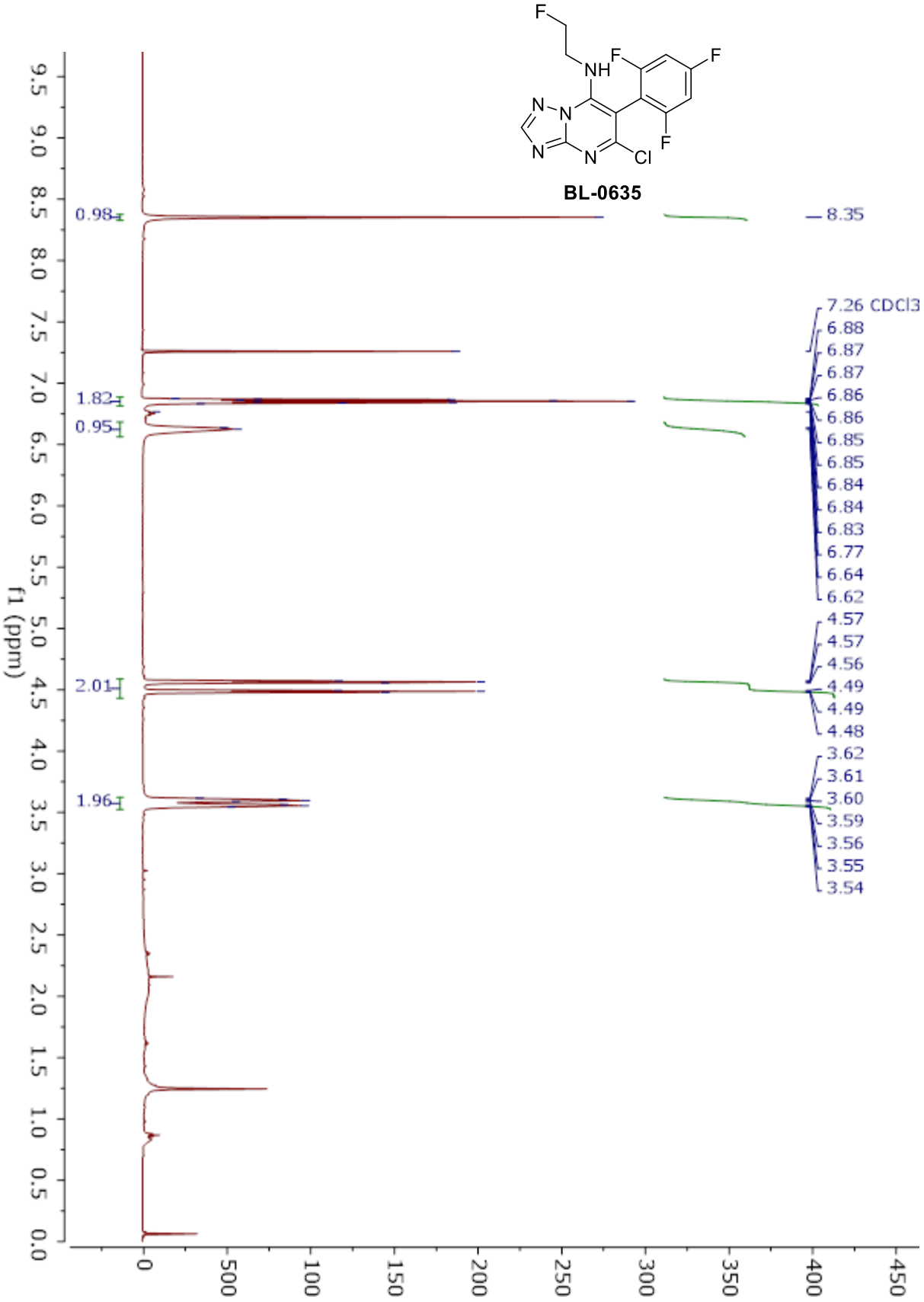
BL-0635
f1 (ppm)
0.98
1.82
0.95
2.01
1.96
8.35
7.26 CDCl3
6.88
6.87
6.87
6.86
6.86
6.85
6.85
6.84
6.84
6.83
6.77
6.64
6.62
4.57
4.57
4.56
4.49
4.49
4.48
3.62
3.61
3.60
3.59
3.56
3.55
3.54

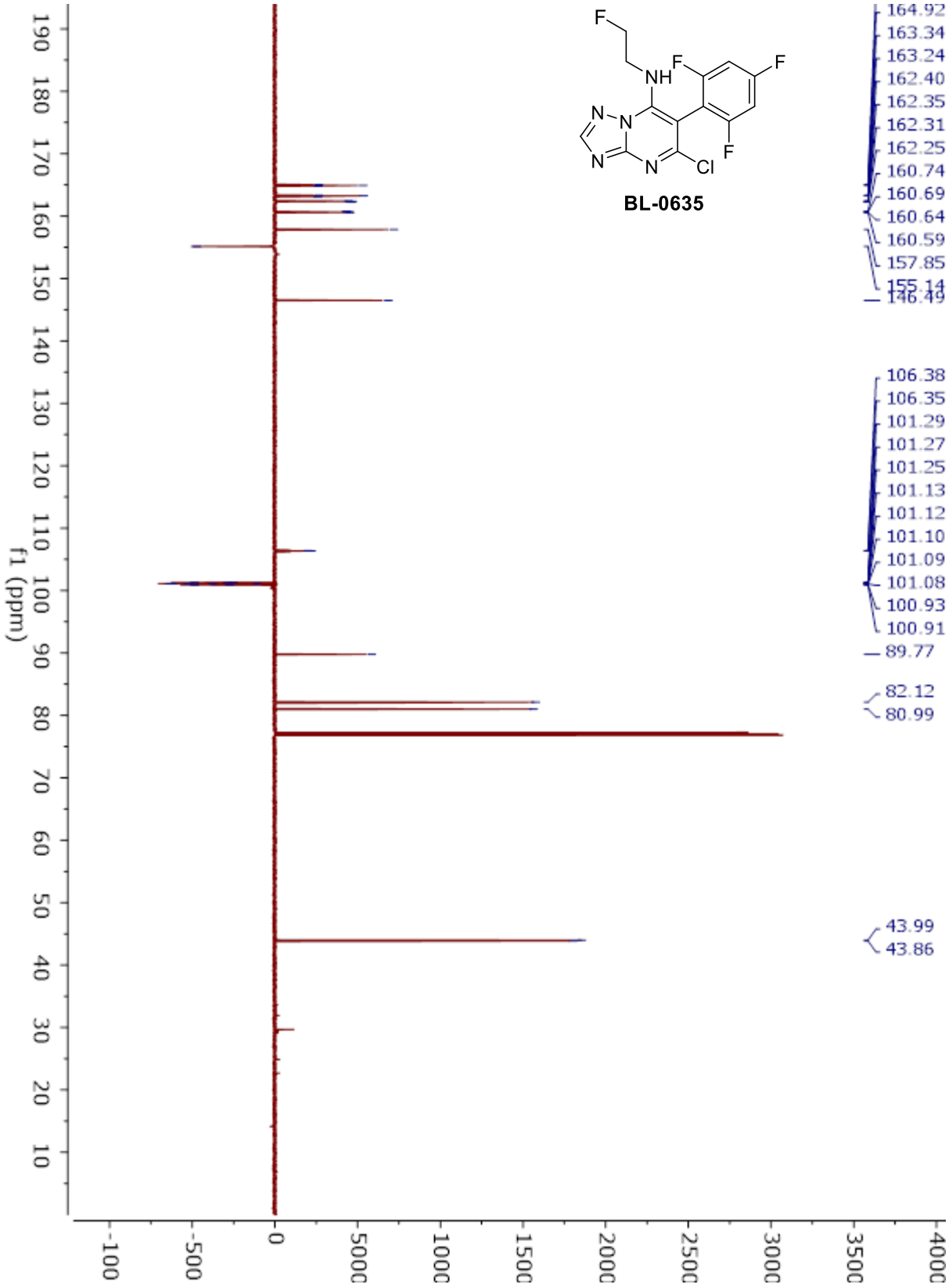
BL-0635
164.92
163.34
163.24
162.40
162.35
162.31
162.25
160.74
160.69
160.64
160.59
157.85
155.14
146.49
106.38
106.35
101.29
101.27
101.25
101.13
101.12
101.10
101.09
101.08
100.93
100.91
89.77
82.12
80.99
43.99
43.86
f1 (ppm)

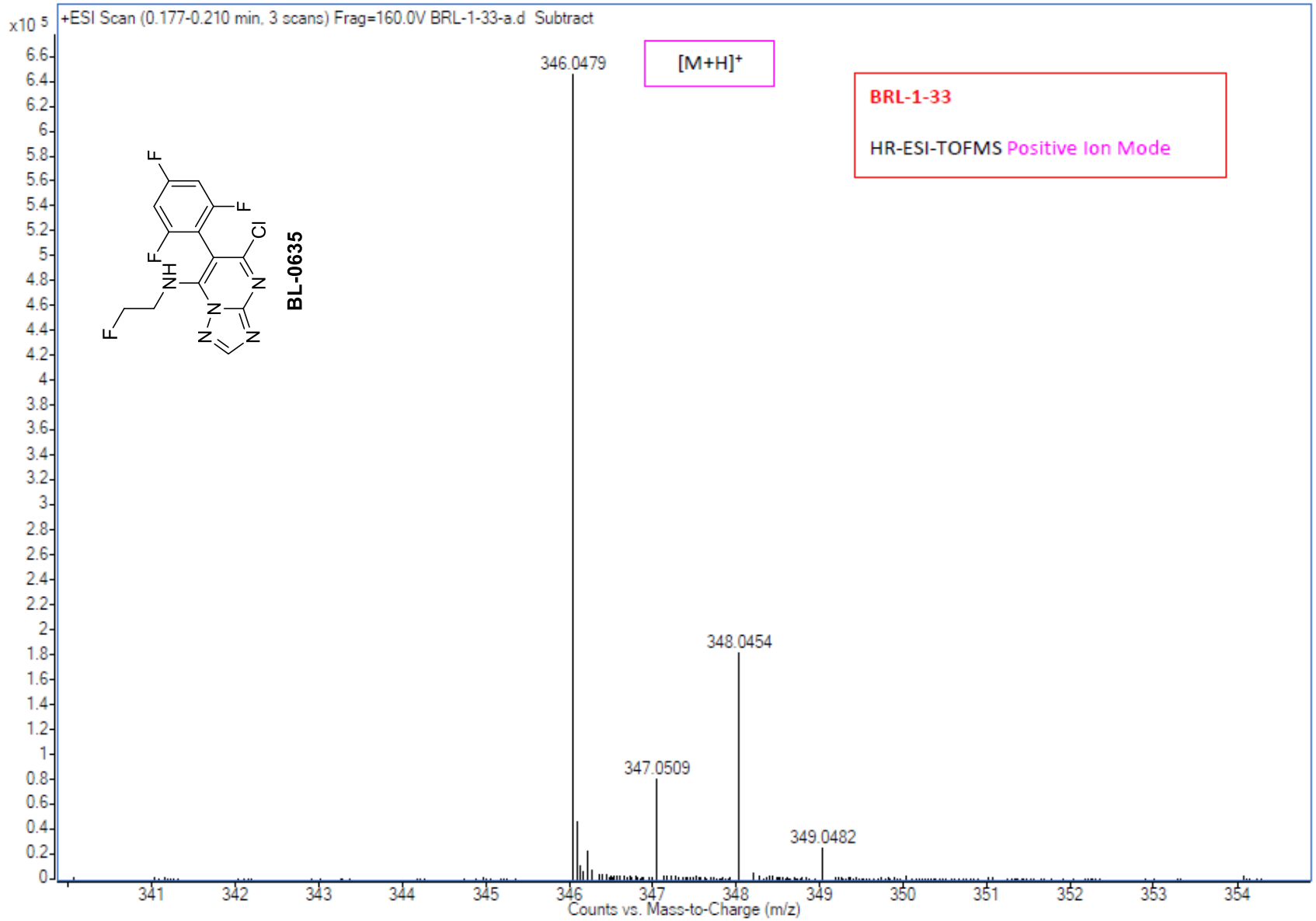
+ESI Scan (0.177-0.210 min, 3 scans) Frag=160.0V BRL-1-33-a.d Subtract
x10 5
346.0479
[M+H]+
BRL-1-33
HR-ESI-TOFMS Positive Ion Mode
BL-0635
348.0454
347.0509
349.0482
Counts vs. Mass-to-Charge (m/z)

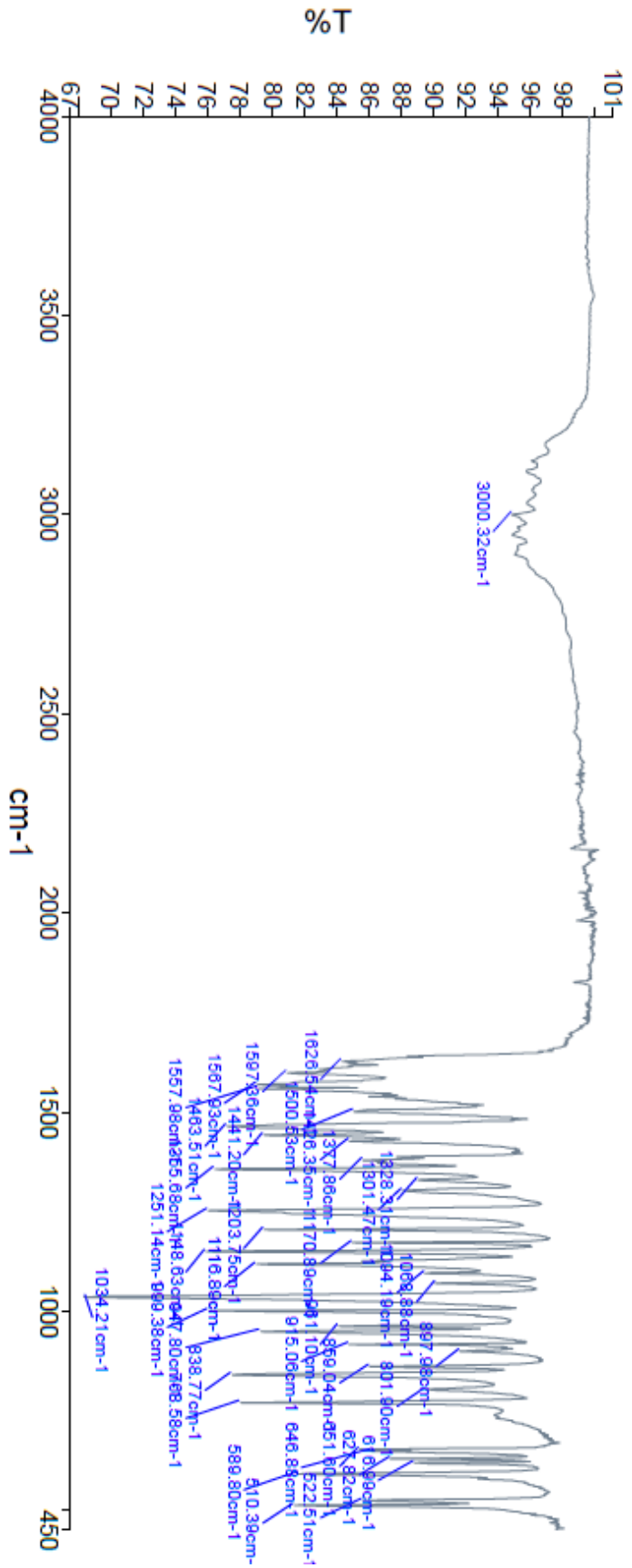

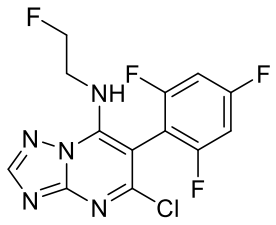

BL-0635

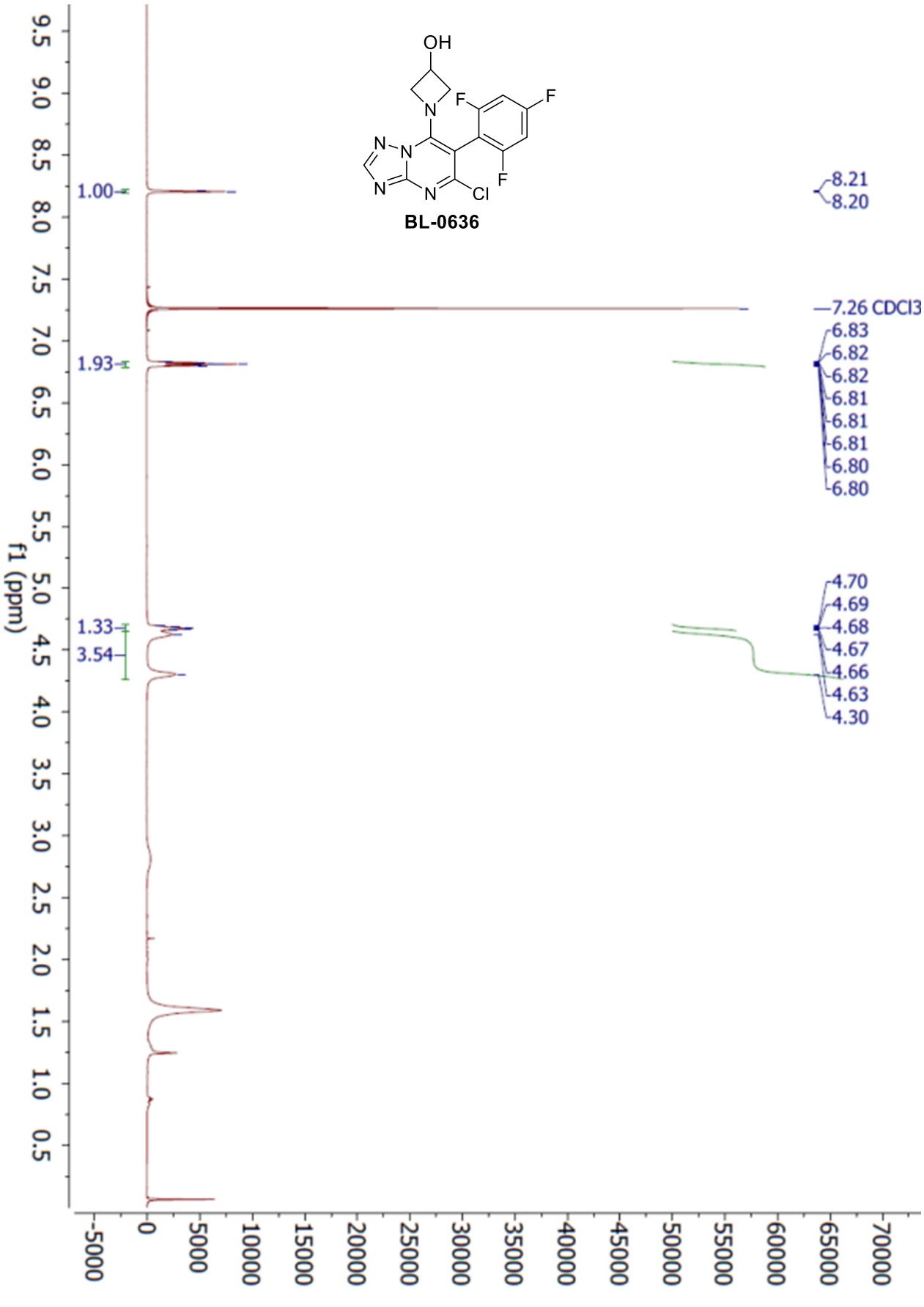
OH
N
F
F
F
N
N
N
N
Cl
BL-0636
1.00
1.93
1.33
3.54
8.21
8.20
7.26 CDCl3
6.83
6.82
6.82
6.81
6.81
6.81
6.80
6.80
4.70
4.69
4.68
4.67
4.66
4.63
4.30
f1 (ppm)
9.5 9.0 8.5 8.0 7.5 7.0 6.5 6.0 5.5 5.0 4.5 4.0 3.5 3.0 2.5 2.0 1.5 1.0 0.5
-5000 0 5000 10000 15000 20000 25000 30000 35000 40000 45000 50000 55000 60000 65000 70000

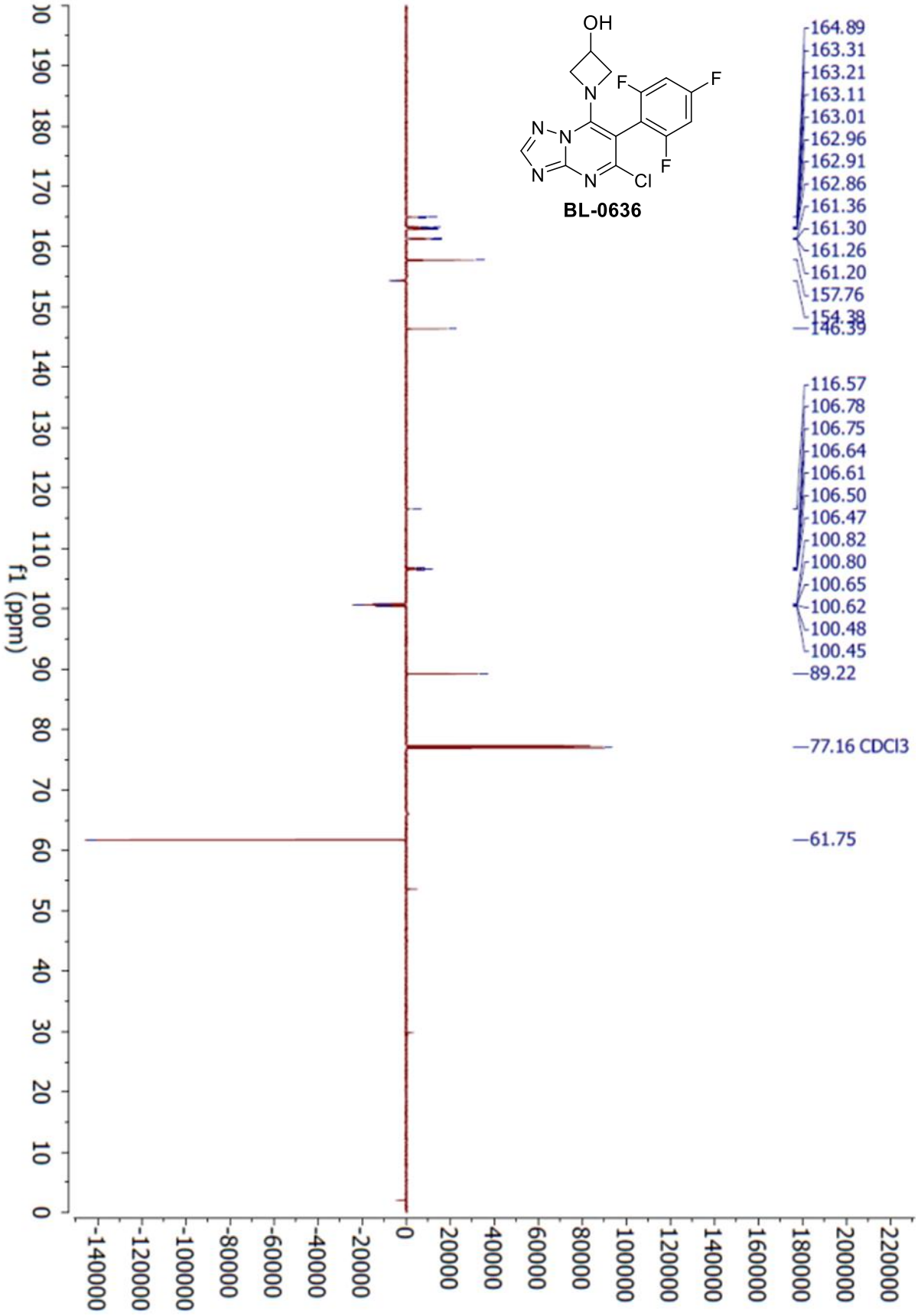
OH
N
F
F
F
N
N
N
N
Cl
BL-0636
164.89
163.31
163.21
163.11
163.01
162.96
162.91
162.86
161.36
161.30
161.26
161.20
157.76
154.38
146.39
116.57
106.78
106.75
106.64
106.61
106.50
106.47
100.82
100.80
100.65
100.62
100.48
100.45
89.22
77.16 CDCl3
61.75
f1 (ppm)

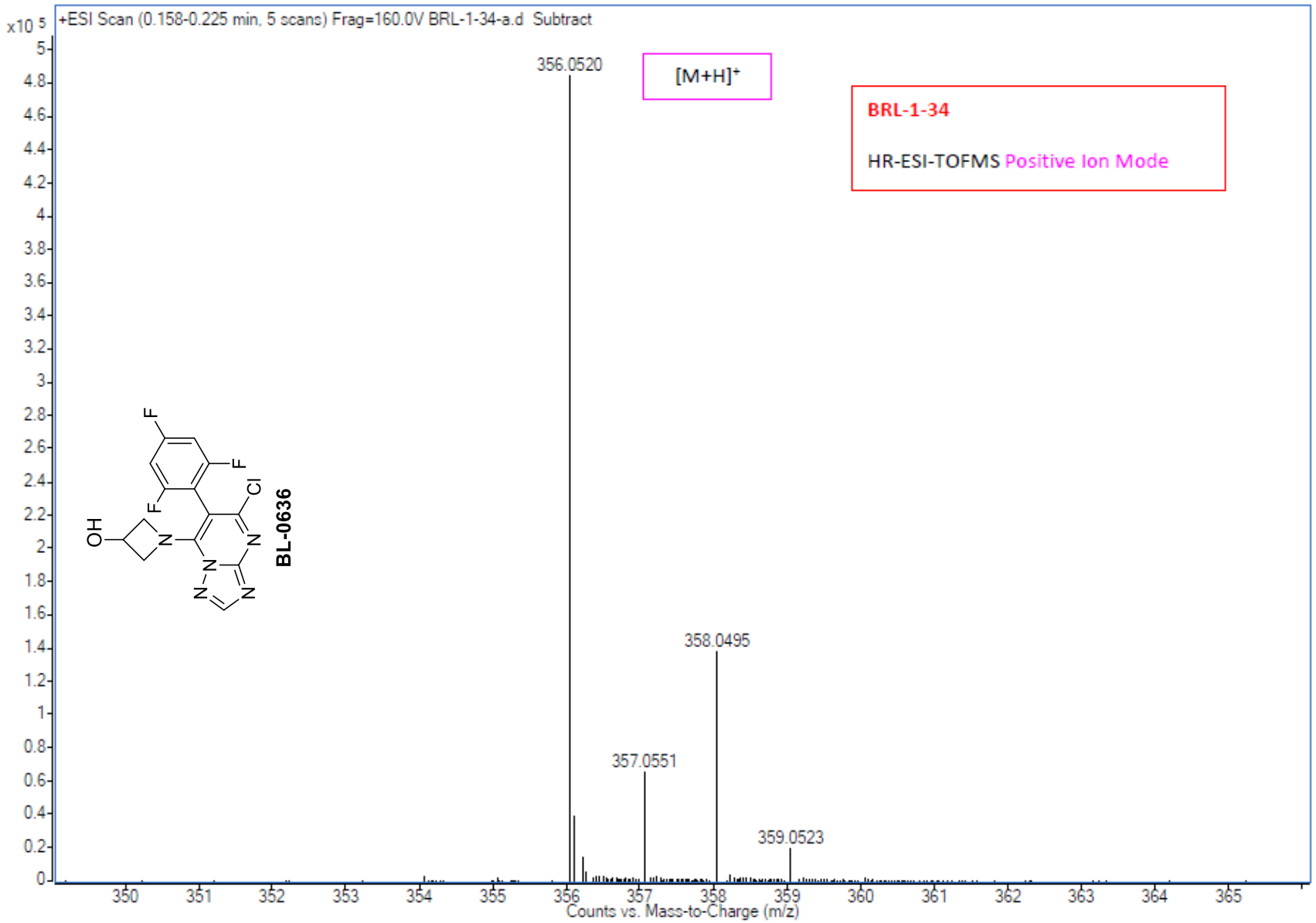
+ESI Scan (0.158-0.225 min, 5 scans) Frag=160.0V BRL-1-34-a.d Subtract
x10 5
356.0520
[M+H]+
BRL-1-34
HR-ESI-TOFMS Positive Ion Mode
358.0495
357.0551
359.0523
BL-0636
Counts vs. Mass-to-Charge (m/z)

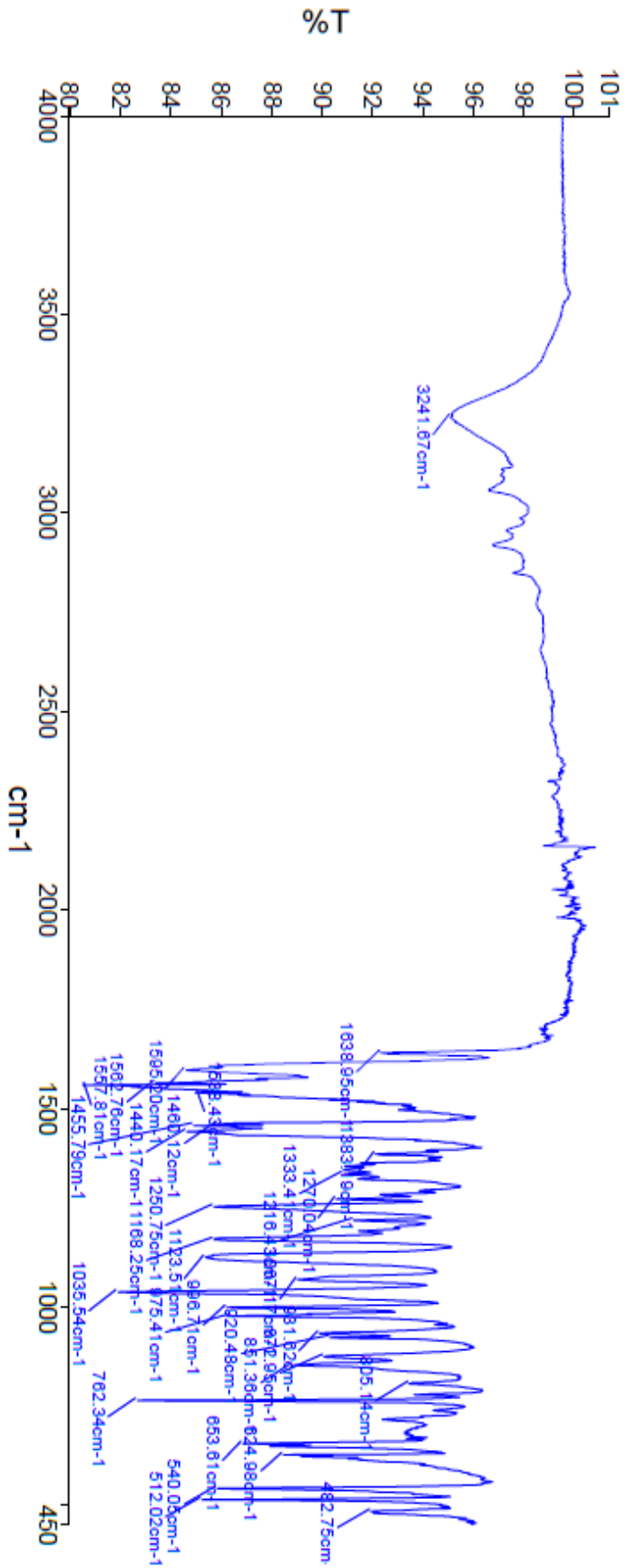
%T
cm-1
3241.67cm-1
1638.95cm-1
1455.79cm-1
1035.54cm-1
762.34cm-1
653.81cm-1
540.05cm-1
512.02cm-1

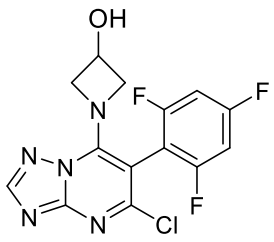
OH
N
F
F
N
N
F
N
N
Cl

BL-0636

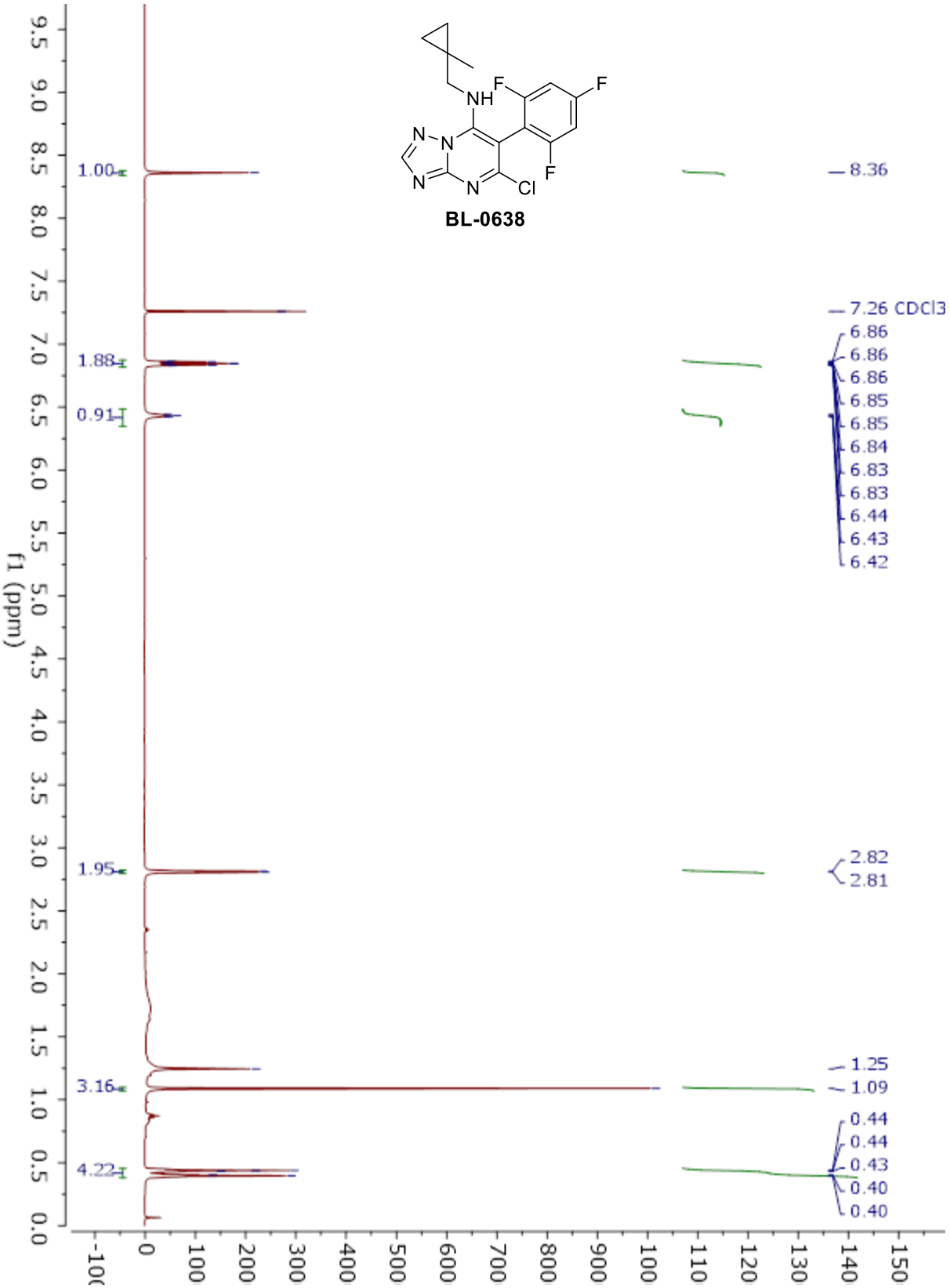
BL-0638
F
F
F
NH
N
N
N
N
Cl
1.00
1.88
0.91
1.95
3.16
4.22
8.36
7.26 CDCl3
6.86
6.86
6.86
6.85
6.85
6.84
6.83
6.83
6.44
6.43
6.42
2.82
2.81
1.25
1.09
0.44
0.44
0.43
0.40
0.40
f1 (ppm)

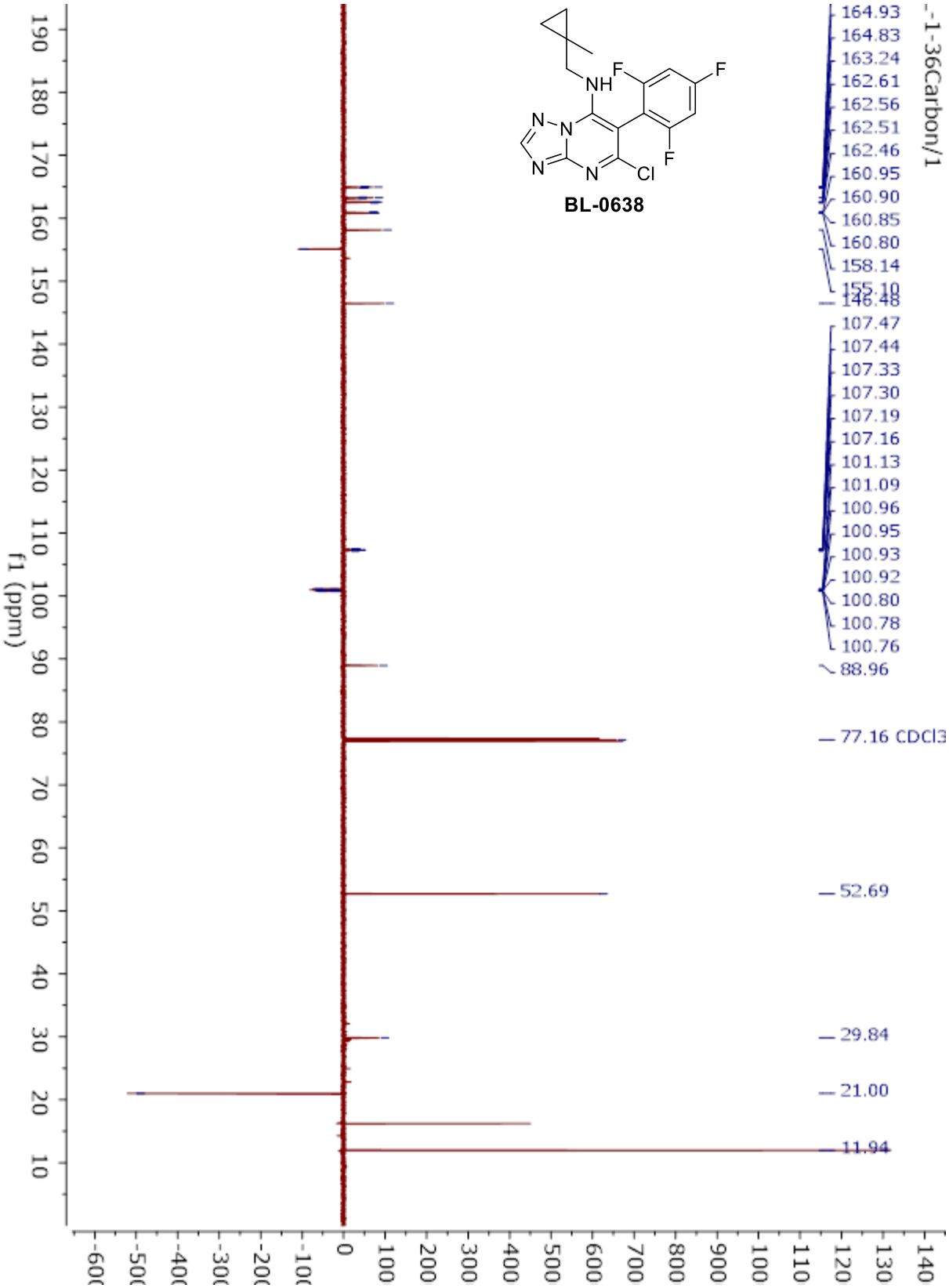
BL-0638
-1-36Carbon/1
164.93
164.83
163.24
162.61
162.56
162.51
162.46
160.95
160.90
160.85
160.80
158.14
155.10
146.48
107.47
107.44
107.33
107.30
107.19
107.16
101.13
101.09
100.96
100.95
100.93
100.92
100.80
100.78
100.76
88.96
77.16 CDCl3
52.69
29.84
21.00
11.94
f1 (ppm)

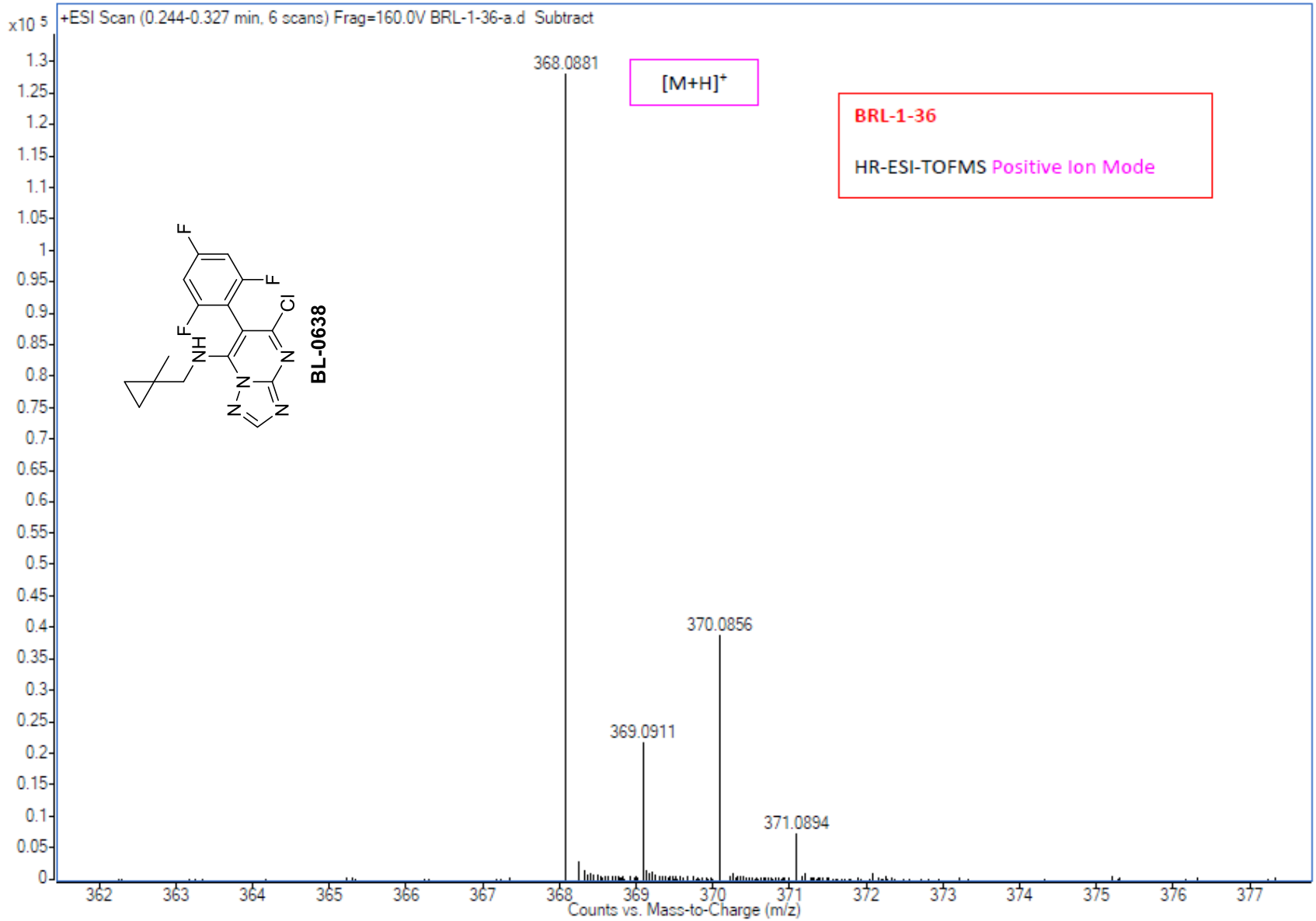
+ESI Scan (0.244-0.327 min, 6 scans) Frag=160.0V BRL-1-36-a.d Subtract
x10 5
1.3
1.25
1.2
1.15
1.1
1.05
1
0.95
0.9
0.85
0.8
0.75
0.7
0.65
0.6
0.55
0.5
0.45
0.4
0.35
0.3
0.25
0.2
0.15
0.1
0.05
0
362
363
364
365
366
367
368
369
370
371
372
373
374
375
376
377
Counts vs. Mass-to-Charge (m/z)
368.0881
[M+H]+
370.0856
369.0911
371.0894
BRL-1-36
HR-ESI-TOFMS Positive Ion Mode
BL-0638
F
F
F
Cl
NH
N
N
N
N

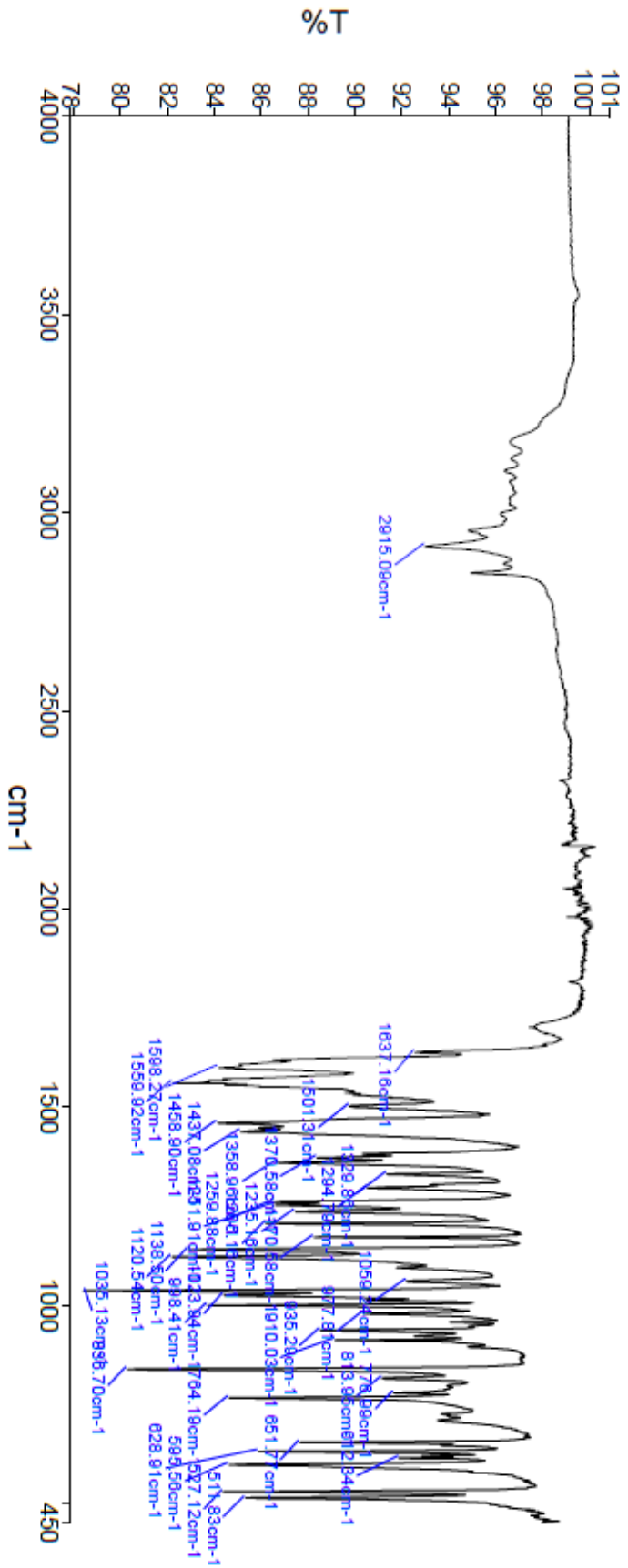
%T
cm-1
2915.09cm-1
1637.16cm-1
1501.31cm-1
1598.27cm-1
1559.92cm-1
1458.90cm-1
1259.88cm-1
1138.50cm-1
1120.54cm-1
1036.13cm-1
998.41cm-1
935.28cm-1
977.81cm-1
1910.03cm-1
813.95cm-1
764.19cm-1
651.27cm-1
628.91cm-1

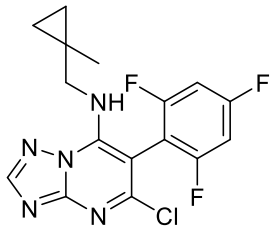
NH
F
F
F
N
N
N
N
Cl

BL-0638

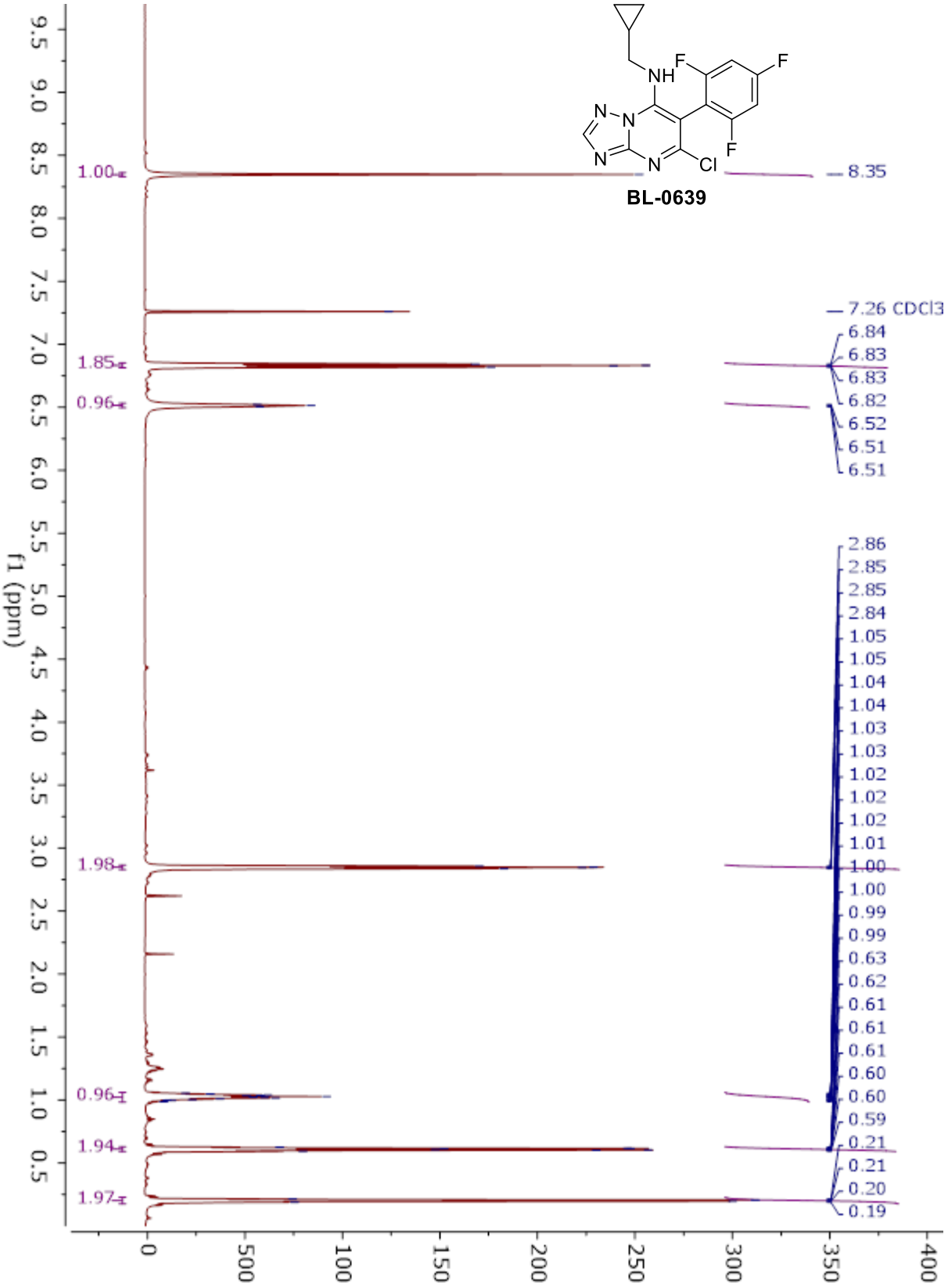
BL-0639
f1 (ppm)
1.00
1.85
0.96
1.98
0.96
1.94
1.97
8.35
7.26 CDCl3
6.84
6.83
6.83
6.82
6.52
6.51
6.51
2.86
2.85
2.85
2.84
1.05
1.05
1.04
1.04
1.03
1.03
1.02
1.02
1.02
1.01
1.00
1.00
0.99
0.99
0.63
0.62
0.61
0.61
0.61
0.60
0.60
0.59
0.21
0.21
0.20
0.19

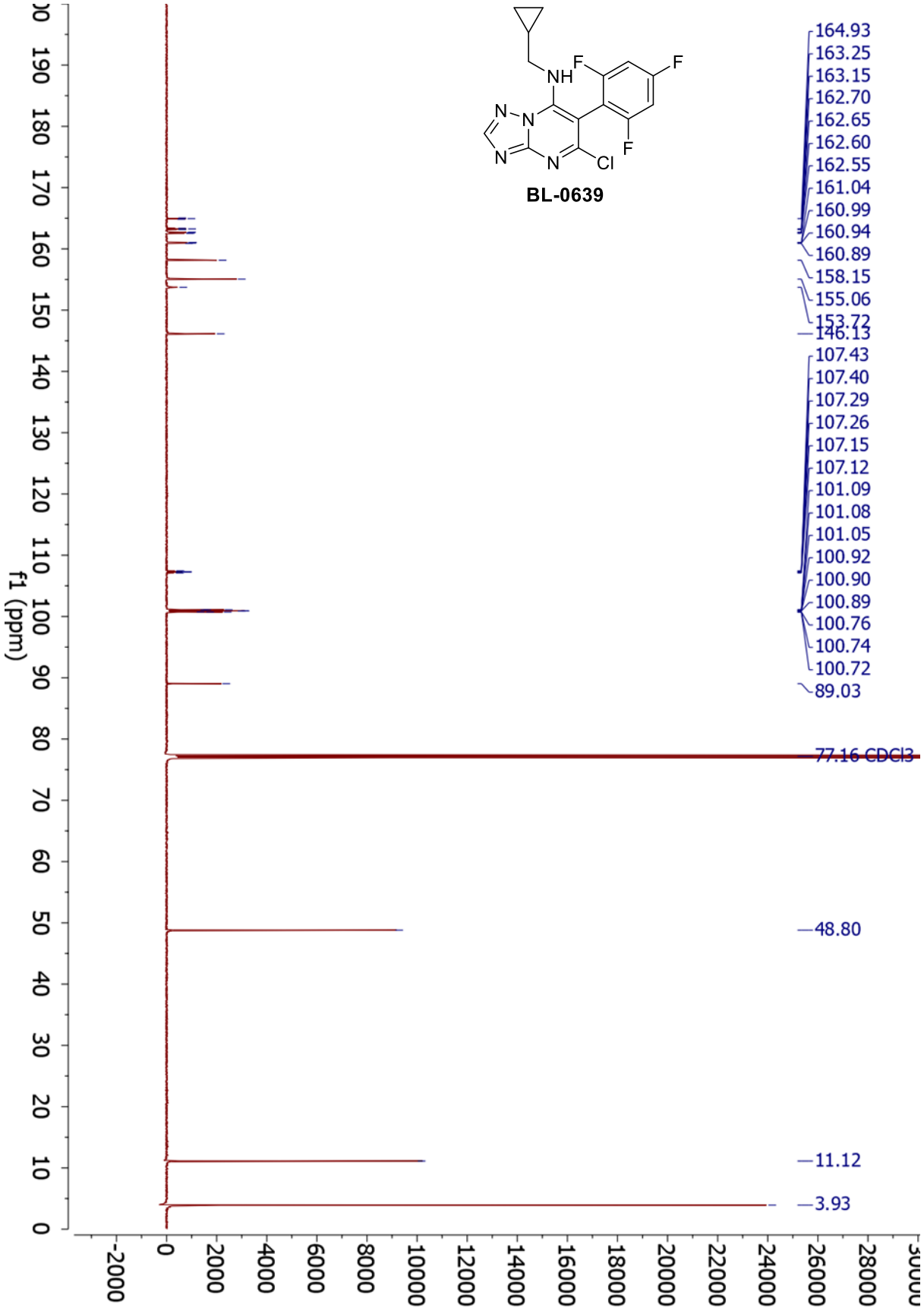
BL-0639
164.93
163.25
163.15
162.70
162.65
162.60
162.55
161.04
160.99
160.94
160.89
158.15
155.06
153.72
146.13
107.43
107.40
107.29
107.26
107.15
107.12
101.09
101.08
101.05
100.92
100.90
100.89
100.76
100.74
100.72
89.03
77.16 CDCl3
48.80
11.12
3.93
f1 (ppm)

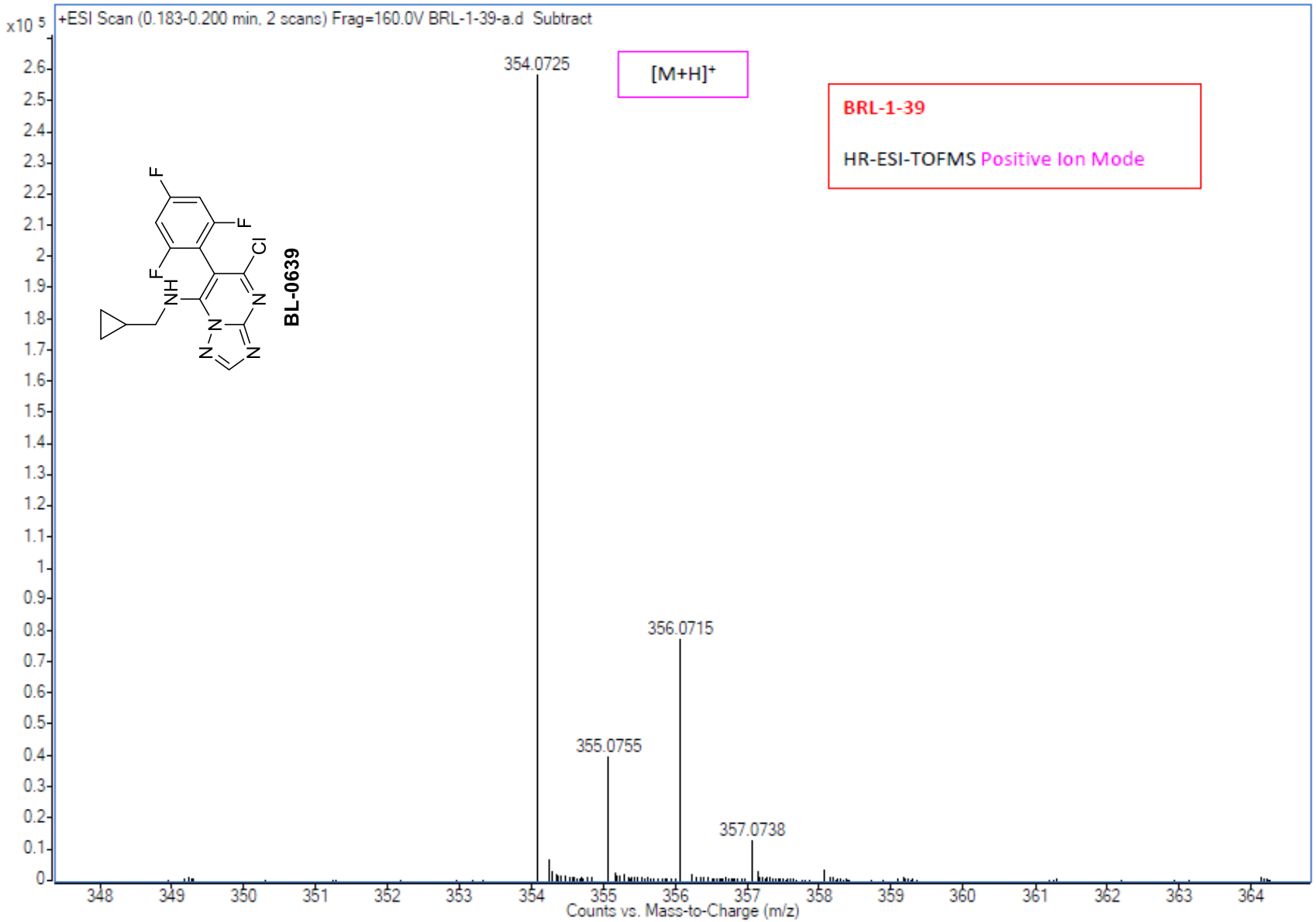
+ESI Scan (0.183-0.200 min, 2 scans) Frag=160.0V BRL-1-39-a.d Subtract
x10 5
354.0725
[M+H]+
BRL-1-39
HR-ESI-TOFMS Positive Ion Mode
BL-0639
356.0715
355.0755
357.0738
Counts vs. Mass-to-Charge (m/z)

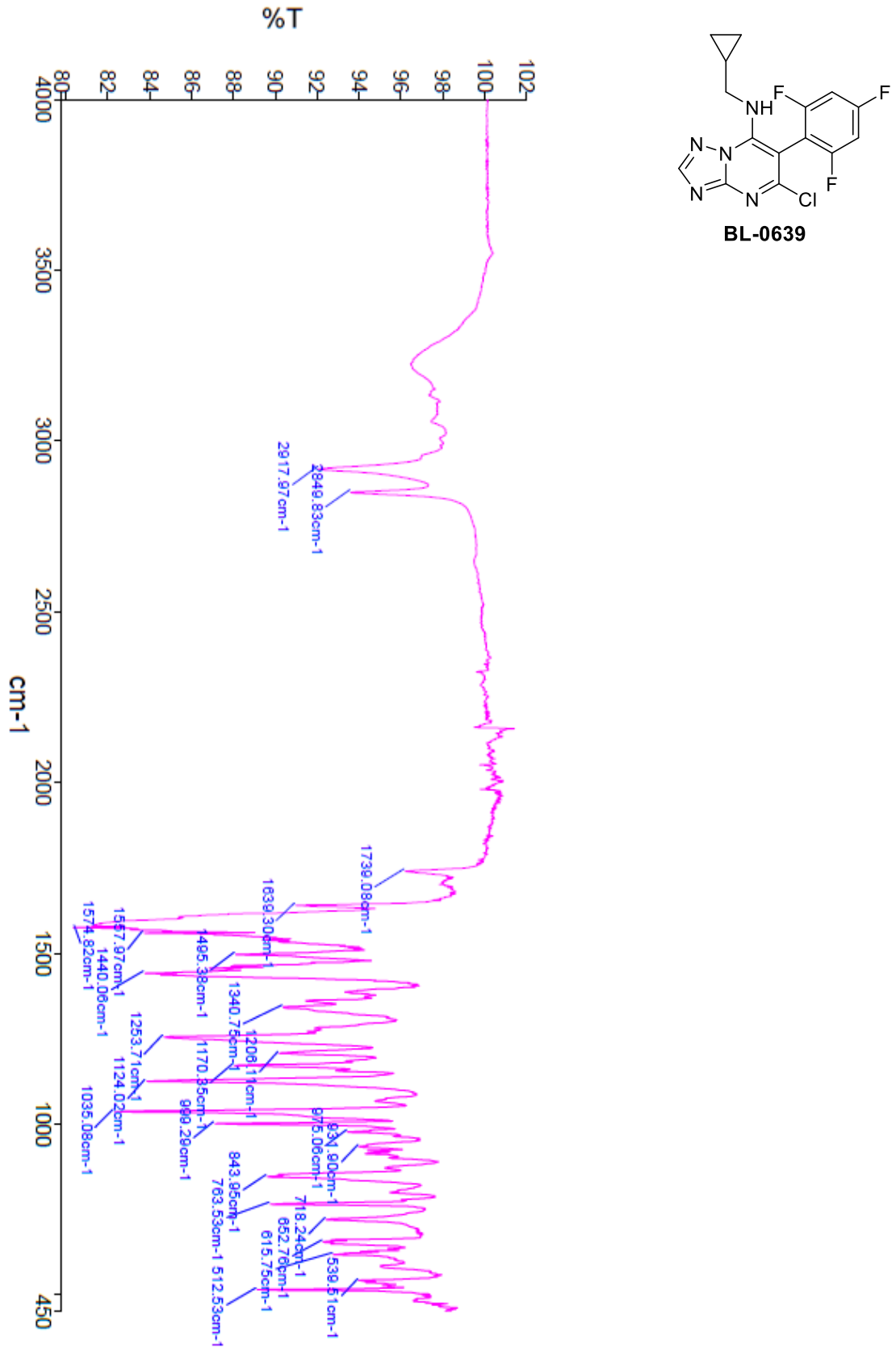
%T
cm-1
2917.97cm-1
2849.83cm-1
1739.08cm-1
1639.30cm-1
1574.82cm-1
1557.97cm-1
1495.38cm-1
1440.06cm-1
1340.75cm-1
1253.71cm-1
1208.11cm-1
1170.85cm-1
1124.02cm-1
1035.08cm-1
999.29cm-1
975.06cm-1
931.90cm-1
843.95cm-1
763.53cm-1
718.24cm-1
652.76cm-1
615.75cm-1
539.51cm-1
512.53cm-1
NH
F
F
F
N
N
N
N
Cl
BL-0639

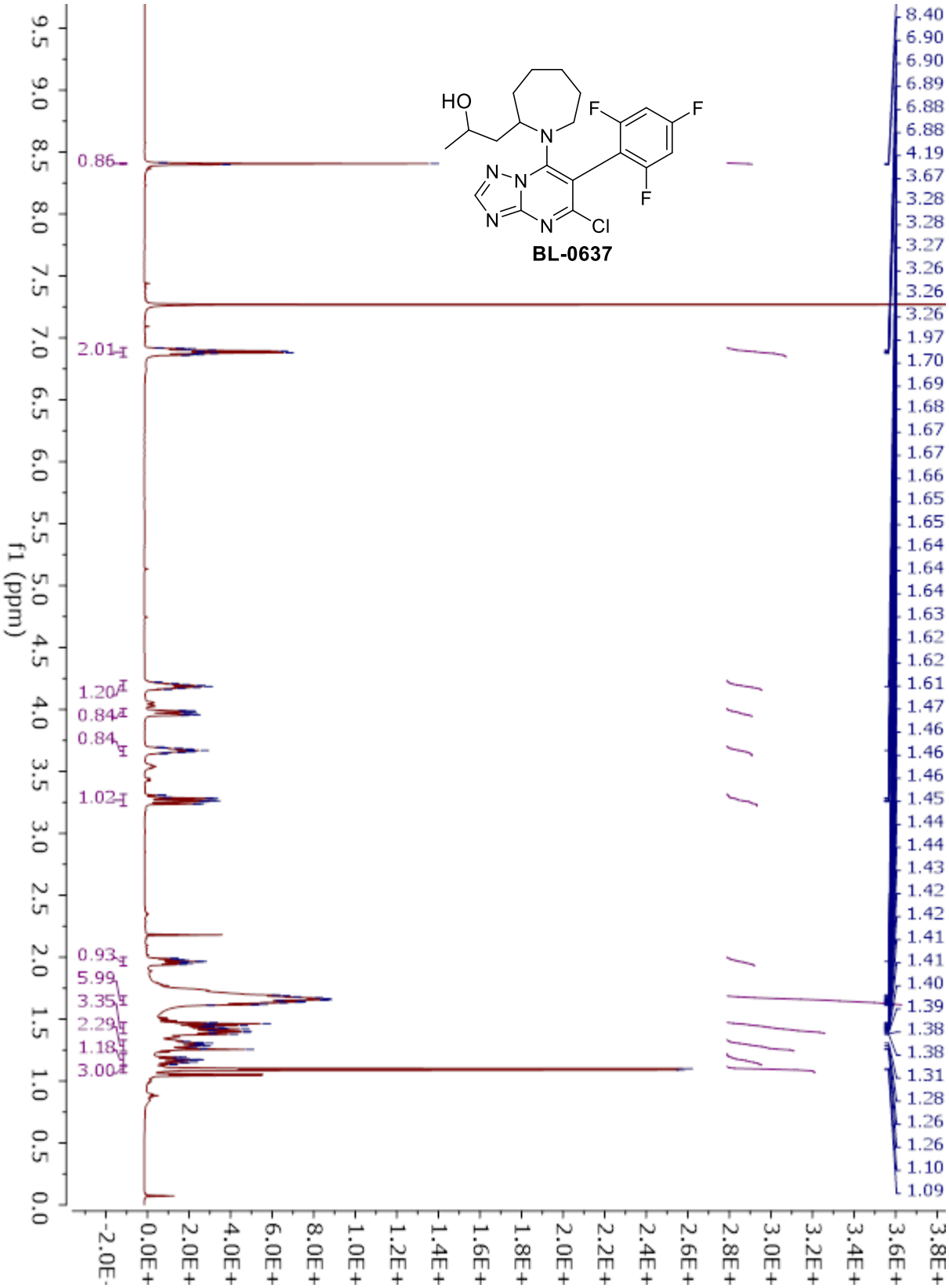
HO
N
F
F
F
N
N
N
N
Cl
BL-0637
f1 (ppm)
0.86
2.01
1.20
0.84
0.84
1.02
0.93
5.99
3.35
2.29
1.18
3.00

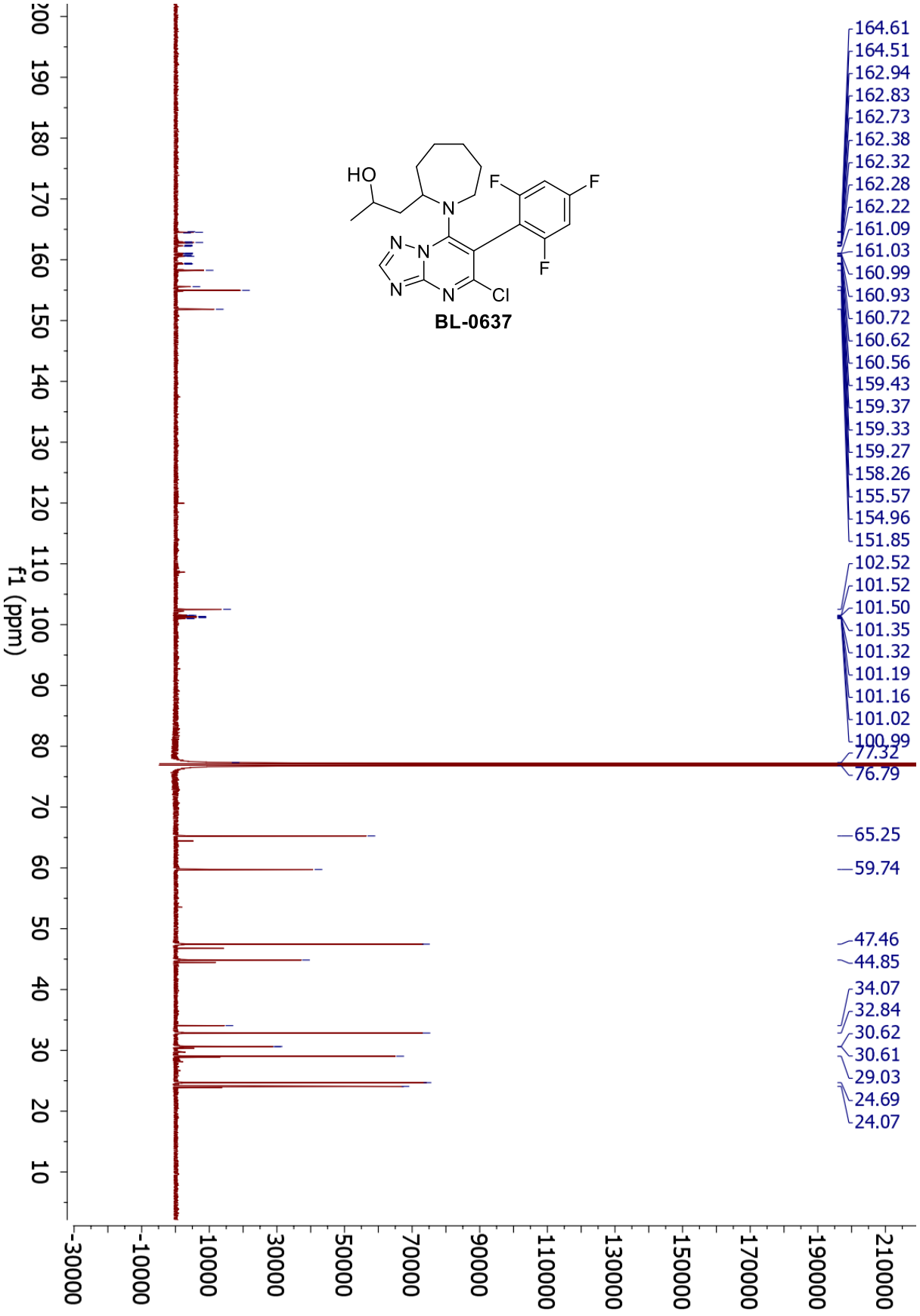
HO
F
F
F
N
N
N
N
N
Cl
BL-0637
164.61
164.51
162.94
162.83
162.73
162.38
162.32
162.28
162.22
161.09
161.03
160.99
160.93
160.72
160.62
160.56
159.43
159.37
159.33
159.27
158.26
155.57
154.96
151.85
102.52
101.52
101.50
101.35
101.32
101.19
101.16
101.02
100.99
77.32
76.79
65.25
59.74
47.46
44.85
34.07
32.84
30.62
30.61
29.03
24.69
24.07
f1 (ppm)

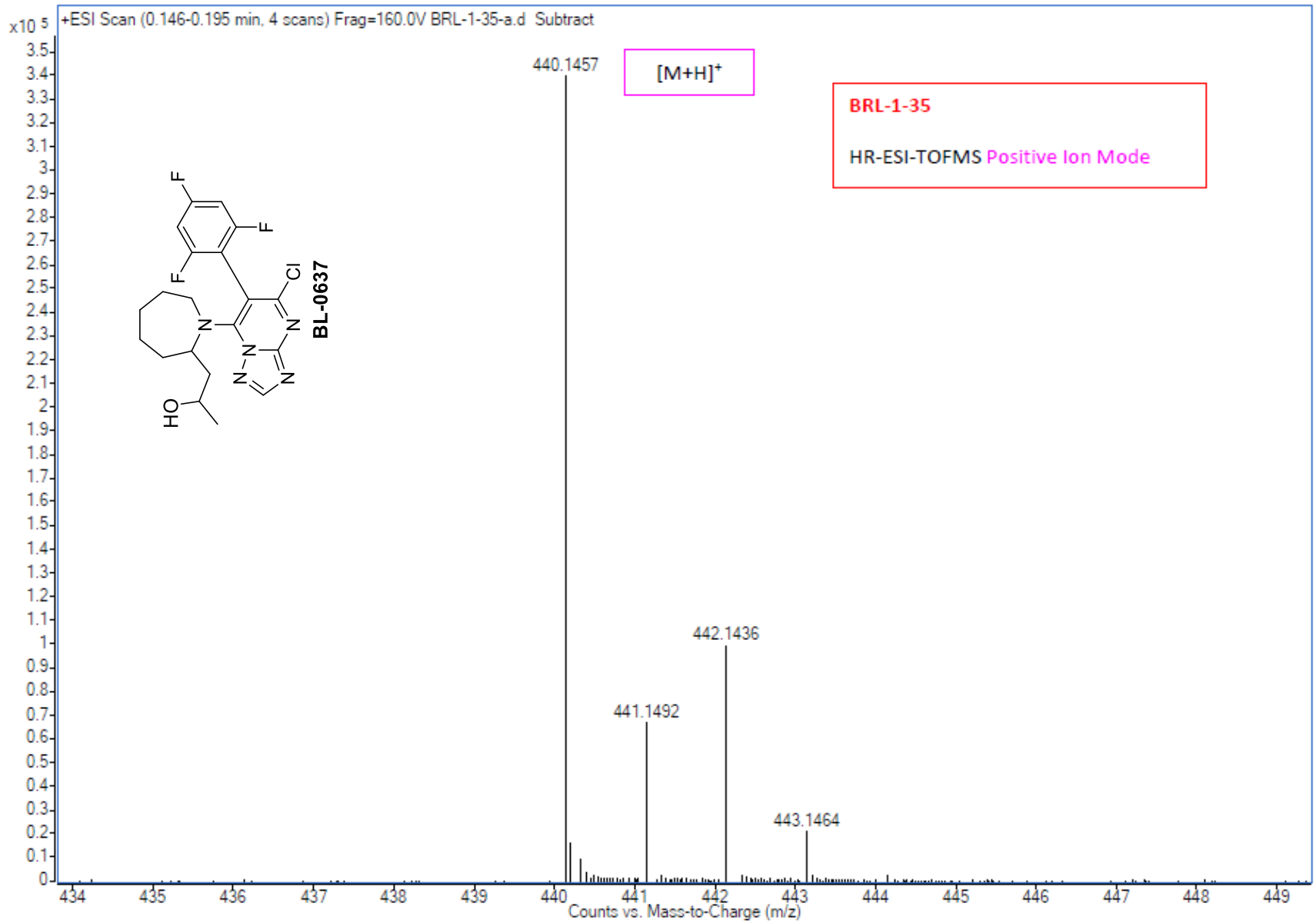
+ESI Scan (0.146-0.195 min, 4 scans) Frag=160.0V BRL-1-35-a.d Subtract
x10 5
440.1457
[M+H]+
BRL-1-35
HR-ESI-TOFMS Positive Ion Mode
BL-0637
442.1436
441.1492
443.1464
Counts vs. Mass-to-Charge (m/z)

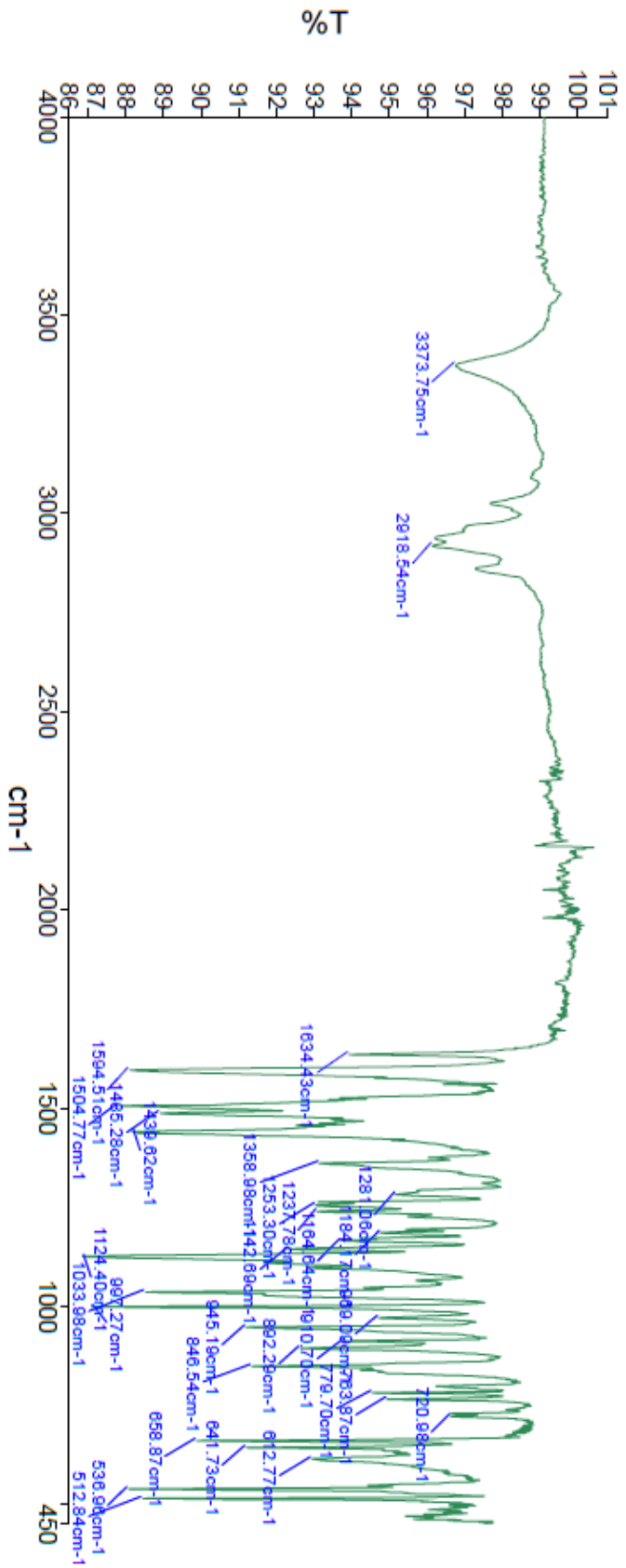
%T
cm-1
3373.75cm-1
2918.54cm-1
1634.43cm-1
1594.51cm-1
1504.77cm-1
1446.28cm-1
1439.62cm-1
1358.98cm-1
1253.30cm-1
1237.78cm-1
1184.64cm-1
1128.40cm-1
1033.98cm-1
999.27cm-1
945.19cm-1
892.29cm-1
846.54cm-1
779.70cm-1
763.87cm-1
720.98cm-1
658.87cm-1
641.73cm-1
612.77cm-1
536.90cm-1
512.84cm-1

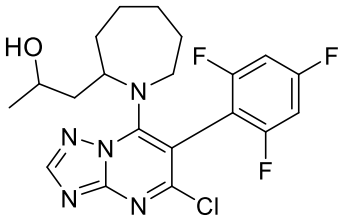
HO
N
F
F
F
N
N
N
N
Cl

BL-0637

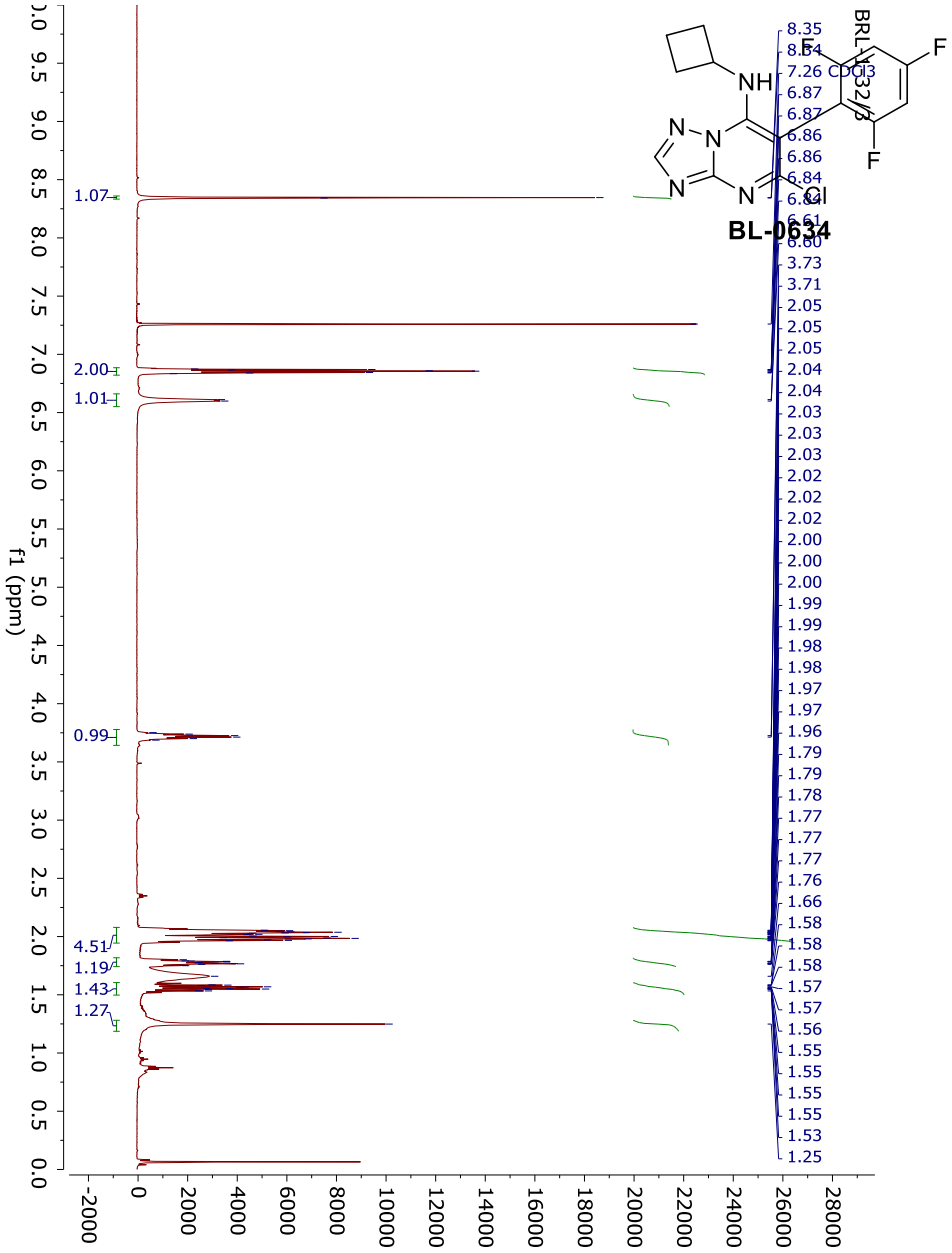
BL-0634
BRL-11532/3
NH
N
N
N
N
F
F
Cl
8.35
8.34
7.26 CDCl3
6.87
6.87
6.86
6.86
6.84
6.84
6.61
6.60
3.73
3.71
2.05
2.05
2.05
2.04
2.04
2.03
2.03
2.03
2.02
2.02
2.02
2.00
2.00
2.00
1.99
1.99
1.98
1.98
1.97
1.97
1.96
1.79
1.79
1.78
1.77
1.77
1.77
1.76
1.66
1.58
1.58
1.58
1.57
1.57
1.56
1.55
1.55
1.55
1.55
1.53
1.25
1.07
2.00
1.01
0.99
4.51
1.19
1.43
1.27
f1 (ppm)

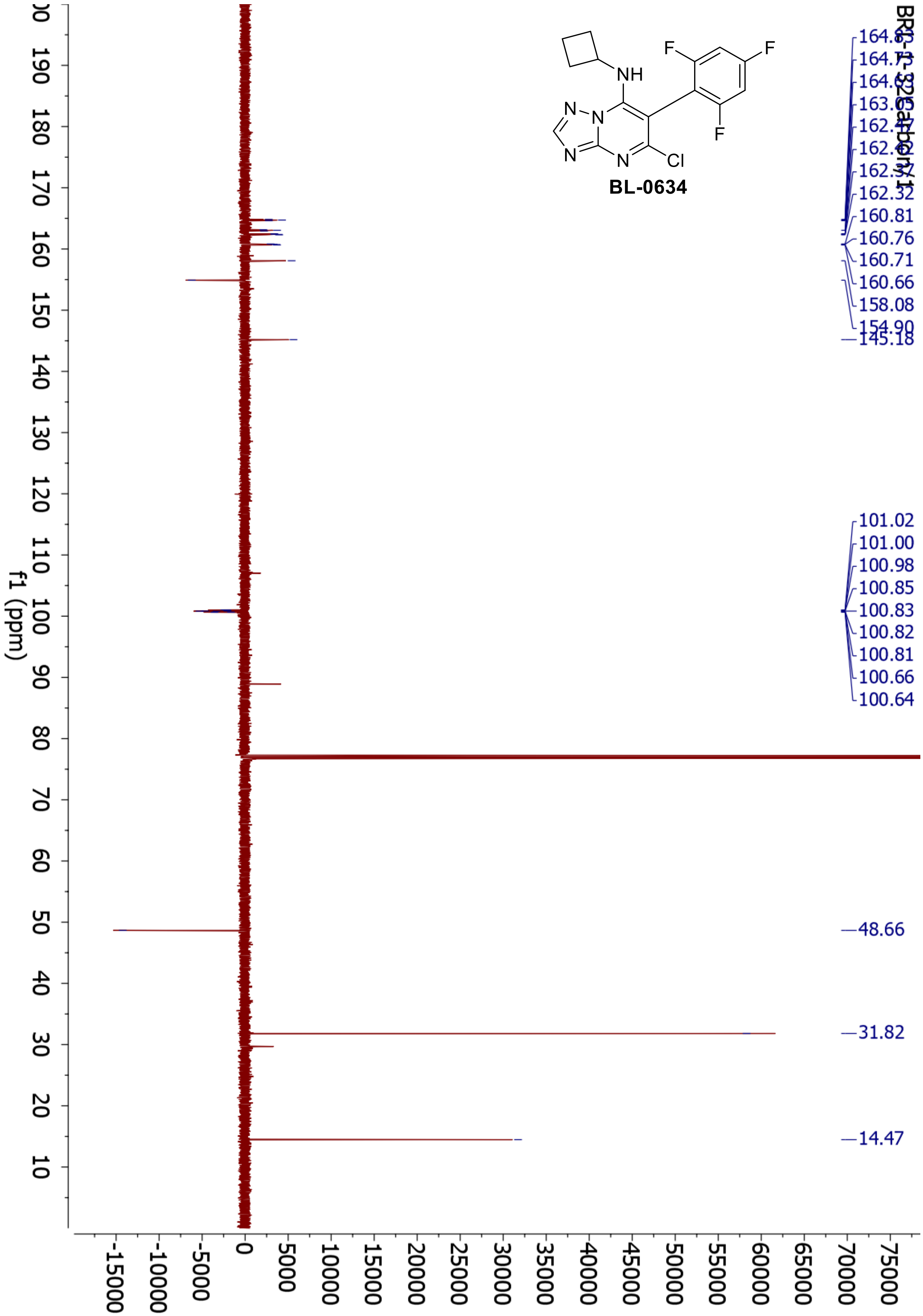
BL-0634
NH
N
F
Cl
162.32
160.81
160.76
160.71
160.66
158.08
145.18
101.02
101.00
100.98
100.85
100.83
100.82
100.81
100.66
100.64
48.66
31.82
14.47
f1 (ppm)

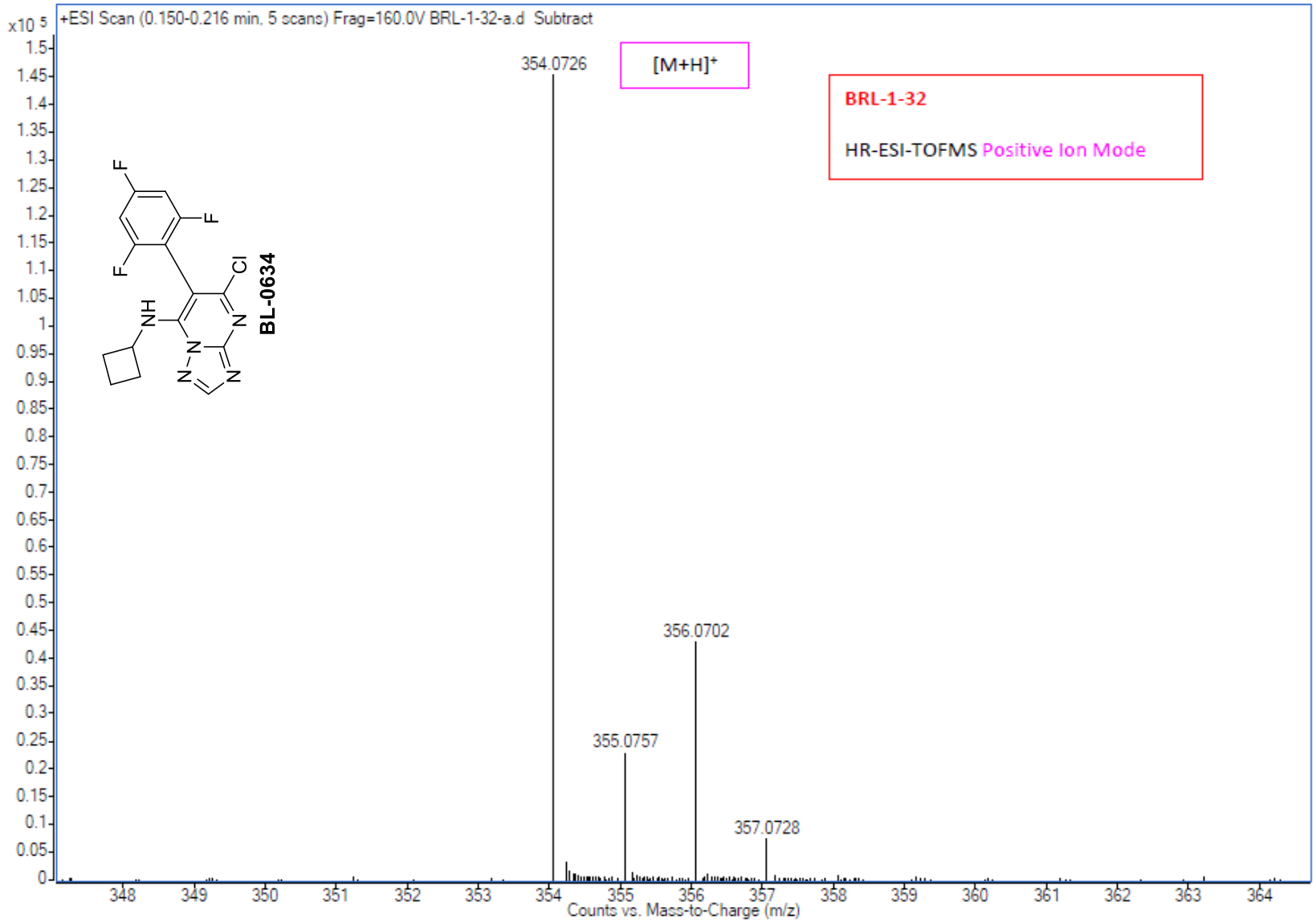
+ESI Scan (0.150-0.216 min, 5 scans) Frag=160.0V BRL-1-32-a.d Subtract
x10 5
[M+H]+
354.0726
356.0702
355.0757
357.0728
BRL-1-32
HR-ESI-TOFMS Positive Ion Mode
BL-0634
Counts vs. Mass-to-Charge (m/z)

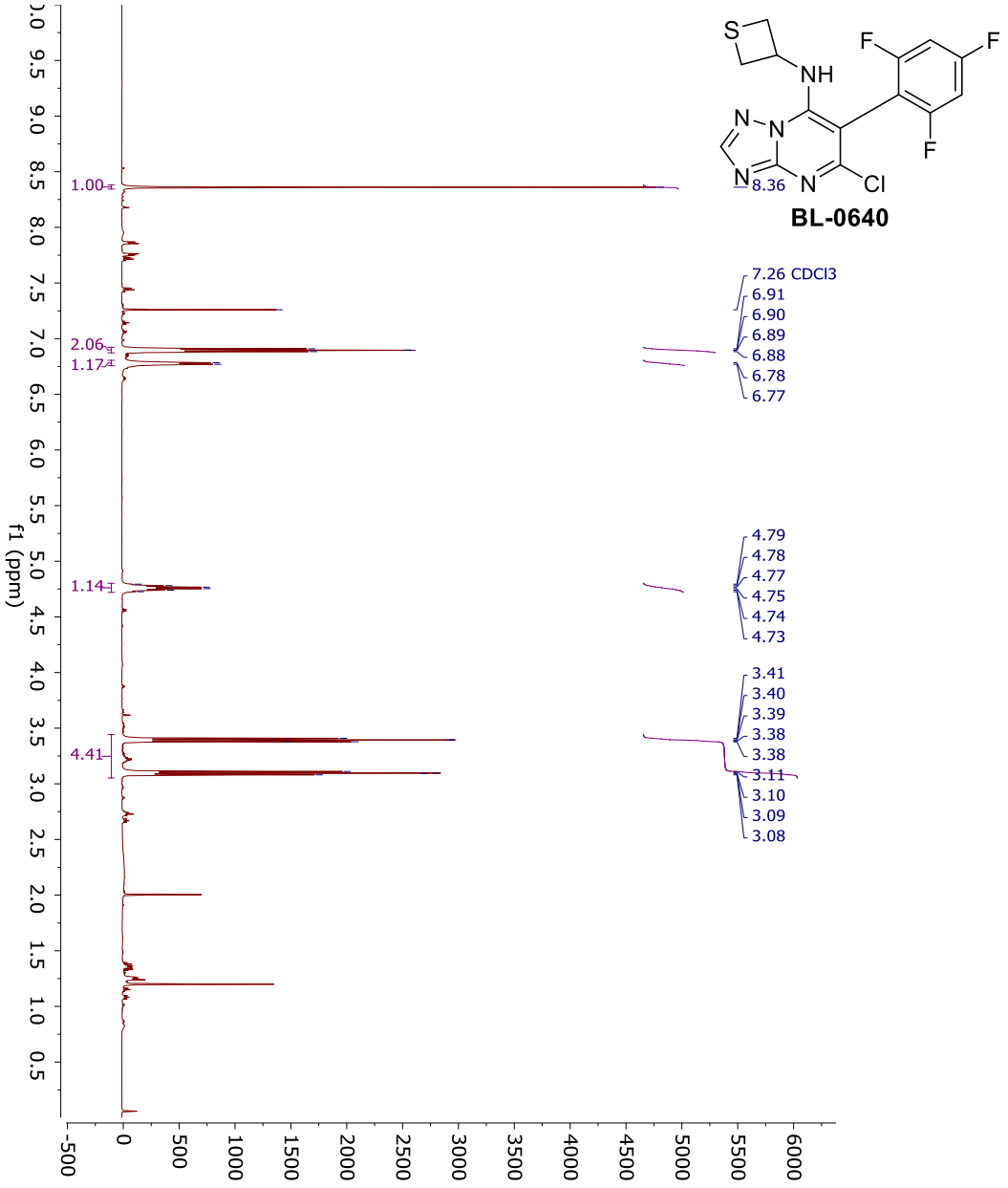
BL-0640
8.36
7.26 CDCl3
6.91
6.90
6.89
6.88
6.78
6.77
4.79
4.78
4.77
4.75
4.74
4.73
3.41
3.40
3.39
3.38
3.38
3.11
3.10
3.09
3.08
1.00
2.06
1.17
1.14
4.41
f1 (ppm)

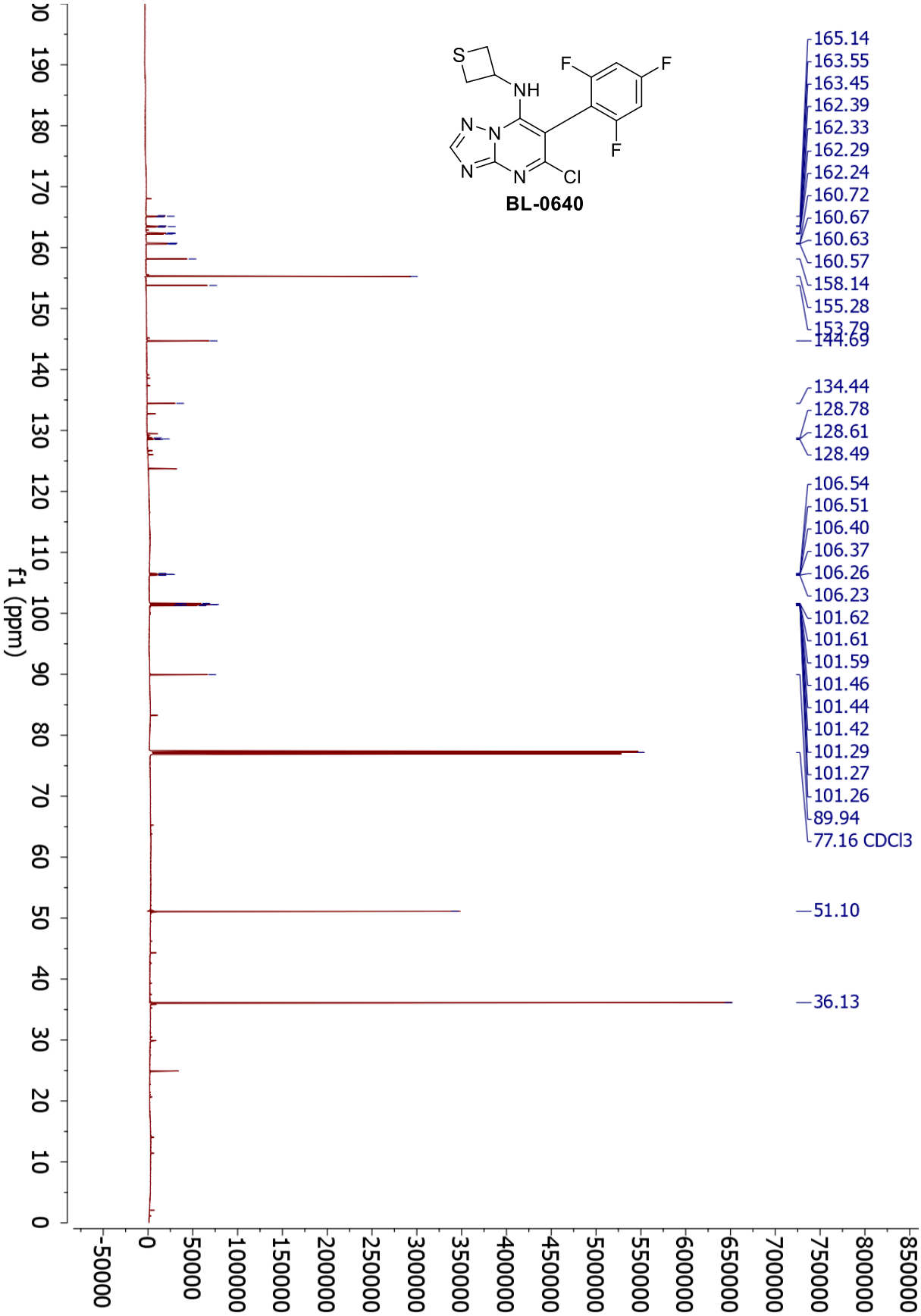
BL-0640
f1 (ppm)
165.14
163.55
163.45
162.39
162.33
162.29
162.24
160.72
160.67
160.63
160.57
158.14
155.28
153.79
144.69
134.44
128.78
128.61
128.49
106.54
106.51
106.40
106.37
106.26
106.23
101.62
101.61
101.59
101.46
101.44
101.42
101.29
101.27
101.26
89.94
77.16 CDCl3
51.10
36.13

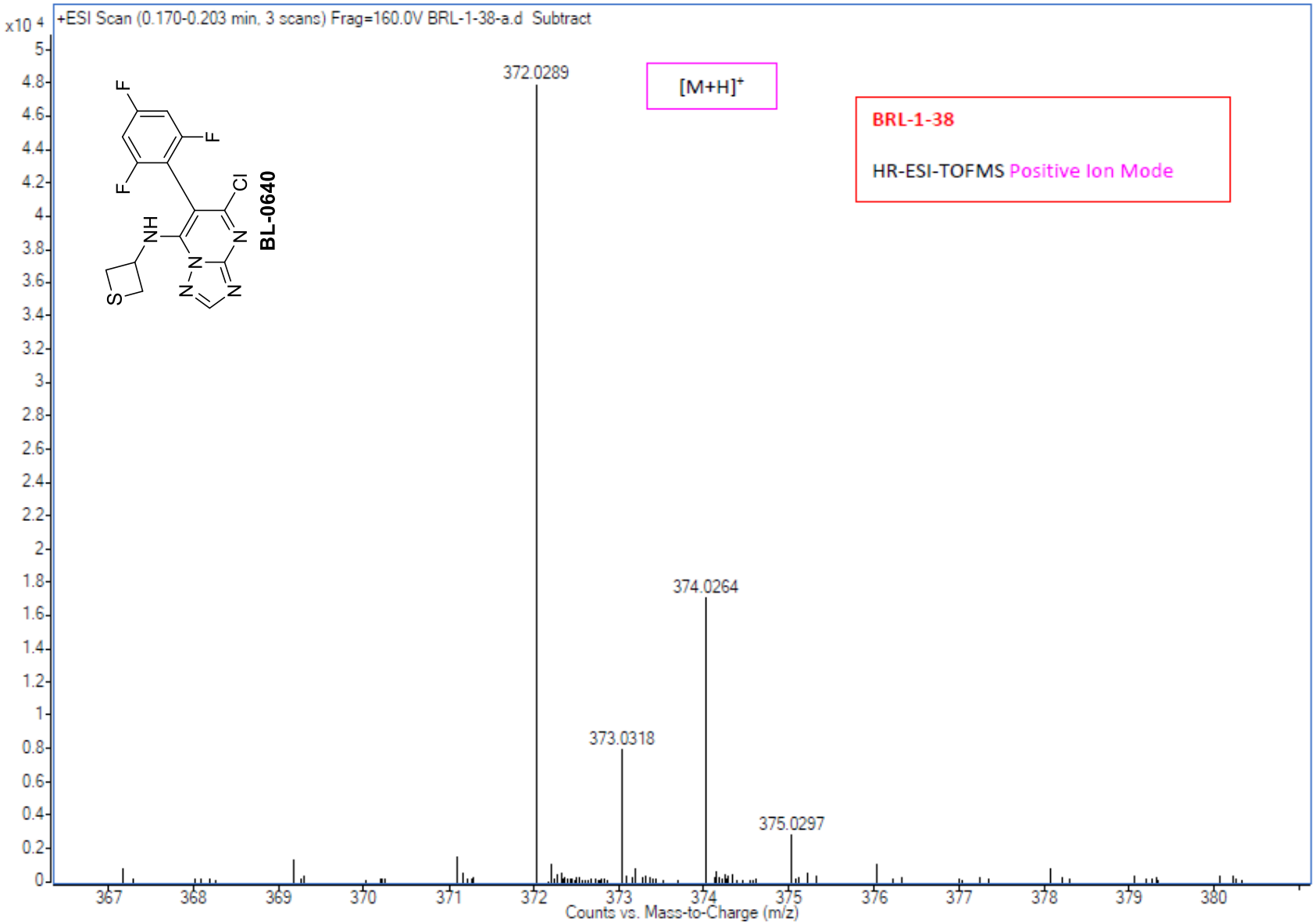
+ESI Scan (0.170-0.203 min, 3 scans) Frag=160.0V BRL-1-38-a.d Subtract
x10 4
5
4.8
4.6
4.4
4.2
4
3.8
3.6
3.4
3.2
3
2.8
2.6
2.4
2.2
2
1.8
1.6
1.4
1.2
1
0.8
0.6
0.4
0.2
0
372.0289
[M+H]+
BRL-1-38
HR-ESI-TOFMS Positive Ion Mode
374.0264
373.0318
375.0297
BL-0640
F
F
Cl
NH
N
N
N
S
367
368
369
370
371
372
373
374
375
376
377
378
379
380
Counts vs. Mass-to-Charge (m/z)

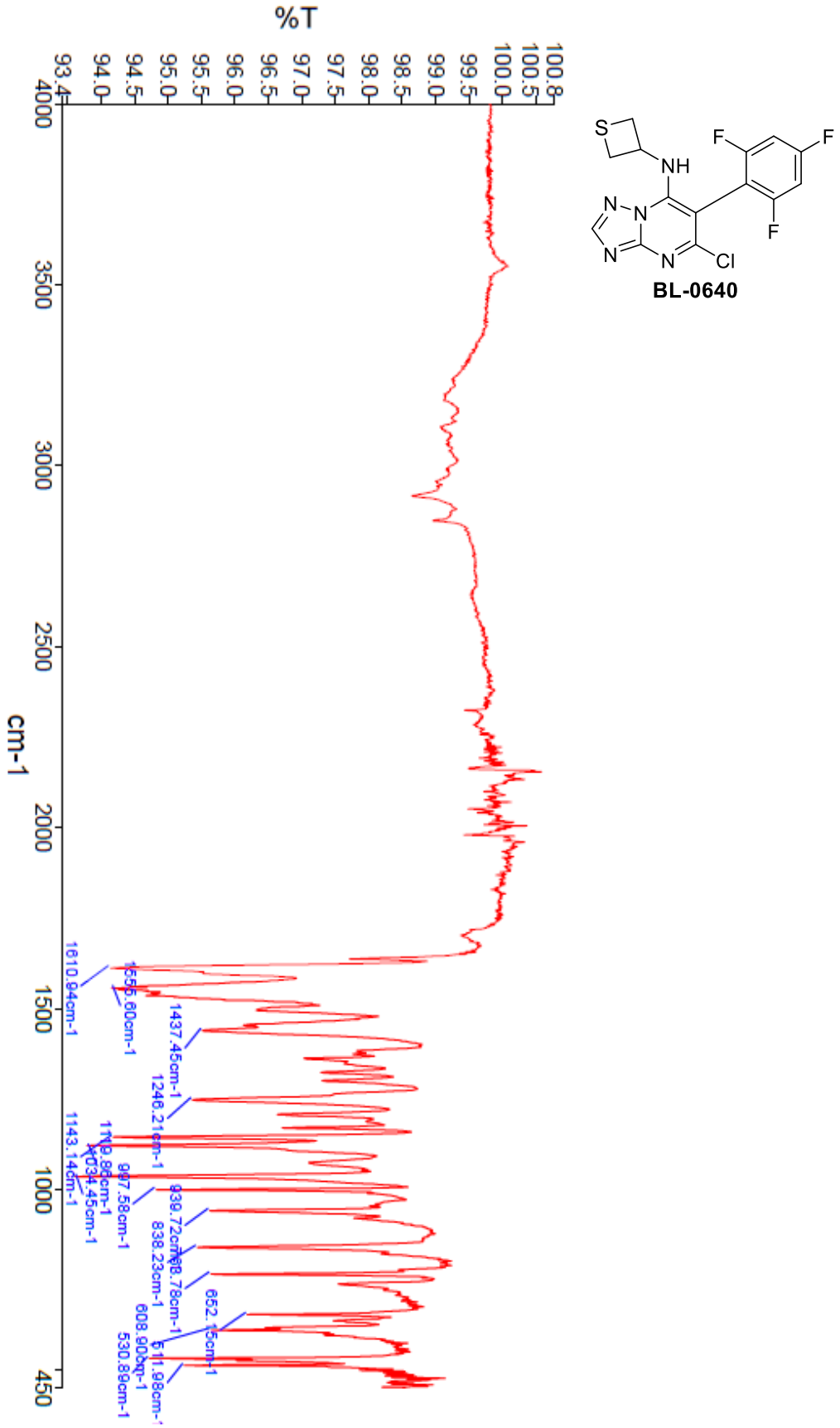
%T
cm-1
1610.84cm-1
1556.60cm-1
1437.45cm-1
1246.21cm-1
1143.14cm-1
1034.45cm-1
997.58cm-1
939.72cm-1
838.23cm-1
652.15cm-1
608.90cm-1
530.89cm-1
S
NH
F
F
F
N
N
N
N
Cl
BL-0640

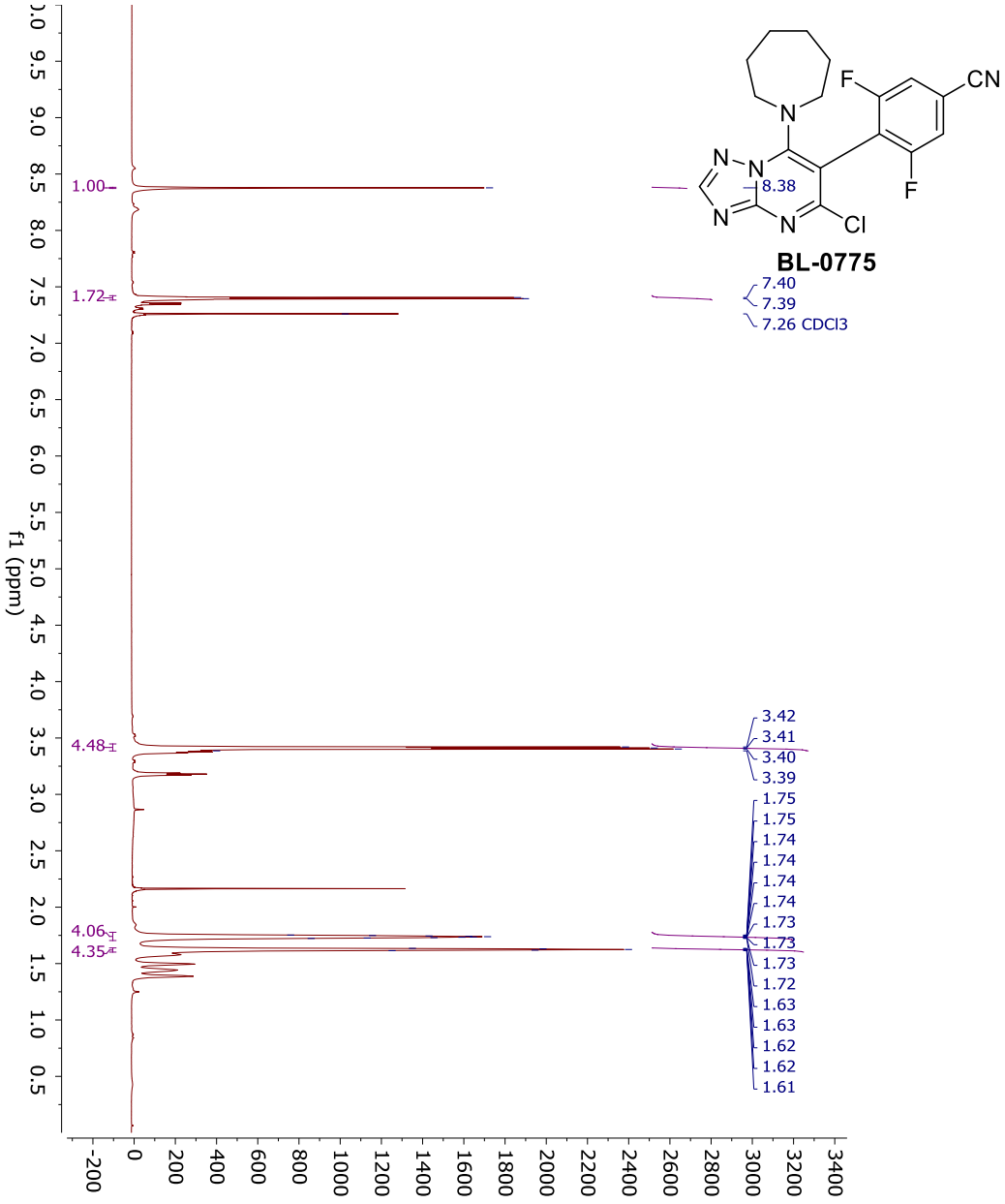
F
CN
N
N
N
8.38
F
N
N
Cl
BL-0775
7.40
7.39
7.26 CDCl3
1.00
1.72
4.48
4.06
4.35
3.42
3.41
3.40
3.39
1.75
1.75
1.74
1.74
1.74
1.74
1.73
1.73
1.73
1.72
1.63
1.63
1.62
1.62
1.61
f1 (ppm)

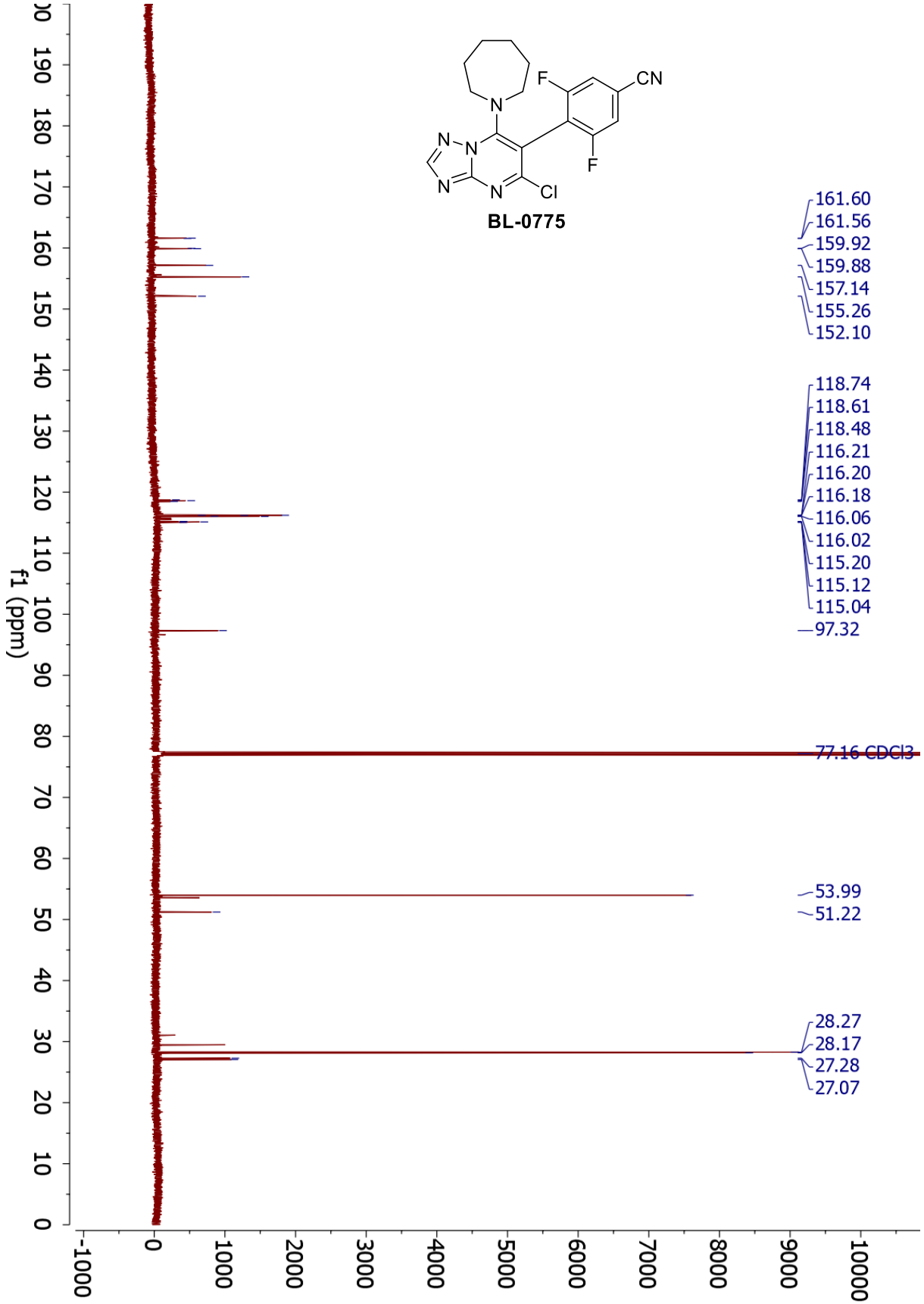
F
CN
N
N
N
N
N
F
Cl
BL-0775
161.60
161.56
159.92
159.88
157.14
155.26
152.10
118.74
118.61
118.48
116.21
116.20
116.18
116.06
116.02
115.20
115.12
115.04
97.32
77.16 CDCl3
53.99
51.22
28.27
28.17
27.28
27.07
f1 (ppm)

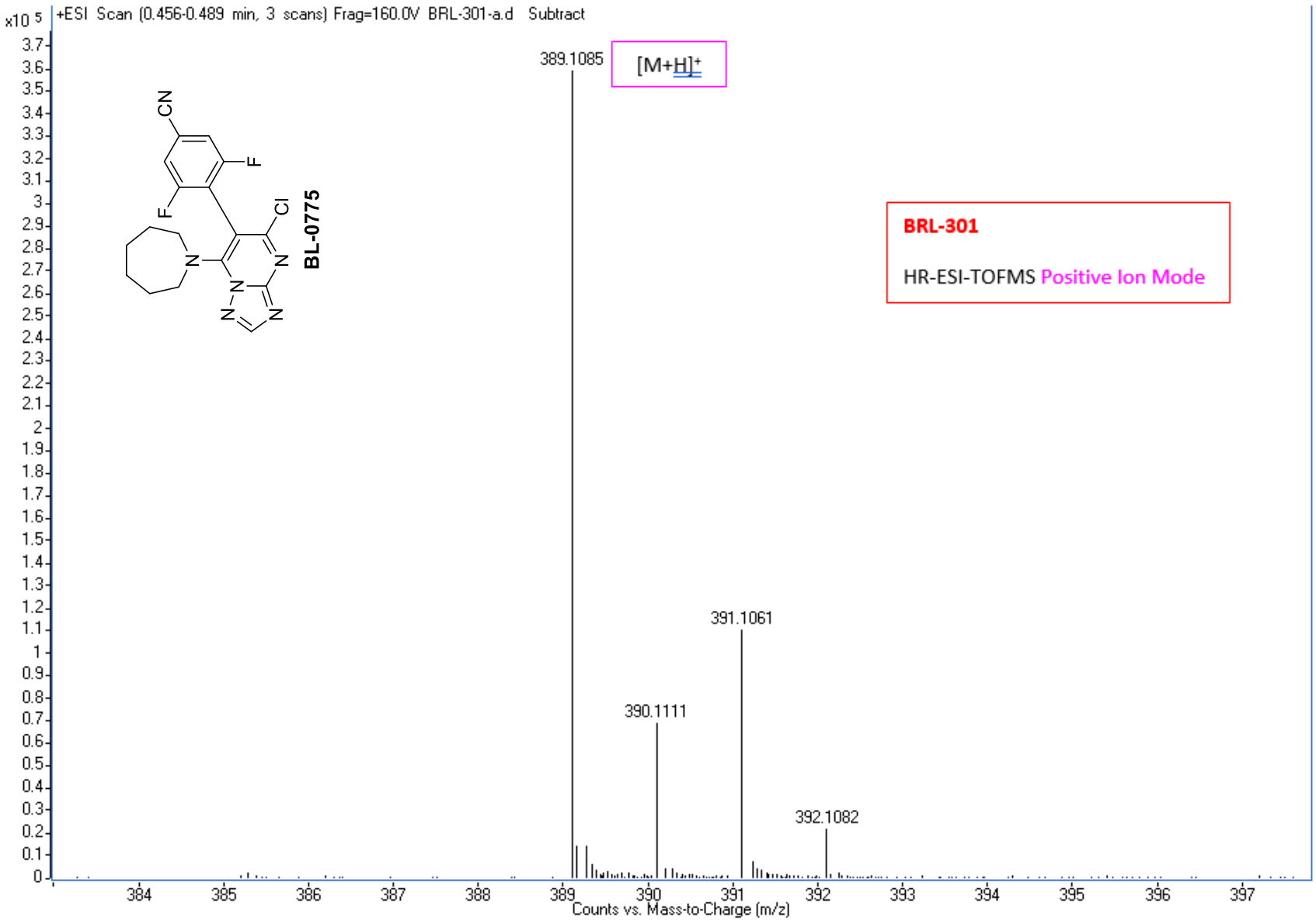
x10 5
+ESI Scan (0.456-0.489 min, 3 scans) Frag=160.0V BRL-301-a.d Subtract
389.1085
[M+H]+
391.1061
390.1111
392.1082
BL-0775
BRL-301
HR-ESI-TOFMS Positive Ion Mode
Counts vs. Mass-to-Charge (m/z)

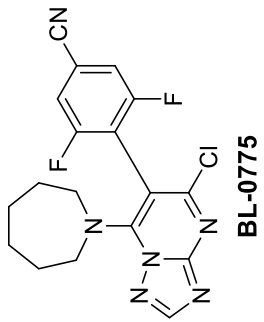
CN
F
F
Cl
N
N
N
N
N

BL-0775

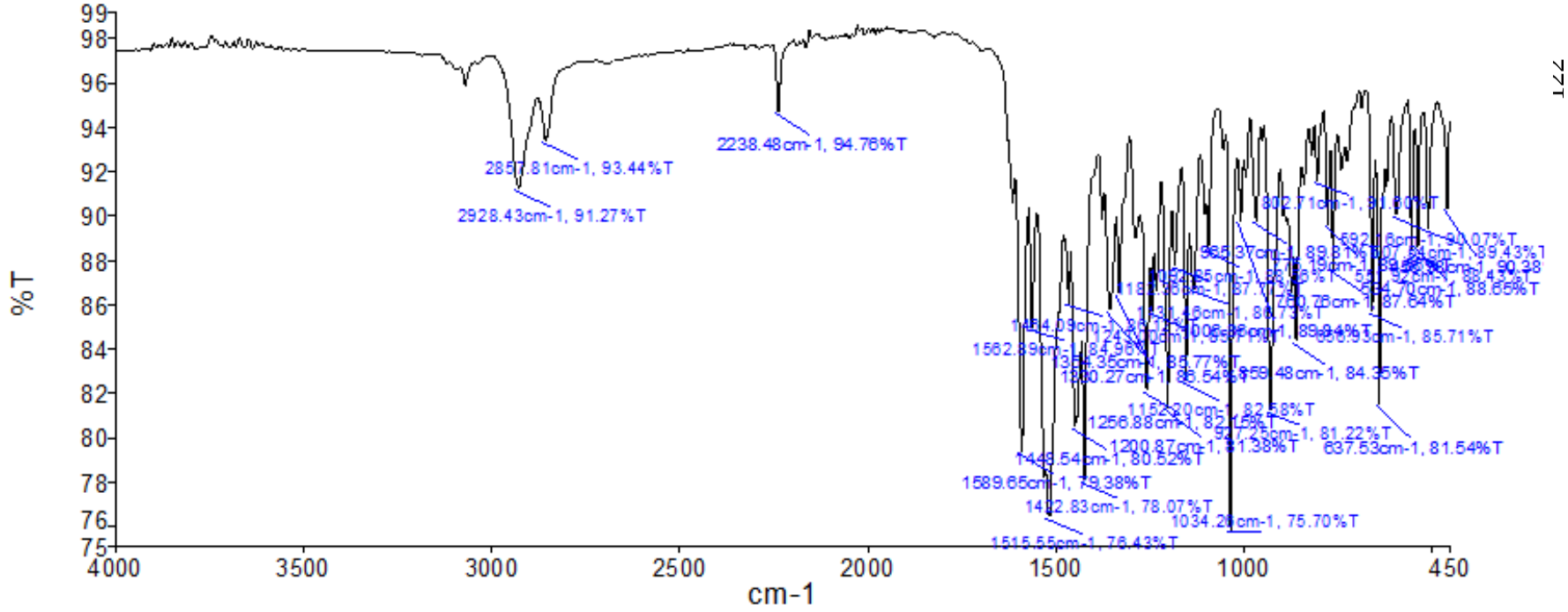
%T
cm-1
2857.81cm-1, 93.44%T
2928.43cm-1, 91.27%T
2238.48cm-1, 94.76%T
1562.89cm-1, 84.96%T
1589.65cm-1, 79.38%T
1422.83cm-1, 78.07%T
1515.55cm-1, 76.43%T
1034.26cm-1, 75.70%T
637.53cm-1, 81.54%T

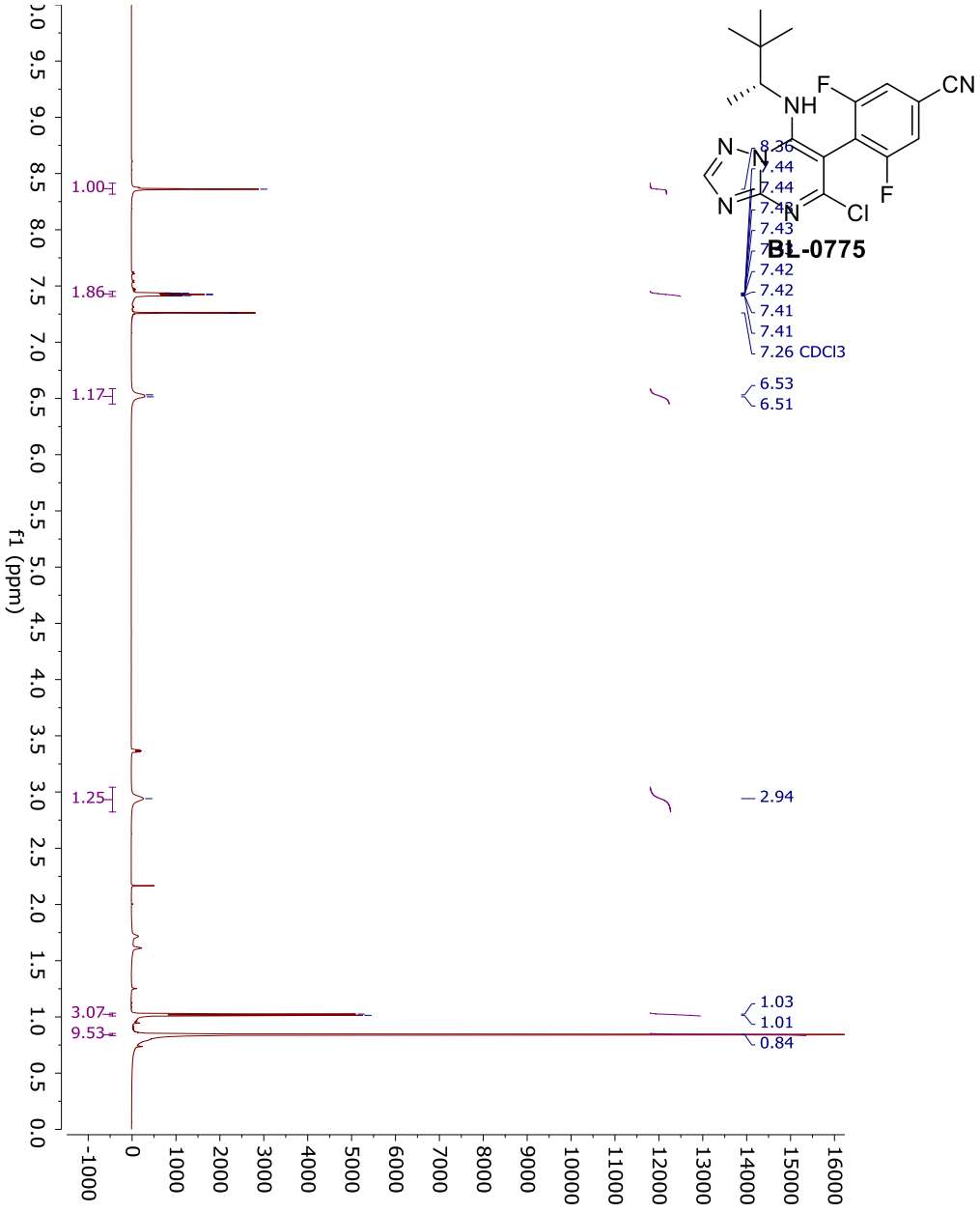
F
CN
NH
N
N
N
N
Cl
F
BL-0775
8.36
7.44
7.44
7.43
7.42
7.42
7.41
7.41
7.26 CDCl3
6.53
6.51
2.94
1.03
1.01
0.84
1.00
1.86
1.17
1.25
3.07
9.53
f1 (ppm)

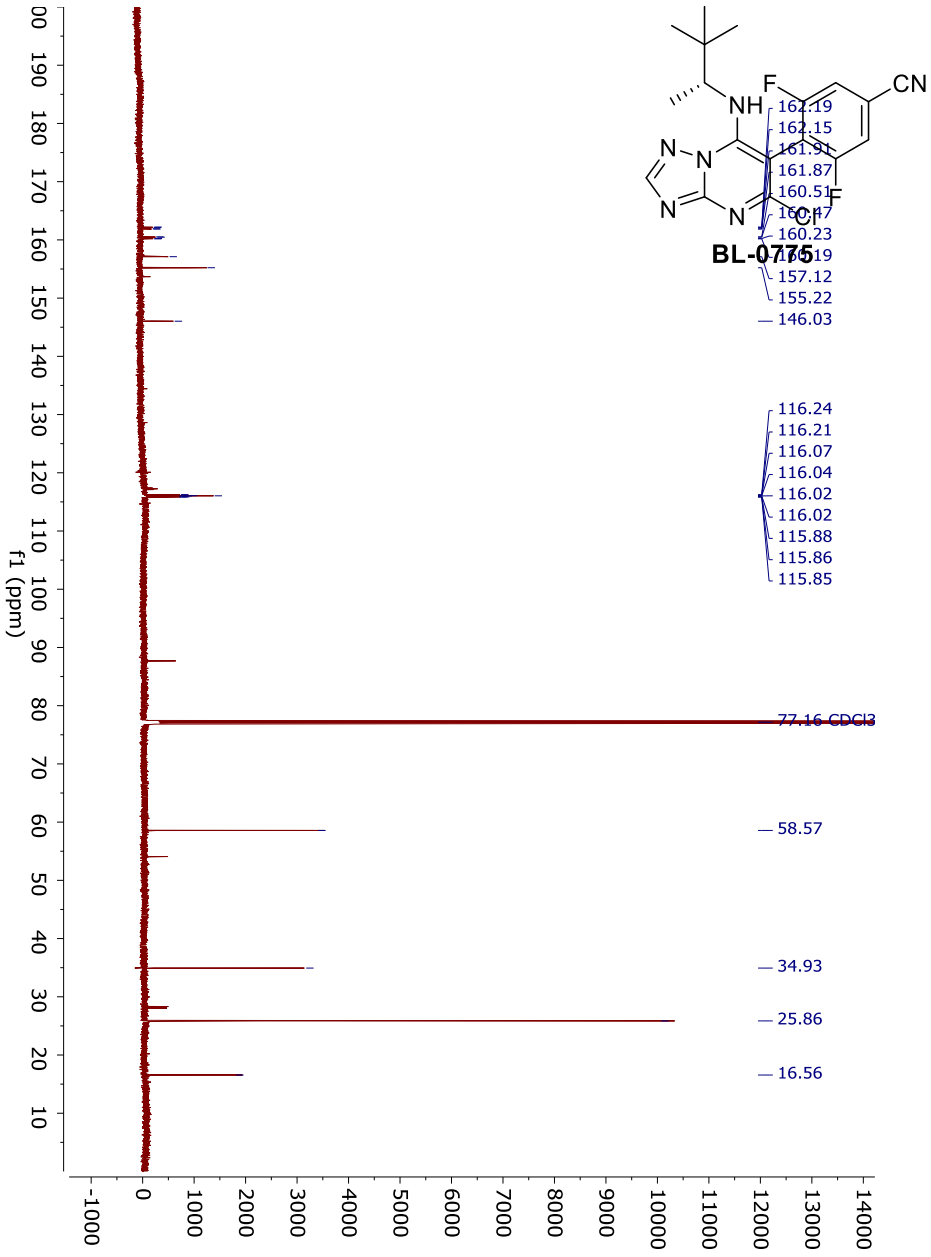
F
CN
NH
N
N
N
N
F
Cl
BL-0775
162.19
162.15
161.91
161.87
160.51
160.47
160.23
157.19
157.12
155.22
146.03
116.24
116.21
116.07
116.04
116.02
116.02
115.88
115.86
115.85
77.16 CDCl3
58.57
34.93
25.86
16.56
f1 (ppm)

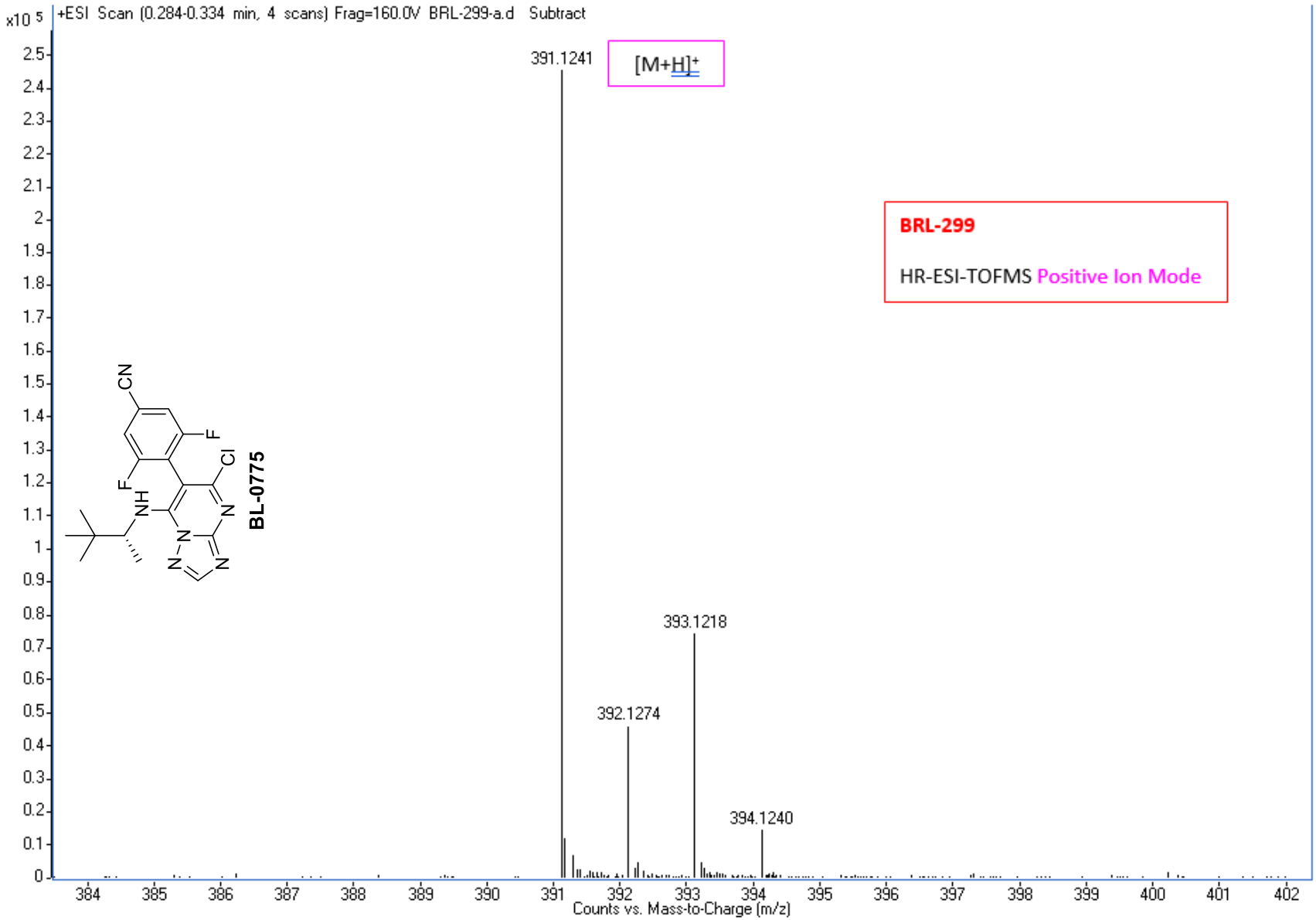
x10 5
+ESI Scan (0.284-0.334 min, 4 scans) Frag=160.0V BRL-299-a.d Subtract
391.1241
[M+H]+
BRL-299
HR-ESI-TOFMS Positive Ion Mode
BL-0775
393.1218
392.1274
394.1240
Counts vs. Mass-to-Charge (m/z)

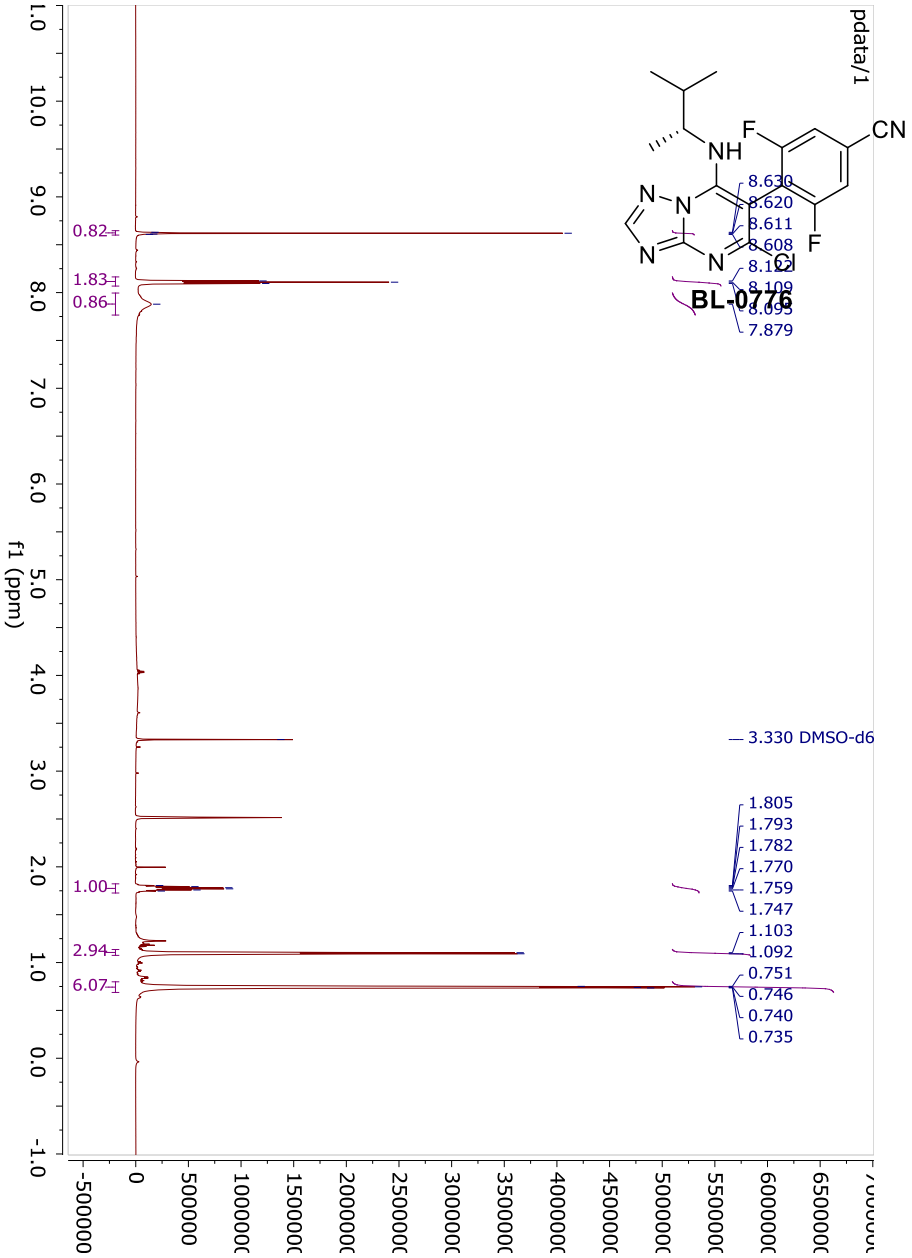
pdata/1
F
CN
NH
N
N
N
N
Cl
F
BL-0776
8.630
8.620
8.611
8.608
8.122
8.109
8.095
7.879
3.330 DMSO-d6
1.805
1.793
1.782
1.770
1.759
1.747
1.103
1.092
0.751
0.746
0.740
0.735
0.82
1.83
0.86
1.00
2.94
6.07
f1 (ppm)

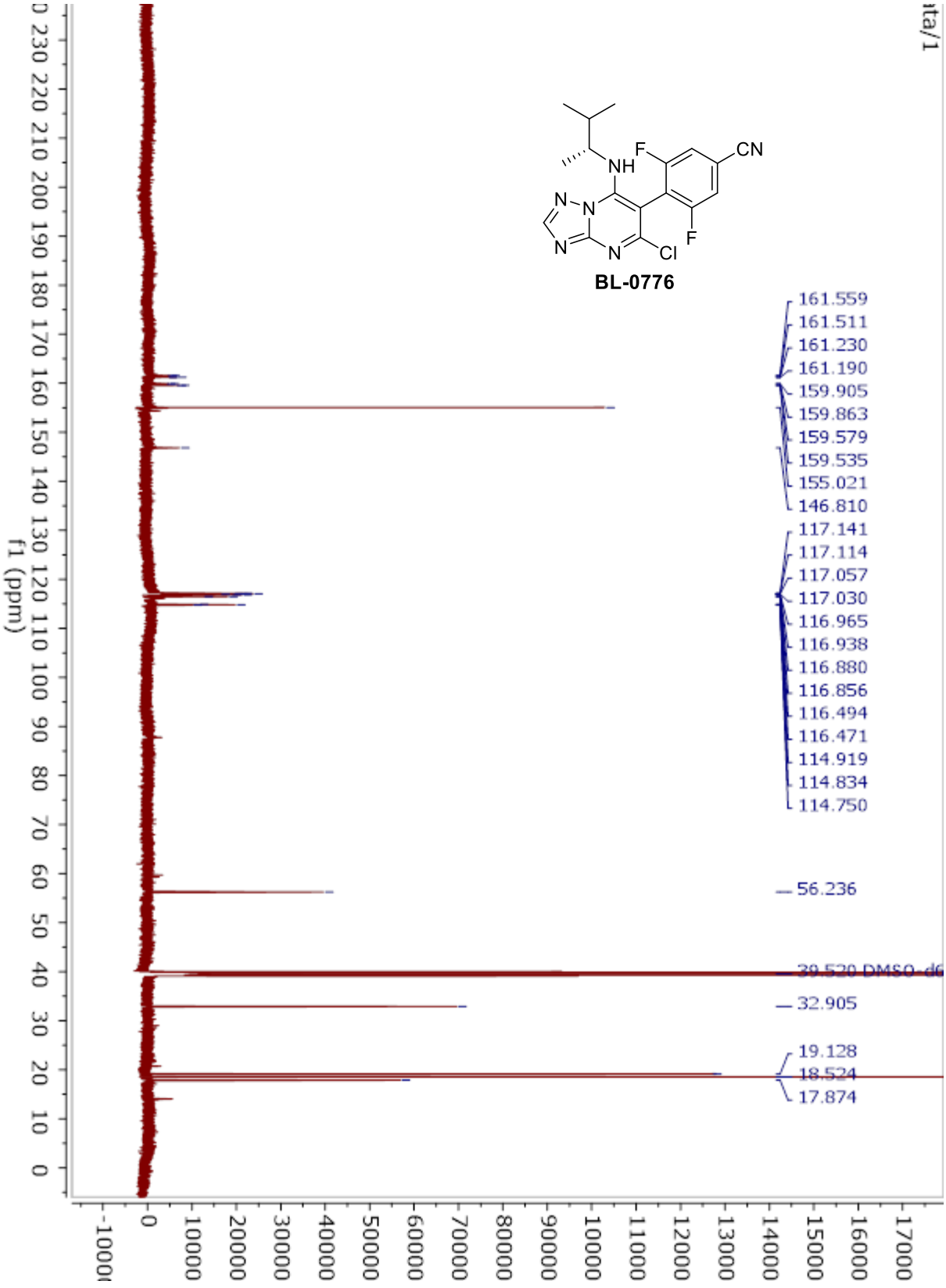
BL-0776
161.559
161.511
161.230
161.190
159.905
159.863
159.579
159.535
155.021
146.810
117.141
117.114
117.057
117.030
116.965
116.938
116.880
116.856
116.494
116.471
114.919
114.834
114.750
56.236
39.520 DMSO-d6
32.905
19.128
18.524
17.874
f1 (ppm)

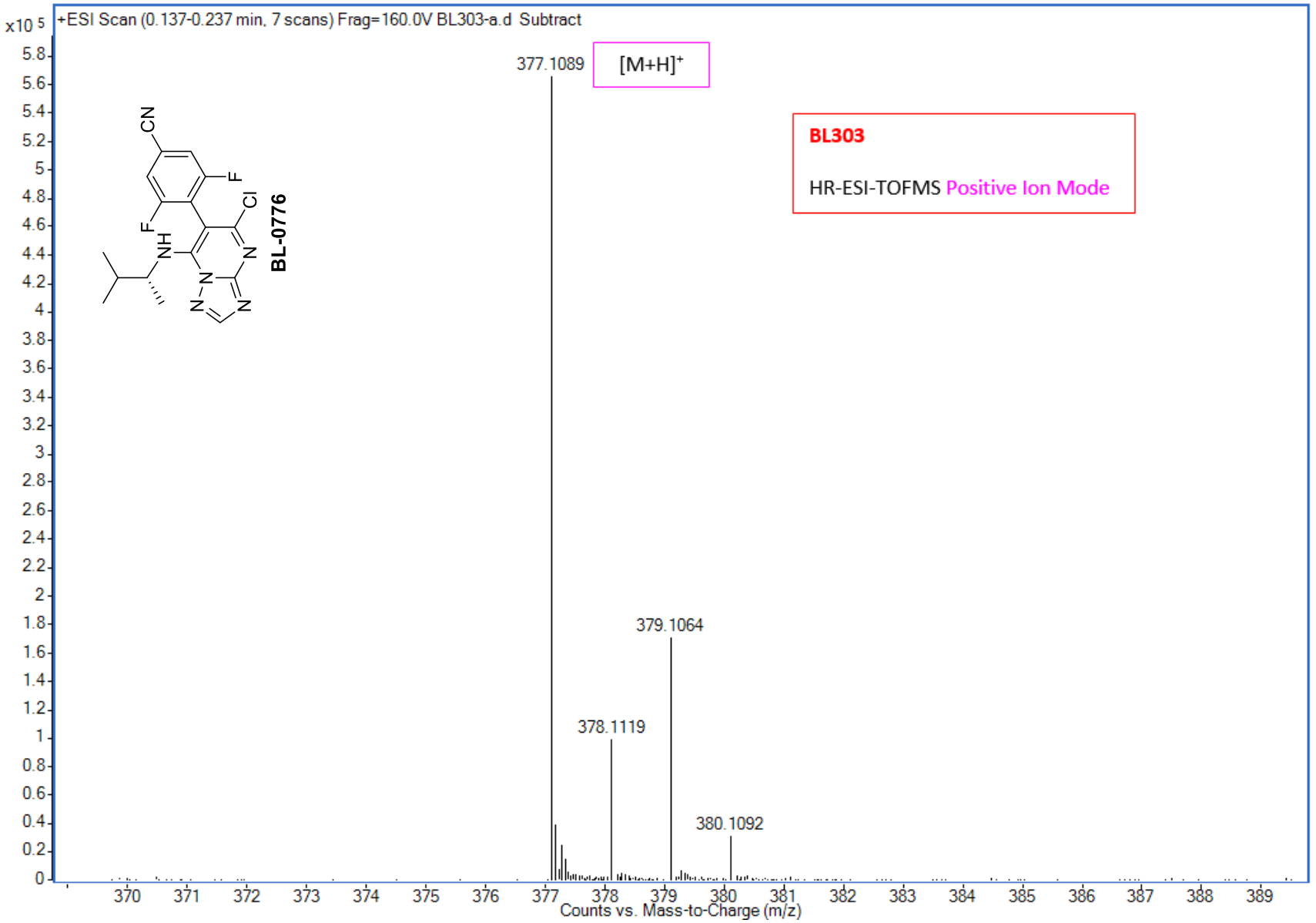
+ESI Scan (0.137-0.237 min, 7 scans) Frag=160.0V BL303-a.d Subtract
x10 5
377.1089
[M+H]+
BL303
HR-ESI-TOFMS Positive Ion Mode
BL-0776
379.1064
378.1119
380.1092
Counts vs. Mass-to-Charge (m/z)

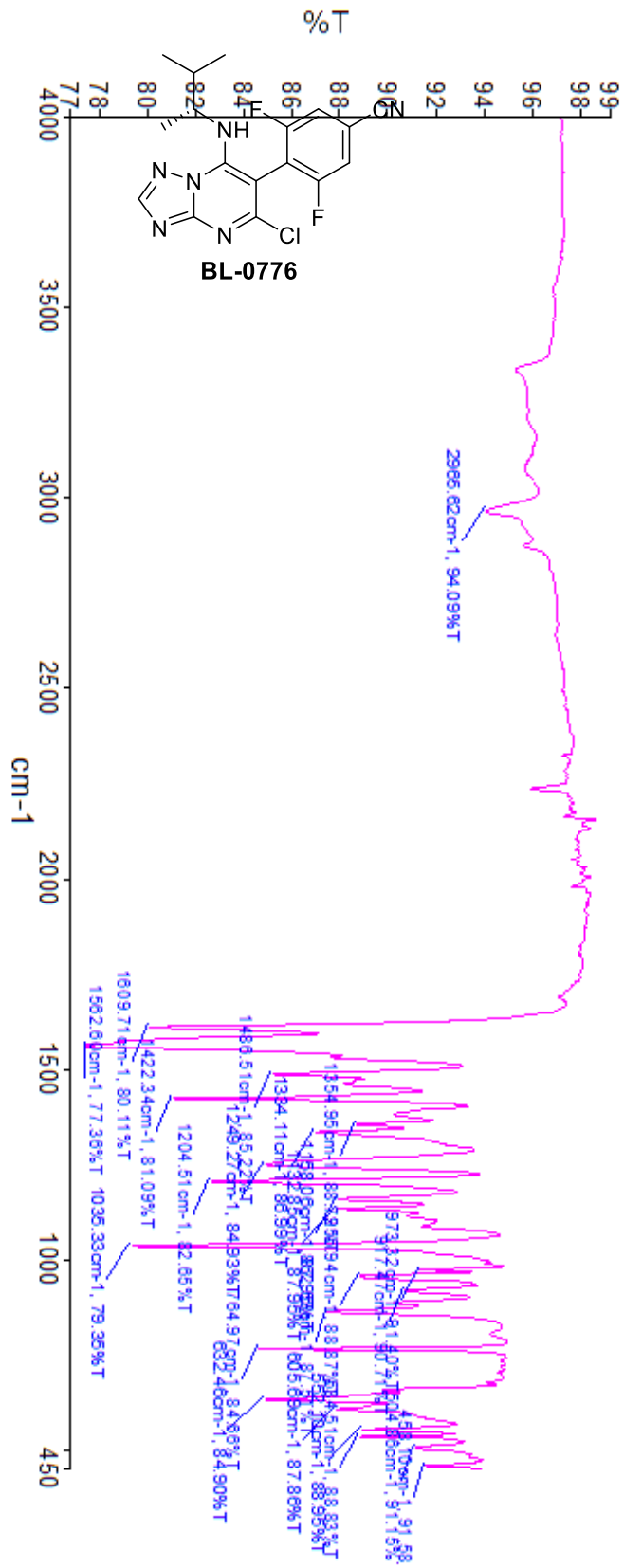
%T
cm-1
BL-0776
2985.62cm-1, 94.09%T
1609.71cm-1, 80.11%T
1582.80cm-1, 77.36%T
1422.34cm-1, 81.09%T
1204.51cm-1, 82.65%T
1035.33cm-1, 79.36%T
832.46cm-1, 84.90%T

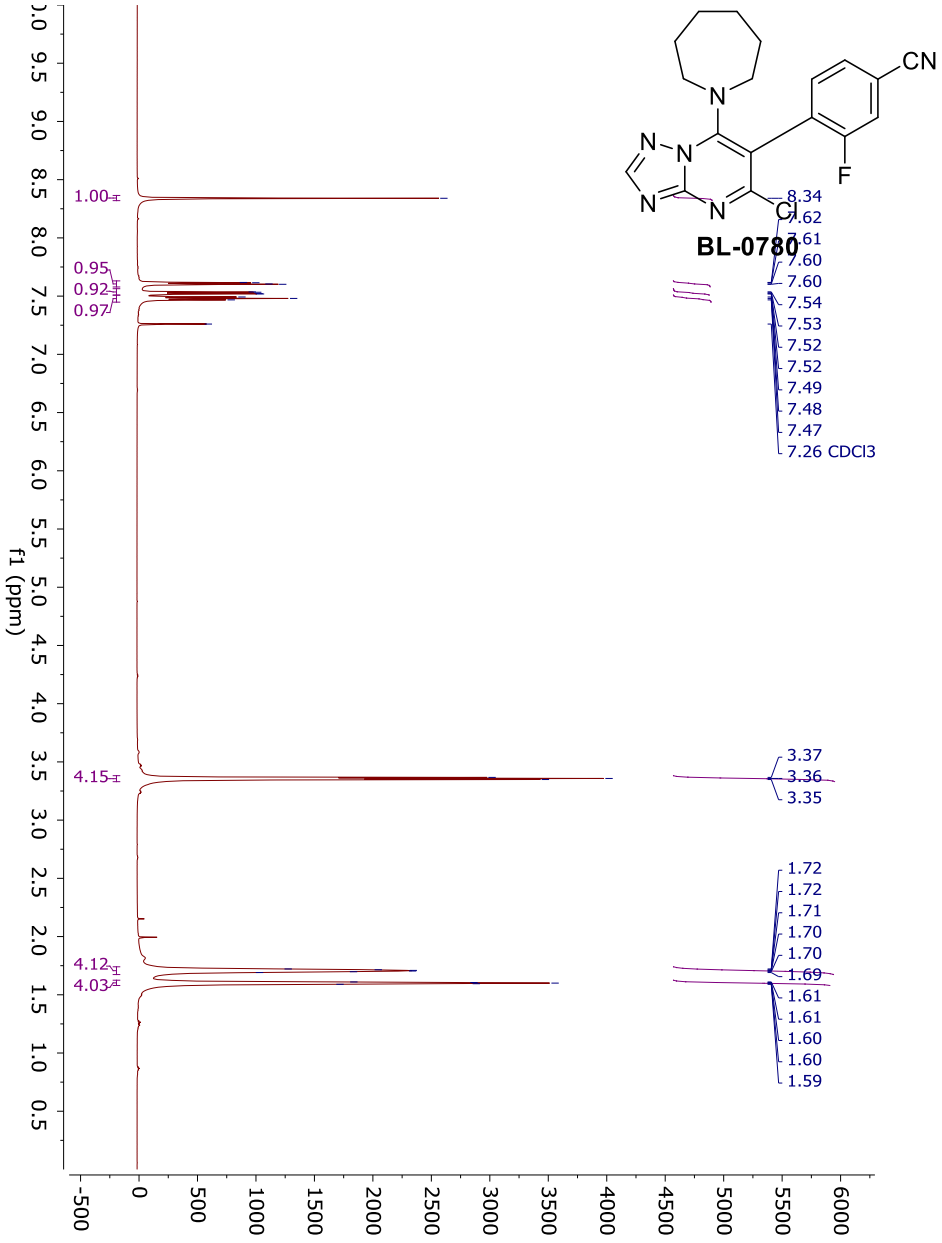
BL-0780
CN
F
Cl
N
N
N
N
N
1.00
0.95
0.92
0.97
4.15
4.12
4.03
8.34
7.62
7.61
7.60
7.60
7.54
7.53
7.52
7.52
7.49
7.48
7.47
7.26 CDCl3
3.37
3.36
3.35
1.72
1.72
1.71
1.70
1.70
1.69
1.61
1.61
1.60
1.60
1.59
f1 (ppm)

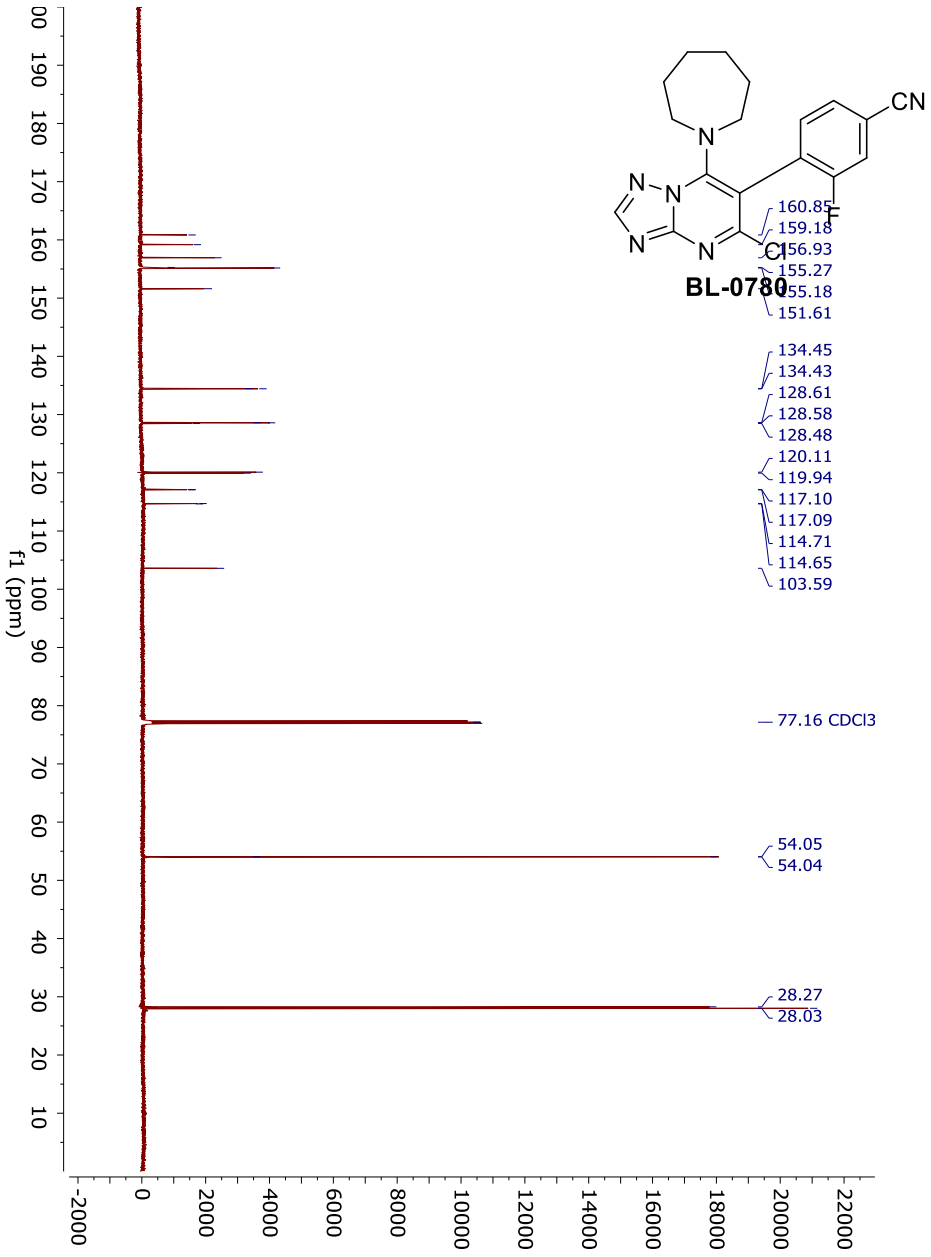
BL-0780
160.85
159.18
156.93
155.27
155.18
151.61
134.45
134.43
128.61
128.58
128.48
120.11
119.94
117.10
117.09
114.71
114.65
103.59
77.16 CDCl3
54.05
54.04
28.27
28.03
f1 (ppm)

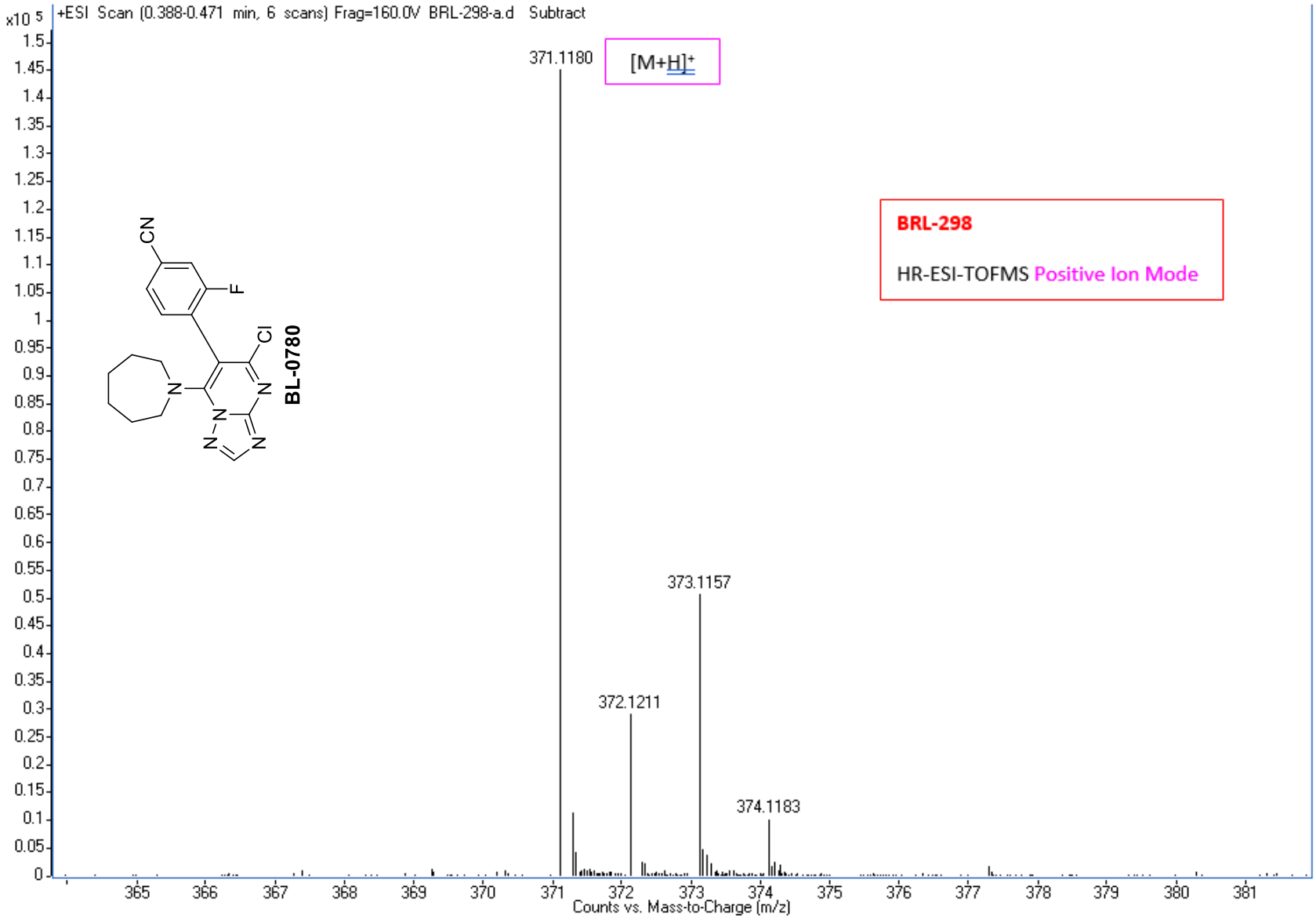
+ESI Scan (0.388-0.471 min, 6 scans) Frag=160.0V BRL-298-a.d Subtract
x10 5
371.1180
[M+H]+
BRL-298
HR-ESI-TOFMS Positive Ion Mode
BL-0780
373.1157
372.1211
374.1183
Counts vs. Mass-to-Charge (m/z)

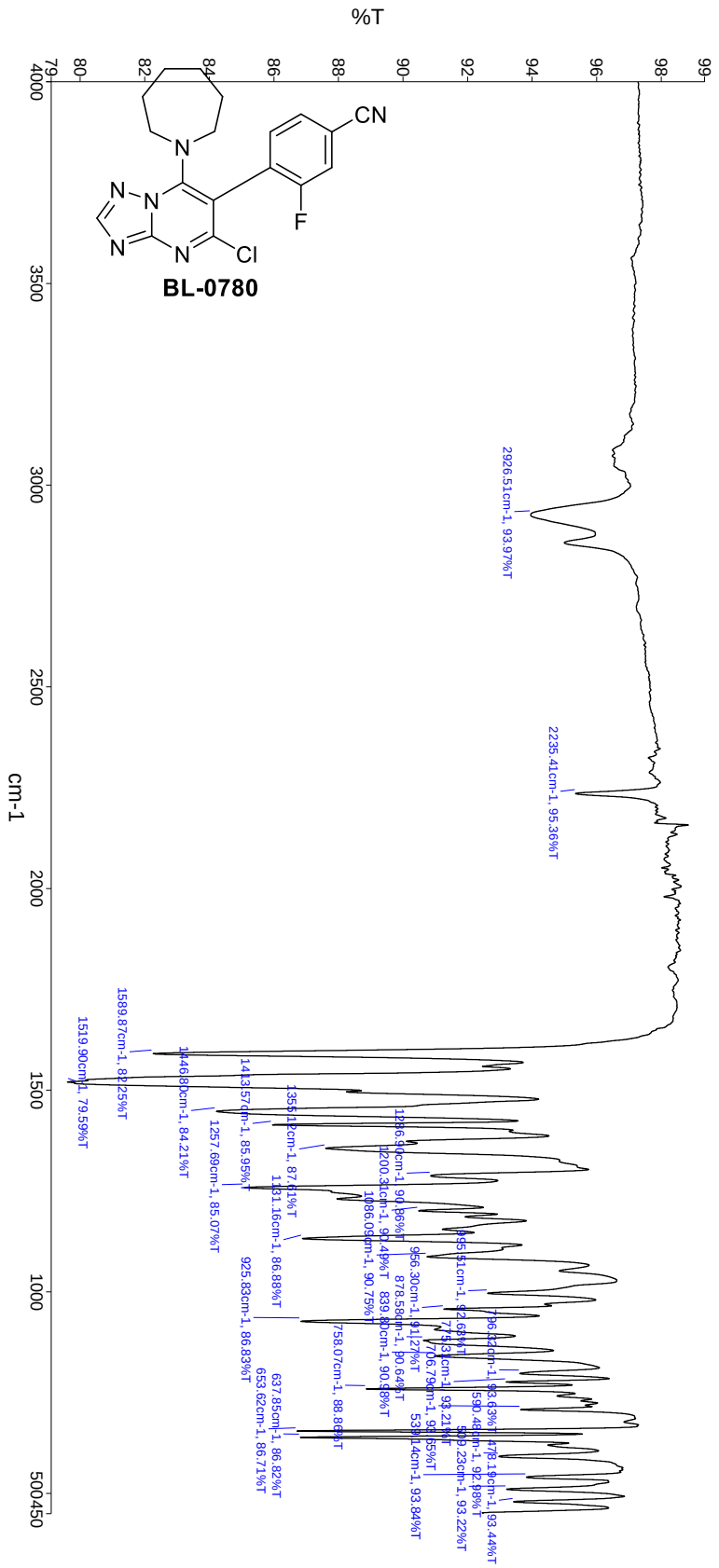
%T
cm-1
BL-0780
2926.51cm-1, 93.97%T
2235.41cm-1, 95.36%T
1589.87cm-1, 82.25%T
1519.90cm-1, 79.59%T
1446.80cm-1, 84.21%T
1413.57cm-1, 85.95%T
1355.11cm-1, 87.81%T
1257.69cm-1, 85.07%T
1181.16cm-1, 86.88%T
1200.31cm-1, 90.49%T
1286.90cm-1, 90.86%T
1086.09cm-1, 90.75%T
956.30cm-1, 91.27%T
925.83cm-1, 86.83%T
878.58cm-1, 90.64%T
839.80cm-1, 90.98%T
758.07cm-1, 88.86%T
637.85cm-1, 86.82%T
653.62cm-1, 86.71%T
795.51cm-1, 92.68%T
796.42cm-1, 93.63%T
706.79cm-1, 90.65%T
530.14cm-1, 93.84%T
590.48cm-1, 92.98%T
609.23cm-1, 93.22%T
478.19cm-1, 93.44%T

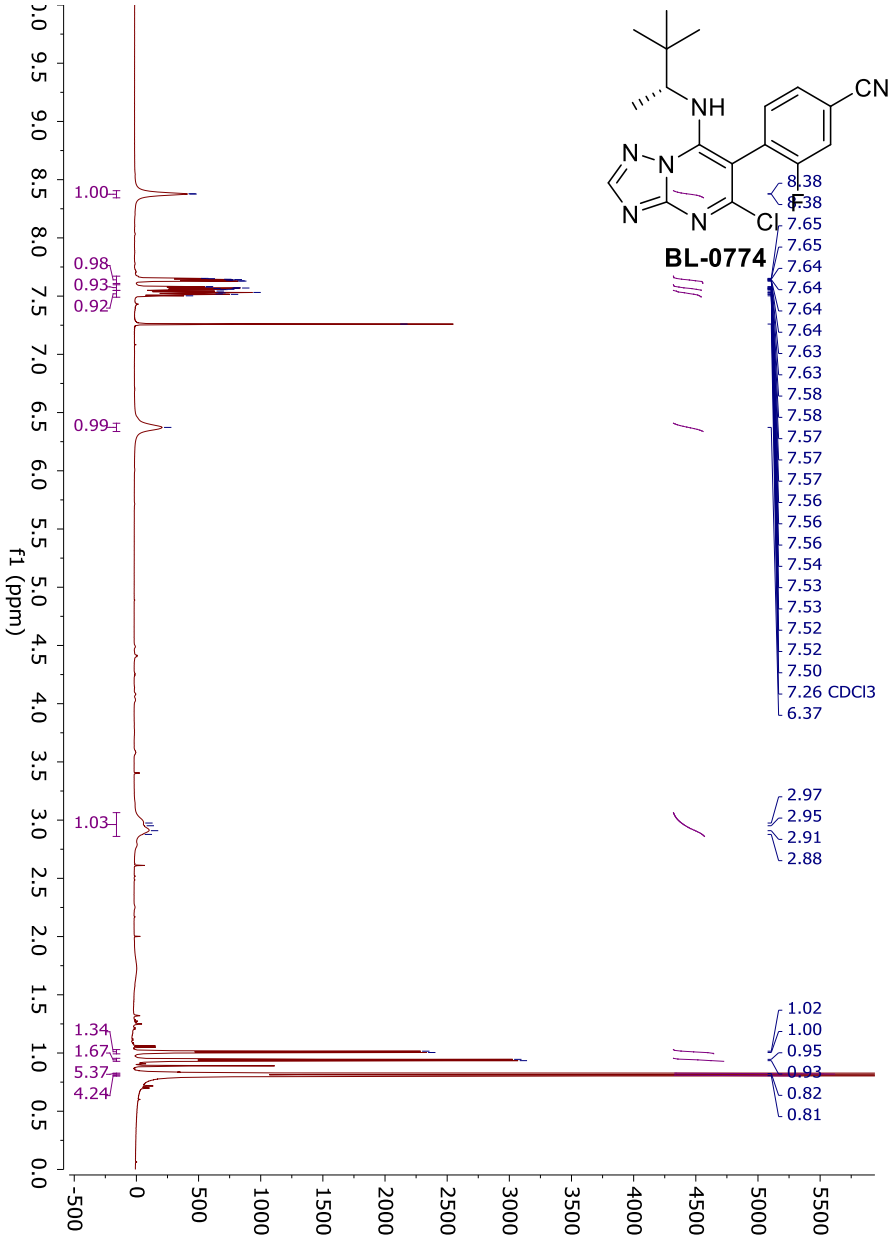
BL-0774
NH
N
N
N
N
Cl
F
CN
f1 (ppm)
1.00
0.98
0.93
0.92
0.99
1.03
1.34
1.67
5.37
4.24
8.38
8.38
7.65
7.65
7.64
7.64
7.64
7.64
7.63
7.63
7.58
7.58
7.57
7.57
7.57
7.56
7.56
7.56
7.54
7.53
7.53
7.52
7.52
7.50
7.26 CDCl3
6.37
2.97
2.95
2.91
2.88
1.02
1.00
0.95
0.93
0.82
0.81

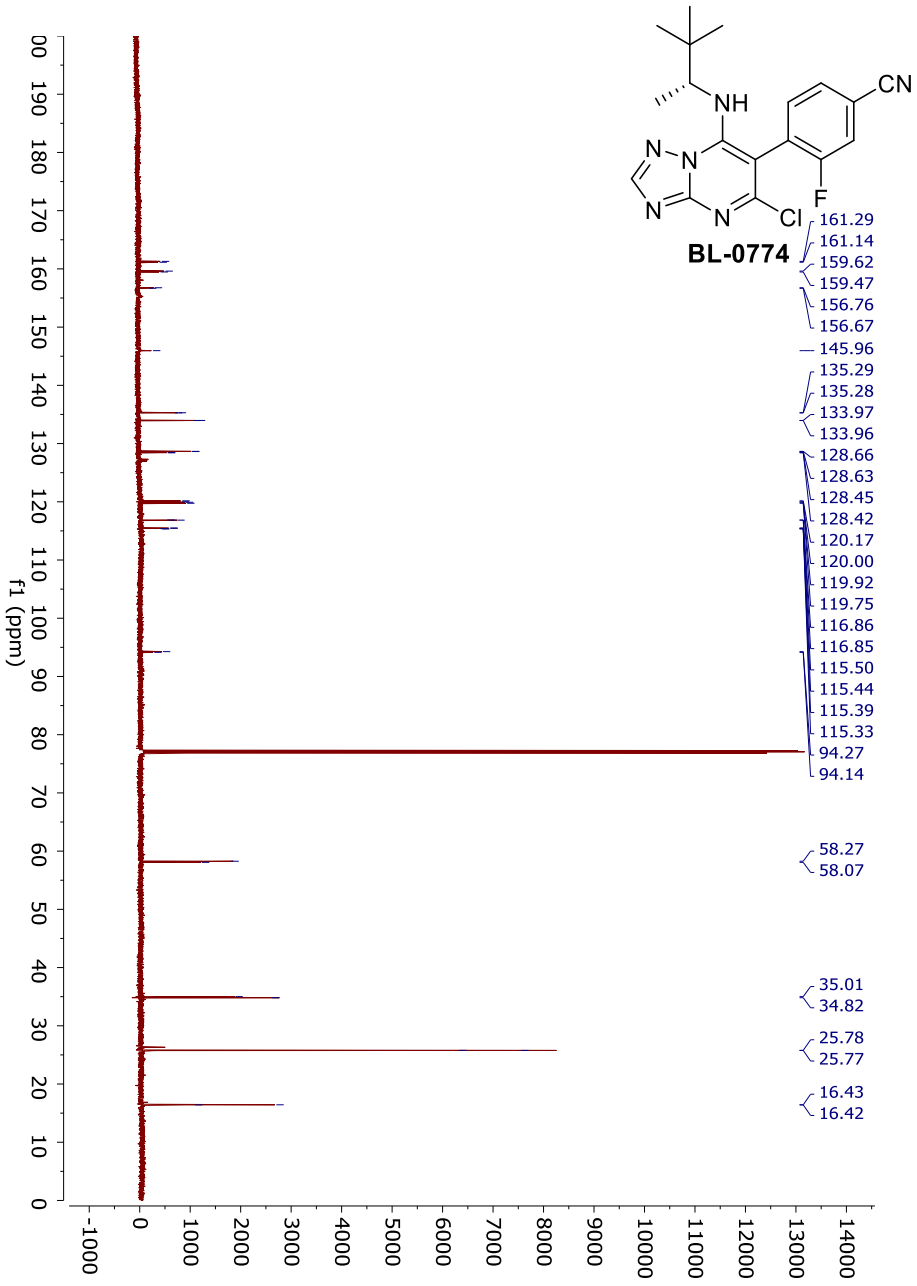
BL-0774
NH
N
N
N
N
Cl
F
CN
161.29
161.14
159.62
159.47
156.76
156.67
145.96
135.29
135.28
133.97
133.96
128.66
128.63
128.45
128.42
120.17
120.00
119.92
119.75
116.86
116.85
115.50
115.44
115.39
115.33
94.27
94.14
58.27
58.07
35.01
34.82
25.78
25.77
16.43
16.42
f1 (ppm)

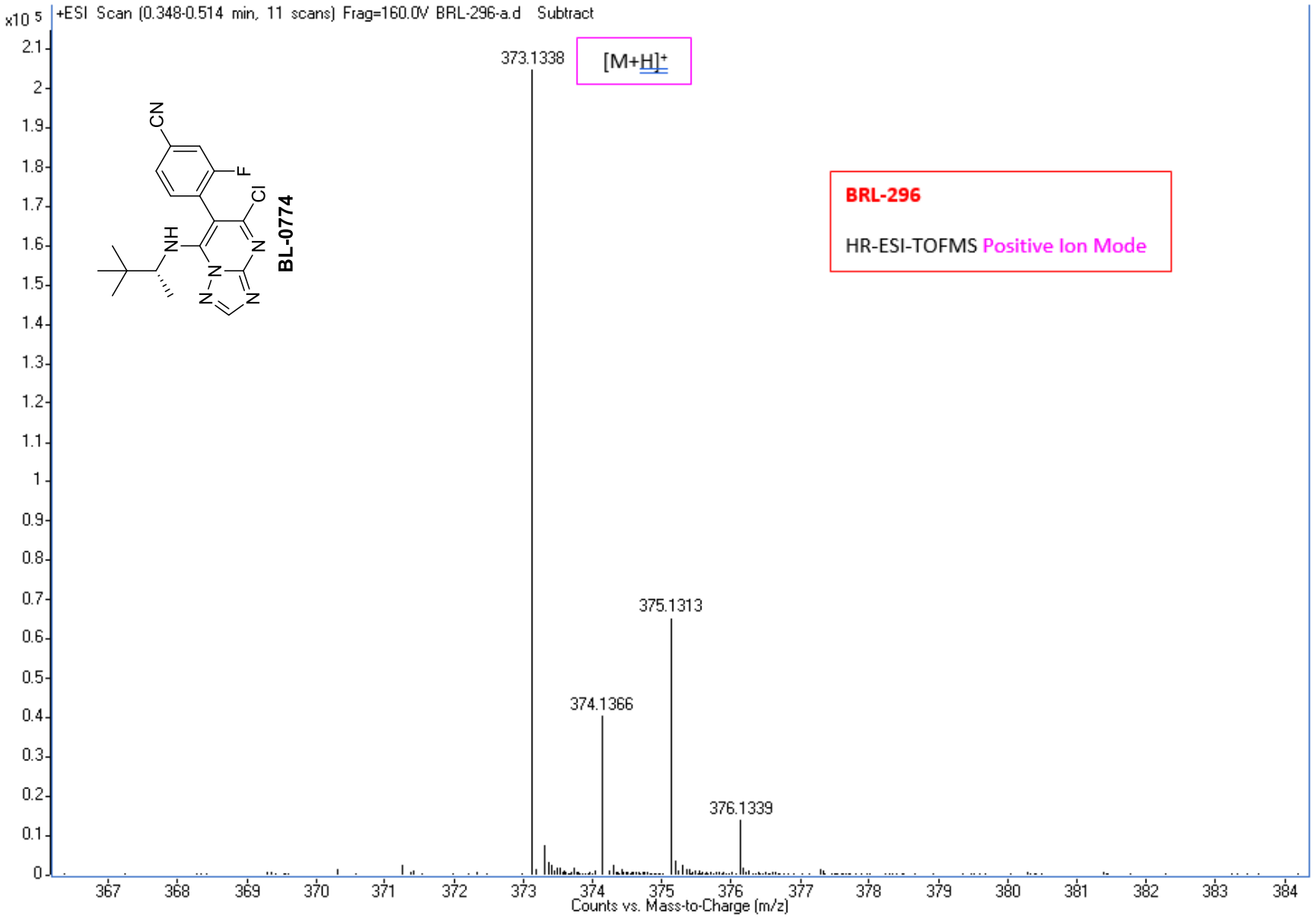
x10 5
+ESI Scan (0.348-0.514 min, 11 scans) Frag=160.0V BRL-296-a.d Subtract
373.1338
[M+H]+
375.1313
374.1366
376.1339
BL-0774
BRL-296
HR-ESI-TOFMS Positive Ion Mode
Counts vs. Mass-to-Charge (m/z)

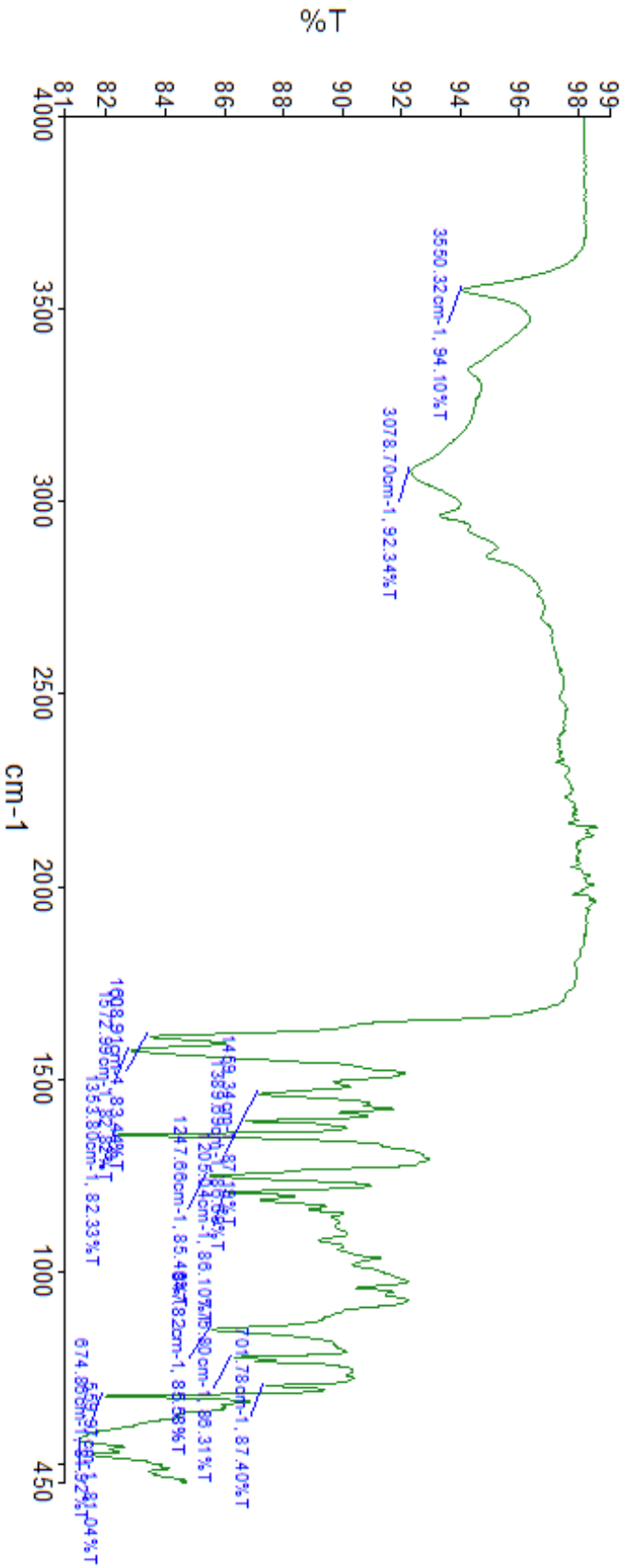
%T
cm-1
3550.32cm-1, 94.10%T
3078.70cm-1, 92.34%T
1572.99cm-1, 83.44%T
1353.80cm-1, 82.33%T
1247.66cm-1, 85.48%T
701.78cm-1, 87.40%T
674.86cm-1, 81.04%T

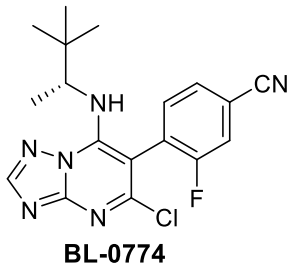
NH
CN
F
Cl
N
N
N
N

BL-0774

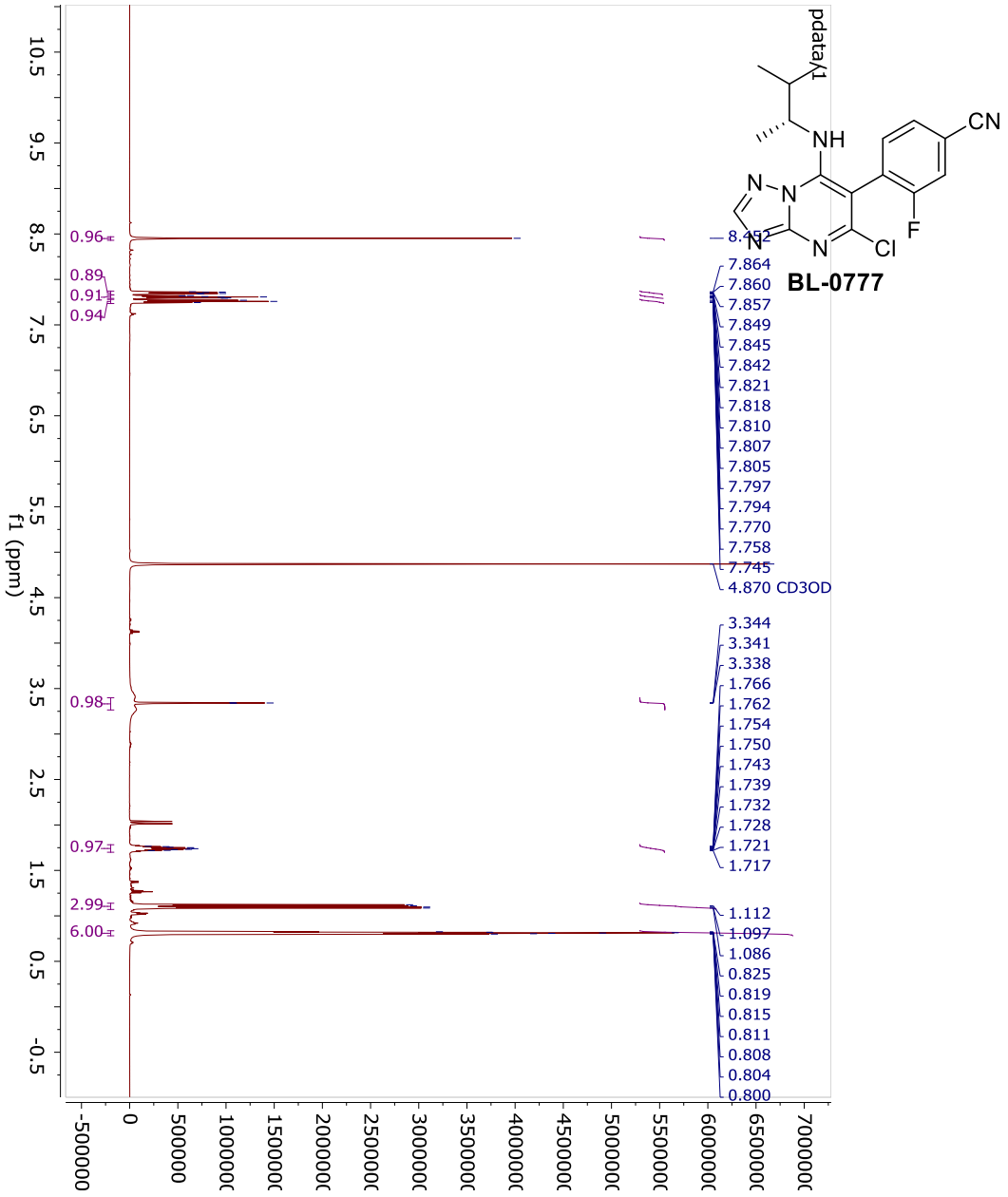
pdata/1
NH
N
N
N
N
Cl
F
CN
BL-0777
0.96
0.89
0.91
0.94
0.98
0.97
2.99
6.00
8.452
7.864
7.860
7.857
7.849
7.845
7.842
7.821
7.818
7.810
7.807
7.805
7.797
7.794
7.770
7.758
7.745
4.870 CD3OD
3.344
3.341
3.338
1.766
1.762
1.754
1.750
1.743
1.739
1.732
1.728
1.721
1.717
1.112
1.097
1.086
0.825
0.819
0.815
0.811
0.808
0.804
0.800
f1 (ppm)

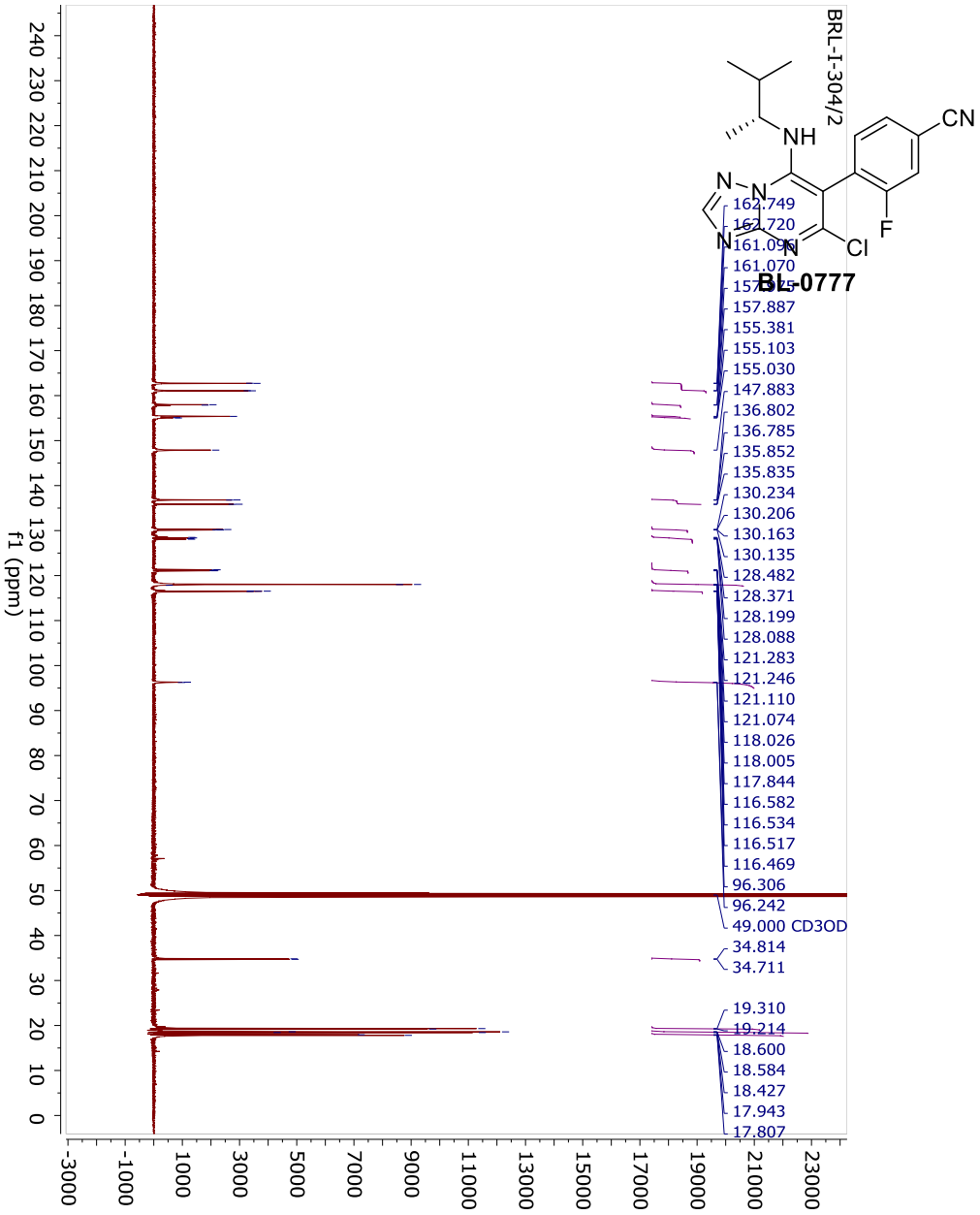
BRL-I-304/2
NH
N
N
N
N
Cl
F
CN
BL-0777
162.749
162.720
161.070
157.887
155.381
155.103
155.030
147.883
136.802
136.785
135.852
135.835
130.234
130.206
130.163
130.135
128.482
128.371
128.199
128.088
121.283
121.246
121.110
121.074
118.026
118.005
117.844
116.582
116.534
116.517
116.469
96.306
96.242
49.000 CD3OD
34.814
34.711
19.310
19.214
18.600
18.584
18.427
17.943
17.807
f1 (ppm)

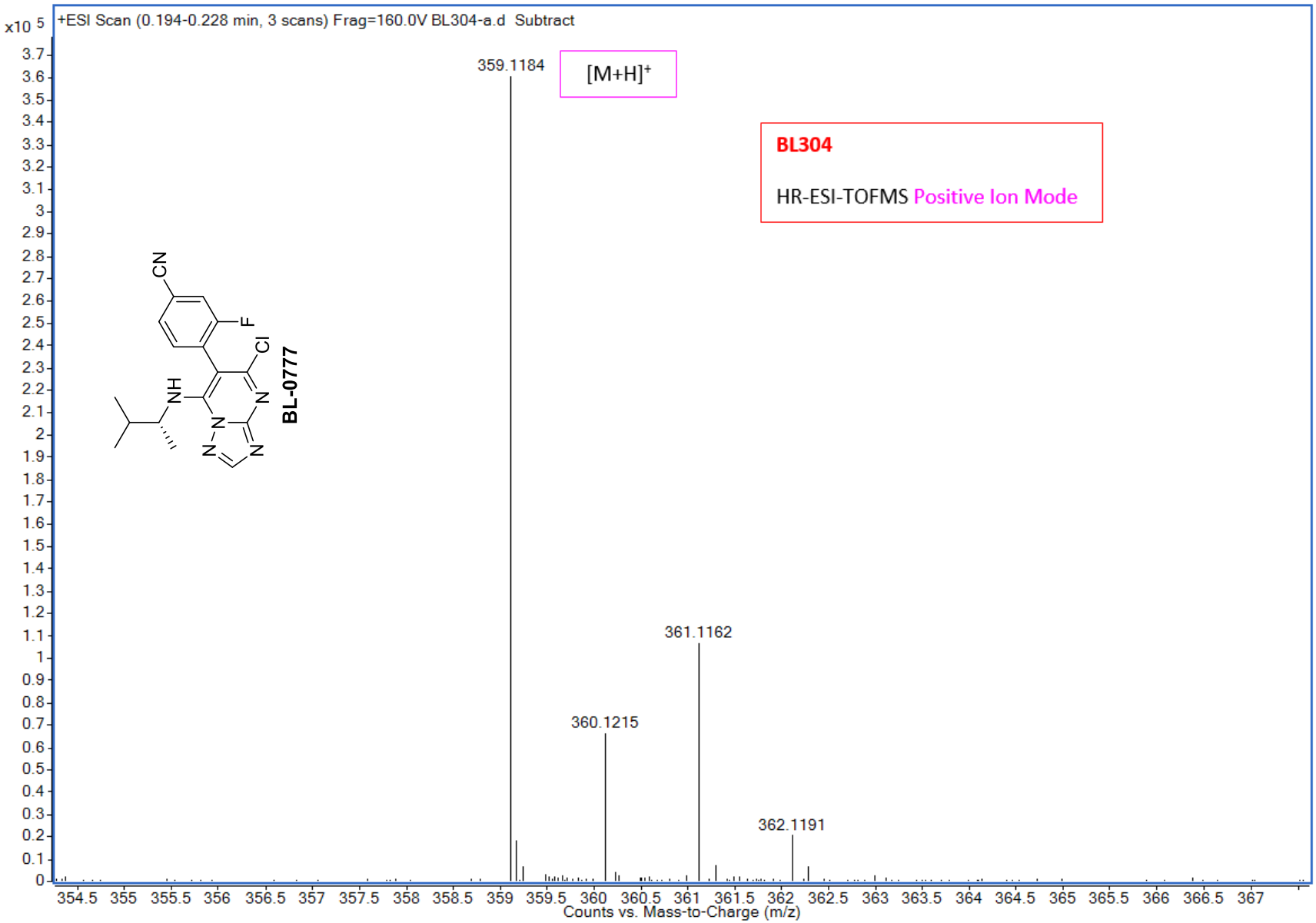
+ESI Scan (0.194-0.228 min, 3 scans) Frag=160.0V BL304-a.d Subtract
x10 5
359.1184
[M+H]+
BL304
HR-ESI-TOFMS Positive Ion Mode
BL-0777
361.1162
360.1215
362.1191
Counts vs. Mass-to-Charge (m/z)

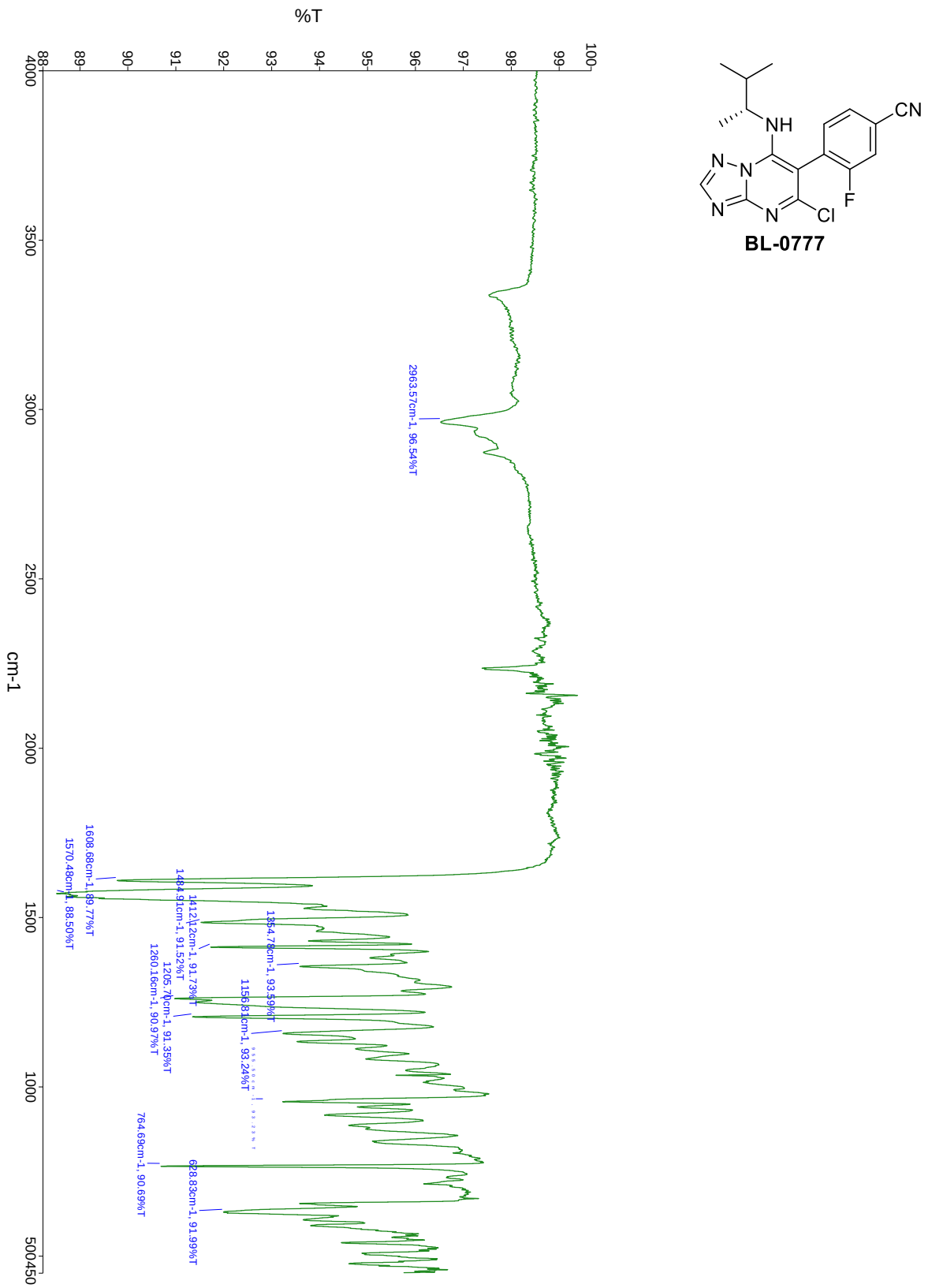
%T
cm-1
2963.57cm-1, 96.54%T
1608.68cm-1, 89.77%T
1570.48cm-1, 88.50%T
1484.91cm-1, 91.52%T
1412.12cm-1, 91.73%T
1354.78cm-1, 93.59%T
1205.70cm-1, 91.35%T
1260.16cm-1, 90.9%T
1156.81cm-1, 93.24%T
764.69cm-1, 90.69%T
628.83cm-1, 91.99%T
NH
CN
F
Cl
N
BL-0777

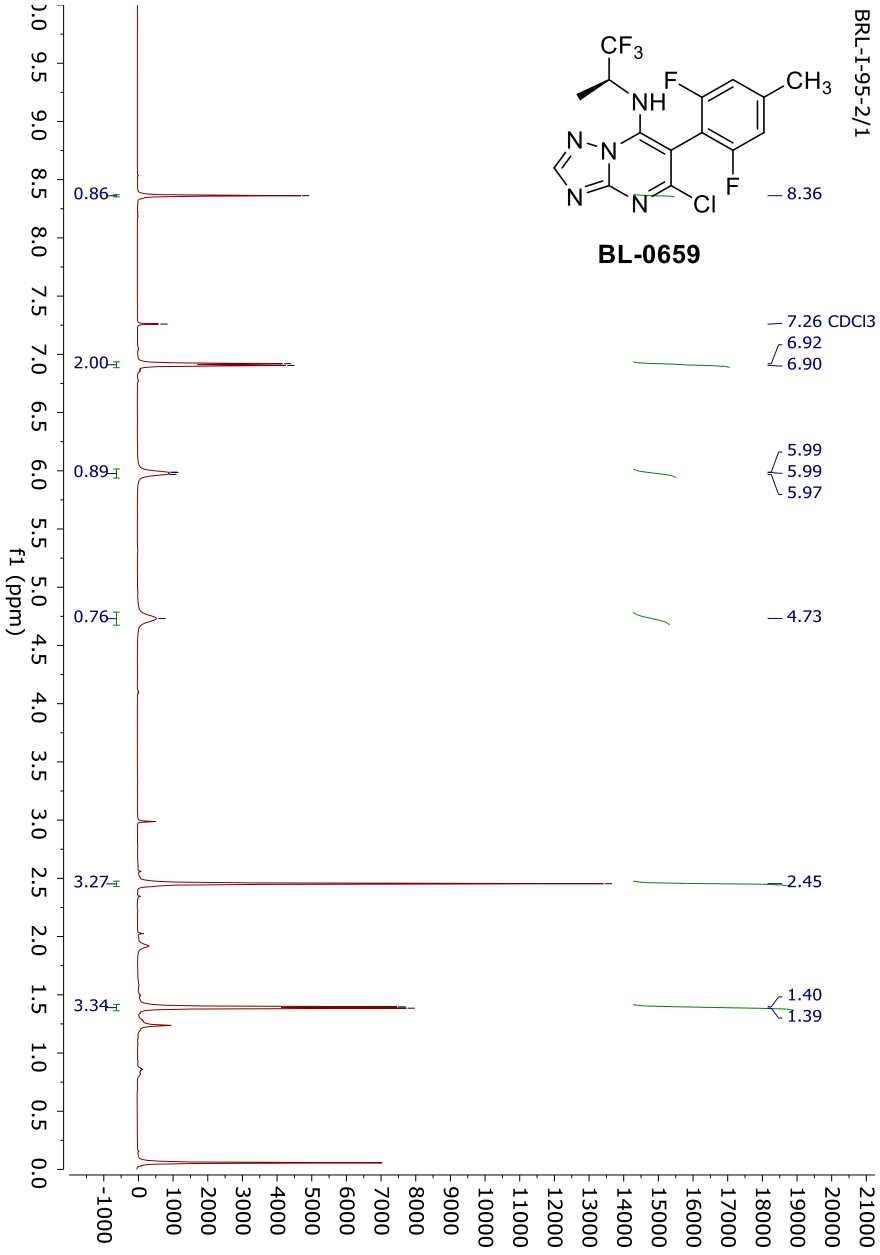
BRL-I-95-2/1
CF3
NH
F
CH3
N
N
N
N
Cl
F
BL-0659
0.86
2.00
0.89
0.76
3.27
3.34
8.36
7.26 CDCl3
6.92
6.90
5.99
5.99
5.97
4.73
2.45
1.40
1.39
f1 (ppm)

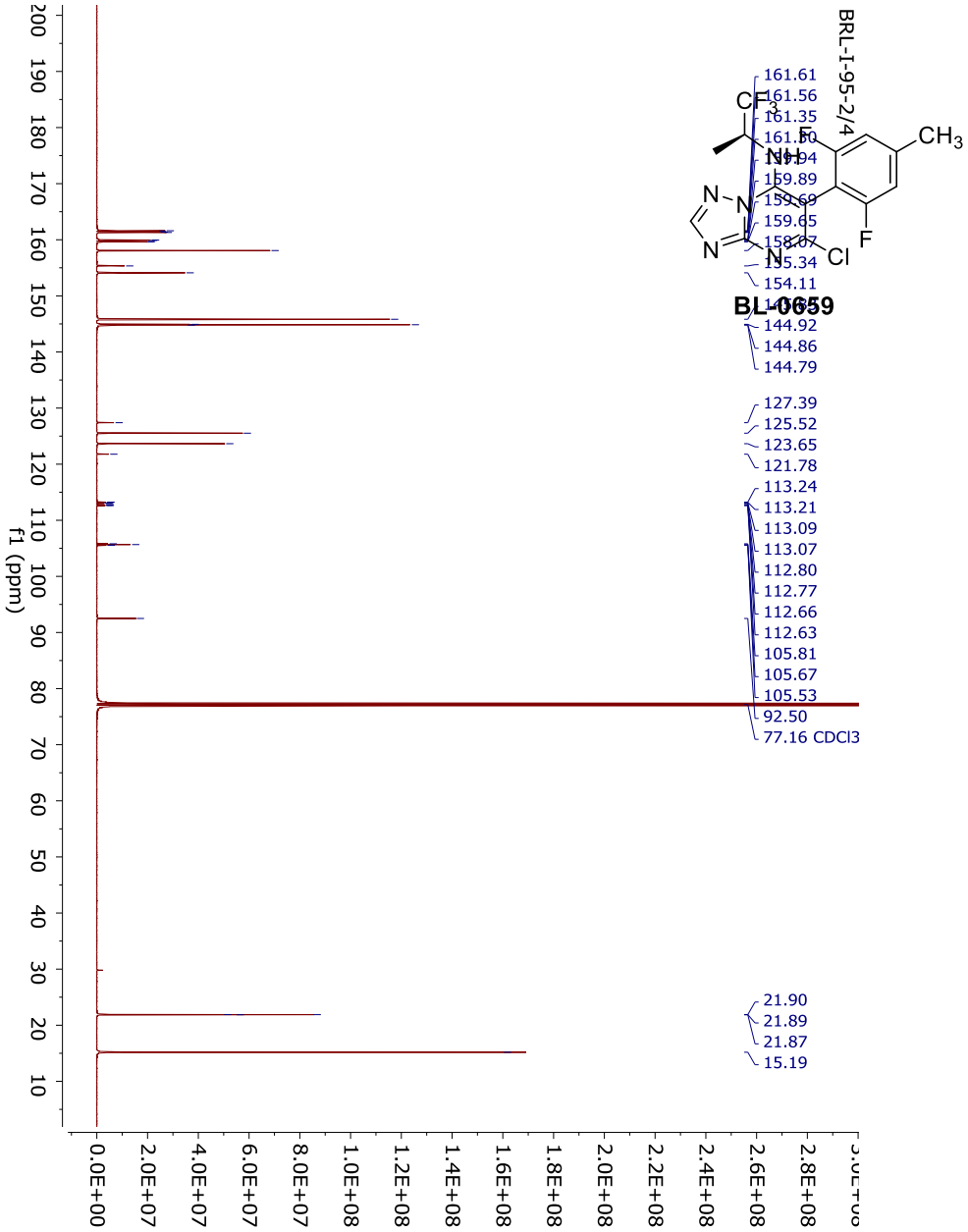
BRL-I-95-2/4
BL-0659
161.61
161.56
161.35
159.89
159.65
154.11
144.92
144.86
144.79
127.39
125.52
123.65
121.78
113.24
113.21
113.09
113.07
112.80
112.77
112.66
112.63
105.81
105.67
105.53
92.50
77.16 CDCl3
21.90
21.89
21.87
15.19
f1 (ppm)

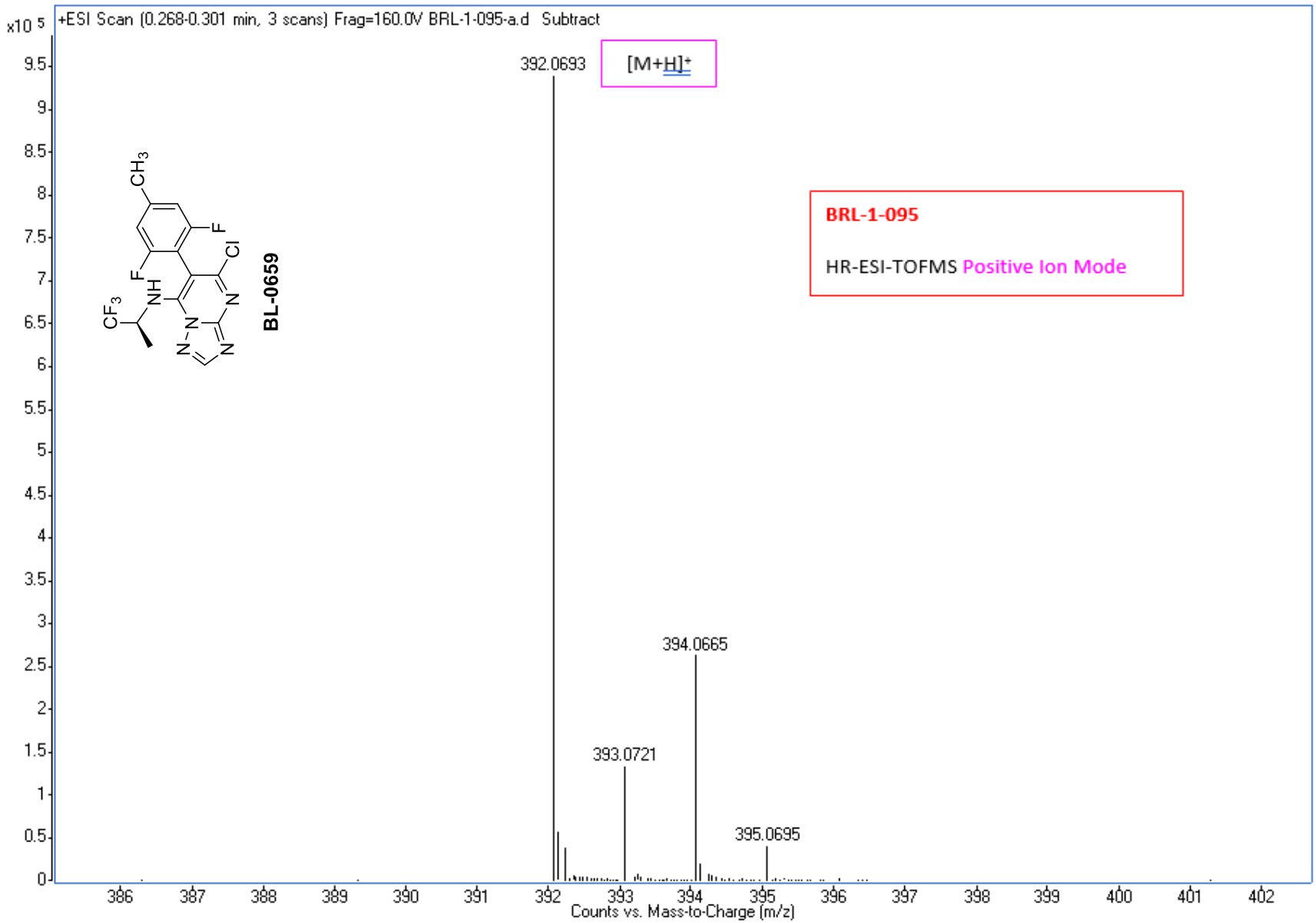
+ESI Scan (0.268-0.301 min, 3 scans) Frag=160.0V BRL-1-095-a.d Subtract
x10 5
392.0693
[M+H]+
394.0665
393.0721
395.0695
BRL-1-095
HR-ESI-TOFMS Positive Ion Mode
BL-0659
Counts vs. Mass-to-Charge (m/z)

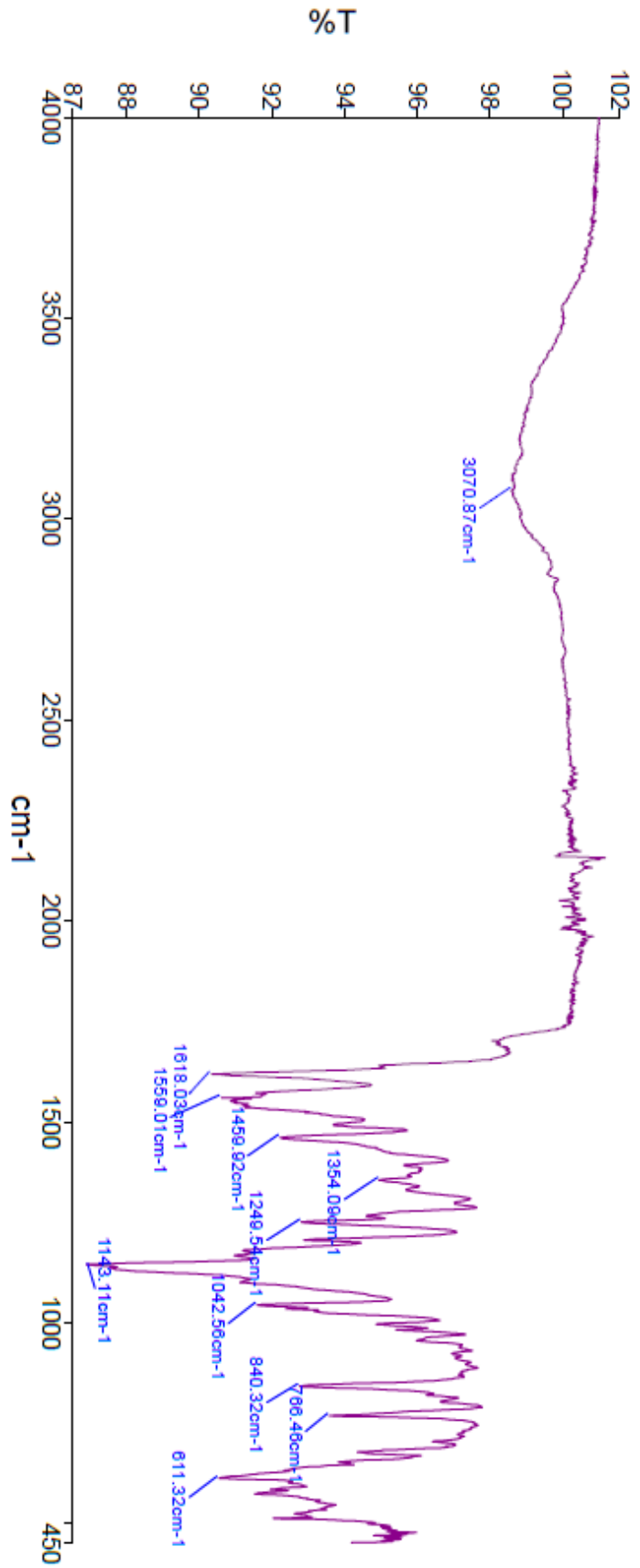
%T
102
100
98
96
94
92
90
88
87
4000
3500
3000
2500
2000
1500
1000
450
cm-1
3070.87cm-1
1618.03cm-1
1559.01cm-1
1459.92cm-1
1354.09cm-1
1249.54cm-1
1143.11cm-1
1042.58cm-1
840.32cm-1
786.48cm-1
611.32cm-1

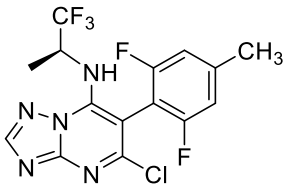
CF3
NH
F
CH3
N
N
N
N
Cl
F

BL-0659

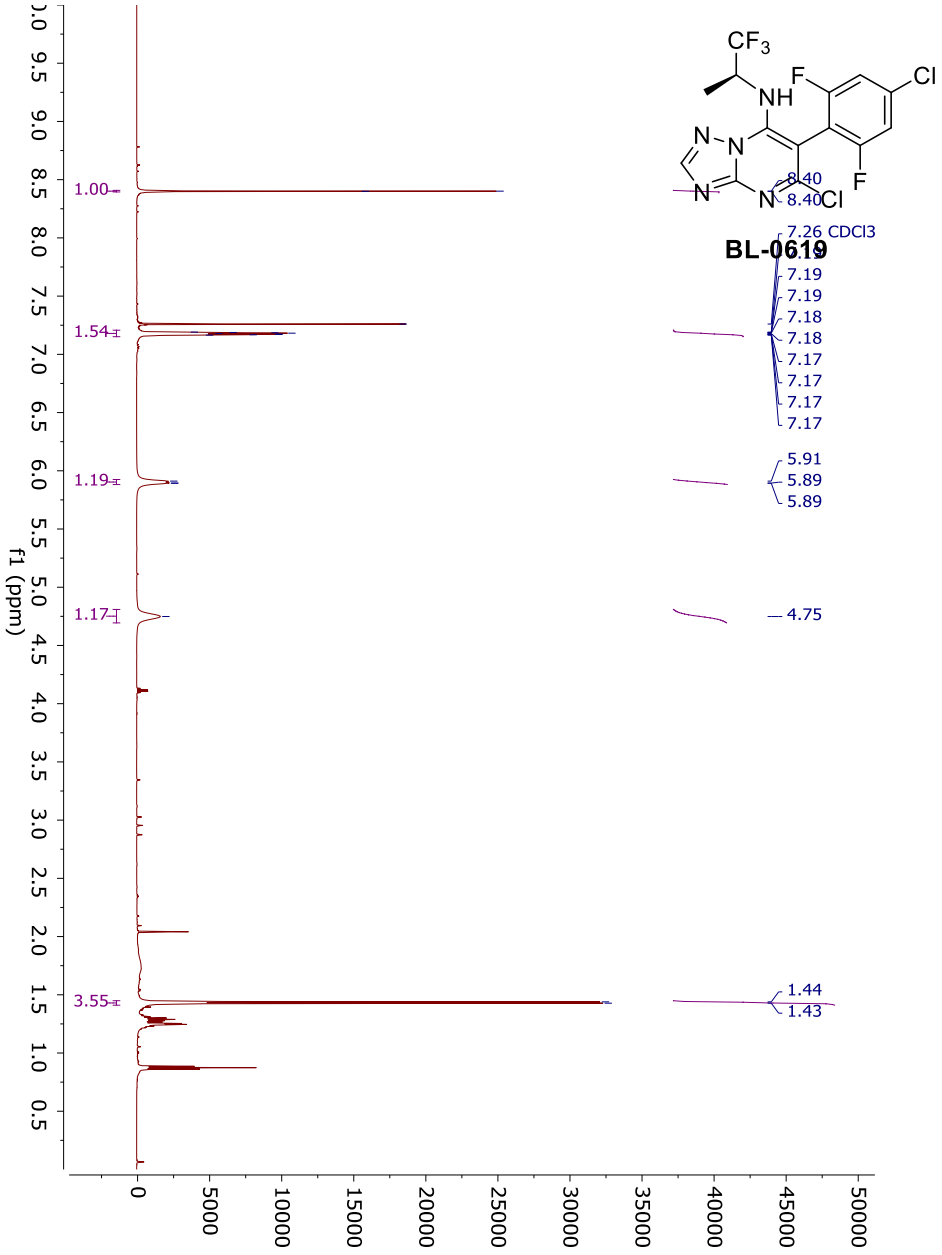
CF3
F
Cl
NH
N
N
N
N
F
Cl
8.40
8.40
7.26 CDCl3
BL-0619
7.19
7.19
7.19
7.18
7.18
7.17
7.17
7.17
7.17
5.91
5.89
5.89
4.75
1.44
1.43
1.00
1.54
1.19
1.17
3.55
f1 (ppm)

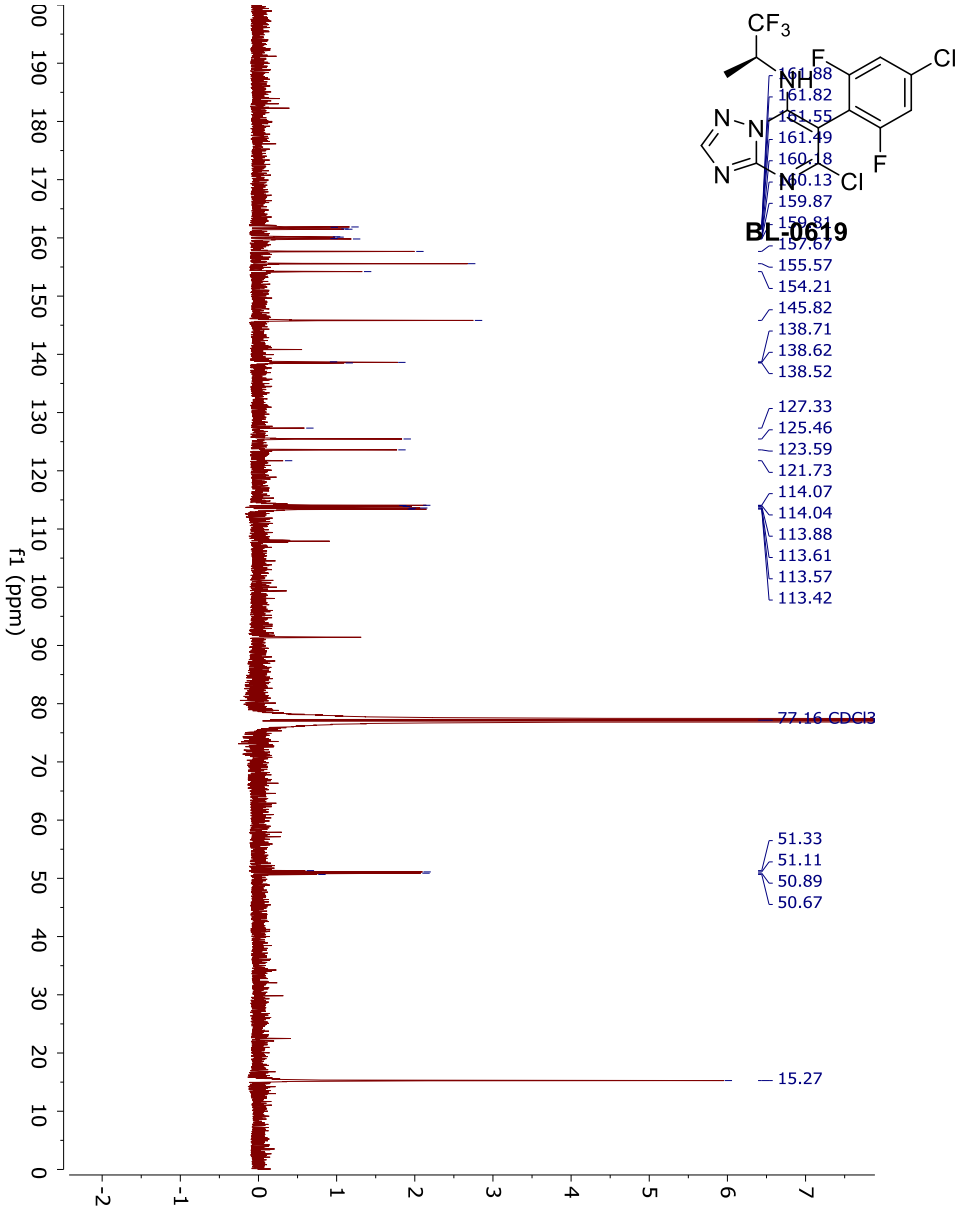
CF3
F
Cl
NH
N
N
N
F
Cl
BL-0619
161.88
161.82
161.55
161.49
160.18
160.13
159.87
155.57
154.21
145.82
138.71
138.62
138.52
127.33
125.46
123.59
121.73
114.07
114.04
113.88
113.61
113.57
113.42
77.16 CDCl3
51.33
51.11
50.89
50.67
15.27
f1 (ppm)

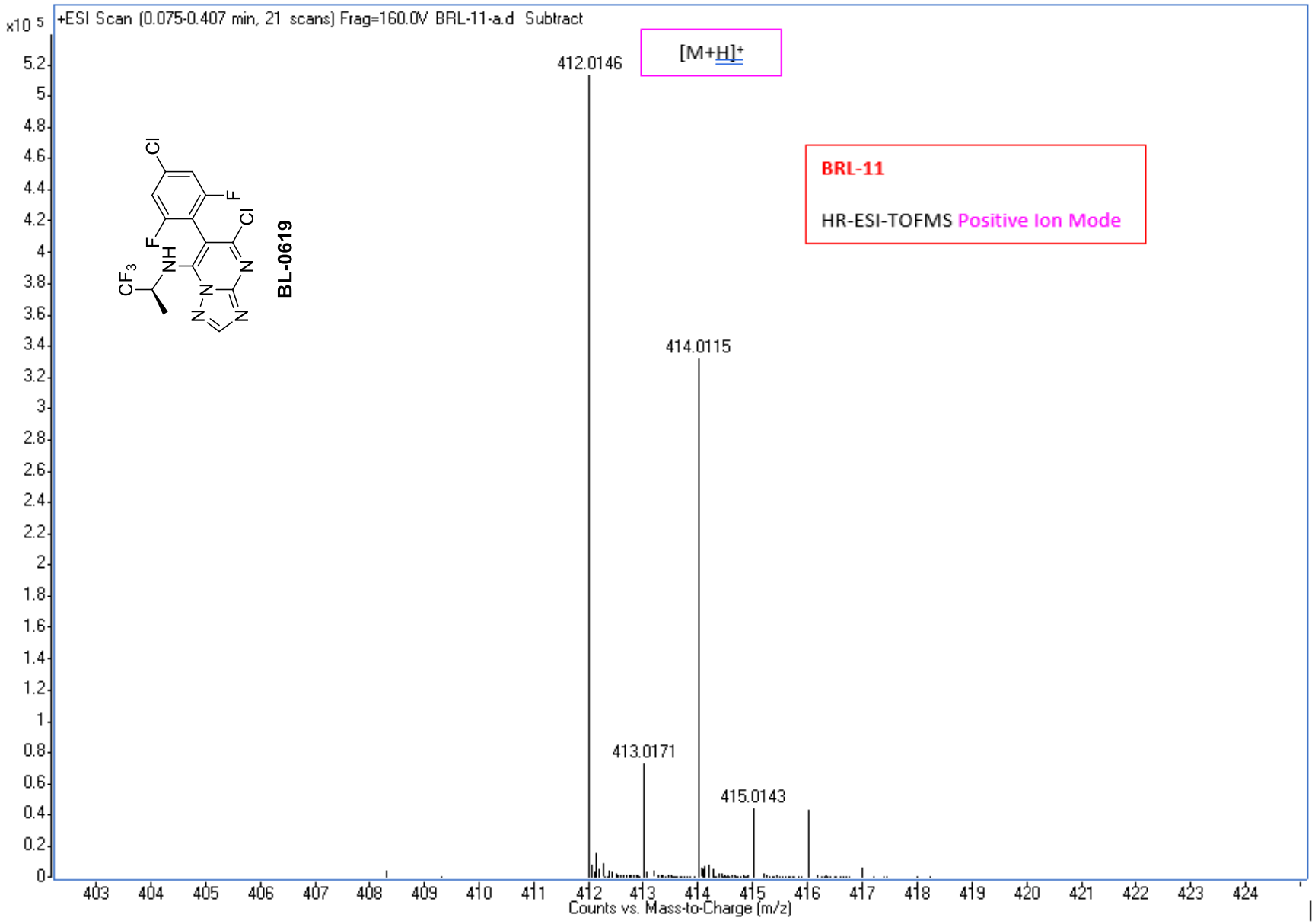
+ESI Scan (0.075-0.407 min, 21 scans) Frag=160.0V BRL-11-a.d Subtract
x10 5
[M+H]+
412.0146
414.0115
413.0171
415.0143
BRL-11
HR-ESI-TOFMS Positive Ion Mode
BL-0619
Counts vs. Mass-to-Charge (m/z)

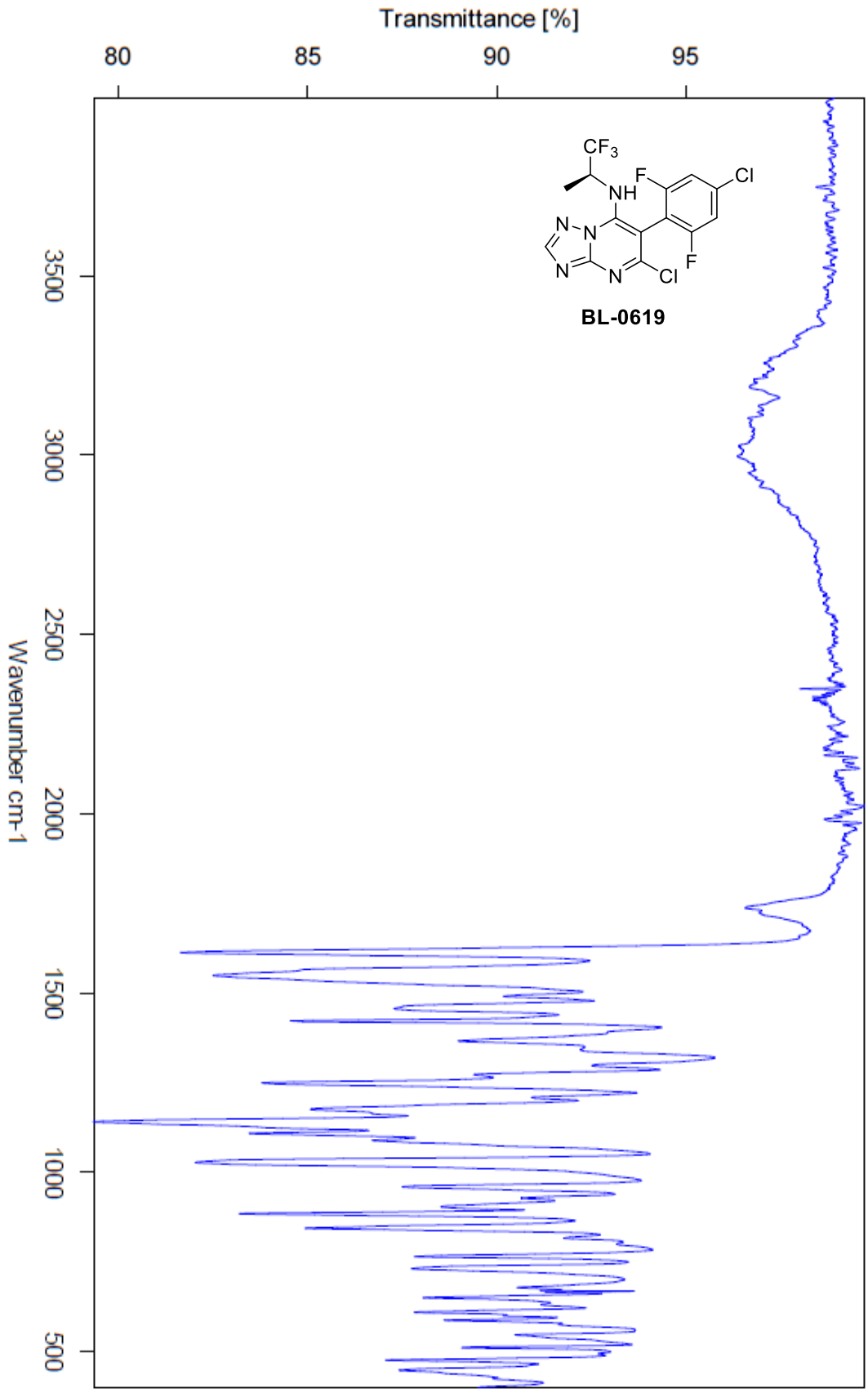
Transmittance [%]
80
85
90
95
Wavenumber cm-1
3500
3000
2500
2000
1500
1000
500
CF3
NH
F
Cl
N
N
N
N
Cl
F
BL-0619

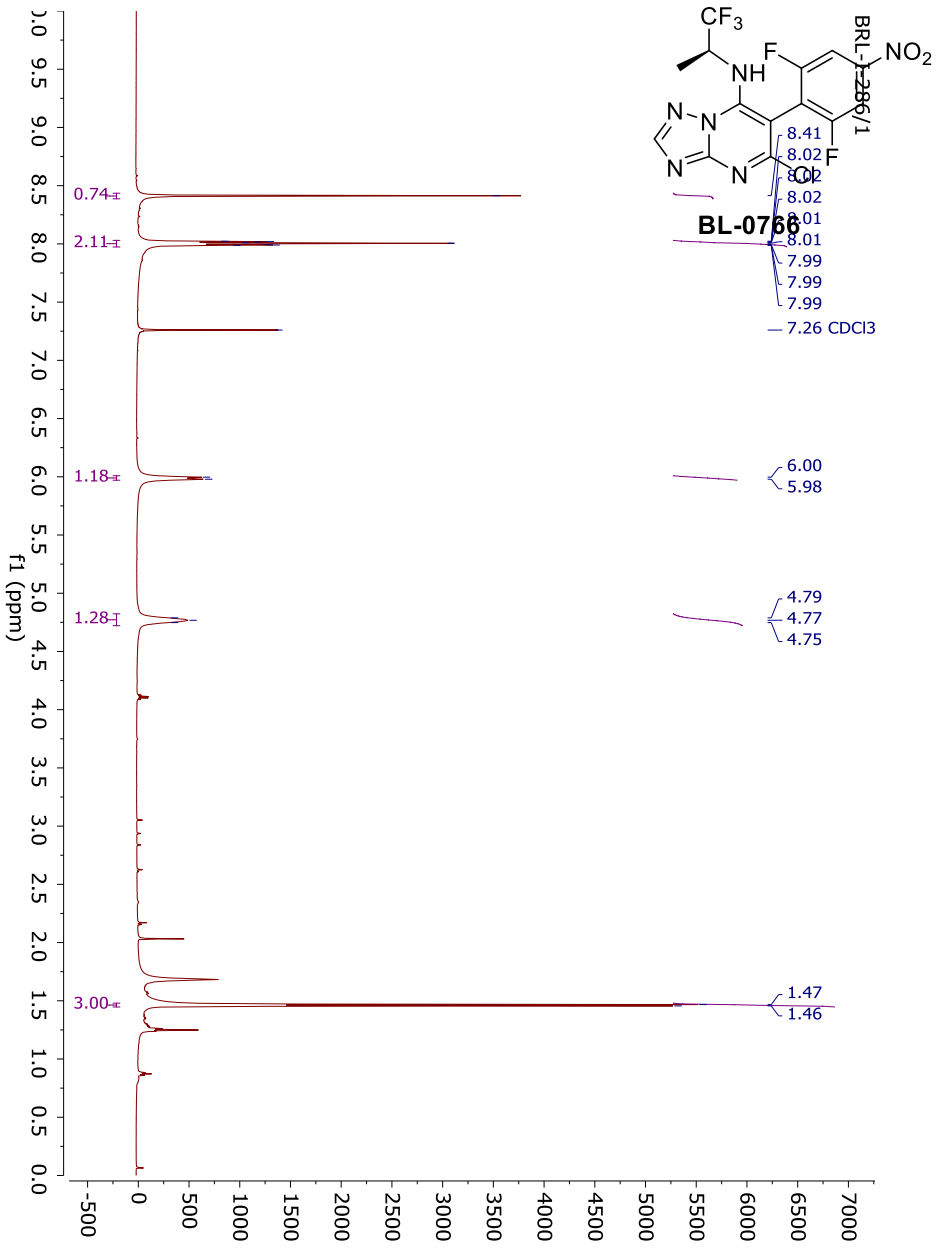
CF3
NH
F
NO2
BRL-1-286/1
F
Cl
BL-0766
8.41
8.02
8.02
8.02
8.01
8.01
7.99
7.99
7.99
7.26 CDCl3
6.00
5.98
4.79
4.77
4.75
1.47
1.46
0.74
2.11
1.18
1.28
3.00
f1 (ppm)

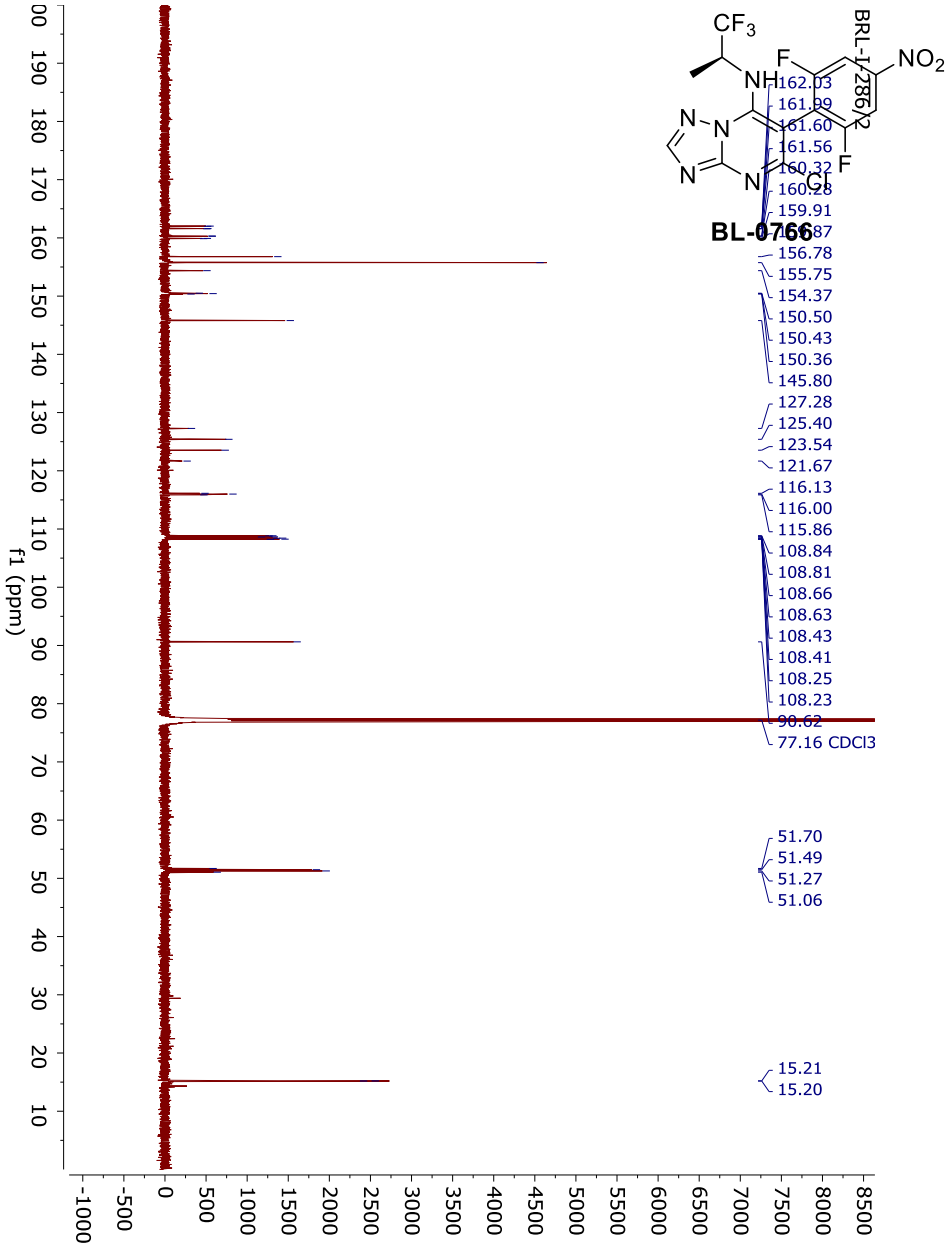
BRL-1/286/2
BL-0766
162.03
161.99
161.60
161.56
160.32
160.28
159.91
156.78
155.75
154.37
150.50
150.43
150.36
145.80
127.28
125.40
123.54
121.67
116.13
116.00
115.86
108.84
108.81
108.66
108.63
108.43
108.41
108.25
108.23
90.62
77.16 CDCl3
51.70
51.49
51.27
51.06
15.21
15.20
f1 (ppm)

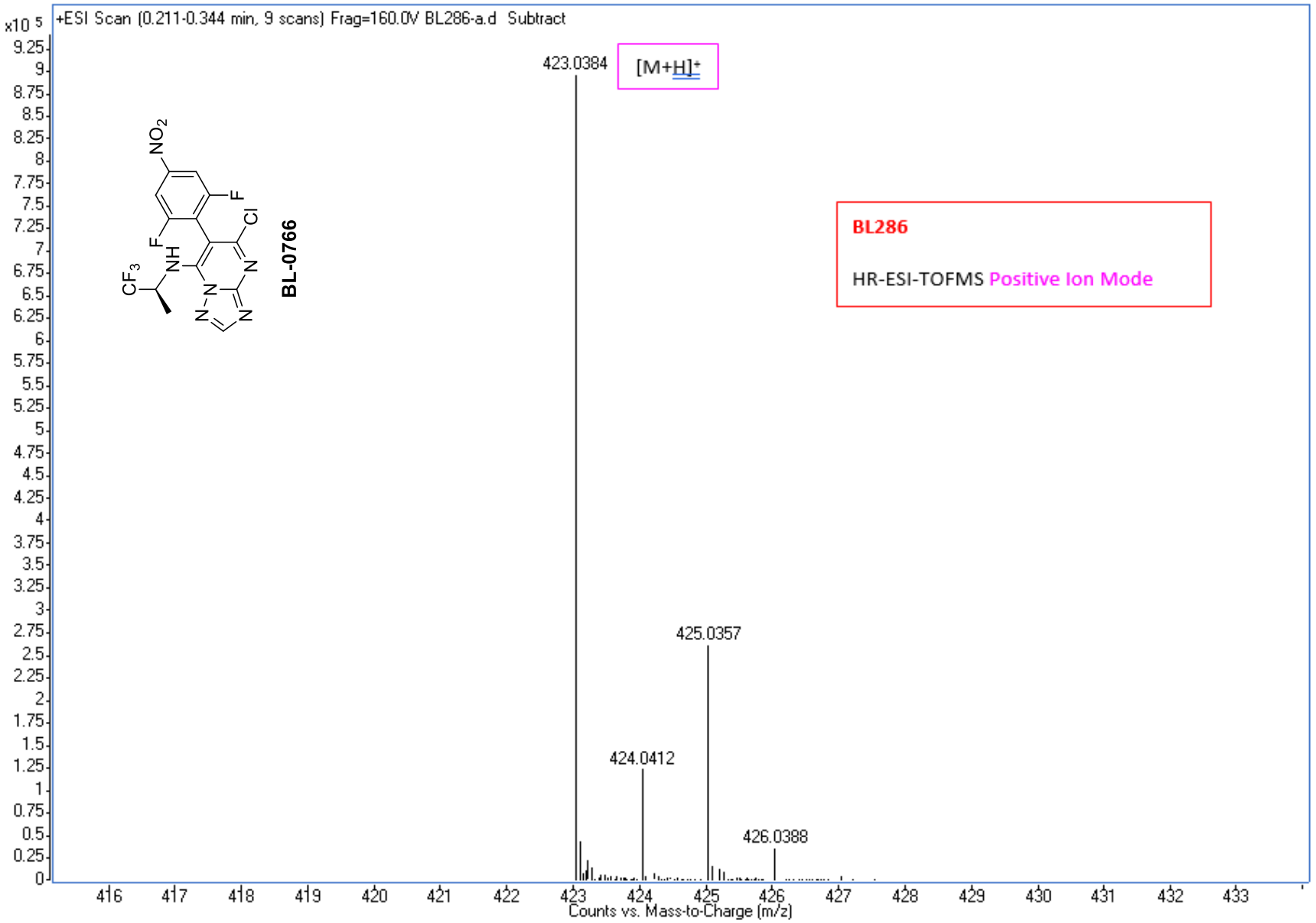
+ESI Scan (0.211-0.344 min, 9 scans) Frag=160.0V BL286-a.d Subtract
x10 5
423.0384
[M+H]+
425.0357
424.0412
426.0388
BL-0766
BL286
HR-ESI-TOFMS Positive Ion Mode
Counts vs. Mass-to-Charge (m/z)

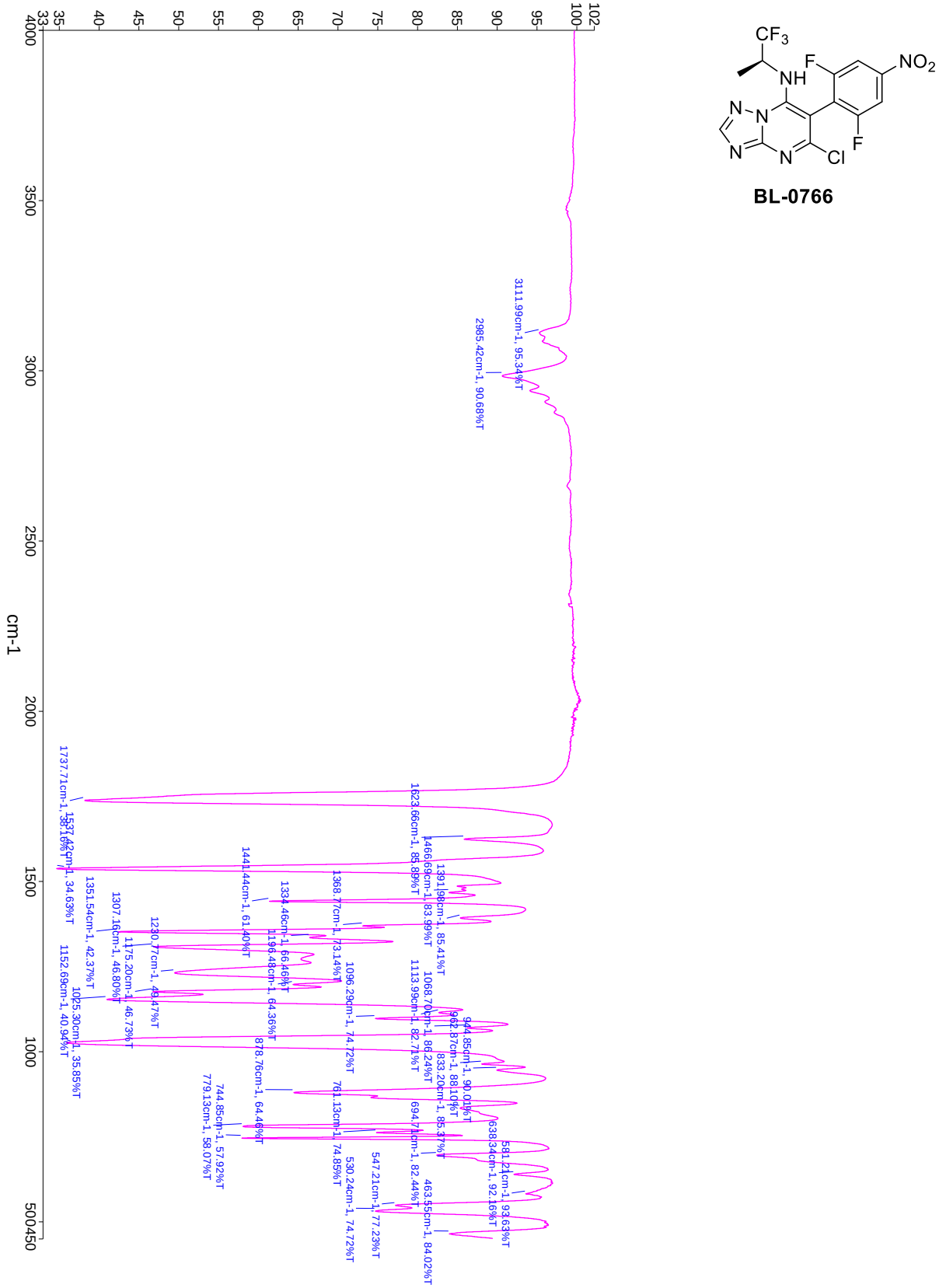
%T
cm-1
3111.99cm-1, 95.34%T
2985.42cm-1, 90.68%T
1623.66cm-1, 85.89%T
1466.69cm-1, 83.99%T
1391.98cm-1, 85.41%T
1368.77cm-1, 73.14%T
1334.46cm-1, 66.46%T
1441.44cm-1, 61.40%T
1196.48cm-1, 64.36%T
1096.29cm-1, 74.72%T
1068.70cm-1, 86.24%T
1113.99cm-1, 82.71%T
962.87cm-1, 88.10%T
944.85cm-1, 90.01%T
833.20cm-1, 85.37%T
878.76cm-1, 64.48%T
761.13cm-1, 74.85%T
694.71cm-1, 82.44%T
638.34cm-1, 92.16%T
581.21cm-1, 93.63%T
547.21cm-1, 77.23%T
530.24cm-1, 74.72%T
463.55cm-1, 84.02%T
744.85cm-1, 57.92%T
779.13cm-1, 58.07%T
1737.71cm-1, 38.16%T
1307.16cm-1, 46.80%T
1230.77cm-1, 49.47%T
1175.20cm-1, 46.73%T
1351.54cm-1, 42.37%T
1025.30cm-1, 35.85%T
1152.69cm-1, 40.94%T

CF3
NH
F
NO2
N
N
N
N
Cl
F

BL-0766

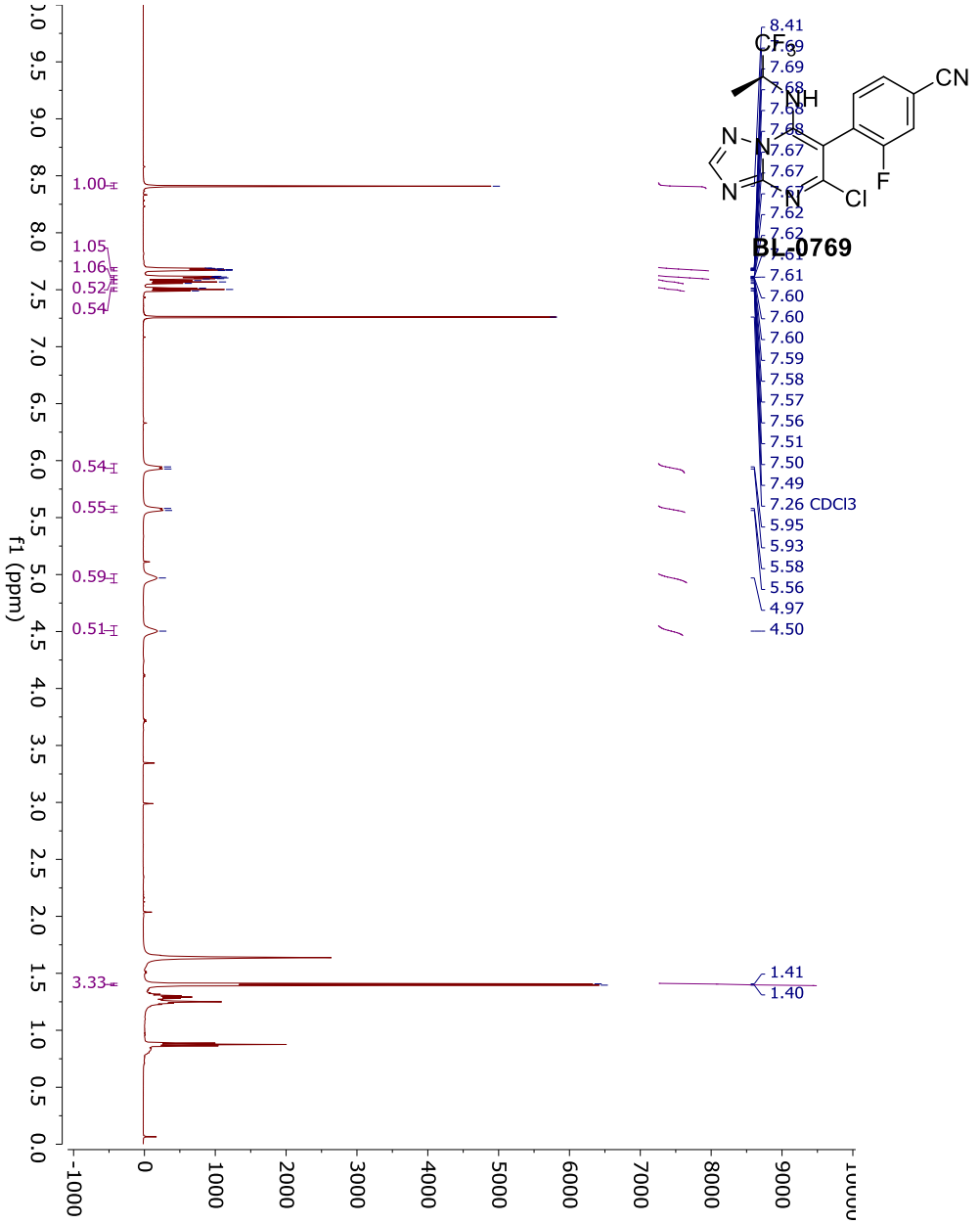
BL-0769
f1 (ppm)
1.00
1.05
1.06
0.52
0.54
0.54
0.55
0.59
0.51
3.33
8.41
7.69
7.69
7.68
7.67
7.67
7.62
7.62
7.61
7.61
7.60
7.60
7.60
7.59
7.58
7.57
7.56
7.51
7.50
7.49
7.26 CDCl3
5.95
5.93
5.58
5.56
4.97
4.50
1.41
1.40
CF3
NH
N
N
N
CN
F
Cl

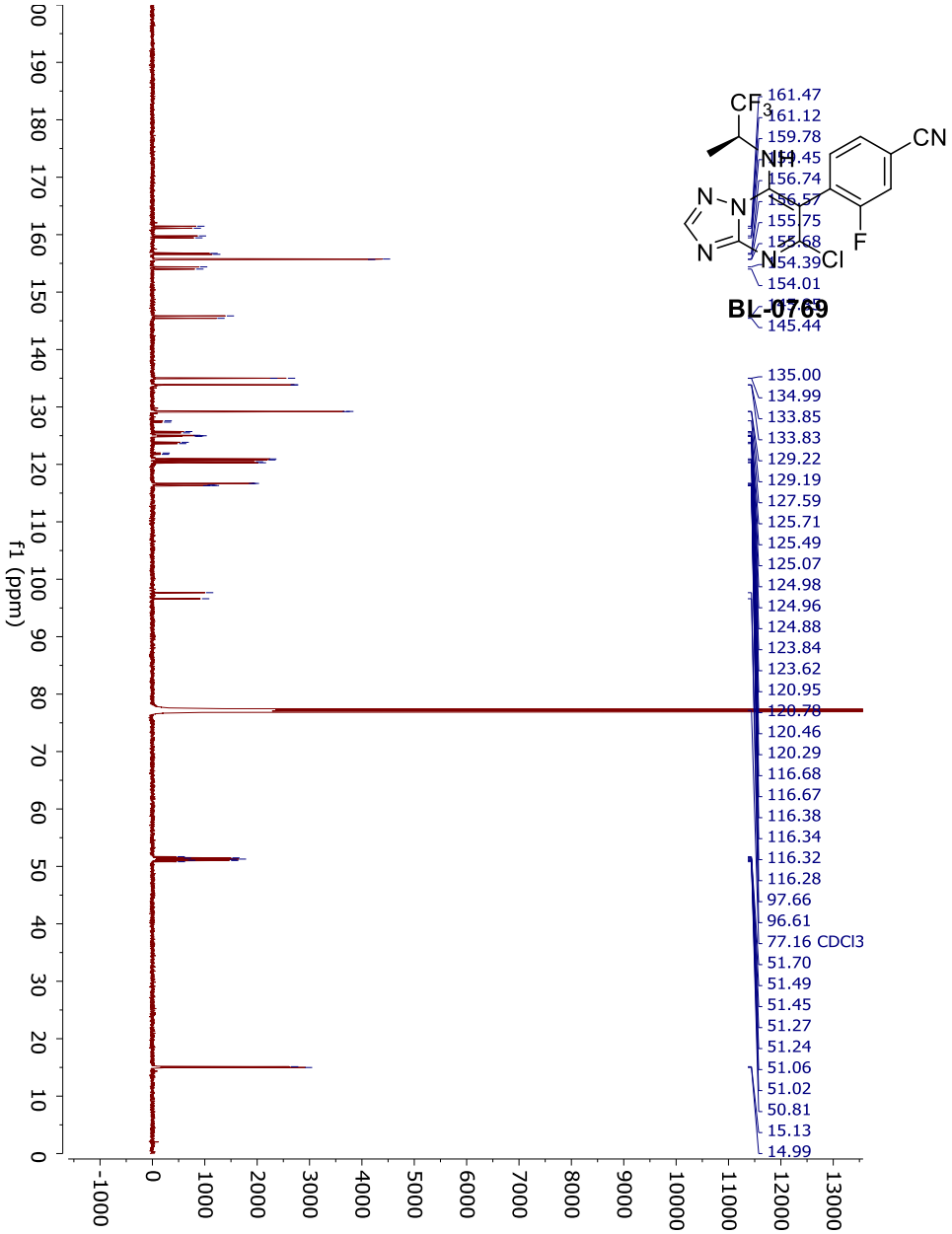
f1 (ppm)
BL-0769
CF3
NH
N
N
N
N
Cl
F
CN
161.47
161.12
159.78
156.74
155.75
154.39
154.01
145.44
135.00
134.99
133.85
133.83
129.22
129.19
127.59
125.71
125.49
125.07
124.98
124.96
124.88
123.84
123.62
120.95
120.46
120.29
116.68
116.67
116.38
116.34
116.32
116.28
97.66
96.61
77.16 CDCl3
51.70
51.49
51.45
51.27
51.24
51.06
51.02
50.81
15.13
14.99

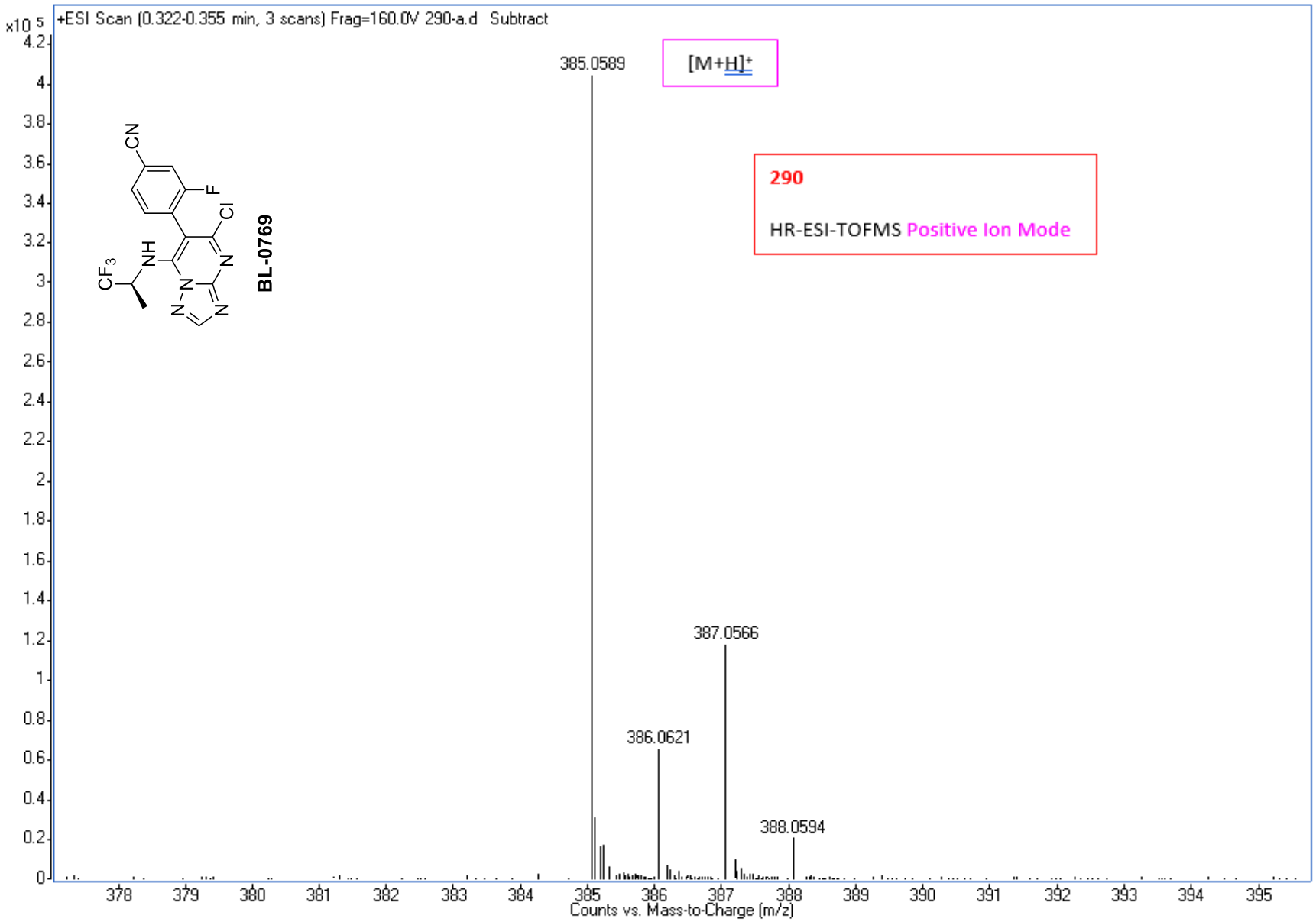
+ESI Scan (0.322-0.355 min, 3 scans) Frag=160.0V 290-a.d Subtract
x10 5
385.0589
[M+H]+
290
HR-ESI-TOFMS Positive Ion Mode
BL-0769
387.0566
386.0621
388.0594
Counts vs. Mass-to-Charge (m/z)

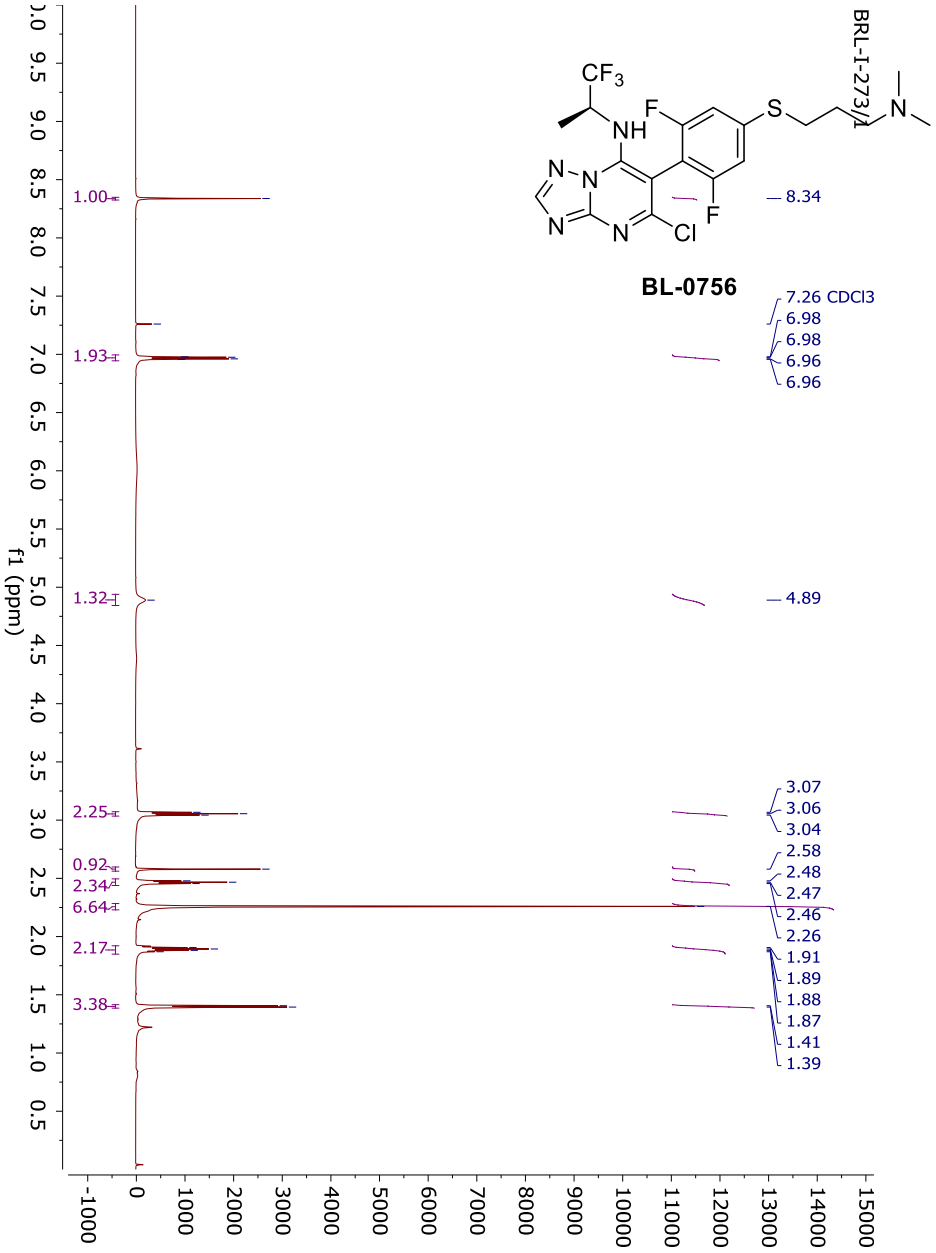
BRL-I-273/1
CF3
F
S
NH
N
N
N
N
F
Cl
8.34
BL-0756
7.26 CDCl3
6.98
6.98
6.96
6.96
4.89
3.07
3.06
3.04
2.58
2.48
2.47
2.46
2.26
1.91
1.89
1.88
1.87
1.41
1.39
1.00
1.93
1.32
2.25
0.92
2.34
6.64
2.17
3.38
f1 (ppm)

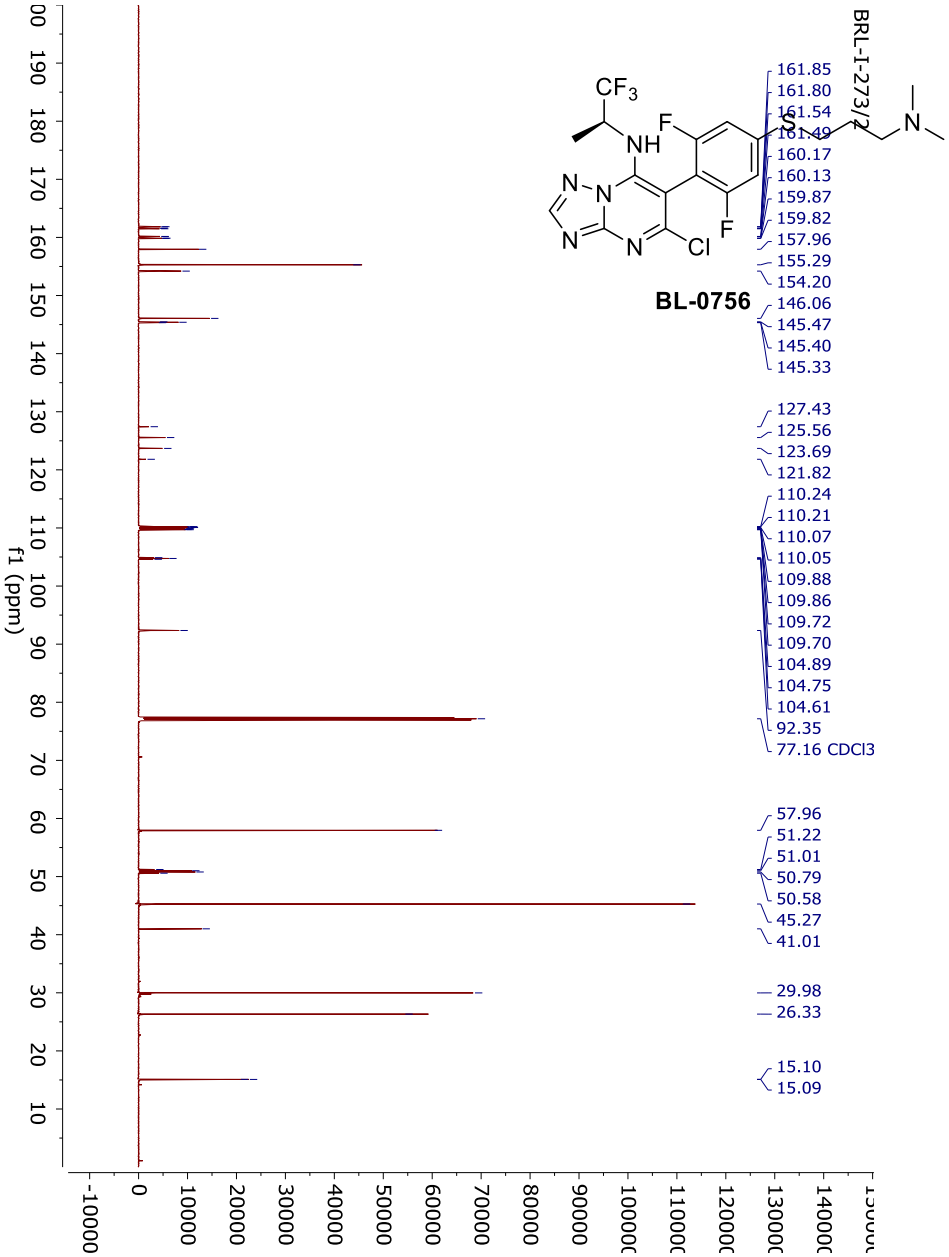
BRL-I-273/2
BL-0756
161.85
161.80
161.54
161.49
160.17
160.13
159.87
159.82
157.96
155.29
154.20
146.06
145.47
145.40
145.33
127.43
125.56
123.69
121.82
110.24
110.21
110.07
110.05
109.88
109.86
109.72
109.70
104.89
104.75
104.61
92.35
77.16 CDCl3
57.96
51.22
51.01
50.79
50.58
45.27
41.01
29.98
26.33
15.10
15.09
f1 (ppm)

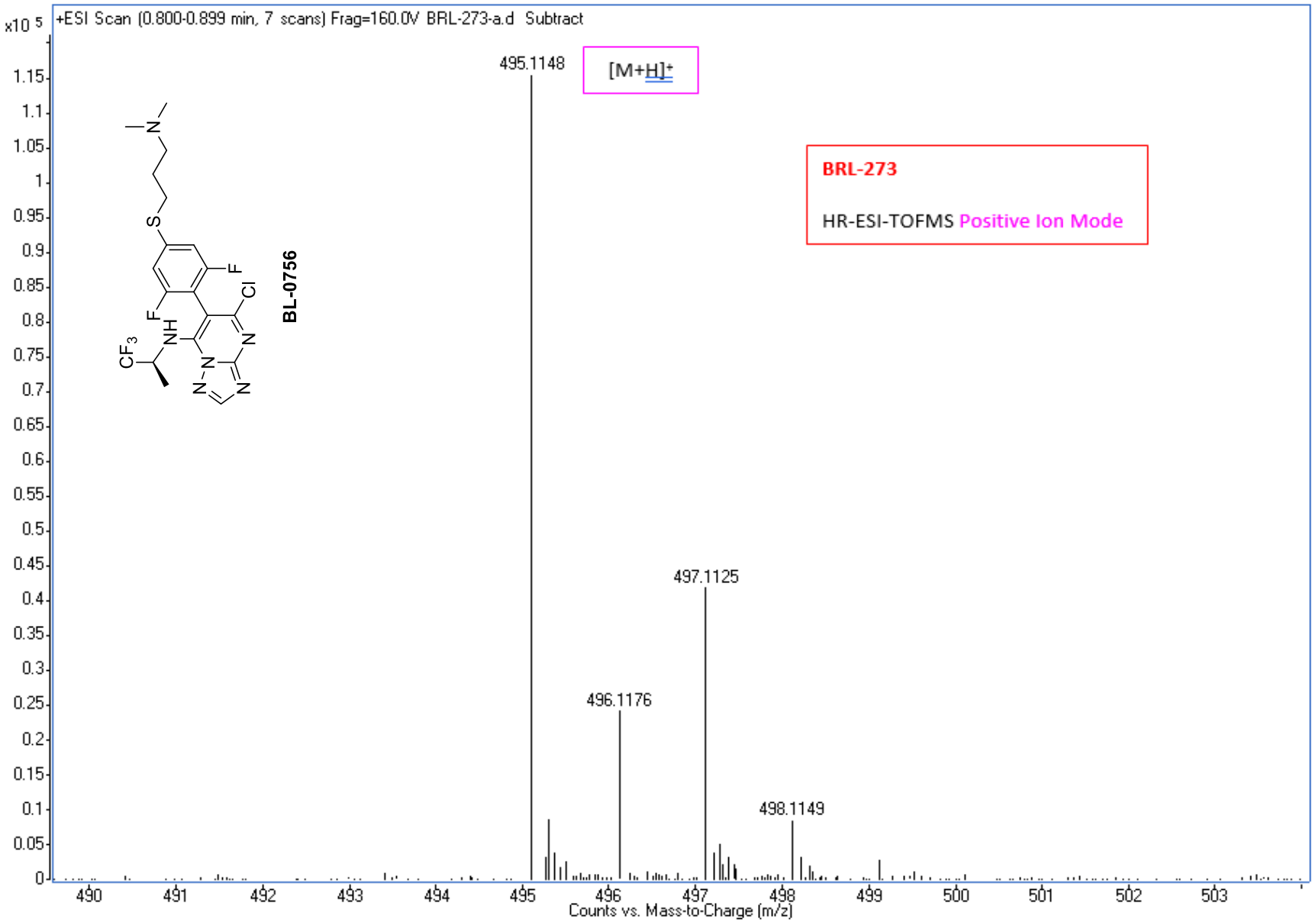
+ESI Scan (0.800-0.899 min, 7 scans) Frag=160.0V BRL-273-a.d Subtract
x10 5
1.15
1.1
1.05
1
0.95
0.9
0.85
0.8
0.75
0.7
0.65
0.6
0.55
0.5
0.45
0.4
0.35
0.3
0.25
0.2
0.15
0.1
0.05
0
495.1148
[M+H]+
BRL-273
HR-ESI-TOFMS Positive Ion Mode
BL-0756
497.1125
496.1176
498.1149
490
491
492
493
494
495
496
497
498
499
500
501
502
503
Counts vs. Mass-to-Charge (m/z)

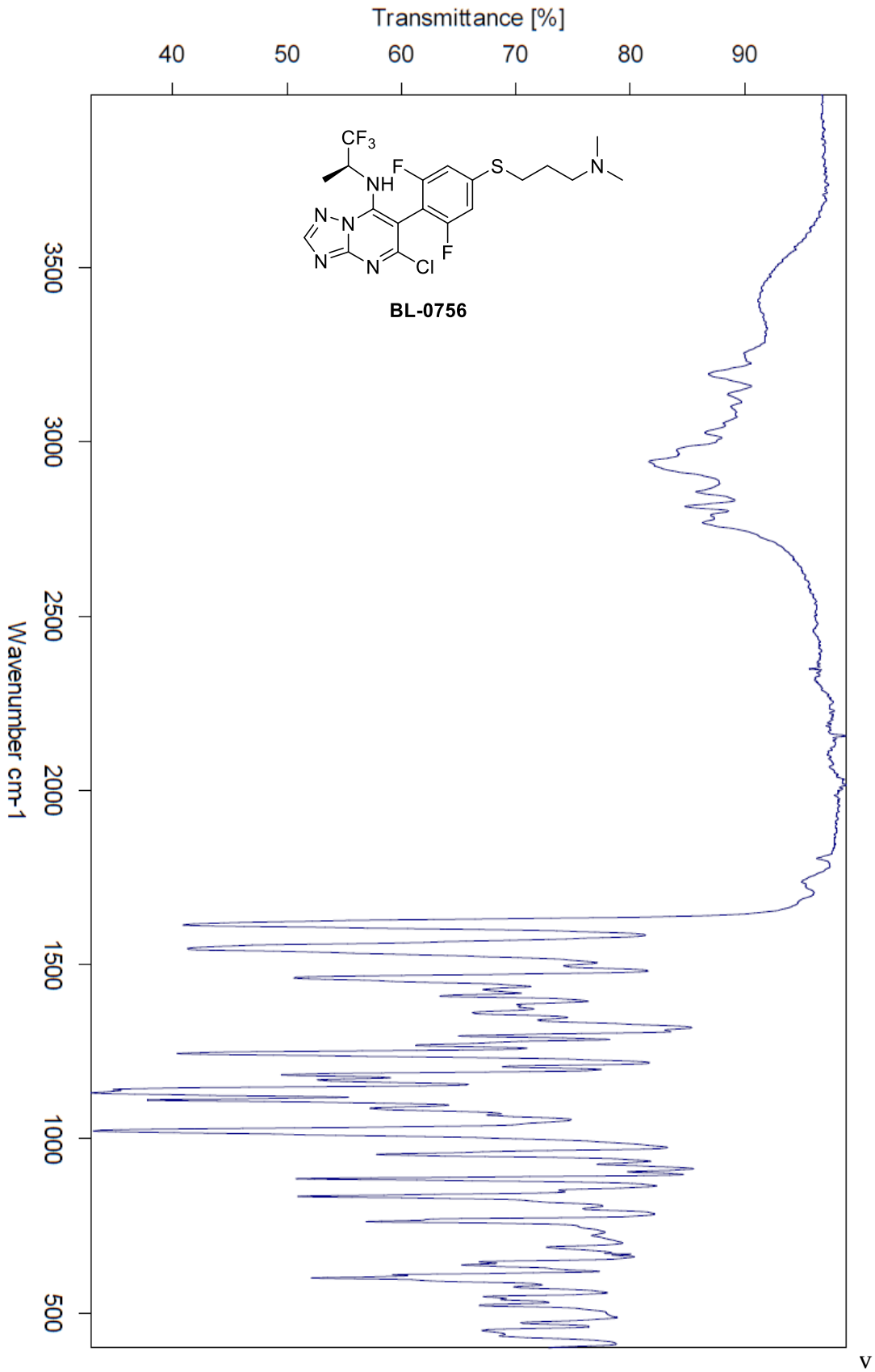
Transmittance [%]
40
50
60
70
80
90
Wavenumber cm-1
3500
3000
2500
2000
1500
1000
500
BL-0756

v

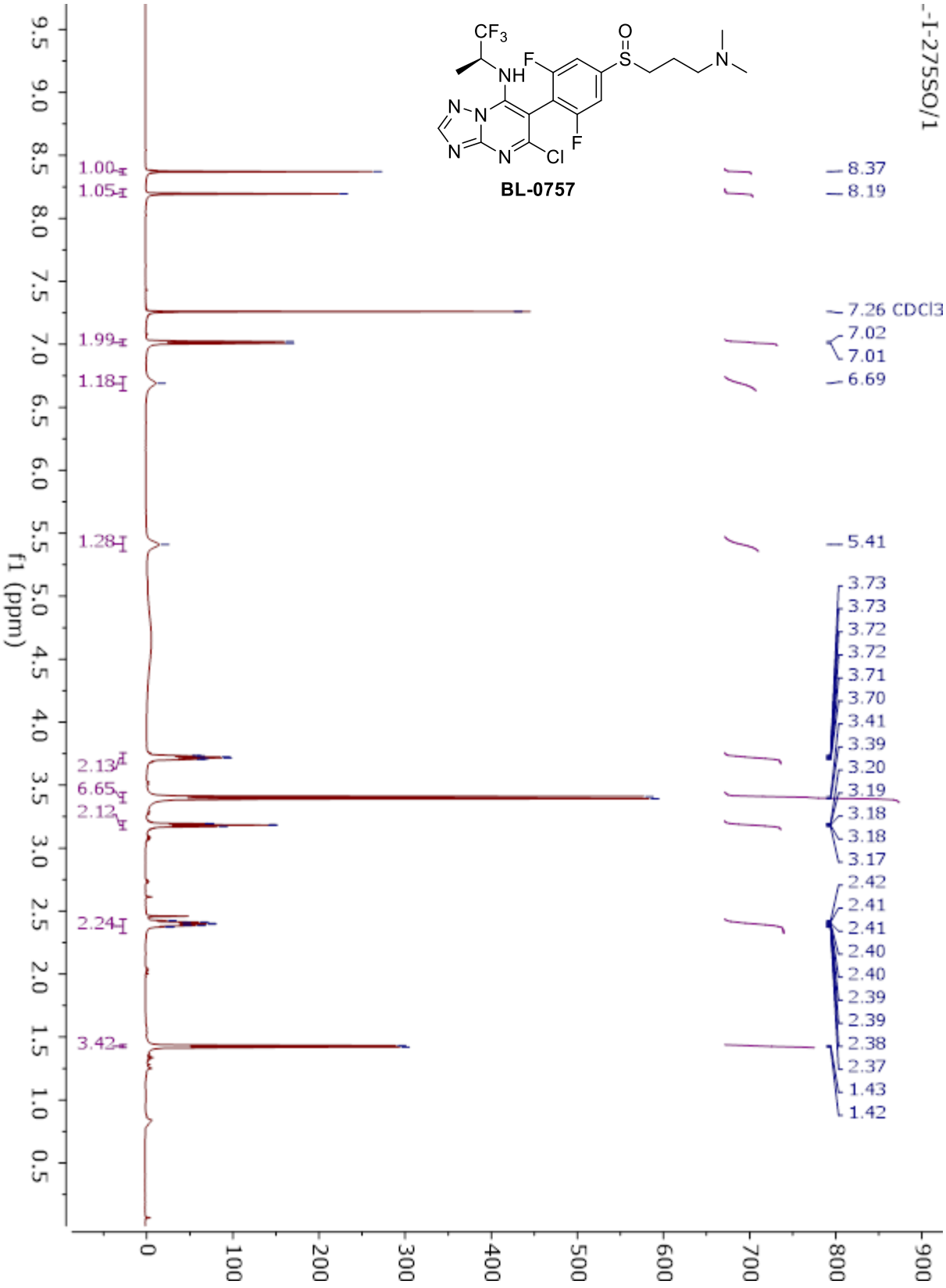
-I-275SO/1
BL-0757
f1 (ppm)
1.00
1.05
1.99
1.18
1.28
2.13
6.65
2.12
2.24
3.42
8.37
8.19
7.26 CDCl3
7.02
7.01
6.69
5.41
3.73
3.73
3.72
3.72
3.71
3.70
3.41
3.39
3.20
3.19
3.18
3.18
3.17
2.42
2.41
2.41
2.40
2.40
2.39
2.39
2.38
2.37
1.43
1.42

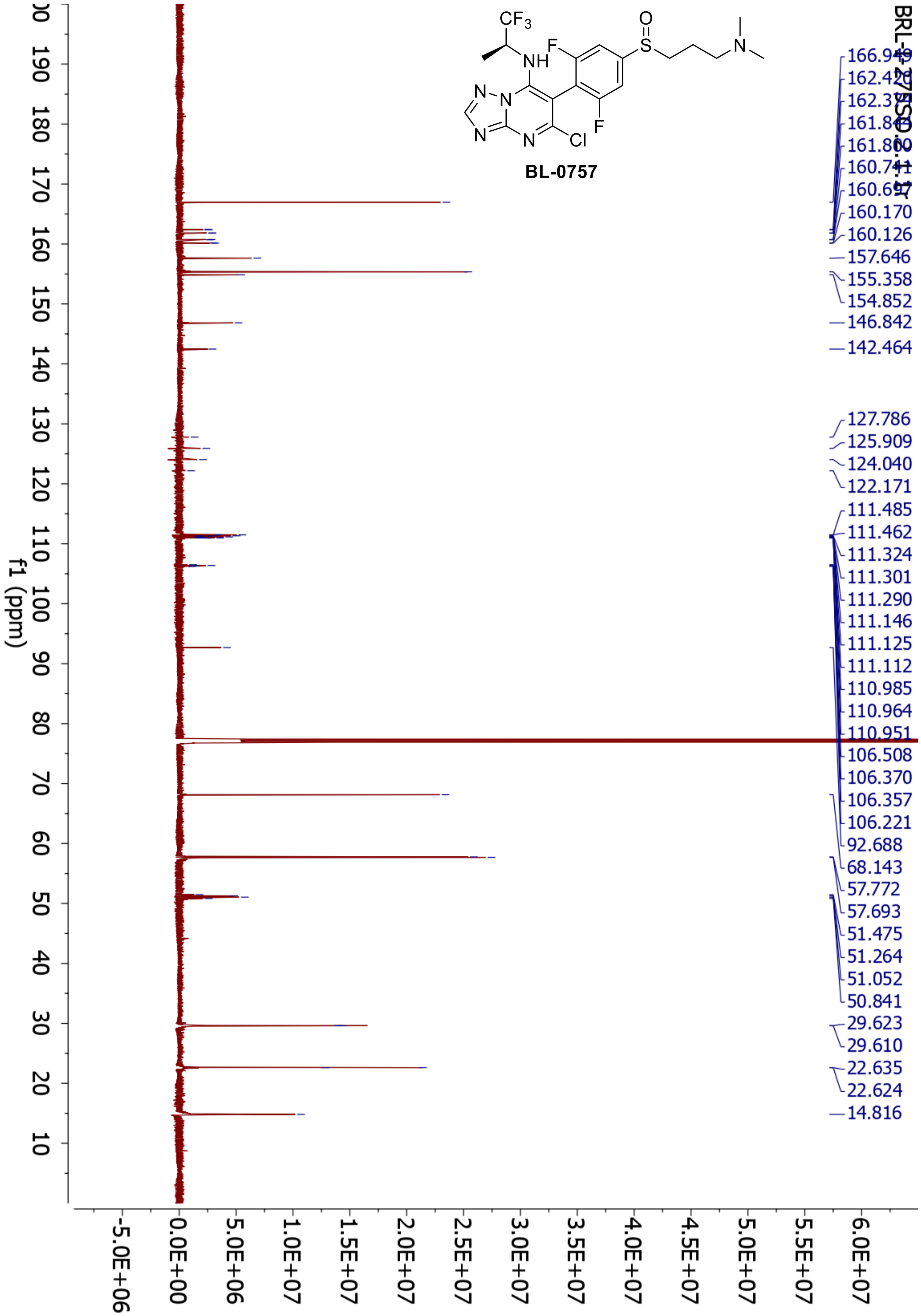
BL-0757
166.949
162.420
162.378
161.844
161.800
160.741
160.697
160.170
160.126
157.646
155.358
154.852
146.842
142.464
127.786
125.909
124.040
122.171
111.485
111.462
111.324
111.301
111.290
111.146
111.125
111.112
110.985
110.964
110.951
106.508
106.370
106.357
106.221
92.688
68.143
57.772
57.693
51.475
51.264
51.052
50.841
29.623
29.610
22.635
22.624
14.816
f1 (ppm)

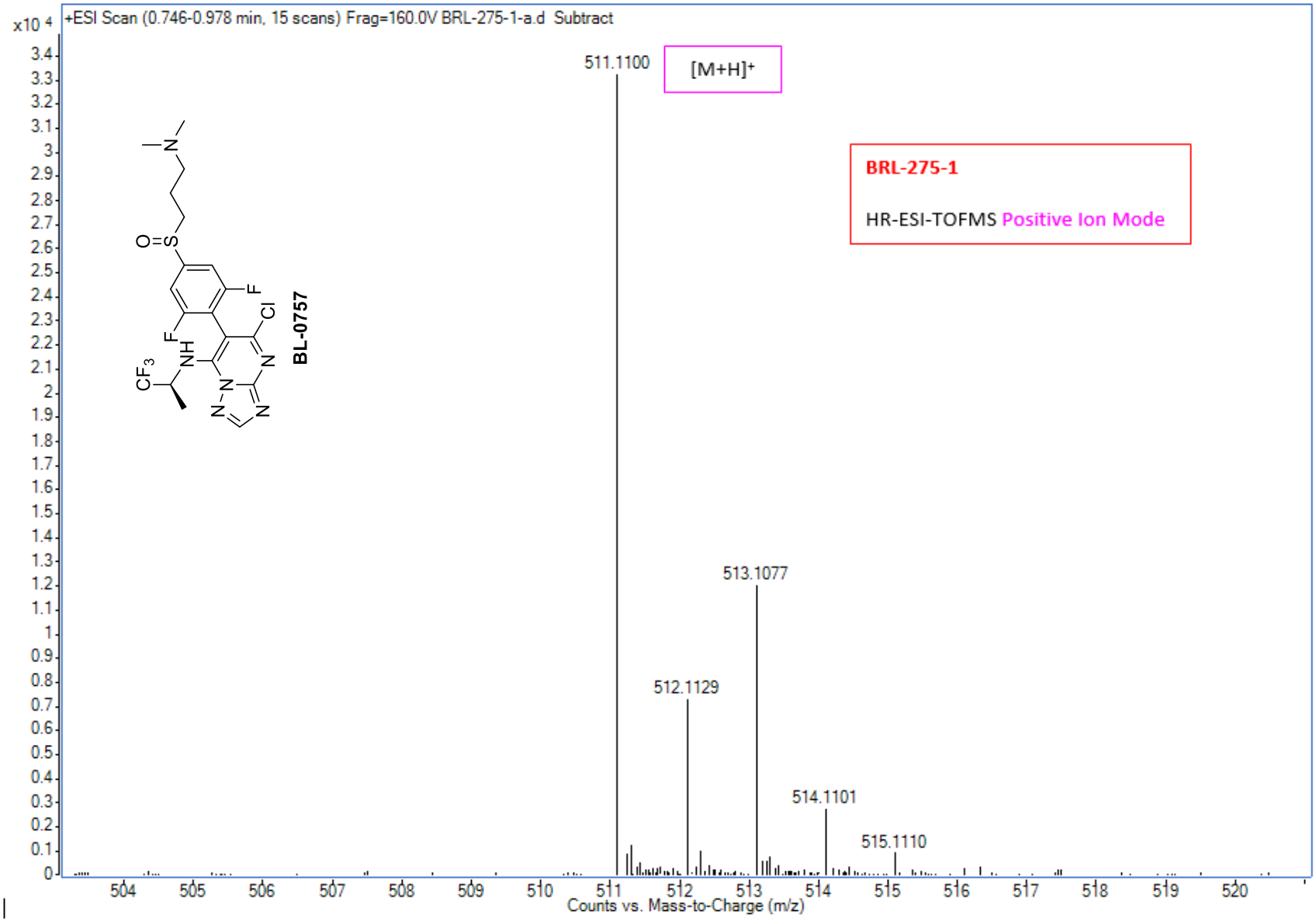
+ESI Scan (0.746-0.978 min, 15 scans) Frag=160.0V BRL-275-1-a.d Subtract
x10 4
511.1100
[M+H]+
BRL-275-1
HR-ESI-TOFMS Positive Ion Mode
BL-0757
513.1077
512.1129
514.1101
515.1110
Counts vs. Mass-to-Charge (m/z)

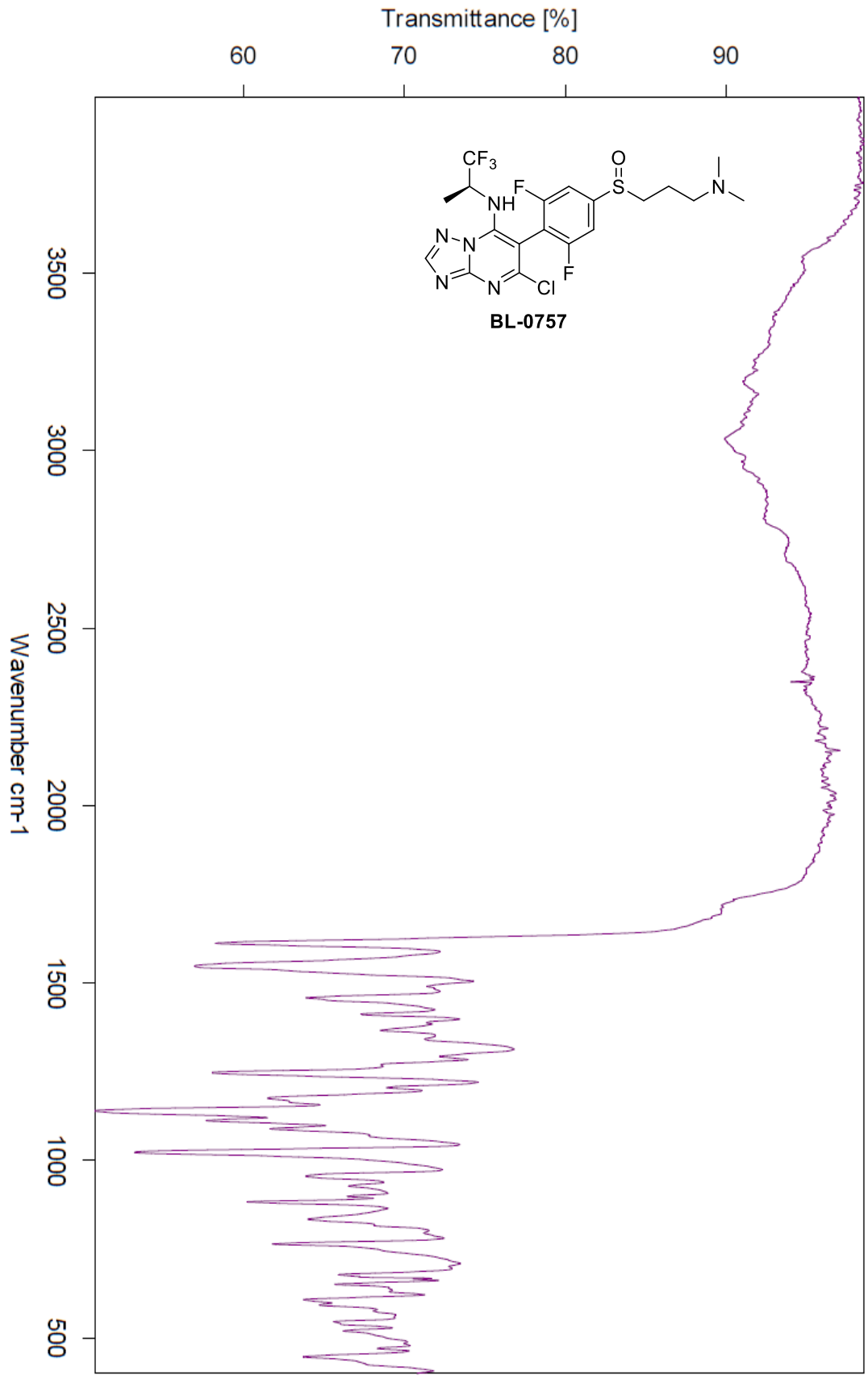
Transmittance [%]
60
70
80
90
Wavenumber cm-1
3500
3000
2500
2000
1500
1000
500
CF3
NH
F
O
S
N
N
N
N
N
Cl
F
BL-0757

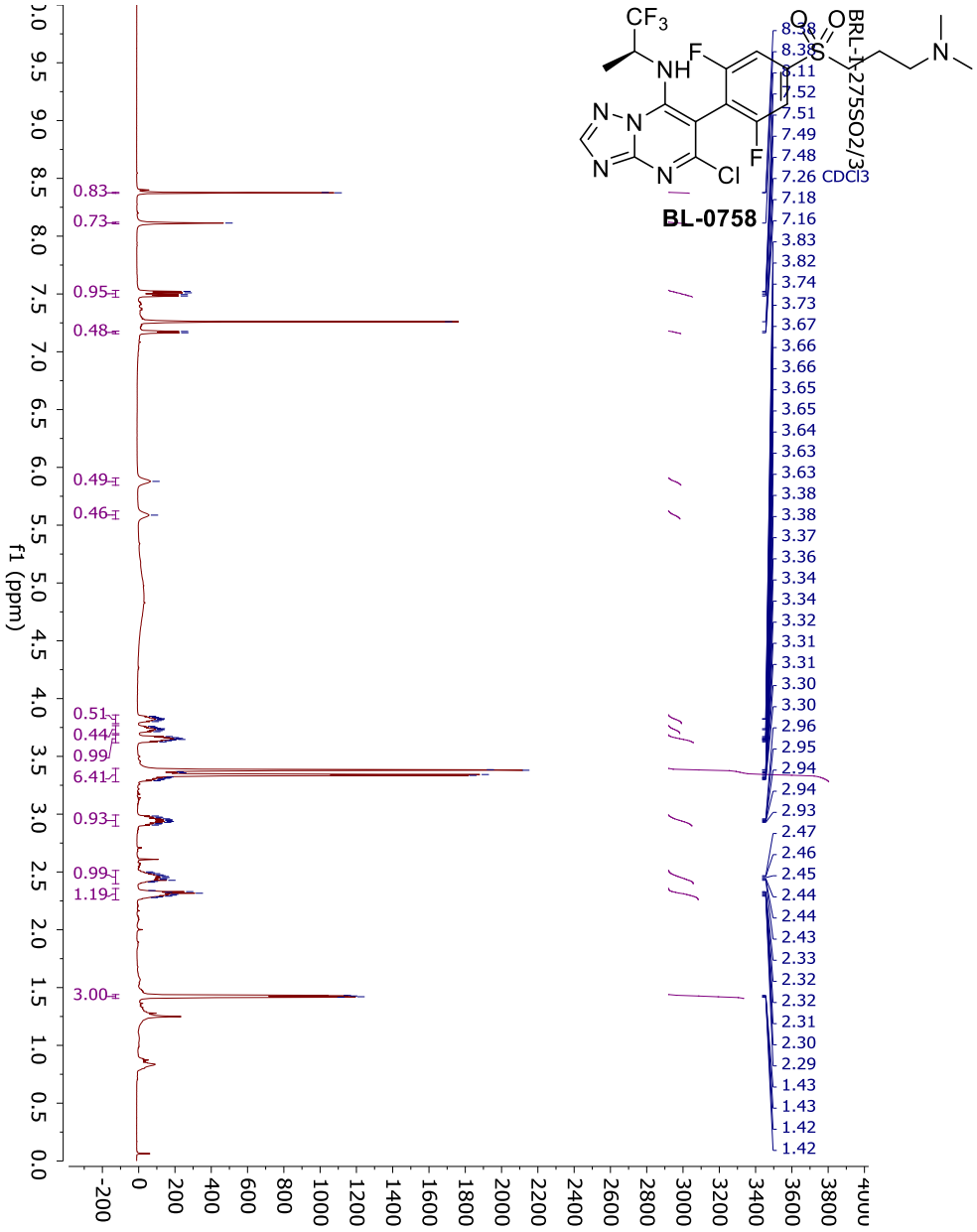
BL-0758
f1 (ppm)
0.83
0.73
0.95
0.48
0.49
0.46
0.51
0.44
0.99
6.41
0.93
0.99
1.19
3.00
CDCl3

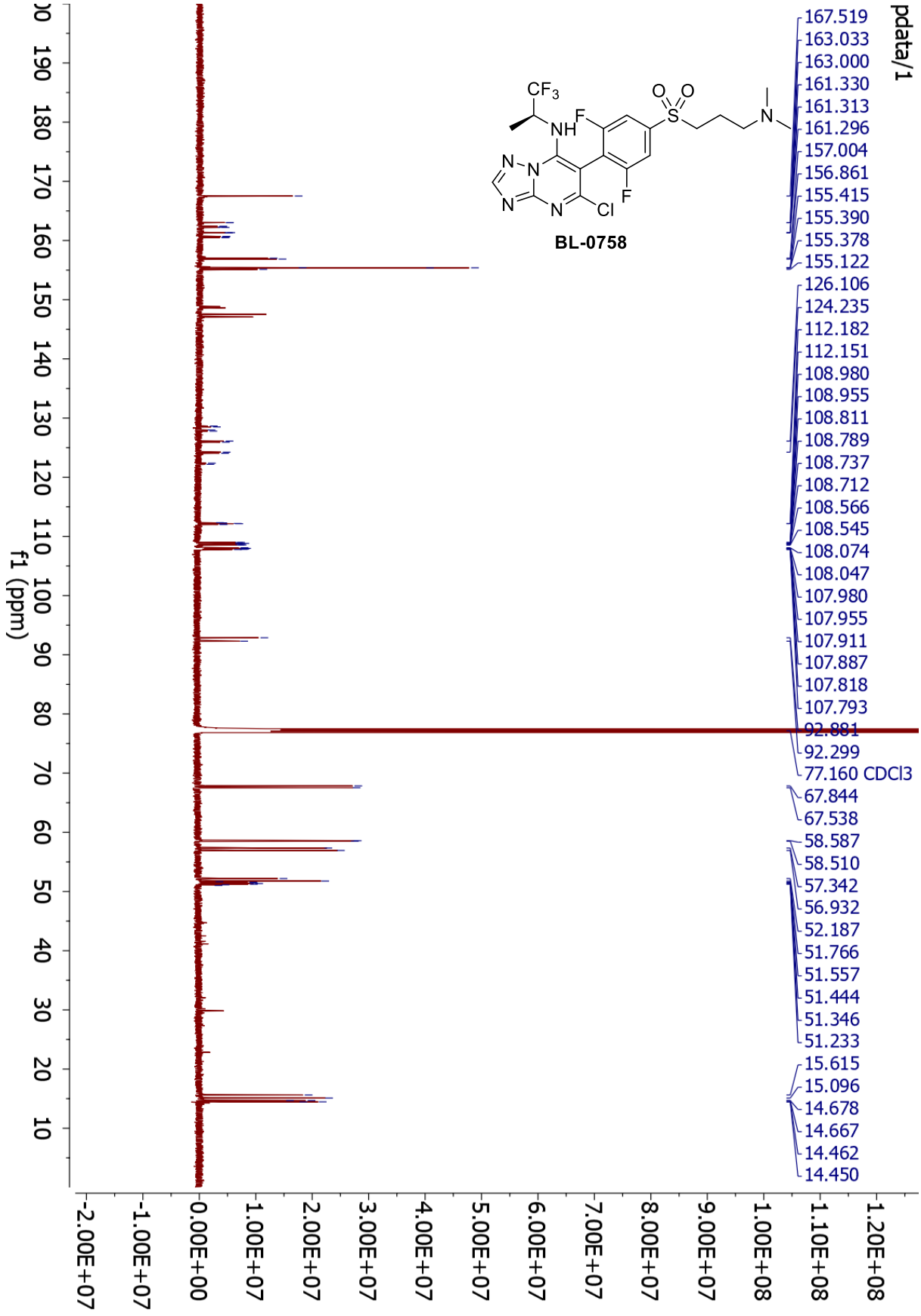
pdata/1
BL-0758
167.519
163.033
163.000
161.330
161.313
161.296
157.004
156.861
155.415
155.390
155.378
155.122
126.106
124.235
112.182
112.151
108.980
108.955
108.811
108.789
108.737
108.712
108.566
108.545
108.074
108.047
107.980
107.955
107.911
107.887
107.818
107.793
92.881
92.299
77.160 CDCl3
67.844
67.538
58.587
58.510
57.342
56.932
52.187
51.766
51.557
51.444
51.346
51.233
15.615
15.096
14.678
14.667
14.462
14.450
f1 (ppm)

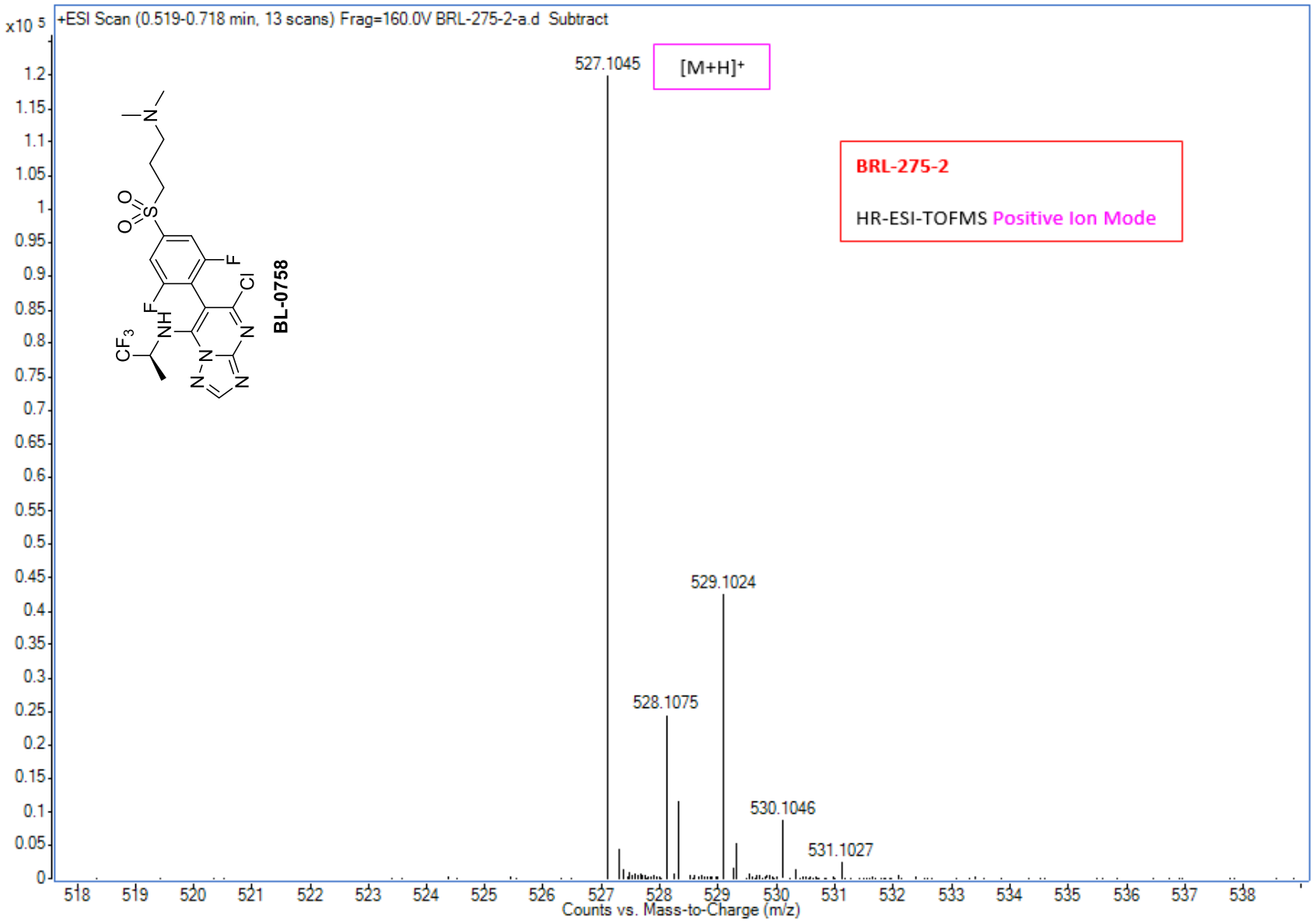
+ESI Scan (0.519-0.718 min, 13 scans) Frag=160.0V BRL-275-2-a.d Subtract
x10 5
527.1045
[M+H]+
BRL-275-2
HR-ESI-TOFMS Positive Ion Mode
BL-0758
529.1024
528.1075
530.1046
531.1027
Counts vs. Mass-to-Charge (m/z)

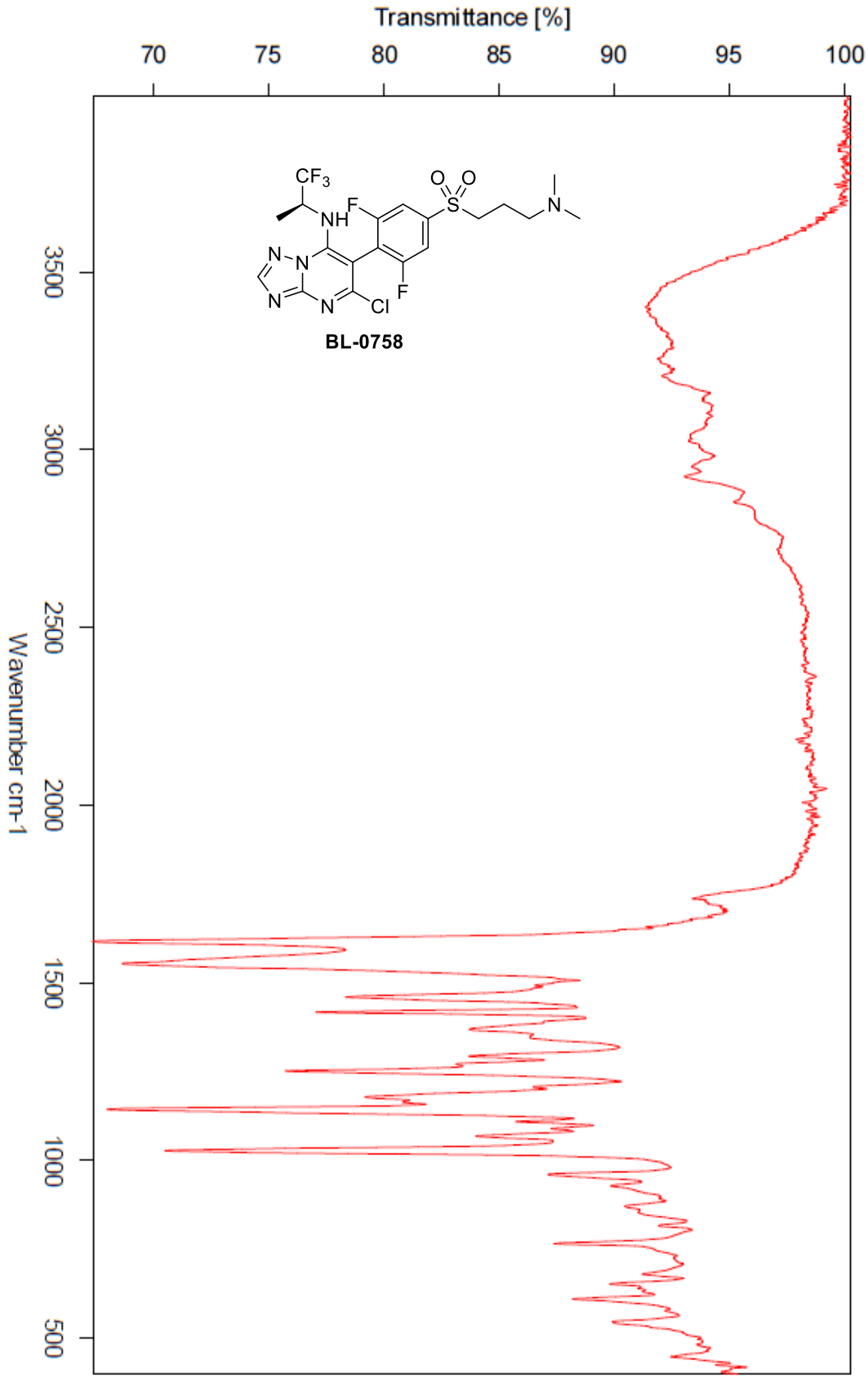
Transmittance [%]
70
75
80
85
90
95
100
Wavenumber cm-1
3500
3000
2500
2000
1500
1000
500
CF3
NH
F
O
O
S
N
N
N
N
N
Cl
F
BL-0758

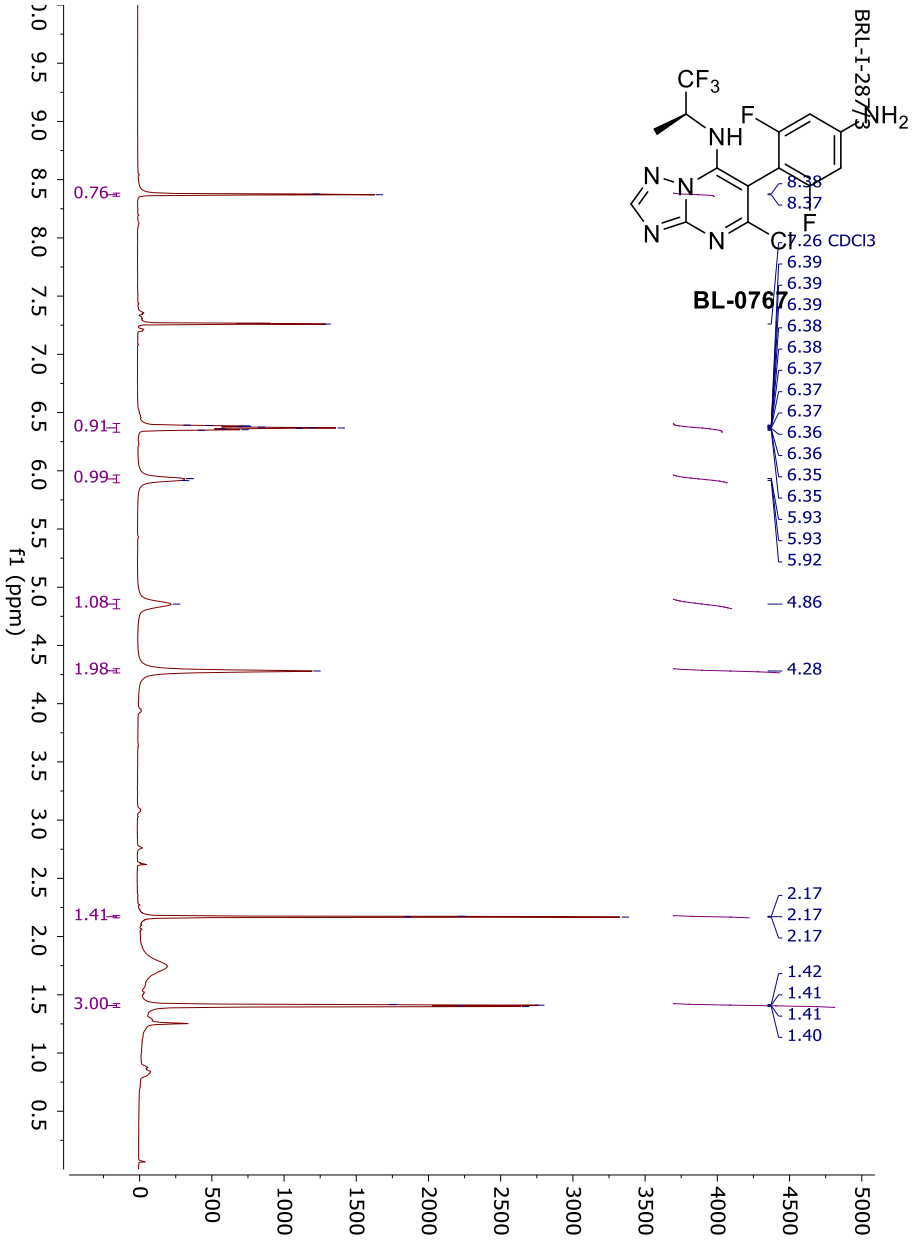
BRL-I-28773
BL-0767
CF3
NH
F
NH2
N
N
N
N
F
Cl
8.38
8.37
7.26 CDCl3
6.39
6.39
6.39
6.38
6.38
6.37
6.37
6.37
6.36
6.36
6.35
6.35
5.93
5.93
5.92
4.86
4.28
2.17
2.17
2.17
1.42
1.41
1.41
1.40
0.76
0.91
0.99
1.08
1.98
1.41
3.00
f1 (ppm)
10.0 9.5 9.0 8.5 8.0 7.5 7.0 6.5 6.0 5.5 5.0 4.5 4.0 3.5 3.0 2.5 2.0 1.5 1.0 0.5
0 500 1000 1500 2000 2500 3000 3500 4000 4500 5000

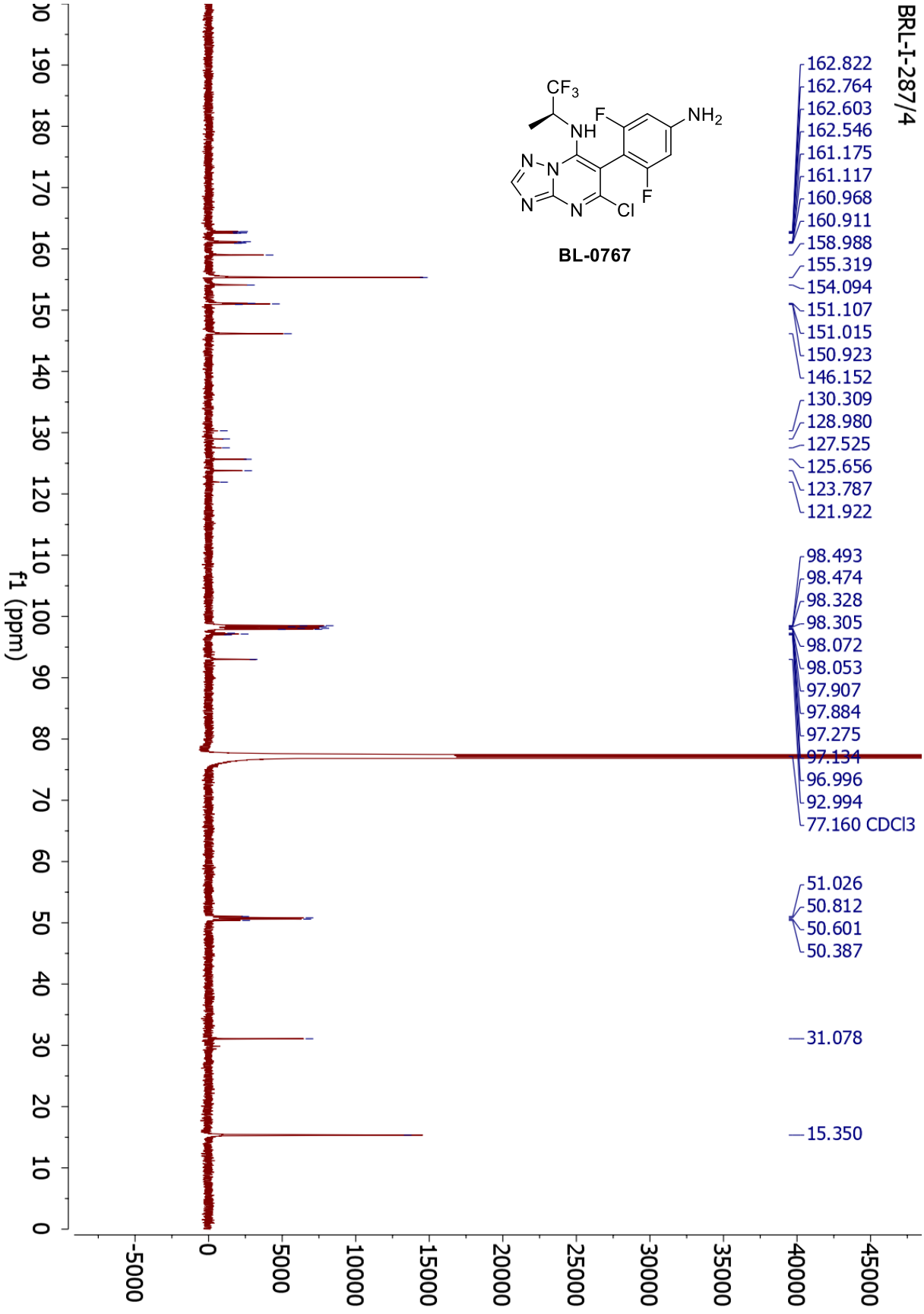
BRL-I-287/4
BL-0767
162.822
162.764
162.603
162.546
161.175
161.117
160.968
160.911
158.988
155.319
154.094
151.107
151.015
150.923
146.152
130.309
128.980
127.525
125.656
123.787
121.922
98.493
98.474
98.328
98.305
98.072
98.053
97.907
97.884
97.275
97.134
96.996
92.994
77.160 CDCl3
51.026
50.812
50.601
50.387
31.078
15.350
f1 (ppm)

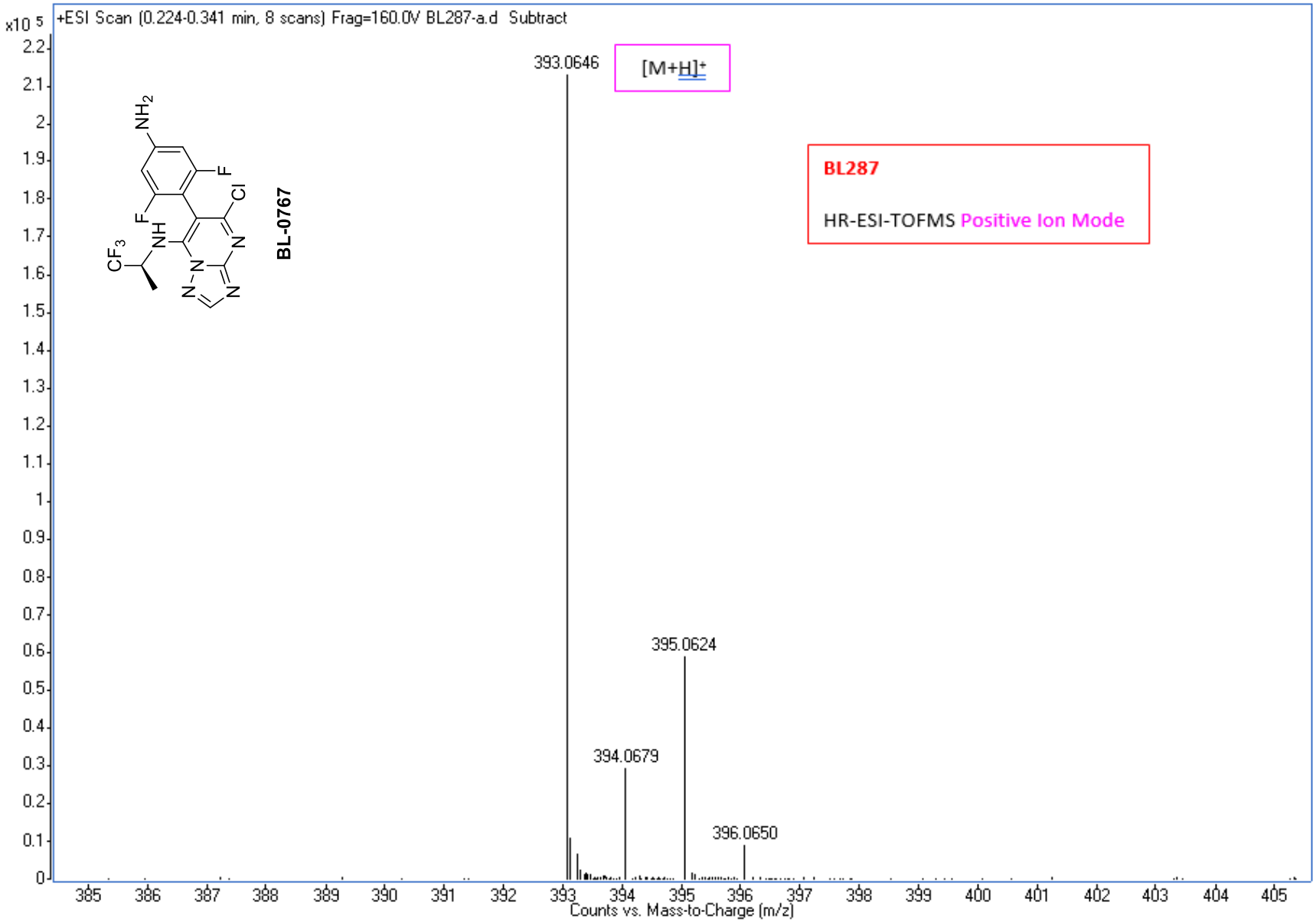
+ESI Scan (0.224-0.341 min, 8 scans) Frag=160.0V BL287-a.d Subtract
x10 5
393.0646
[M+H]+
395.0624
394.0679
396.0650
BL287
HR-ESI-TOFMS Positive Ion Mode
BL-0767
Counts vs. Mass-to-Charge (m/z)

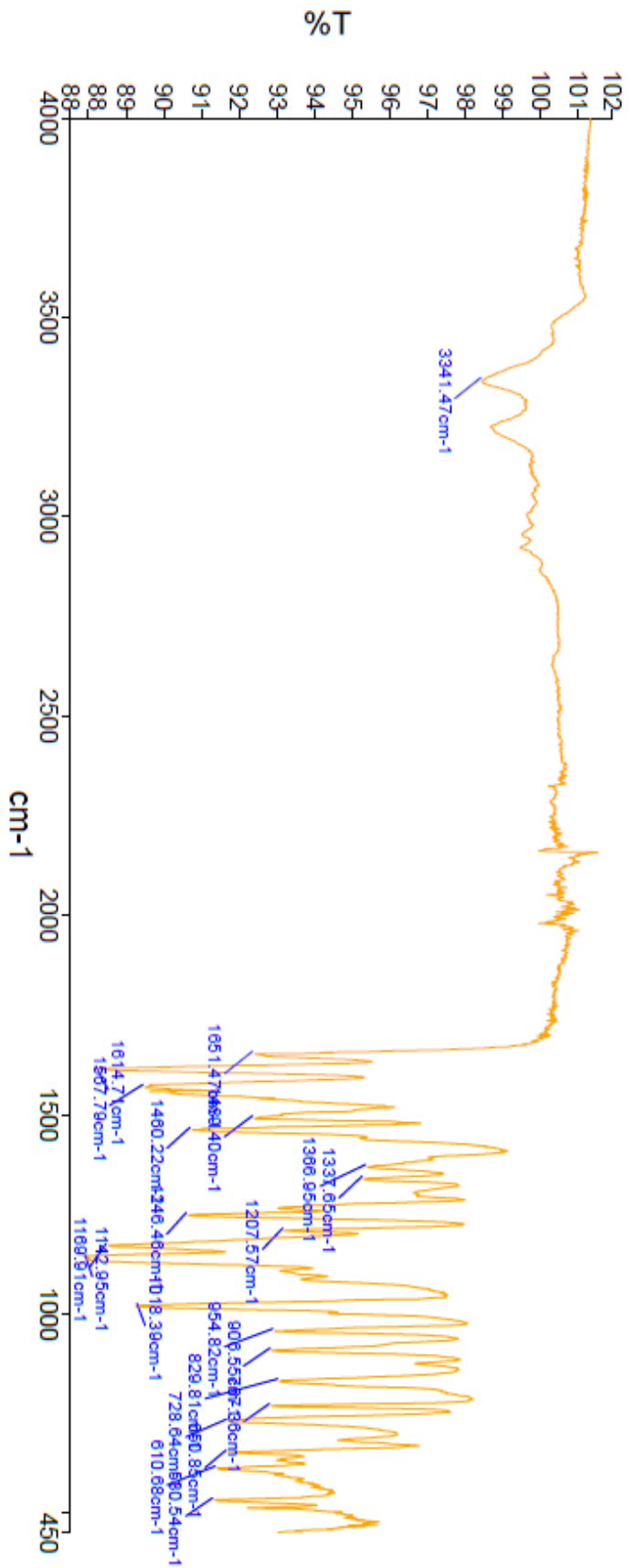
%T
cm-1
3341.47cm-1
1651.47cm-1
1614.71cm-1
1567.79cm-1
1460.22cm-1
1386.95cm-1
1207.57cm-1
1142.95cm-1
1018.39cm-1
954.82cm-1
829.81cm-1
728.64cm-1
610.68cm-1

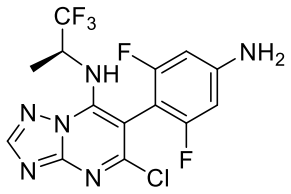
CF3
NH
F
NH2
N
N
N
N
Cl
F

BL-0767

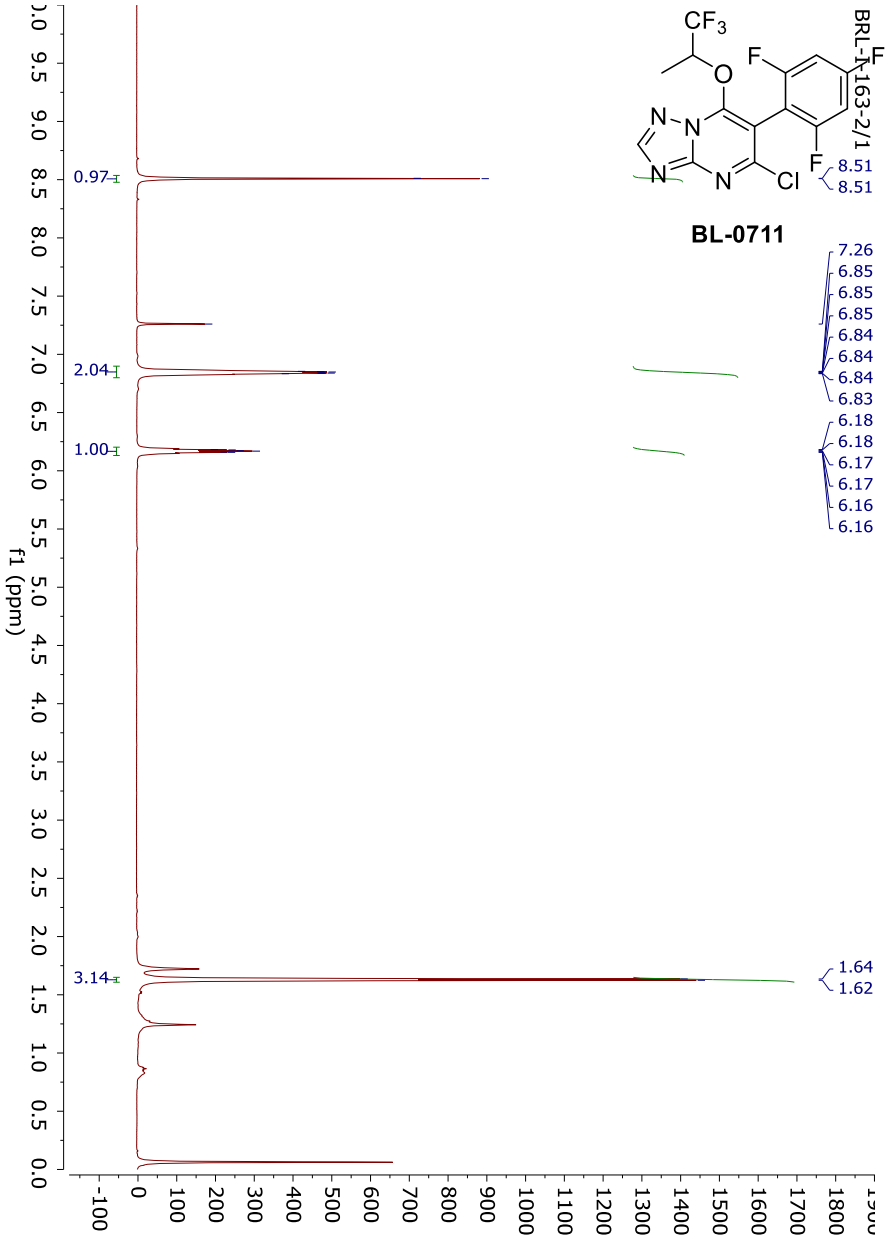
BRL-163-2/1
BL-0711
0.97
2.04
1.00
3.14
8.51
8.51
7.26
6.85
6.85
6.85
6.84
6.84
6.84
6.83
6.18
6.18
6.17
6.17
6.16
6.16
1.64
1.62
f1 (ppm)

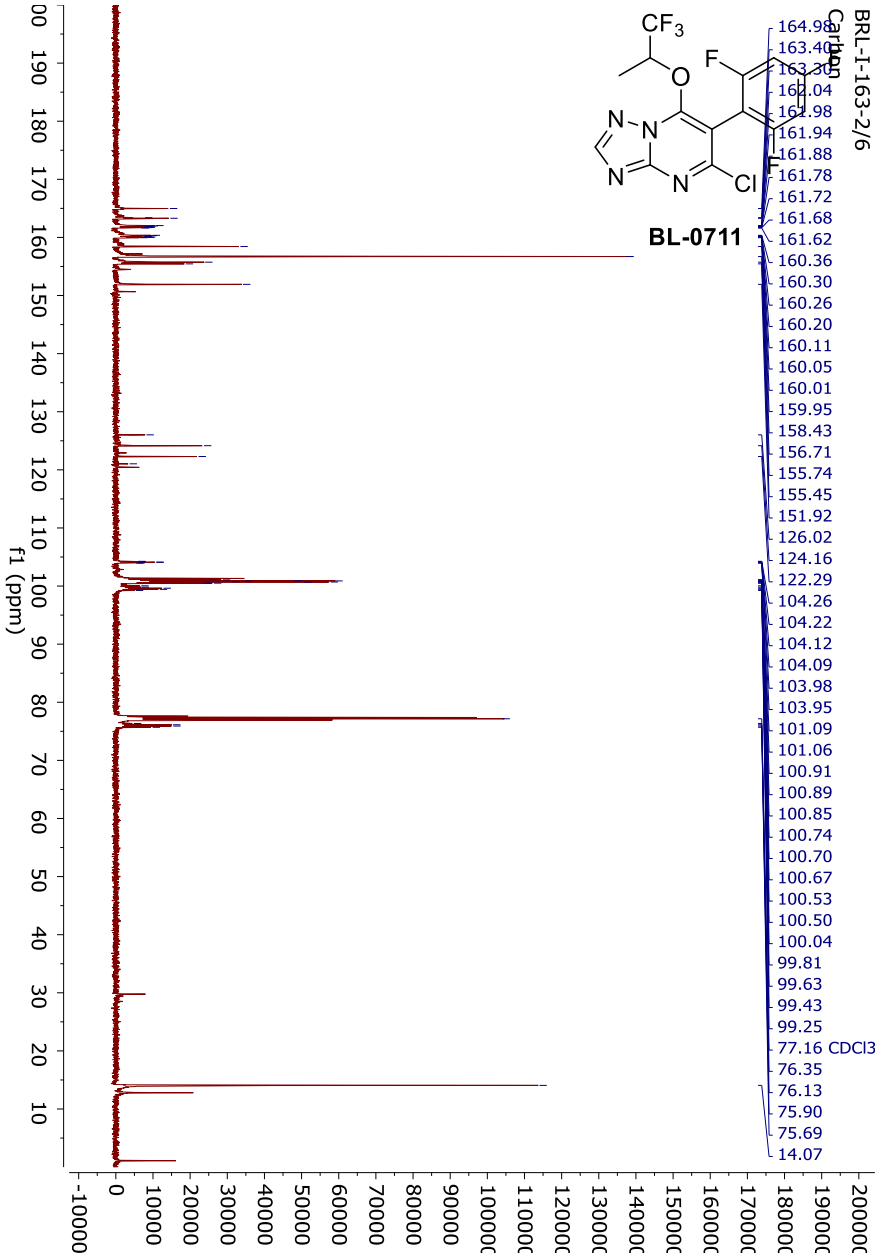
BRL-I-163-2/6
Carbon
BL-0711
164.98
163.40
163.30
162.04
161.98
161.94
161.88
161.78
161.72
161.68
161.62
160.36
160.30
160.26
160.20
160.11
160.05
160.01
159.95
158.43
156.71
155.74
155.45
151.92
126.02
124.16
122.29
104.26
104.22
104.12
104.09
103.98
103.95
101.09
101.06
100.91
100.89
100.85
100.74
100.70
100.67
100.53
100.50
100.04
99.81
99.63
99.43
99.25
77.16 CDCl3
76.35
76.13
75.90
75.69
14.07
f1 (ppm)

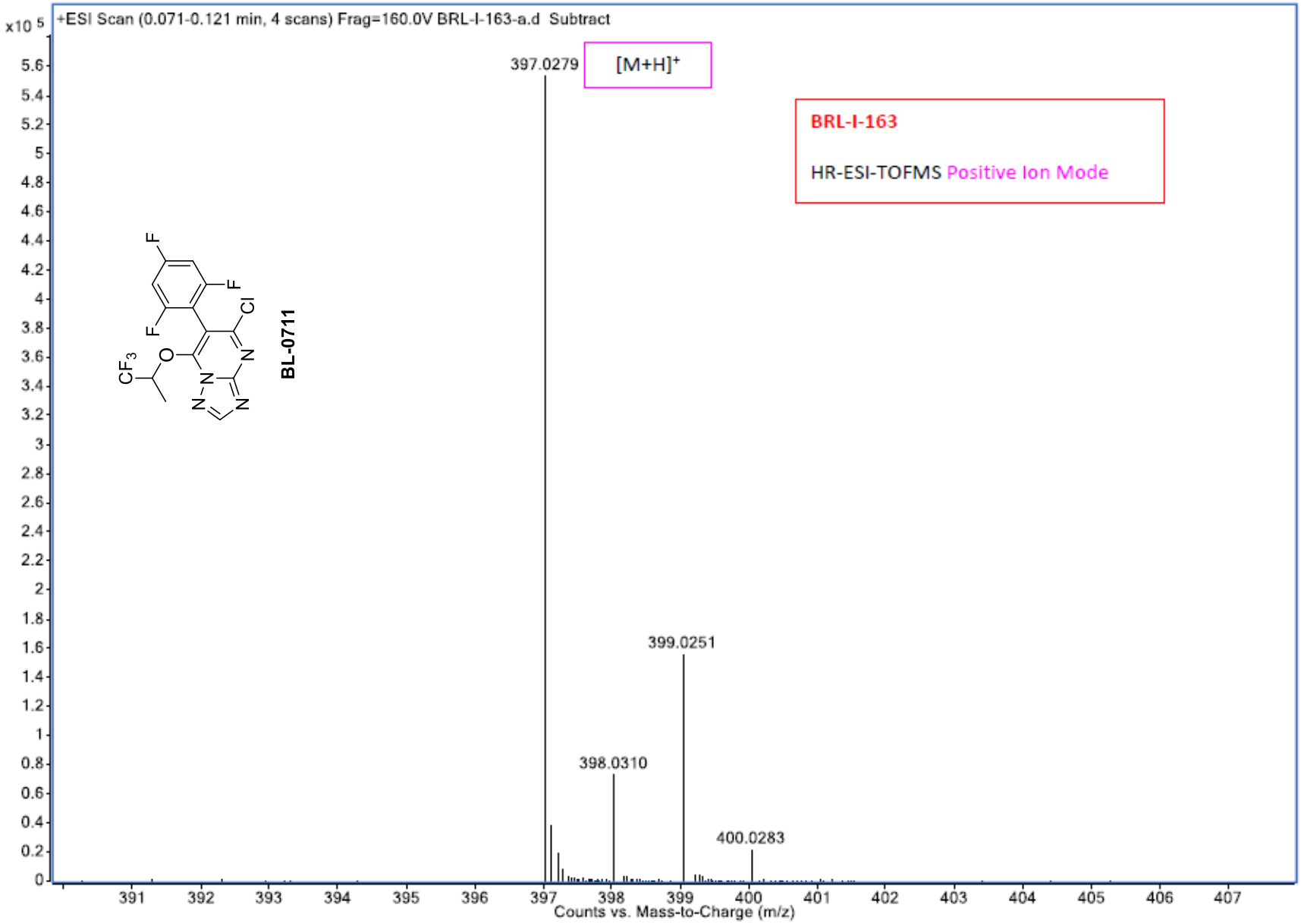
+ESI Scan (0.071-0.121 min, 4 scans) Frag=160.0V BRL-I-163-a.d Subtract
x10 5
397.0279
[M+H]+
BRL-I-163
HR-ESI-TOFMS Positive Ion Mode
BL-0711
399.0251
398.0310
400.0283
Counts vs. Mass-to-Charge (m/z)

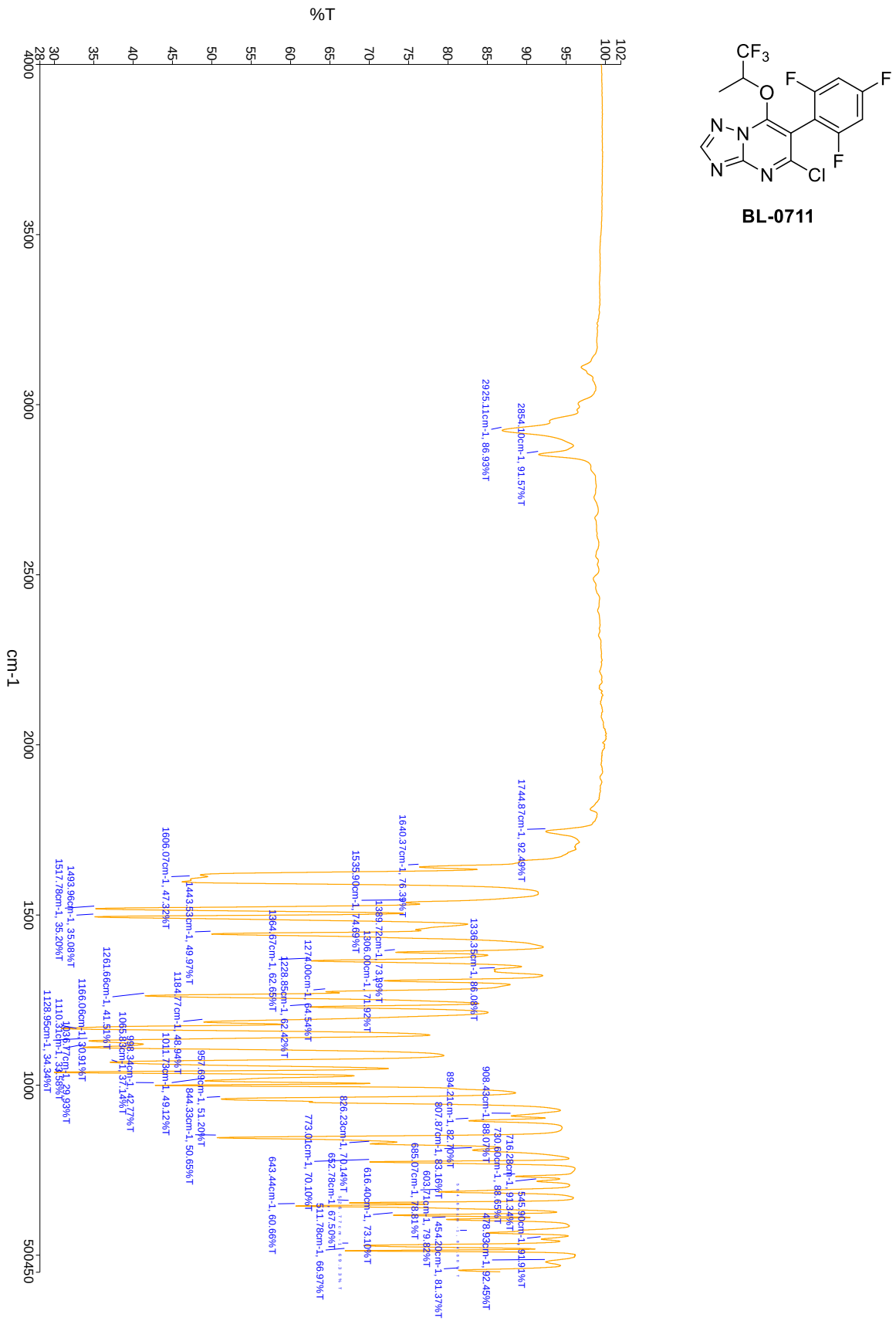
%T
cm-1
2925.11cm-1, 86.93%T
2854.10cm-1, 91.57%T
1744.87cm-1, 92.49%T
1640.37cm-1, 76.39%T
1535.90cm-1, 74.69%T
1389.72cm-1, 73.89%T
1364.67cm-1, 62.65%T
1338.35cm-1, 86.08%T
1306.00cm-1, 71.92%T
1274.00cm-1, 64.54%T
1228.85cm-1, 62.42%T
1606.07cm-1, 47.32%T
1443.53cm-1, 49.97%T
1261.66cm-1, 41.51%T
1184.77cm-1, 48.94%T
1166.06cm-1, 30.91%T
1128.95cm-1, 34.34%T
1110.31cm-1, 33.56%T
1493.96cm-1, 35.08%T
1517.78cm-1, 35.20%T
1011.72cm-1, 49.12%T
957.68cm-1, 51.20%T
844.33cm-1, 50.65%T
908.43cm-1, 88.07%T
894.21cm-1, 92.70%T
826.23cm-1, 70.14%T
773.01cm-1, 70.10%T
643.44cm-1, 60.66%T
807.87cm-1, 83.16%T
685.07cm-1, 78.81%T
730.60cm-1, 88.65%T
716.28cm-1, 91.34%T
652.78cm-1, 67.50%T
616.40cm-1, 73.10%T
603.71cm-1, 79.82%T
545.90cm-1, 91.91%T
511.78cm-1, 66.97%T
478.93cm-1, 92.45%T
454.20cm-1, 81.37%T

CF3
F
F
O
N
N
N
N
F
Cl

BL-0711

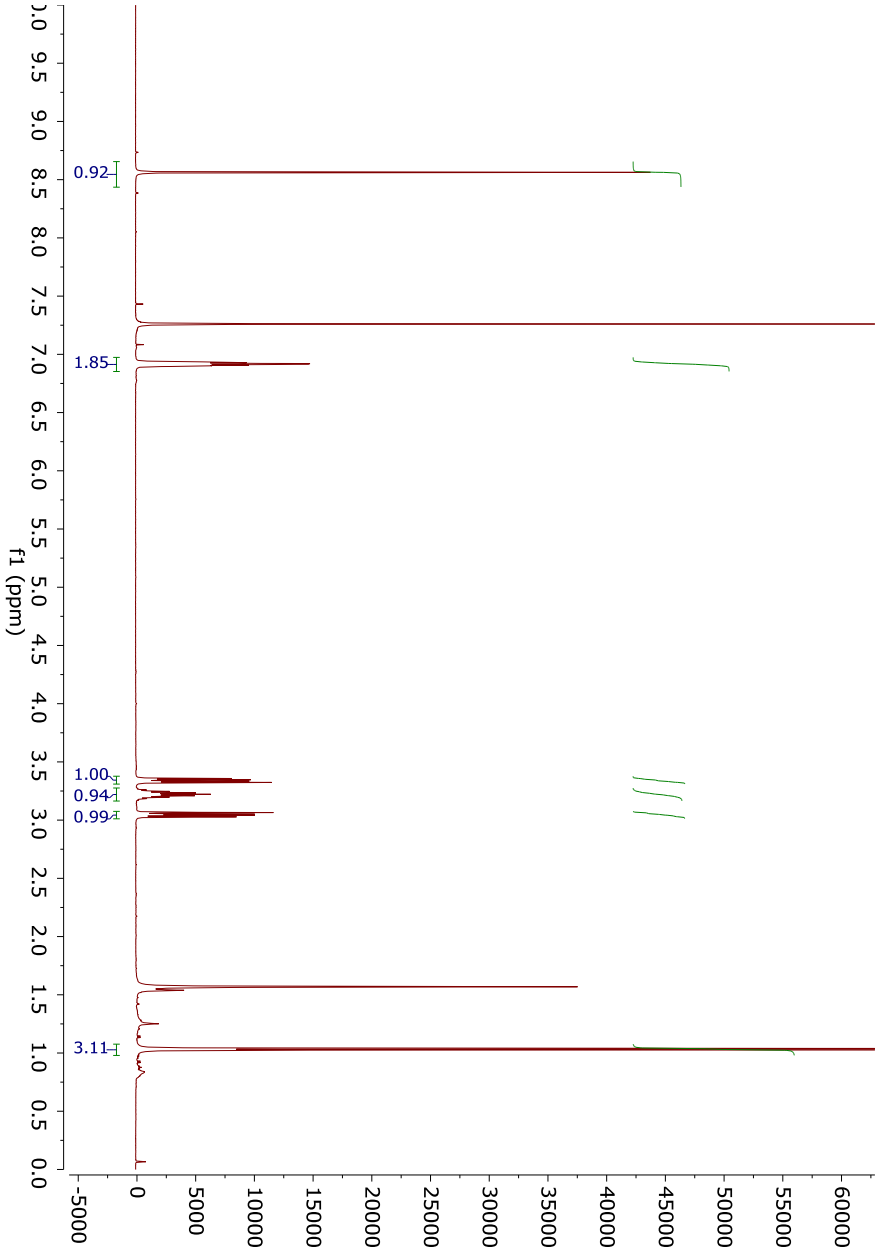

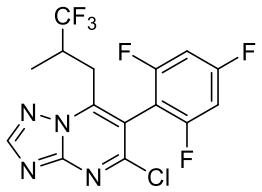

BL-0711

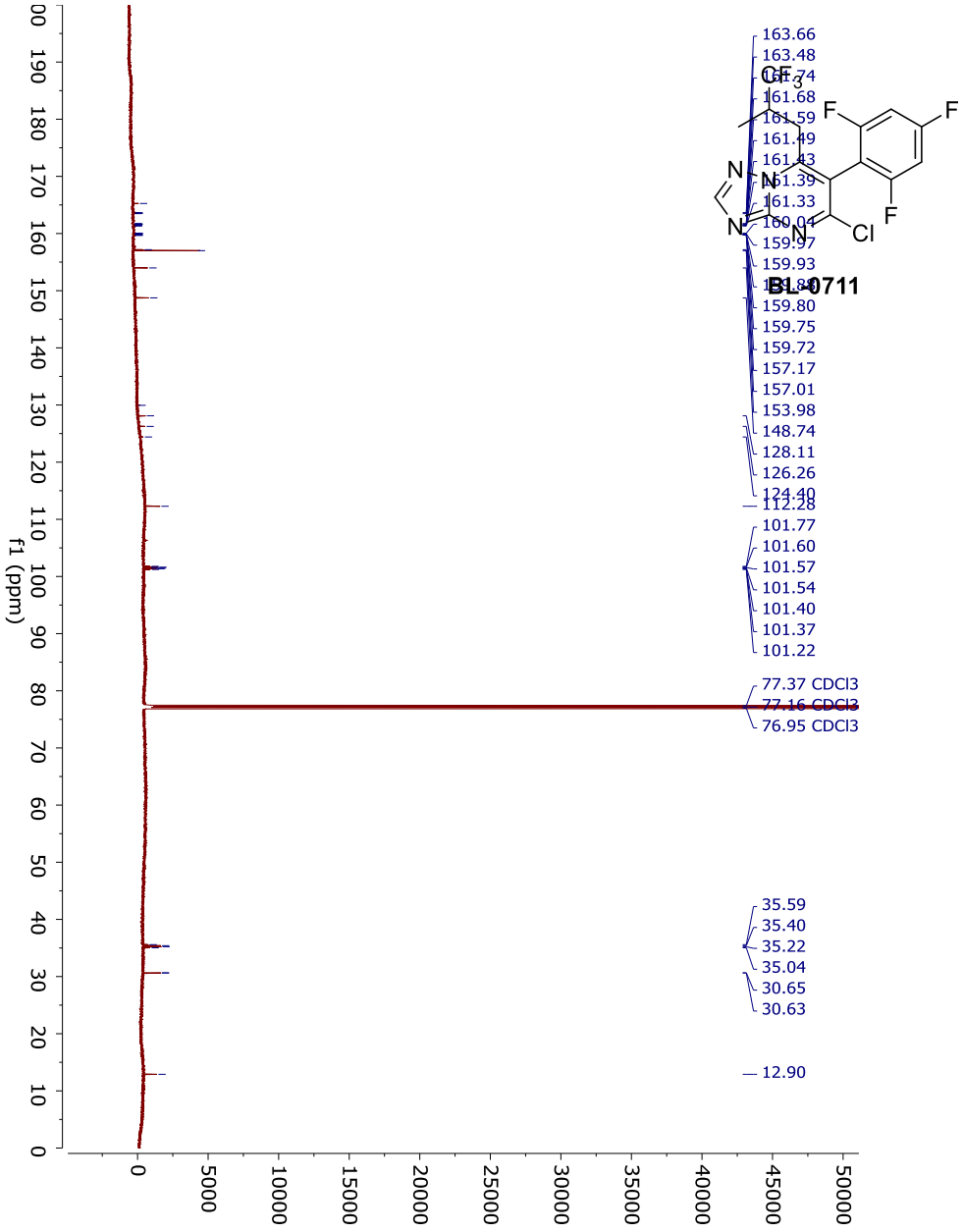
163.66
163.48
161.68
161.59
161.49
161.43
161.39
161.33
160.04
159.97
159.93
159.80
159.75
159.72
157.17
157.01
153.98
148.74
128.11
126.26
124.40
112.28
101.77
101.60
101.57
101.54
101.40
101.37
101.22
77.37 CDCl3
77.16 CDCl3
76.95 CDCl3
35.59
35.40
35.22
35.04
30.65
30.63
12.90
BL-0711
F
F
F
Cl
N
N
N
f1 (ppm)

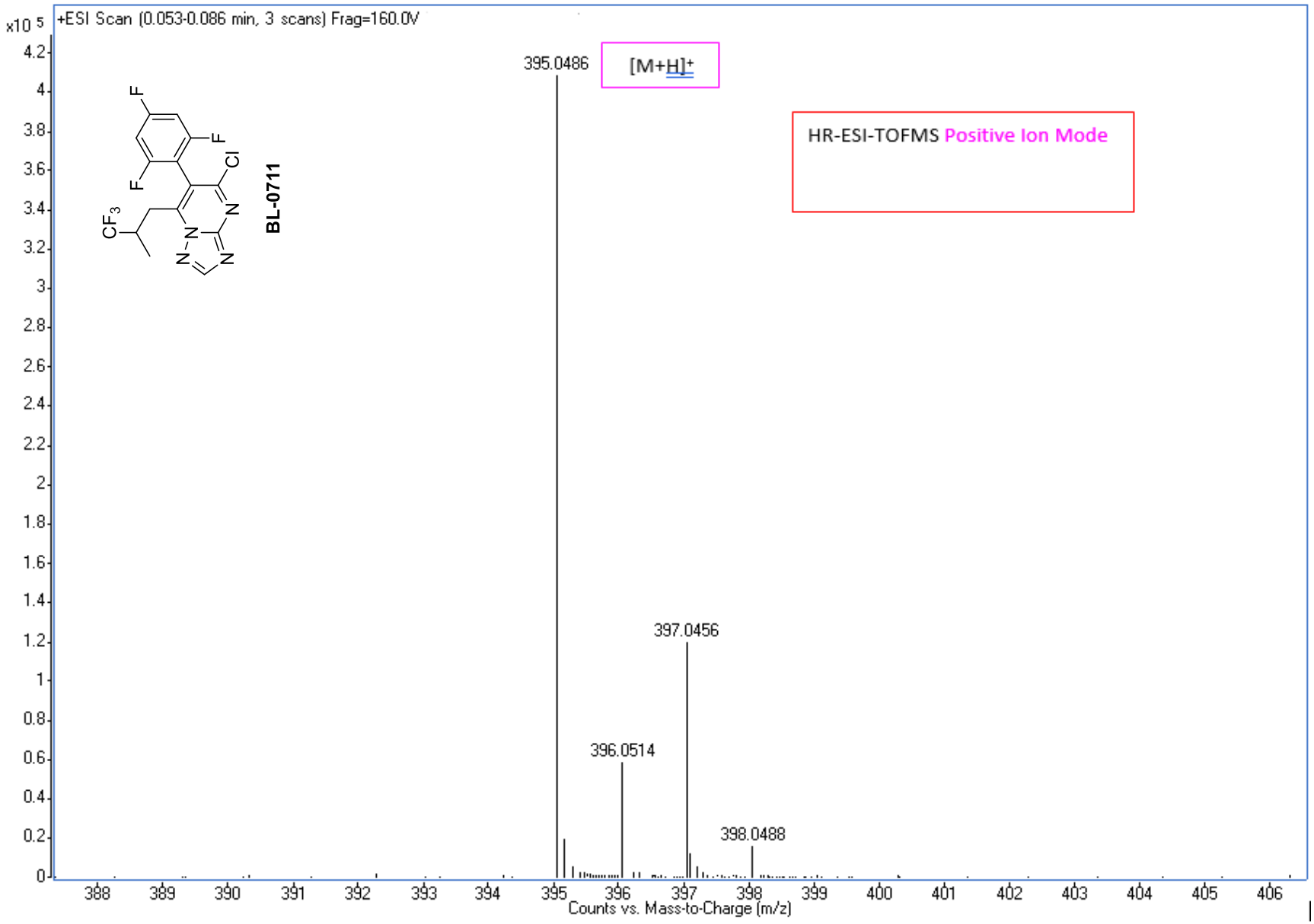
+ESI Scan (0.053-0.086 min, 3 scans) Frag=160.0V
x10 5
395.0486
[M+H]+
HR-ESI-TOFMS Positive Ion Mode
BL-0711
397.0456
396.0514
398.0488
Counts vs. Mass-to-Charge (m/z)

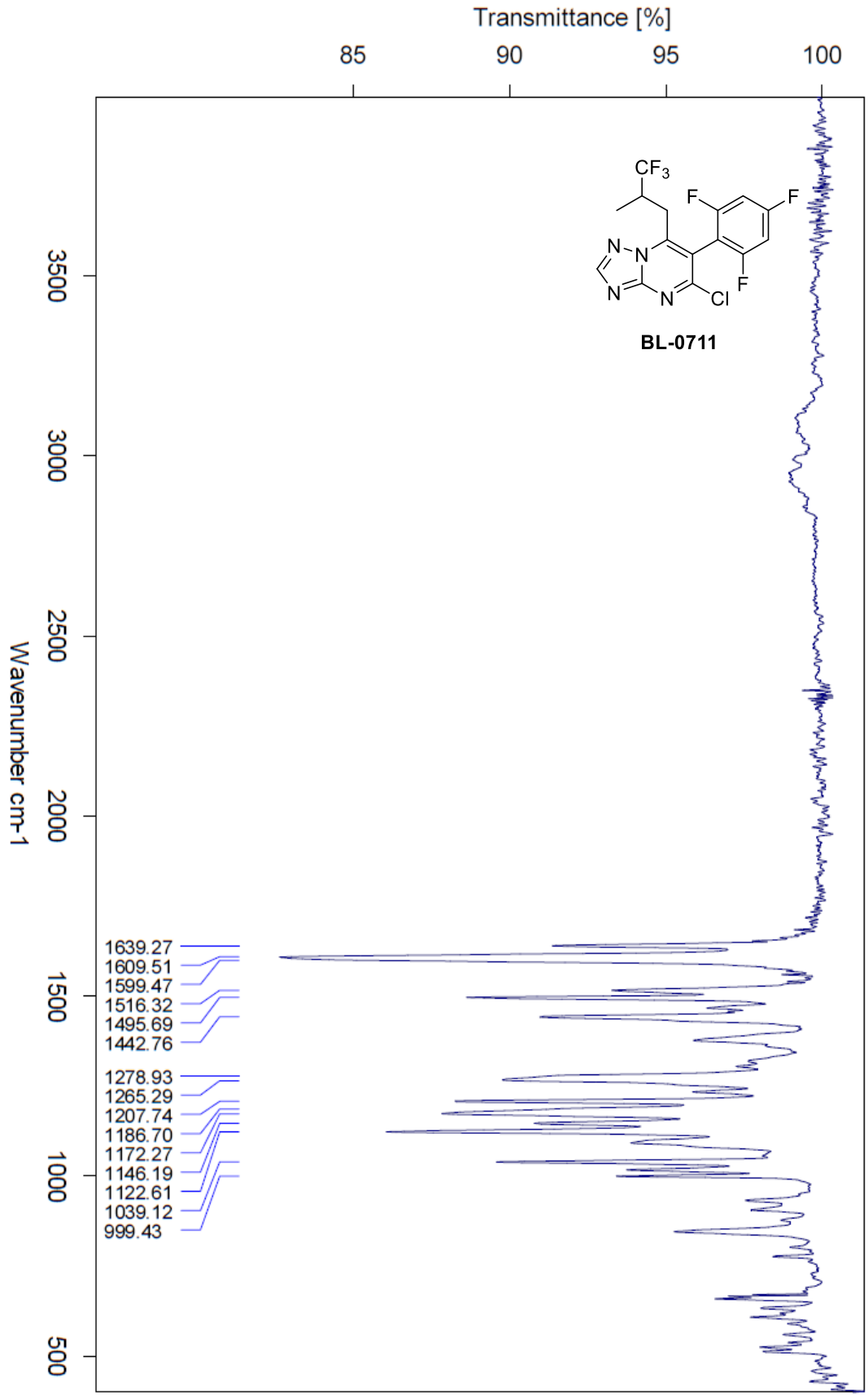
Transmittance [%]
85
90
95
100
Wavenumber cm-1
3500
3000
2500
2000
1500
1000
500
1639.27
1609.51
1599.47
1516.32
1495.69
1442.76
1278.93
1265.29
1207.74
1186.70
1172.27
1146.19
1122.61
1039.12
999.43
CF3
F
F
F
N
N
N
N
Cl
BL-0711

References

1. Hyman, B. T., The neuropathological diagnosis of Alzheimer's disease: clinical-pathological studies. *Neurobiology of Aging* **1997,** *18* (4 Suppl), S27-32.

2. Ball, M.; Braak, H.; Coleman, P.; Dickson, D.; Duyckaerts, C.; Gambetti, P.; Hansen, L.; Hyman, B.; Jellinger, K.; Markesbery, W.; Perl, D.; Powers, J.; Price, J.; Trojanowski, J.; Wisniewski, H.; Phelps, C.; Khachaturian, Z., Consensus recommendations for the postmortem diagnosis of Alzheimer's disease. *Neurobiology of Aging* **1997,** *18* (4), S1-S2.

3. Brunden, K. R.; Ballatore, C.; Crowe, A.; Smith, A. B.; Lee, V. M.; Trojanowski, J. Q., Tau-directed drug discovery for Alzheimer's disease and related tauopathies: a focus on tau assembly inhibitors. *Experimental Neurology* **2010,** *223* (2), 304-10.

4. Goedert, M., Tau gene mutations and their effects. *Movement Disorders* **2005,** *20 Suppl 12*, S45-52.

5. Goedert, M.; Jakes, R., Mutations causing neurodegenerative tauopathies. *Biochim Biophys Acta* **2005,** *1739* (2-3), 240-50.

6. Hutton, M.; Lendon, C. L.; Rizzu, P.; Baker, M.; Froelich, S.; Houlden, H.; Pickering-Brown, S.; Chakraverty, S.; Isaacs, A.; Grover, A.; Hackett, J.; Adamson, J.; Lincoln, S.; Dickson, D.; Davies, P.; Petersen, R. C.; Stevens, M.; de Graaff, E.; Wauters, E.; van Baren, J.; Hillebrand, M.; Joosse, M.; Kwon, J. M.; Nowotny, P.; Che, L. K.; Norton, J.; Morris, J. C.; Reed, L. A.; Trojanowski, J.; Basun, H.; Lannfelt, L.; Neystat, M.; Fahn, S.; Dark, F.; Tannenberg, T.; Dodd, P. R.; Hayward, N.; Kwok, J. B.; Schofield, P. R.; Andreadis, A.; Snowden, J.; Craufurd, D.; Neary, D.; Owen, F.; Oostra, B. A.; Hardy, J.; Goate, A.; van Swieten, J.; Mann, D.; Lynch, T.; Heutink, P., Association of missense and 5'-splice-site mutations in tau with the inherited dementia FTDP-17. *Nature* **1998,** *393* (6686), 702-5.

7. Lee, V. M.; Goedert, M.; Trojanowski, J. Q., Neurodegenerative tauopathies. *Annual Review Neuroscience* **2001,** *24*, 1121-59.

8. Desai, A.; Mitchison, T. J., Microtubule polymerization dynamics. *Annual Review of Cell and Developmental Biology* **1997,** *13*, 83-117.

9. Drechsel, D. N.; Hyman, A. A.; Cobb, M. H.; Kirschner, M. W., Modulation of the dynamic instability of tubulin assembly by the microtubule-associated protein tau. *Molecular Biology of the Cell* **1992,** *3* (10), 1141-54.

10. Dixit, R.; Ross, J. L.; Goldman, Y. E.; Holzbaur, E. L., Differential regulation of dynein and kinesin motor proteins by tau. *Science* **2008,** *319* (5866), 1086-9.

11. Vershinin, M.; Carter, B. C.; Razafsky, D. S.; King, S. J.; Gross, S. P., Multiple-motor based transport and its regulation by Tau. *Proceedings of the National Academy of Sciences of the United States of America* **2007,** *104* (1), 87-92.

12. Yu, W.; Qiang, L.; Solowska, J. M.; Karabay, A.; Korulu, S.; Baas, P. W., The microtubule-severing proteins spastin and katanin participate differently in the formation of axonal branches. *Molecular Biology of the Cell* **2008,** *19* (4), 1485-98.

13. Sudo, H.; Baas, P. W., Strategies for diminishing katanin-based loss of microtubules in tauopathic neurodegenerative diseases. *Human Molecular Genetics* **2011,** *20* (4), 763-78.

14. Buée, L.; Bussière, T.; Buée-Scherrer, V.; Delacourte, A.; Hof, P. R., Tau protein isoforms, phosphorylation and role in neurodegenerative disorders. *Brain Research reviews* **2000,** *33* (1), 95-130.

15. Kuret, J.; Chirita, C. N.; Congdon, E. E.; Kannanayakal, T.; Li, G.; Necula, M.; Yin, H.; Zhong, Q., Pathways of tau fibrillization. *Biochim Biophys Acta* **2005,** *1739* (2-3), 167-78.

16. Brunden, K. R.; Zhang, B.; Carroll, J.; Yao, Y.; Potuzak, J. S.; Hogan, A. M.; Iba, M.; James, M. J.; Xie, S. X.; Ballatore, C.; Smith, A. B.; Lee, V. M.; Trojanowski, J. Q., Epothilone D improves microtubule density, axonal integrity, and cognition in a transgenic mouse model of tauopathy. *Journal of Neuroscience* **2010,** *30* (41), 13861-6.

17. Zhang, B.; Maiti, A.; Shively, S.; Lakhani, F.; McDonald-Jones, G.; Bruce, J.; Lee, E. B.; Xie, S. X.; Joyce, S.; Li, C.; Toleikis, P. M.; Lee, V. M.; Trojanowski, J. Q., Microtubule-binding drugs offset tau sequestration by stabilizing microtubules and reversing fast axonal transport deficits in a tauopathy model. *Proc Natl Acad Sci U S A* **2005,** *102* (1), 227-31.

18. Lee, V. M.; Daughenbaugh, R.; Trojanowski, J. Q., Microtubule stabilizing drugs for the treatment of Alzheimer's disease. *Neurobiology of Aging* **1994,** *15 Suppl 2*, S87-9.

19. Brunden, K. R.; Yao, Y.; Potuzak, J. S.; Ferrer, N. I.; Ballatore, C.; James, M. J.; Hogan, A. M.; Trojanowski, J. Q.; Smith, A. B.; Lee, V. M., The characterization of microtubule-stabilizing drugs as possible therapeutic agents for Alzheimer's disease and related tauopathies. *Pharmacological Research* **2011,** *63* (4), 341-51.

20. Bollag, D. M.; McQueney, P. A.; Zhu, J.; Hensens, O.; Koupal, L.; Liesch, J.; Goetz, M.; Lazarides, E.; Woods, C. M., Epothilones, a new class of microtubule-stabilizing agents with a taxol-like mechanism of action. *Cancer Research* **1995,** *55* (11), 2325-33.

21. Zhang, B.; Carroll, J.; Trojanowski, J. Q.; Yao, Y.; Iba, M.; Potuzak, J. S.; Hogan, A. M.; Xie, S. X.; Ballatore, C.; Smith, A. B.; Lee, V. M.; Brunden, K. R., The microtubule-stabilizing agent, epothilone D, reduces axonal dysfunction, neurotoxicity, cognitive deficits, and Alzheimer-like pathology in an interventional study with aged tau transgenic mice. *Journal of Neuroscience* **2012,** *32* (11), 3601-11.

22. Barten, D. M.; Fanara, P.; Andorfer, C.; Hoque, N.; Wong, P. Y.; Husted, K. H.; Cadelina, G. W.; Decarr, L. B.; Yang, L.; Liu, V.; Fessler, C.; Protassio, J.; Riff, T.; Turner, H.; Janus, C. G.; Sankaranarayanan, S.; Polson, C.; Meredith, J. E.; Gray, G.; Hanna, A.; Olson, R. E.; Kim, S. H.; Vite, G. D.; Lee, F. Y.; Albright, C. F., Hyperdynamic microtubules, cognitive deficits, and pathology are improved in tau transgenic mice with low doses of the microtubule-stabilizing agent BMS-241027. *Journal of Neuroscience* **2012,** *32* (21), 7137-45.

23. Pettit, G.; Cichacz, Z.; Gao, F.; Boyd, M.; Schmidt, J., Isolation and Structure of the Cancer Cell Growth Inhibitor Dictyostatin 1. *Journal of the Chemical Society, Chemical Communications* **1994**, 9, 1111-12.

24. Brunden, K. R.; Gardner, N. M.; James, M. J.; Yao, Y.; Trojanowski, J. Q.; Lee, V. M.; Paterson, I.; Ballatore, C.; Smith, A. B., MT-Stabilizer, Dictyostatin, Exhibits Prolonged Brain Retention and Activity: Potential Therapeutic Implications. *ACS Medicinal Chemistry Letters* **2013,** *4* (9), 886-9.

25. Makani, V.; Zhang, B.; Han, H.; Yao, Y.; Lassalas, P.; Lou, K.; Paterson, I.; Lee, V. M.; Trojanowski, J. Q.; Ballatore, C.; Smith, A. B.; Brunden, K. R., Evaluation of the brain-penetrant microtubule-stabilizing agent, dictyostatin, in the PS19 tau transgenic mouse model of tauopathy. *Acta Neuropathologica Communications* **2016,** *4* (1), 106.

26. Cirrito, J. R.; Deane, R.; Fagan, A. M.; Spinner, M. L.; Parsadanian, M.; Finn, M. B.; Jiang, H.; Prior, J. L.; Sagare, A.; Bales, K. R.; Paul, S. M.; Zlokovic, B. V.; Piwnica-Worms, D.; Holtzman, D. M., P-glycoprotein deficiency at the blood-brain barrier increases amyloid-beta deposition in an Alzheimer disease mouse model. *Journal of Clinical Investigation* **2005,** *115* (11), 3285-90.

27. Westermann, S.; Weber, K., Post-translational modifications regulate microtubule function. *National Review of Molecular Cellular Biology* **2003,** *4* (12), 938-47.

28. Lou, K.; Yao, Y.; Hoye, A. T.; James, M. J.; Cornec, A. S.; Hyde, E.; Gay, B.; Lee, V. M.; Trojanowski, J. Q.; Smith, A. B.; Brunden, K. R.; Ballatore, C., Brain-penetrant, orally bioavailable microtubule-stabilizing small molecules are potential candidate therapeutics for Alzheimer's disease and related tauopathies. *Journal of Medicinal Chemistry* **2014,** *57* (14), 6116-27.

29. Zhang, N.; Ayral-Kaloustian, S.; Nguyen, T.; Afragola, J.; Hernandez, R.; Lucas, J.; Gibbons, J.; Beyer, C., Synthesis and SAR of [1,2,4]triazolo[1,5-a]pyrimidines, a class of anticancer agents with a unique mechanism of tubulin inhibition. *Journal Medicinal Chemistry* **2007,** *50* (2), 319-27.

30. Kovalevich, J.; Cornec, A. S.; Yao, Y.; James, M.; Crowe, A.; Lee, V. M.; Trojanowski, J. Q.; Smith, A. B.; Ballatore, C.; Brunden, K. R., Characterization of brain-penetrant pyrimidine-containing molecules with differential microtubule-stabilizing activities developed as potential therapeutic agents for Alzheimer's disease and related tauopathies. *Journal of Pharmacology and Experimental Therapeutics* **2016,** *357* (2), 432-50.

31. Fukushima, N.; Furuta, D.; Hidaka, Y.; Moriyama, R.; Tsujiuchi, T., Post-translational modifications of tubulin in the nervous system. *Journal of Neurochemistry* **2009,** *109* (3), 683-93.

32. Sáez-Calvo, G.; Sharma, A.; Balaguer, F. d. A.; Barasoain, I.; Rodríguez-Salarichs, J.; Olieric, N.; Muñoz-Hernández, H.; Berbís, M. Á.; Wendeborn, S.; Peñalva, M. A.; Matesanz, R.; Canales, Á.; Prota, A. E.; Jímenez-Barbero, J.; Andreu, J. M.; Lamberth, C.; Steinmetz,

M. O.; Díaz, J. F., Triazolopyrimidines Are Microtubule-Stabilizing Agents that Bind the Vinca Inhibitor Site of Tubulin. *Cell Chemical Biology* **2017,** *24* (6), 737-750 e6.

33. Meyer, O.; Eisenacht, R. Process for the Preparation of Halogenated Phenylmalonates. 6,156,925, 2000.

34. Pfrengle, W.; Pees, K.; Albert, G.; Carter, P.; A, R. Fungicidal Trifluoromethylalkylamino-triazolopyrimidines. 1999.

35. Hurtley, W., Replacement of Halogen in orthoBromobenzoic Acid. *Journal of Chemical Society* **1929**, 1870-1873.

36. MCKILLOP, A.; RAO, D., COPPER-CATALYZED DIRECT ARYLATION OF ALPHA-SUBSTITUTED BETA-DICARBONYL COMPOUNDS WITH 2-BROMOBENZOIC ACID. *Synthesis-Stuttgart* **1977,** (11), 759-760.

37. Bacon, R.; Murray, J.; Metal-Ions and Complexes in Organic Reactions. Copper Catalized Reactions of Aromatic Bromo-carboxylates with Carbanions, Giving Oxo-Acids, Isocoumarins, and Related Products. *Journal of the Chemical Society-Perkin Transactions 1* **1975,** (13), 1267-1272.

38. Beletskaya, I. P.; Fedorov, A. Y., Modern Copper-Catalyzed Hurtley Reaction: Efficient C-Arylation of CH-Acid Derivatives. In *Copper-Mediated Cross-Coupling Reactions*, 2013; pp 281-311.

39. Bechamp, A. J., *Ann. Chim. Phys.* **1854,** *42*.

40. Werner, J. Amination By Reduction. *Industrial and Engineering Chemistry* **1949,** *41* (9), 1841-1846.

41. Gomez, L.; Massari, M. E.; Vickers, T.; Freestone, G.; Vernier, W.; Ly, K.; Xu, R.; McCarrick, M.; Marrone, T.; Metz, M.; Yan, Y. G.; Yoder, Z. W.; Lemus, R.; Broadbent, N. J.; Barido, R.; Warren, N.; Schmelzer, K.; Neul, D.; Lee, D.; Andersen, C. B.; Sebring, K.; Aertgeerts, K.; Zhou, X.; Tabatabaei, A.; Peters, M.; Breitenbucher, J. G., Design and Synthesis of Novel and Selective Phosphodiesterase 2 (PDE2a) Inhibitors for the Treatment of Memory Disorders. *Journal of Medicinal Chemistry* **2017,** *60* (5), 2037-2051.

42. Krapcho, A. Synthetic Applications of Dealkoxycarbonylations of Malonate Esters, Beta-Keto-Esters, Alpha-Cyano Esters, and Related-Compounds in Dipolar Aprotic Media. *Synthesis-Stuttgart* **1982,** (11), 893-914.

43. Barnes-Seeman, D.; Jain, M.; Bell, L.; Ferreira, S.; Cohen, S.; Chen, X.-H.; Amin, J.; Snodgrass, B.; Hatsis, P., Metabolically Stable tert-Butyl Replacement. *ACS Medicinal Chemistry Letters* **2013,** *4* (6), 514-516.